University of Strathclyde

Strathclyde Institute of Pharmacy and Biomedical Science

Development of a novel combination radio-chemotherapy for glioblastoma multiforme

David Scott

A thesis submitted in fulfilment of the requirements for the degree of Doctor of Philosophy

2019

Declaration

This thesis is the result of the author's original research. It has been composed by the author and has not been previously submitted for examination which has led to the award of a degree.

Signed:

Date:

Acknowledgements

I would first and foremost like to thank my supervisors Professor Alex Mullen and Dr Marie Boyd for all their help, support and guidance over the last 4 years and beyond. Without them this thesis wouldn't be extant. Furthermore, I owe a huge amount to Drs Annette Sorensen, Pamela McCall and Tony McClusky, your help has been appreciated more than I can explain. The same goes for everyone in the Boyd group I have had the pleasure of sharing bench space with; PF, RG, NM, KA, KM, MA, LB, AA, RA, RA, ML, WA, IA & anyone else who I have forgotten.

A huge thank you again to everyone who I've shared HW513, 512 & 501 with over the years, PT, RS, LK, JM, IB, LR, KW, EB, MB, CW, KH, MA, JC, JD, FL, KB, DL, GM, SW, BR, MHC, and again, anyone else who I have forgotten.

I also wish to thank both of my sponsors, Medical Research Scotland and Medac GbmH for all the support I have received over the past years. I wish to thank in particular Professor Philip Winn, Dr Alex Graham and Alastair McMurray for all their support, and advice, as well as the opportunities that have been afforded to me.

A huge thank you to my family: Lorraine, Brian and Niamh.

Table of contents

List of figures

Chapter 1

Chapter 3

Chapter 4

Chapter 5

Chapter 6

List of tables

List of abbreviations

ACTB – β-actin

AKT – α-serine/threonine-protein kinase

ALDH – Aldehyde dehydrogenase

ARE – Antioxidant response element

ASK1 – Apoptosis signal-regulating kinase 1

ATCC – American Type Culture Collection

ATM – Ataxia telangiectasia mutated

ATP – Adenine triphosphate

ATR – Ataxia telangiectasia and Rad3-related protein

AUC – Area under the curve

BCNU – bis-chloroethylnitrosourea

BRCA1 – Breast cancer type 1 susceptibility protein

BSA – Bovine serum albumin

BSO – Buthionine sulfoximine

CD – Cluster of differentiation

CDDO-im – 1[2-Cyano-3,12-dioxooleana-1,9(11)-dien-28-oyl] imidazole

CHK – Checkpoint kinase

CI – Combination index

CNS – Central nervous system

DCFDA – 2′,7′-dichlorodihydrofluorescein diacetate

DEP – Dose effect plot

DICE – Dexamethasone, ifosamide, cisplatin & etoposide

DIPG – Diffuse intrinsic pontine glioma

DMF – Dimethyl fumarate

DMSO – Dimethyl sulphoxide

DNA – Deoxyribonucleic acid

DT – Doubling time

DTNB – 5,5'-dithiobis-(2-nitrobenzoic acid)

EGFR – Epidermal growth factor receptor

ELISA – Enzyme linked immune-sorbent assay

EORTC – European Organisation for Research and Treatment of Cancer

ESMO – European Society for Medical Oncology

fa/fu – fraction affected/fraction unaffected

FACE – Fast activated cell-based ELISA

FACs – Fluorescence-activated cell sorting

FITC – Fluorescein isothiocyanate

FOLFOX – Folinic acid, 5-fluorouracil & oxaliplatin

GBM – Glioblastoma multiforme

GST – Glutathione-s-tranferase

H2a.X – H2A histone family member X

HFSTR – Hyperfractionated stereotactic radiotherapy

HGG – High-grade glioma

HIF – Hypoxia inducible factor

HMOX-1 – Haem oxygenase (decycling) 1

HO-1 – Haem oxygenase 1

IDH – Isocitrate dehydrogenase

IL – Interleukin

IMRT – Intensity modulated radiotherapy

iNOS – inducible nitric oxide synthetase

JNK – c-Jun N-terminal kinases

KEAP-1 – Kelch-like ECH-associated protein 1

LET – Linear energy transfer

MAP-k – Mitogen associated protein kinase

MCTS – Multicellular tumour spheroid

MEP – Median effect plot

MGMT – Methylguanine methyltransferase

MMP – Matrix metalloproteinase

MMR – Mismatch repair

MTIC – 5-(3-methyltriazen-1-yl) imidazole-4-carboxamide

mTKI – Multiple tyrosine kinase inhibitor

NAC – N-acetylcysteine

NADPH – Nicotinamide adenine dinucleotide phosphate

NF-κB – Nuclear factor κ-light-chain-enhancer of activated B-cells

NHEJ – Non-homologous end joining

NICE – National Institute for Health and Care Excellence

NIH – National Institute of Health

NOS – Nitric oxide synthetase

NQO-1 – NAD(P)H quinone dehydrogenase 1

NRF2 – Nuclear factor (erythroid-derived 2)-like 2

PBS – Phosbo-buffered saline

PCR – Polymerase chain reaction

PCV – Probarbazine, lomustine & vincristine

PI – Propidium iodide

PI3K – Phosphoinositide 3-kinase

PTEN – Phosphatase and tensin homolog

RNA – Ribonucleic acid

ROS – Reactive oxygen species

RT – Reverse transcriptase

SF2 – Survival fraction at 2Gy

SHH – Sonic hedgehog

SOD – Superoxide dismutase

SOX – Sex determining region Y-box 2

TERT – Telomerase reverse transcriptase

TMZ – Temozolomide

TNF-α – Tumour necrosis factor

ToF-Sims – Time of flight-Secondary ion mass spectrometry

TSC – Tuberous sclerosis

VEGF – Vascular endothelial growth factor

VHEE – Very high energy electrons

VHL – Von-Hippel Landau

WHO – World Health Organisation

XTBR – External beam radiotherapy

Abstract

Glioblastoma multiforme is an invariably terminal cancer, with 5-year survival rates as low as 1.9% in some patient groups. The current treatment for glioblastoma is surgery, external beam radiotherapy and adjuvant and concomitant temozolomide chemotherapy. Treatment will fail due to an inherent treatment resistance, and as a result, current treatment for glioblastoma has been designated as an unmet clinical need, meaning that new and more efficacious treatment options are needed. Dimethyl fumarate is a clinically available immunomodulatory drug, currently used to treat multiple sclerosis. One of the targets of dimethyl fumarate is glutathione, a potent chemo- and radio-resistance factor. We hypothesised that the use of dimethyl fumarate as an adjuvant to standard of care chemo-radiotherapy would increase the efficacy of treatment via glutathione inhibition and subsequent amplification of chemo-radiotherapy effects on a molecular level. We have shown, using bespoke combinations of temozolomide and dimethyl fumarate in two glioblastoma cell lines, that our hypothesis was correct. Cell line specific combinations of temozolomide and dimethyl fumarate significantly increased cell kill in a dose dependent manner. Unfortunately, a precise mechanism for this combination was unable to be elucidated. There was no significant increase in DNA double strand breaks, cell cycle arrest or apoptotic induction when temozolomide treatment and X-irradiation was combined with dimethyl fumarate. We were able to positively identify glutathione as a chemoresistance factor in these cell lines, as well as rule out the role of reactive oxygen species. We have also shown however, that dimethyl fumarate is capable of activating the chemo- and radioresistance factor NRF2. We believe that this is the first mechanistic interrogation of dimethyl fumarate being used to potentiate combined chemo-radiotherapy, however future work is needed before potential clinical deployment of dimethyl fumarate as an anti-neoplastic agent.

Chapter 1

Introduction

1.1 Cancer

Cancer is a leading global killer, responsible for over 8 million deaths worldwide in 2012 (Torre *et al*., 2015). The incidence of cancer is increasing, and it is now estimated that 1 in 2 people will be diagnosed with at least one type of over 200 cancers at some point during their lifetime (Torre *et al*., 2015). Fortunately for many cancers, this high incidence rate is matched by high survival rates including breast, testicular, prostate cancers and malignant melanoma, all of which have 5-year survival rates of greater than 85% (Bray *et al*., 2018; CRUK, 2015; Torre *et al*., 2015).

Conversely, a number of cancers have 5-year survival rates of significantly lower than 20%. These cancers include lung, stomach, pancreatic and brain cancers (CRUK, 2015). The low survival rates for these cancers can in part be attributed to a lack of effective treatment options, as well as fewer effective diagnostic markers, meaning these cancers are often diagnosed at a later stage. Treatment for these high-grade cancers (WHO Grade III-IV) is often considered palliative, meaning that only symptoms that the cancer are treated, with no curative intent.

1.1.1 Brain, Central Nervous System and Intracranial tumours

There are a large number of different brain and central nervous system malignancies, and these cancers account for 2.8% of the total number of cancer diagnoses in the United Kingdom in 2011, and 3.2% of all cancer deaths (CRUK, 2015). The incidence of brain cancer has increased consistently between 1979 and 2010 (CRUK, 2015), however this increase can be partly attributed to advances in diagnostic imaging, which can allow for more accurate detection and diagnosis (McKinney, 2004). The same trend can be observed when comparing overall incidence of all CNS tumours diagnosed between 1975-1979 and 1996-1999 (Hoffman *et al*., 2006; Legler *et al*., 1999). There is increased worldwide mortality and incidence of CNS cancers in both males and females in more developed compared to less developed areas (Torre *et al*., 2015), suggesting

that a westernised lifestyle may play a role in the development of these cancers. Alternatively, the fact that CNS cancers tend to be diagnosed in older patients may play a role in these statistics as these more developed areas tend to have populations with a longer lifespan. It is also possible that less developed areas lack the equipment, resources and clinical expertise to accurately diagnoses these cancers, potentially skewing the data.

Very few CNS cancers are preventable, with statistics in the UK indicating that less than 1% of all diagnosed brain, CNS and intracranial tumours are preventable (CRUK, 2015). The only indicated causative factors are high dose X-rays, such as those used in radiotherapy and chemicals used in the petrochemical industry, however these factors can only be attributed to a very small number of cases (Adamson *et al*., 2009). There is no evidence that mobile phones, smoking, alcohol or infection from specific pathogens can cause brain or CNS cancers (McKinney, 2004).

A limited number of genetic factors have been implicated to be causative of brain and CNS cancers. Exemplar genetic conditions which are associated with an increased rate of brain and CNS tumours include neurofibromatosis (*NF1* gene), tuberous sclerosis (*TSC1/2* gene), Von-Hippel Landau disease (*VHL* gene), Li-Frauman syndrome (*p53* or *CHK2* gene) and Turcot syndrome, also known as mismatch repair cancer syndrome (*MLH1, MSH2, MSH6* or *PMS2* genes) (Goodenberger and Jenkins, 2012). These conditions all result in oncogenesis due to a loss of tumour suppressor gene function, an increase in oncogene activity, or a failure to repair mutagenic DNA damage.

Despite considerable research and clinical advancements, the survival rates for brain and CNS tumours have remained low, with overall 5-year survival rising from 7% to only 19% over the past 40-years (Cancer Research, 2014), this low survival is matched with an increasing incidence.

1.1.1.1 Glioma incidence and survival

The most common brain or CNS cancer is glioma, accounting for 80% of all malignant brain tumours (Omuro and DeAngelis, 2013). Glioma can arise from a number of glial cells, such as astrocytes, oligodendrocytes or ependymal cells. Astrocyte derived cancers – astrocytomas – make up 75% of all gliomas and 34% of all brain or CNS

cancers (Ostrom *et al*., 2014). Gliomas are most commonly found in the frontal, temporal, parietal and occipital lobes (Larjavaara *et al*., 2007)

The World Health Organization grades glioma based on aggressiveness and the level of differentiation of the cells within the tumour. Grade I and II tumours can be viewed as benign (Dolecek *et al*., 2012), but if left unchecked they will invariably progress to an aggressive, malignant growth (Omuro and DeAngelis, 2013). Grade III and IV gliomas are highly differentiated and aggressive cancers with poor survival rates (Ostrom *et al*., 2014).

Grade III gliomas are either anaplastic astrocyotmas, oligodendrogliomas or oligoastrocytomas, with astrocytomas featuring the lowest survival of these, showing a 5-year survival of between only 22 and 25.6% (Omuro and DeAngelis, 2013; Smoll and Hamilton, 2014). Grade IV glioma is commonly known as Glioblastoma Multiforme or simply Glioblastoma. Glioblastoma multiforme originates and presents through two distinct pathways which result in either a primary or secondary glioblastoma. Both primary and secondary glioblastoma, as the two distinct tumours are described, are WHO grade IV and are treated identically. Secondary glioblastoma can develop directly from WHO grade II astrocytoma or from grade II astrocytoma that has progressed to grade III anaplastic astrocytoma before further progression to glioblastoma. (Louis *et al*., 2016; Ohgaki and Kleihues, 2013)

Due to the aggressiveness of this cancer, glioblastoma is considered terminal, with 5-year survival historically being as low as 1.9% in some patient groups, (Perry *et al.,* 2012). However, 5-year survival has increased to between 8-10% with the introduction of more effective treatment options (Perry *et al*., 2012; Preusser *et al*., 2011).

Median survival from high-grade glioma diagnosis is typically less than 4 months, and this pattern of increasing glioma incidence and continued low survival rates has precipitated a need for new and effective treatment options, and a deeper understanding of the molecular biology of glioma has given rise to a number of exploitable targets.

Diagnosis	WHO Grade	Anaplastic	5-year Survival (%)	Incidence/100,000
Pilocytic Astrocytoma	I		86.6	0.36
Oligoastrocytoma	II	No	50	0.19
Oligodendroglioma			68.5	0.19
Astrocytoma			18.5	0.31
Oligoastrocytoma	III	Yes	49.4	0.15
Oligodendroglioma			35.4	0.08
Glioblastoma Multiforme	IV		3.4	2.58

Table 1.1: The age adjusted survival and incidence of glioma, highlighting the difference between survival in high grade and low-grade glioma, as well as the higher incidence of astrocytomas and glioblastoma multiform (Adapted from Ostrom *et al*., 2014).

1.2.Biology of glioblastoma

There are a number of features common to glioma that combine to make these cancers aggressive and difficult to treat, including aberrant gene expression, hypoxia and a highly invasive phenotype. An increased knowledge of the cellular and molecular basis of glioma has raised expectation that these traits can be exploited to deliver tumour targeted treatment options (Omuro and DeAngelis, 2013; Parsons *et al*., 2008; Perry *et al*., 2012).

1.2.1 Primary and secondary glioblastoma

Glioblastoma multiforme originates and presents through two distinct pathways which result in either a primary or secondary glioblastoma. Both primary and secondary glioblastoma, as the two distinct tumours are described, are WHO grade IV and are treated identically, but display distinct genetic, transcriptomic and molecular patterns (Kim *et al*., 2015; Ohgaki and Kleihues, 2013; Tso *et al*., 2006).

Primary glioblastoma is a *de novo* tumour that typically presents in the older population with no prior clinical manifestation, whereas secondary glioblastoma is a progression from previously diagnosed glioma. Secondary glioblastoma can develop directly from WHO grade II astrocytoma or from grade II astrocytoma that has progressed to grade III

anaplastic astrocytoma before further progression to glioblastoma (Agnihotri *et al*., 2013; Louis *et al*., 2016). This process is illustrated in Figure 1.1.

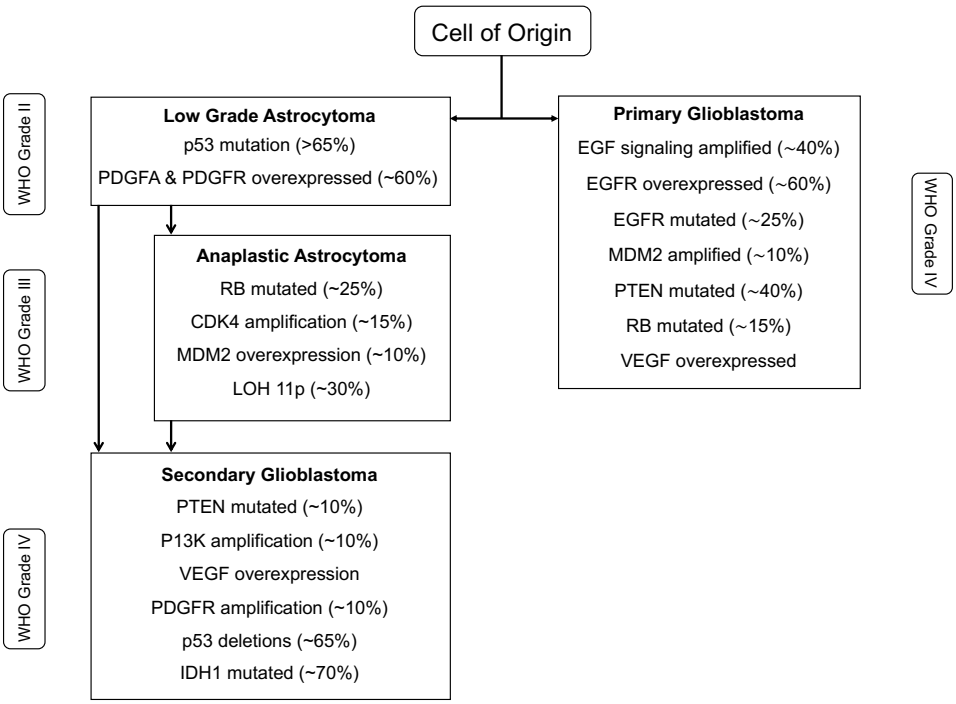

Figure 1.1: Development of primary and secondary glioblastoma from an undefined cell of origin. Mutations associated with each cancer are also shown. Adapted from (Agnihotri *et al*., 2013; Louis *et al*., 2016).

The cell of origin in Figure 1.1 is left undefined as there is no common consensus from which cell brain cancers such as glioma develop from. Recent work, however, has identified oligodendrocyte precursor-cells as the putative cell of origin in glioma (Liu *et al*., 2011). This work also indicated that although oligodendrocyte precursor cells appear to be the cell of origin for glial cancers, the mutation that induces these malignancies can occur in neural stem cells, the precursor to oligodendrocyte precursor-cells. Furthermore, Mutations in p53, NF1 and TERT have been identified as drivers of this malignant divergence (Lee *et al*., 2018; Liu *et al*., 2011). This is illustrated in Figure 1.2.

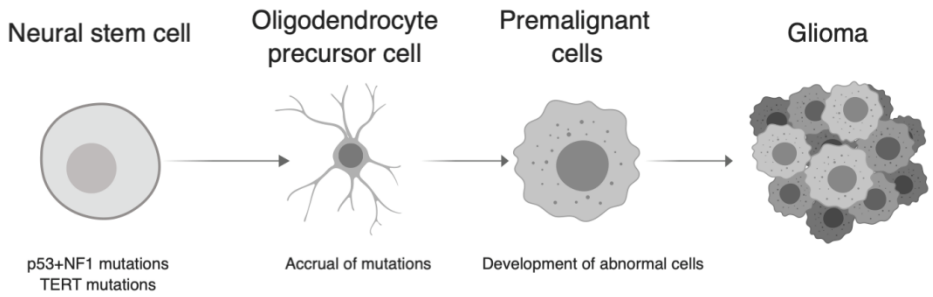

Figure 1.2: Current paradigm for the origin of glioma as a divergence from typical neurodevelopment. Adapted from (Liu *et al*., 2011).

Secondary glioblastoma generally has a more favourable prognosis than primary glioblastoma (7.8 vs 4.7 months) (Louis *et al*., 2016; Ohgaki and Kleihues, 2013). This is partially due to secondary glioblastoma presenting in younger patients who are more resilient to a more robust treatment regimen than the older population in which primary glioblastoma typically presents. As secondary glioblastoma is a progression from a WHO grade II or III astrocytoma, there is a clinical history attached to each patient. A more detailed clinical history will allow clinicians to make a more informed decisions based around treatment deployment in secondary glioblastoma than in *de novo* primary glioblastoma. Unfortunately, although secondary glioblastoma has significantly better prognosis, primary glioblastoma makes up the bulk of glioblastoma multiforme diagnosis. 94.7% of cases of glioblastoma multiforme fulfil the clinical conditions required for diagnoses of primary glioblastoma.

More so than clinical history and tumour grade at diagnosis, there is a distinct mutational, transcriptomic and metabolomic profile associated with primary and secondary glioblastoma. This is observed more so on the transcriptomic level (Tso *et al*., 2006), with neural, classical (described as proliferative by (Phillips *et al*., 2006)), mesenchymal and proneural profiles being well defined and described in the literature (Lottaz *et al*., 2010; Phillips *et al*., 2006; Verhaak *et al*., 2010). However, there is now evidence the neural subtype is not a true glioma subtype, but is in fact contamination by healthy brain tissue (Li *et al*., 2017; Sidaway, 2017; Wang *et al*., 2017) as highlighted by the lack of genetic abnormalities in this grouping (Brennan *et al*., 2013).

These three profiles have now been validated in a number of patient samples, and further analysis has shown that median survival differs between each subtype. The classical, mesenchymal and proneural subtypes have median survival of 14.7, 11.5 and 17 months respectively (Wang *et al*., 2017). Increased survival in the proneural subtype is likely due to the virtually exclusive presence of mutant IDH within this group (Aldape *et al*., 2015). Characteristic differential gene signatures are shown in Table 1.2. The classical subtype (described by Phillips as proliferative) was described in this way due to the typical glioblastoma presentation of chromosome 7 amplification and chromosome 10 deletion (Phillips *et al*., 2006).

All of these profiles have been associated with primary glioblastoma, with a proneural profile being seen in both primary and secondary glioblastoma. Unique to secondary glioblastoma, a DNA hypermethylation phenotype, known as the glioma-CpG island methylator phenotype (G-CIMP), has been identified. This group is seen more commonly in proneural tumours. This population was first identified by Noushmehr and the population in which this phenotype was first identified is consistent with the secondary glioblastoma patient population (Noushmehr *et al*., 2010).

Neural	Classical	Mesenchymal	Proneural
	EGFR VIII mutation	NF1 mutation	IDH1 mutation p53 mutation
	EGFR amplification		PDGFRA amplification
	INK4A/ARF loss PTEN loss	CDKN2A loss p53 loss PTEN loss	INK4A/ARF loss PTEN loss
EGFR overexpression Elevated neural marker expression HER2 overexpression	Nestin overexpression	CD44 overexpression CHI3L1 overexpression MET overexpression VEGF overexpression	
	Notch activation SHH activation	NFκB activation TNF family activation	HIF-1α activation PDGFRA activation PI3K activation
Brain tissue gene signature	Chromosome 7 amplification & chromosome 10 deletion	Mesenchymal tissue gene signature	Proneural cell gene signature

Table 1.2: Table showing the differences between the 4 main glioblastoma subtypes. The neural subtype is separated to highlight the differences, or lack thereof, that distinguish this group from typical brain tissue. Adapted from (Agnihotri *et al*., 2013; Behnan *et al*., 2019; Ludwig and Kornblum, 2017; Noushmehr *et al*., 2010; Phillips *et al*., 2006; Verhaak *et al*., 2010).

It has now been evidenced that transition between these subtypes is a feature of glioma progression and development (Wang *et al*., 2017), and in some cases progression appears to be strongly influenced by the tumour microenvironment, particularly the immune response to, and the immune infiltrates within, the tumour (Wang *et al*., 2017).

Glioblastoma has a remarkable level of genetic heterogeneity on an intratumoral level, meaning that a case of glioblastoma is likely present with molecular features of more than of the groups described above (Sottoriva *et al*., 2013). This is likely to occur through one of two mechanisms; early divergent mutations from the cell of origin of glioblastoma or clonal evolution from stem cells, giving rise to genetically diverse populations within the tumour mass (Parker *et al*., 2015). Due to evolutionary divergence occurring early in the development of glioblastoma, heterogeneity on a genetic level is a common feature of glioblastoma. By developing mutations early in the oncogenic process, either through stem cell differentiation and expansion or through germ line cell mutation, glioblastoma develops as a genetically diverse cancer, with unique subpopulations throughout the tumour mass (Brennan *et al*., 2013; Wang *et al*., 2017). These subpopulations can feature genetic overlap, or remain distinct, however it is common for a tumour to have the characteristics of more than one glioblastoma subtype as seen in Table 1.2.

A point of interest around primary and secondary glioblastoma is the ‘storm, form and norm’ of the cancer stem cell hypothesis; the controversial proposition of the concept of glioma stem cells, the re-evaluation of clinical and lab findings to incorporate the paradigm of cancerous stem cells and then finally the normalisation of glioma stem cells as an established scientific phenomenon.

1.2.2 Physiological, molecular and genetic aspects of glioblastoma

Cancer is a disease of the genes; accrual of genetic damage leads to alteration of gene activity in the form of mutations. Genetic damage can affect the way in which mutated genes are expressed, with genes commonly being epigenetically modified, constitutively expressed, or silenced (Stratton *et al*., 2009). This often results in uncontrolled cellular proliferation. However, there is not one single genetic alteration that gives rise to a malignancy. There are often more than 5 mutations leading to dysplasia and hyperplasia, before a tissue becomes cancerous (Yokota, 2000). Mutations can be caused by a number of factors, such as exposure to ionising radiation, ultraviolet-light or toxic chemicals; mutations can also occur organically as a part of the DNA synthesis and replication process.

The mutations that lead to cancer are often found in genes associated with control of cell growth, for example genes involved in regulation of the cell cycle. Therefore, cell cycle

dysfunction is a common motif of almost every cancer. Due to the importance of the cell cycle, it is tightly regulated by a series of phosphorylation cascades, underpinned by a complex interplay of cyclin-dependent kinases, DNA damage repair proteins and other gene families, such as tumour suppressor genes and proto-oncogenes (Collins *et al*., 1997; Kastan and Bartek, 2004; Zhivotovsky and Orrenius, 2010). Checkpoints at each phase of the cell cycle ensure that the synthesis and fidelity of DNA is conserved to prevent introduction of oncogenic or fatal mutations. These checkpoints prevent cells with incorrectly replicated DNA from proceeding through the cycle until the damage has been repaired, or forces the cell to undergo apoptosis (Kastan & Bartek, 2004).

Tumour suppressor genes act to maintain and regulate the normal proliferation of the cell by controlling the cell cycle. These genes include p53, p16, MGMT and BRCA1, which act as cell cycle regulators, cyclin-dependent kinase inhibitors, and DNA damage repair genes respectively (Garinis *et al*., 2002). For a tumour suppressor gene to fail, an individual must be homozygous for the mutant gene, and an inherited mutation can predispose an individual to certain types of cancer. These mutations are almost always loss-of-function mutations (Lee & Muller, 2010; Sherr, 2004).

Proto-oncogenes are drivers of cellular proliferation, and commonly mutate to oncogenes; these are typically gain of function mutations that stimulate cell growth, division and survival (Lee and Muller, 2010). These mutations push the cell through the cell cycle, forcing rapid cell division, which can lead to tumour formation. Ras is the most commonly mutated oncogene in cancer, with the K-Ras isoform mutated in up to 30% of all cancers (Fernandez-Medarde & Santos, 2011). The mutated Ras gene has a large number of functions in cancers, but one of its main roles is to promote constitutive cell cycling by constitutive Ras signalling through ERK, P13K/AKT and PKC pathways.

As with many cancers, there are a number of genes that are commonly mutated or overexpressed in glioma. These include the DNA damage repair protein MGMT, the pro-inflammatory transcription factor NF-κB and the isocitrate dehydrogenase gene family. This section aims to describe several of these genetic, molecular and physiological features of high-grade glioma and their role in treatment outcome. However, this is not exhaustive, as there are a large number of other genetic, molecular and physiological markers associated with glioblastoma.

1.2.2.1 MGMT

There are a plethora of DNA repair mechanism that aim to repair DNA damage which accumulates in glioma cells. One of these DNA damage repair proteins is MGMT (O^6-methylguanine DNA methyltransferase). Under normal conditions, MGMT acts to primarily to prevent genes, such as tumour suppressor genes, from being epigenetically silenced via methylation (Christmann *et al*., 2011; Nakamura *et al*., 2001). MGMT acts specifically to undo methylation in the O^6 position of the base guanine by transferring the unwanted methyl group to a nearby cysteine base. Removal of the methyl group form the O^6-position of guanine by MGMT is an irreversible reaction, meaning that the active site of the enzyme is irreversibly poisoned.

The methylation of guanine to O^6-methylguanine is rare, accounting for less than 8% of all DNA alkylation events (Fan *et al*., 2013; Kaina *et al*., 2007). Although rare, O^6 methylation of guanine is incredibly toxic due to the inability of the cell to successfully pair the methylated guanine with a complementary base pair. This leads to induction of the mismatch repair pathway. Sustained inability of the cell to successfully pair the methylated guanine base leads to aborted mismatch repair cycles, which generates DNA double strand breaks.

Methylation of the O^6-position of guanine is the main mechanism of the alkylating agent temozolomide. Because of this, expression of the DNA damage repair protein O^6-methylguanine DNA methyltransferase (MGMT) is used clinically to predict response to the standard of care for glioblastoma, temozolomide (Section 1.3.3.1). Patient survival in MGMT positive tumours is discussed in Section 1.3.3.1.

However, in high grade glioma, epigenetic methylation of the *MGMT* promoter occurs Promoter methylation prevents expression of the MGMT protein, and therefore increases response to temozolomide therapy. Promoter methylation and therefore null expression occurs more commonly in low-grade astrocytoma (48%) and in 75% of secondary glioblastomas (WHO grade IV) that have progressed from low-grade astrocytoma. The frequency of *MGMT* promoter methylation has been found to significantly lower in primary glioblastomas (36%) (Nakamura *et al*., 2001). This indicates that methylation of the MGMT promoter may be an early event in the development of these cancers, and null activity of MGMT in secondary glioblastoma may explain why these cancers have a

significantly better response to temozolomide therapy (Ohgaki and Kleihues, 2013).

1.2.2.2 Isocitrate dehydrogenase

Isocitrate dehydrogenase (IDH) 1 and 2 are metabolic enzymes that produce the Kreb's Cycle intermediate α-ketoglutarate (Reitman *et al*., 2011). Mutated IDH1 is more often found in secondary glioblastoma than primary glioblastoma and these mutations are believed to occur early in the development of these cancers (Frezza *et al*., 2010). As discussed, secondary glioblastoma occurs as a progression from lower grade glioma, typically anaplastic astrocytoma (Louis *et al*., 2016; Ohgaki and Kleihues, 2013). IDH mutations are more commonly found in secondary glioblastoma than primary glioblastoma. Expression of mutant IDH in secondary glioblastoma is likely an artefact of progression from anaplastic astrocytoma as IDH mutation at codon 132 has been found in 60% of anaplastic astrocytoma but only 7.2% of primary glioblastoma cases (Hartmann *et al*., 2010; Sanson *et al*., 2009).

IDH normally exists as a homodimer, but following mutation it will exist as a heterodimer, composed of one wild-type and one mutant subunit (Zhao *et al*., 2009). Atypically for a tumour suppressor gene, only one allele needs to mutate for loss of function to occur. This mutation decreases intracellular levels of α-ketoglutarate, which increases the intracellular levels of the hypoxia marker, hypoxia inducible factor 1-α (HIF1-α), as α-ketoglutarate is involved in the oxygen-dependent degradation of HIF (Fu *et al*., 2010). Despite mutation in a tumour suppressor gene, patients displaying an IDH mutation have significantly higher survival rates, and this is believed to be due to mutant IDH consuming, rather than producing NADPH. This will prevent appropriate reduction of the free-radical scavenger glutathione occurring, resulting in chemo- and radiosensitisation (Christensen *et al*., 2010; Fu *et al*., 2010; Houillier *et al*., 2010). This is illustrated in Figure 1.3.

Overall survival for secondary glioblastoma patients with mutant IDH1/2 was found to be 4.3 months longer than with IDH1/2 wild type (8.4 months vs 12.7 months) (SongTao *et al*., 2012) and 2.7 years longer (1.1 years vs 3.8 years) in patients with IDH1 mutation (Parsons *et al*., 2008). Overall, patients with both mutant IDH and MGMT promotor methylation perform better than patients with either MGMT promoter methylation or IDH mutation (1311 days mean survival vs 331 days mean survival) (Hartmann *et al*., 2010;

Molenaar *et al*., 2014)

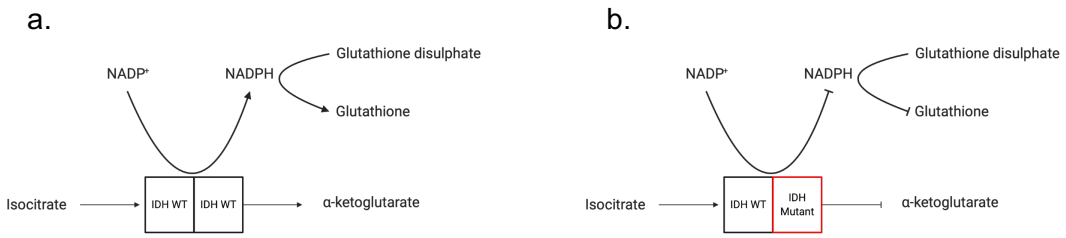

Figure 1.3: Function of isocitrate dehydrogenase in glioma. **a.** shows normal metabolism of isocitrate by the wild type isocitrate dehydrogenase with associated reduction of glutathione. **b.** shows dysfunctional metabolism of isocitrate by the mutant isocitrate dehydrogenase with no associated reduction of glutathione, resulting in chemo and radiosensitisation.

1.2.2.3 p53, PTEN and monosomy of chromosomes 10 & 17

p53 is the most commonly mutated tumour suppressor gene in human cancers (Lai *et al*., 2012). In healthy cells p53 acts as cell cycle checkpoint protein as part of the ARF/MDM2/p53 pathway, holding the cell at the G_1 and G_2/M checkpoint, where damaged DNA can be repaired by DNA damage repair proteins, which can also be induced by p53 (Sherr and McCormick, 2002). If the damage is too severe, and the DNA cannot be repaired, apoptosis will be induced. However, in p53 mutant cancer, the cell can still divide with damaged DNA, resulting in cells that will have unstable genetic content. If there is a high degree of instability, then these cells will eventually die. Cells with lower levels of instability may continue to grow aberrantly, and develop further mutations (Vakifahmetoglu *et al*., 2008). This also allows cells which have had DNA damaged by chemotherapy or radiotherapy to continue to replicate instead of initiating apoptosis, resulting in many chemotherapeutic drugs operating in a p53 dependent manner.

As reported by The Cancer Genome Atlas, the ARF/MDM2/p53 pathway is dysregulated in 84% of glioblastoma cases, with *TP53* dysregulation observed in 22% of glioblastoma (Parsons *et al*., 2008; The Cancer Genome Atlas Research Network, 2008). The majority of these mutations are missense mutations in the DNA binding domain of the *TP53* gene which leads to inhibition of transcription factor activity and therefore lower levels of

oncogenic gene transcription (Labussière *et al*., 2016). Mutant p53 has been shown to be more oncogenic than the more common loss of wild type p53 (Bastien *et al*., 2015; Khani *et al*., 2019). This is due to mutant p53 acting as a gain of function mutation that is capable of interacting with p63, p73 and VDR (Vitamin D receptor) (Zhang *et al*., 2018), which are associated with malignant progression, resulting in an increase in cellular proliferation, migration and invasion.

The *TP53* gene is found on chromosome 17, and 60% of WHO grade II and III astrocytomas have a loss of heterozygosity of chromosome 17, and this is commonly associated with mutant p53 activity (Fults *et al*., 1992), and has been suggested to be a mediator of malignant progression (Deimling *et al*., 1992; Watanabe *et al*., 1997). As mutant p53 is found more commonly in grade II-III glioma, p53 is more commonly seen in secondary glioblastoma, with over 70% of secondary glioblastoma displaying mutant p53 (Crespo *et al*., 2011; Zawlik *et al*., 2009). p53 has been shown to be mutated in response to chemotherapy, with 37.5% and 58% of untreated and treated glioblastomas showing mutant p53 (Parsons *et al*., 2008; The Cancer Genome Atlas Research Network, 2008), this is likely due to positive selection of mutant cells due to the reliance of competent p53 for many chemotherapeutic drugs to elicit cytotoxicity (Hirose *et al*., 2001).

Due to the increase oncogenic activity associated with mutant p53, wild type p53 expression in high-grade glioma is correlated with higher 5-year survival than mutant p53 (46% vs. 21%). Mutant p53 is associated with poor response to temozolomide therapy. This is believed to occur as the length of the G_2/M arrest induced by temozolomide is dependent on wild type p53 (Hirose *et al*., 2001), and arrest at the G_2/M checkpoint is needed for the temozolomide treated cells to induce apoptosis (Hermisson *et al*., 2006; Roos *et al*., 2007). Interestingly, mutant p53 is associated with methylation of the MGMT promoter, which confers temozolomide sensitivity (Hermisson *et al*., 2006; Nakamura *et al*., 2001).

p53 mutation has been associated with dysfunction of another tumour suppressor gene, Phosphatase and tensin homolog (PTEN). PTEN acts as a tumour suppressor by negatively regulating PI3K which forms an intrinsic part of the PI3K/AKT pathway (Endersby and Baker, 2008). In glioma, activation of receptor tyrosine kinases has been shown to signal through the PI3K/AKT axis to increase cell growth and prevent induction

of apoptosis (Fan and Weiss, 2010). The *PTEN* gene is found on chromosome 10, and monosomy of chromosome 10 is commonly seen in primary glioblastoma (Lopez-Gines *et al*., 2005), with between 60 and 90% of glioblastoma cases showing whole chromosome loss of chromosome 10. In secondary glioblastoma loss of chromosome 10q is more common than deletion (Fujisawa *et al*., 2000). As a result of this, deletion of PTEN is more common than mutation.

Loss of PTEN results in increased or constitutive PI3K/AKT signalling and is commonly associated with an increase in EGFR (epidermal growth factor receptor) signalling (Parsons *et al*., 2008; Smith *et al*., 2001; Stichel *et al*., 2018; The Cancer Genome Atlas Research Network, 2008). Mutations or deletions with in the EGFR/PTEN/PI3K/AKT pathway have been demonstrated in 88% of glioblastoma diagnoses (The Cancer Genome Atlas Research Network, 2008). Furthermore, PTEN mutation or deficiency is correlated with a significantly worse outcome for glioblastoma multiforme and anaplastic astrocytoma patients (Chakravarti *et al*., 2004; Smith *et al*., 2001).

As mentioned, PTEN is a negative regulator of PI3K and AKT. Activation of AKT and PI3K is associated with apoptotic resistance following treatment (Duronio, 2008; Franke *et al*., 2003; Li *et al*., 2016). This occurs through up regulation of anti-apoptotic factors such as NF-κB and BCL-2, and inhibition of pro-apoptotic factors such as Caspases 3 & 8, Bad and Bax (Hay and Sonenberg, 2004; Hu *et al*., 2005; Malla *et al*., 2010; Nan *et al*., 2017; Zhang *et al*., 2012). Evasion of programmed cell death pathways leads to increased tumour growth, and it is believed that the loss of PTEN as a positive regulator of apoptosis is responsible for the poor outcome in PTEN deficient patient groups (Chakravarti *et al*., 2004; Han *et al*., 2016; Smith *et al*., 2001).

Downstream targets of PI3K and AKT include mammalian target of rapamycin 1 & 2 (mTOR1&2). mTOR is a highly conserved serine/threonine kinase that controls cell growth and metabolism in response to nutrients, growth factors, cellular energy, and stress. mTOR acts downstream of AKT to facilitate signal transduction. Due to the constitutive activation of AKT/PI3K signalling in PTEN negative cancers, mTOR mediated signal transduction is highly active. mTOR is also highly druggable, with everolimus, sirolimus and rapamycin showing strong inhibitory properties. Everolimus, an immunosuppressive mTOR inhibitor, has been approved for WHO grade I subependymal giant cell astrocytoma (SEGA) which is associated with tuberous

sclerosis (Krueger *et al*., 2010) and mTOR inhibitors have shown promise in *in vivo* models of glioblastoma with constitutive AKT signalling (Hu *et al*., 2005) as well as showing synergy with temozolomide in both *in vivo* and *in vitro* models of glioblastoma (Luchman *et al*., 2014). However, this has not translated clinically. Initial studies using rapamycin in PTEN deficient glioblastoma showed promising results (Cloughesy *et al*., 2008), but larger studies combining everolimus with the standard of care showed an increase in toxicity with no associated survival benefit (Ma *et al*., 2015a). Careful patient selection must be performed in order to determine if mTOR inhibitors can be of use in select patient groups (Don and Zheng, 2011).

1.2.2.4 EGFR VIII expression and chromosome 7 trisomy

A common feature of high-grade glioma is trisomy of chromosome 7. Chromosome 7 contains the *EGFR* gene and gain of chromosome 7 is associated with over expression of the epidermal growth factor receptor (EGFR) in glioblastoma patients. EGFR signalling has been shown to be amplified primarily in primary glioblastoma (Parsons *et al*., 2008; Stichel *et al*., 2018; The Cancer Genome Atlas Research Network, 2008; Verhaak *et al*., 2010), with 55-70% of primary glioblastomas overexpressing EGRF (Ohgaki and Kleihues, 2013; Ohgaki *et al*., 2004). This is not seen in lower grade astrocytoma (Agosti *et al*., 1992).

As well as overexpression of EFGR, a mutant EGFR variant is commonly expressed in glioblastoma (Nishikawa *et al*., 1994; Szerlip *et al*., 2012). EGFR vIII features deletion of a sequence of 267 amino acids in the extracellular ligand-binding domain, resulting in constitutive low level EGF signalling even in the absence of ligand binding (Ekstrand *et al*., 1992). EGFR activation results in a cacophony of signal transduction, including RAS/ERK/MAPK, PI3K/AKT, NF-κB and STAT3 signalling. Stimulation of these pathways results in suppression of apoptosis and sustained growth as well as an increase in angiogenesis and invasion (An *et al*., 2018; Normanno *et al*., 2006; Sigismund *et al*., 2019).

As a result of the activation of oncogenic targets amplification of EGFR and presence of EGFR vIII is associated with poor patient outcome (Bieńkowski *et al*., 2013; Smith *et al*., 2001) and poor response to radiotherapy (Barker *et al*., 2001) and chemotherapy (Montano *et al*., 2011). However, a number of studies have shown that EGFR vIII is not

a prognostic indicator in glioblastoma multiforme (Donato *et al*., 2007; Felsberg *et al*., 2017; Heimberger *et al*., 2005). The use of EGFR vIII as a prognostic factor has not been validated in large scale trials.

Due to the high level of EGFR activation in glioblastoma multiforme, targeting EGFR has become been an attractive therapeutic option (Raymond *et al*., 2000). EGFR has shown itself to be an attractive and highly druggable treatment option, with small molecule EGFR inhibitors such as erlotinib (Shepherd *et al*., 2005; Tsao *et al*., 2005) and gefitinib (Maemondo *et al*., 2010; Mok *et al*., 2009), and monoclonal antibodies such as cetuximab (Cunningham *et al*., 2004; Van Cutsem *et al*., 2009) being approved for a number of cancers. However, despite the level of efficacy seen in other tumour types, EGFR inhibition has largely failed as a treatment option for glioblastoma (Westphal *et al*., 2017).

Erlotinib has been shown to cross the blood brain barrier in an orthotopic model of glioblastoma (Liu *et al*., 2013), but numerous studies have shown to show no improvement in overall or progression free survival when the standard of care for glioblastoma is supplemented with erlotinib (van den Bent *et al*., 2009; Peereboom *et al*., 2010; Prados *et al*., 2009; Raizer *et al*., 2010). The use of erlotinib has been associated with an increase in unacceptable side effects (Peereboom *et al*., 2010). Unfortunately, in a study using the small molecule EGFR inhibitor gefitinib, there was no significant increase in overall or progression free survival compared to the standard of care (Chakravarti *et al*., 2013; Uhm *et al*., 2011). Interestingly, patients who had a gefitinib associated adverse events did see an increase in overall survival (Uhm *et al*., 2011). The lack of response of glioblastoma to EGFR targeted therapies and incidence of adverse events associated with therapy has prevented deployment of these therapies in glioblastoma.

1.2.2.5 Hypoxia, vascularisation and the invasive phenotype of glioblastoma

As described in The Hallmarks of Cancer (Hanahan and Weinberg, 2000, 2011), tumour vascularisation, hypoxia and sustained angiogenesis are prominent features of high-grade glioma, and all are closely linked. Over expression of vascular endothelial growth factor (VEGF) is associated with an increase in angiogenesis as well as increasing vascular permeability of the blood brain barrier. Hypoxia and angiogenesis are closely

linked in glioblastoma. Glioma tends to be highly vascularized, likely through the differentiation of glioma stem cells to endothelial-like cells and increased levels of VEGF found in the largely hypoxic tumour (Bristow and Hill, 2008; Ricci-Vitiani *et al*., 2010). Large quantities of VEGF are produced in response to hypoxia and the production of Hypoxia Inducible Factor (HIF), this leads to increased tumour vascularisation, as well as an increase in tumour growth (Jensen *et al*., 2006).

Hypoxia is a feature of many solid tumours, and is characterized by an oxygen level lower than 10mmHg, compared to normal tissue, which has typical oxygen levels of 40-60mmHg (Brown, 2000). The induction and accumulation of the transcription factors Hypoxia Inducible Factor (HIF) 1α and HIF-2α occurs in hypoxic tissue, as HIF-1 and 2 both degrade in an oxygen dependent manner (Semenza, 2012). This results in increased binding of HIFs to hypoxia specific promoter regions, known as hypoxic response elements on the DNA, and increased translation of a number of genes which contribute to tumour growth, therapy resistance and angiogenesis (Kaur *et al*., 2005). Hypoxic response elements are found upstream of a large number of genes including; the vascular endothelial growth factor (*VEGFA*) gene, which promotes angiogenesis, the *GLUT1* gene, which increases growth and glycolytic metabolism, and the carbonic anhydrase IX (*CA9*) gene, which regulates intracellular pH (Bristow and Hill, 2008).

Resistance to treatment is commonly associated with hypoxia. HIF mediated overexpression of the xenobiotic efflux pump p-glycoprotein (p-GP) results in broad-spectrum chemotherapy resistance (Wartenberg *et al*., 2003), and the pH regulating carbonic anhydrase IX results in resistance to alkylating agents (Bristow and Hill, 2008; Shannon *et al*., 2003). HIF-1α has also been shown to induce MGMT expression, resulting in a temozolomide resistant cell population (Persano *et al*., 2012). These factors combine to make chemotherapy largely ineffective against the hypoxic core of the tumour. This hypoxic region is also 2-3 times more resistant to radiation than normoxic tumour cells (Harrison, 2002) .This is due to the absence of oxygen, which is converted to free radicals by ionising radiation (Cooke *et al*., 2003). However, the free-radical scavenger glutathione is known to inhibit HIF activity, but reduced glutathione, as found in cells following radiotherapy, has no effect on HIF binding to hypoxic response elements (Tajima *et al*., 2009), meaning that radiation may indirectly promote HIF binding and activity.

As the tumour progresses, the hypoxic fraction of the tumour will also increase in size, leading to further VEGF synthesis and action. In solid tumours, increased vascularisation and vascular permeability is associated with metastasis (Arvelo *et al*., 2016). Instead of metastasising, glioma is highly invasive along white matter tracts. There are four steps to invasion; detachment of cells from the tumour mass, adhesion to the extracellular matrix, degradation of the extracellular matrix through the action of matrix metalloproteinases and invasion by increased cell motility (Tate and Aghi, 2009). The production of VEGF in glioma is associated with growth and invasion through CXCR4 signalling (Hong *et al*., 2006; Zagzag *et al*., 2006). Anti-VEGF therapies have been shown to increase survival (Section 1.3.3.3), but have also been shown to induce a compensatory increase in glioma cell invasion (Keunen *et al*., 2011). This invasive phenotype can render both surgical resection and radiotherapy ineffective, and it believed that recurrence is partly due to these deeply infiltrating cells (Demuth and Berens, 2004; Tate and Aghi, 2009).

1.2.2.6 Cancer stem cells

As chemotherapy is highly toxic, it will often kill non-cancerous cells. This off-target effect is most commonly associated with cells with a high mitotic index, such as hematopoietic cells, gametocytes and epithelial cells. There is also emerging evidence that cells that do not rapidly divide can also be adversely affected by chemotherapy. This is seen in particular with neural tissue, with so-called “chemo-fog” affecting healthy brain tissue (Wefel and Schagen, 2012). One of the main problems with treating brain cancers is that neural tissue has limited self-renewal, despite having a high degree of plasticity (Antonelli *et al*., 2012). This means that non-cancerous cells that are killed or damaged by chemotherapy are incapable of regrowth, which can have immediate or delayed effects on cognition, motor skills, or speech, limiting the overall acceptable toxicity of the chemotherapy regime (Vives and Piepmeier, 1999; Wefel and Schagen, 2012).

However, the cancer stem cell population reported to be present in glioma contains a high level of self-renewal potential, and this contributes to the development and resurgence of the tumour mass (Peitzsch *et al*., 2017). Cancer stem cells are now a widely accepted phenomenon, with properties similar to the healthy stem cell population. These cells are particularly long lived and have a high replicative ability and are therapy resistant. Glioma stems cells have the ability to self-renew and the potential to

differentiate widely, which may explain the heterogeneity of glioma (Vescovi *et al*., 2006).

Due to the high proliferative capacity and self-renewal potential exhibited by these cells, they are often highly treatment resistant and failure to destroy the cancer stem cell population will result in regrowth of the tumour mass (Bao *et al*., 2006; Jordan *et al*., 2006; Lathia *et al*., 2015). The known stem cell marker CD133 evidences this; $CD133^+$ cells have been shown to be able to generate tumours in *in vivo* models (Singh *et al*., 2004) and recurrent gliomas also have much higher levels of $CD133^+$ cells, suggesting that the glioma stem cell population is responsible for recurrence of the tumour mass (Rich, 2007).It has been suggested that this occurs due to the stem cell population evading chemo- and radiotherapy by cycling slowly, and then increasing growth in response to treatment (Bao *et al*., 2006; Rich, 2007)

The detoxification enzyme aldehyde dehydrogenase 1 (ALDH1A1) is another common stem cell marker in a number of cancers (Ginestier *et al*., 2007), and is associated with poor prognosis and resistance to temozolomide and radiation (Croker and Allan, 2012; Schäfer *et al*., 2012). ALDH removes oxidized and peroxidised membrane lipids that have the potential to bind and react with DNA and protein structures within the cell, resulting in cell death (Schäfer *et al*., 2012). Expression of ALDH is associated with poor treatment outcome, and the over expression of ALDH in glioma stem cells is likely to contribute to the treatment refractory nature of this population (Croker and Allan, 2012; Schäfer *et al*., 2012)

The development, maintenance and differentiation of the glioma stem cell population is strongly influenced by hypoxia (Heddleston *et al*., 2009). Hypoxia inducible factor (HIF) -2α is preferentially upregulated by glioma stem cells, and it believed to be vital for the survival of this cell population (Li *et al*., 2009). The undifferentiated phenotype of these cells is also maintained by hypoxia (Mohyeldin *et al*., 2010), and hypoxia increases stem cell numbers, as well as the expression of CD133 and a separate stem cell marker, SOX-2 (Bar *et al*., 2010). This corresponds with the invasive nature of glioma, as SOX-2 is involved in matrix-metalloproteinase-9 mediated invasion of surrounding brain tissue (Park *et al*., 2006), and stem cells are highly involved in invasion and treatment resistance (Yan *et al*., 2013).

Glioma stem cells are highly treatment refractory, with both chemotherapy and

radiotherapy having little effect on cancer stem cell survival (Sakariassen *et al*., 2007). A number of stem cell markers are associated with treatment resistance and understanding these resistance mechanisms may enable the development of more effective treatment options. The stem cell population is inherently radioresistant, and this is believed to be due to a preferential activation of the ATM/CHK1/CHK2 DNA damage response pathway following radiotherapy, rather than an induction of apoptosis (Bao *et al*., 2006; Rich, 2007). Another of these resistance mechanisms is the overexpression of the DNA damage repair protein MGMT, which has been reported to be driven by hypoxia-mediated CD133 expression (Liu, 2006; Pistollato *et al*., 2010).This results in resistance to the alkylating agents carmustine and temozolomide (Esteller *et al*., 2000), which are the gold standard treatments used in the majority of glioma patients.

1.3 Current Treatment of Glioma

The three main treatment options for glioma are surgery, radiotherapy and chemotherapy, most usually delivered in combination. Due to the delicate nature of the brain, glioma can cause severely life limiting side effects, such as seizures, vision problems and migraines, and these symptoms are treated as they emerge on an individual basis. The current standard of care for glioma is surgery, radiotherapy with concomitant and adjuvant temozolomide as seen in Figure 1.4. This has improved overall survival from 12.1 months to 14.6 months compared to patients who received radiotherapy only (Stupp *et al*., 2005).

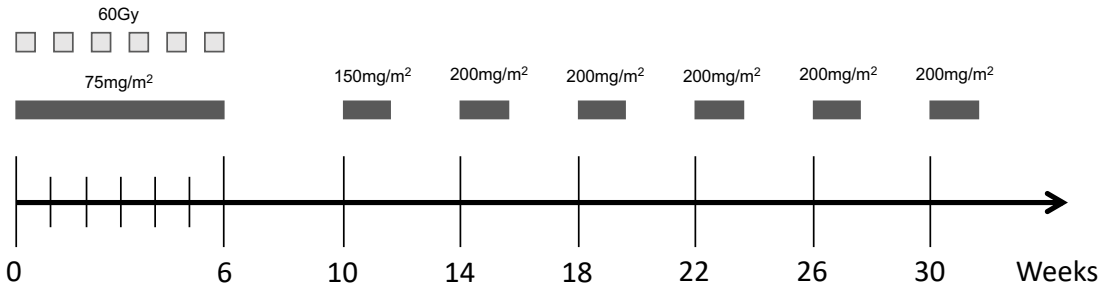

Figure 1.4: The standard of care for high-grade glioblastoma as suggested by the EORTC. 60Gy of hyperfractionated stereotactic radiotherapy (HFSRT) is given in 6 rounds of 10Gy in 2Gy fractions (light grey boxes) Concomitant temozolomide is given at a dose of 75mg/m^2 daily. Adjuvant temozolomide is given in 6 rounds of either 150 or 200mg/m^2 for 5 days every 4 weeks (dark grey boxes). Adapted from (Omuro *et al*., 2014; Stupp *et al*., 2005, 2007, 2009, 2010).

1.3.1 Surgery

Surgery is used only when appropriate and safe to do so, but still remains the first course of action for every suitable glioma patient. Follow-up treatment of radiotherapy and chemotherapy can be used to destroy residual cancer cells, which have the potential to reform a tumour. Conversely, chemotherapy and radiotherapy can be used before surgery to reduce tumour mass (Reed, 2009). This is not always a valid treatment option, for example in brain stem gliomas located deep within the brain or diffuse tumours such as diffuse intrinsic pontine glioma (DIPG).

One of the main limiting factors of surgery is the location of the tumour mass. Glioma is predominantly found in the eloquent cortexes of the brain, and surgeons will err on the side of caution when debulking the tumour mass, as damaging these areas could massively affect a persons motor control and speech (Vives and Piepmeier, 1999). However, resection is often needed in these areas, as the tumour exerts a mass effect, which can affect the quality of life of a patient (Mikuni and Miyamoto, 2010).

The sensitive areas within which glioma develops, and the invasive nature of glioma makes the tumour margins difficult to determine and fully resect. Glioma has a high affinity for myelinated tracts, and is able to cross the corpus callosum to invade the contralateral hemisphere using these tracts (Giese *et al*., 2003). Glioma is so invasive that even extreme surgical procedures such as radical hemispherectomy have not been curative (Dandy, 1928). Surgery has been improved by the use of 5-aminolevulinic (5-ALA), a fluorescent dye is metabolised by the haem pathway. As glioblastoma has altered expression and activity of haem pathway enzymes that increase the conversion of 5-ALA to the fluorescent protoporphyrin IX, 5-ALA accumulates in glioblastoma more so than normal brain tissue (Colditz *et al*., 2012). Use of 5-ALA has significantly increases the extent of surgical resection and the time to tumour progression compared to non-fluorescent guided surgery (Eljamel, 2015; Ishizuka *et al*., 2011)

Peripheral, established ‘invader’ glioma cells have the ability to regrow and reform the tumour mass, this is invariably a terminal, treatment refractory cancer (Sneed *et al*., 1994). This recurrence typically occurs within 7-9 months, and in over 90% of cases this recurrence is located within 2cm of the tumour margins (De Bonis *et al*., 2013). This study also showed that following extended resection of the tumour mass, recurrence was

seen in over 65% of cases, and following a basic resection, recurrence was seen in over 85% of cases of high grade glioma and glioblastoma multiforme (De Bonis *et al*., 2013). Interestingly, recurrence distant from the initial tumour site has significant genomic divergence from the initial tumour. This genomic divergence is not seen to the same extent in local recurrence (Kim *et al*., 2015).

In low-grade glioma, where patients have a significantly improved prognosis, patients whose cancer is less than 70% resected will see a significantly lower 5-year survival rate (41%) compared to patients who had greater-than 70% tumour resection (84%) (Ius *et al*., 2012). However, this surgery can delay malignant progression and reduce the risk of anaplastic transformation (Keles *et al*., 2006). This highlights the need for maximal resection in glioma. However, In high-grade glioma, there is some controversy regarding the efficacy of surgery as a treatment option. It is accepted that tumour debulking can increase survival rates (Pang *et al*., 2007), but it is controversial as whether aggressive debulking is an appropriate treatment option (Mitchell *et al*., 2005). However, removing the tumour mass can increase the efficacy of chemotherapy (Ng *et al*., 2007) and this itself may be a valid reason for surgery.

1.3.2 Radiotherapy

Radiotherapy is used in almost every glioma patient when safe to do so, and radiotherapy following surgery is the current standard of care and has been since the 1970s. This is almost always external beam radiation from an X-ray source which is given in 1.8-2Gy increments up to 60Gy (Weller, 2011). However, there is increasing interest in the use of stereotactic radiotherapy, which provides very high doses of radiation to a very specific area of the brain in fewer exposures (Baskar *et al*., 2012; Fogh *et al*., 2010).

Intensity-modulated radiation therapy (IMRT) has been available since the late 1990s. IMRT is a newer form of external beam radiotherapy that uses extremely precise X-rays to deliver radiation to the tumour. This has been shown to spare critical structures such as the brain stem from being unduly exposed to ionising radiation, while preventing the dose reaching the target from being lowered (Hermanto *et al*., 2007). However, studies suggest that there is no significant improvement in survival when IMRT is used to treat high-grade glioma, and that the costly nature of IMRT may not merit its usage in all cases

(Fuller *et al*., 2007).

Proton beam therapy is an emerging treatment option for glioma but is more commonly used to treat paediatric neurological malignancies. Proton beam therapy deposits high-energy protons to a highly localised area (Loeffler and Durante, 2013). If this area includes the area glioma is likely to invade, high-grade glioma can be contained by ionising radiation with follow up proton beam therapy (Mizumoto *et al*., 2015). However, in the United Kingdom, proton beam therapy is not routinely available for the treatment of glioma (As of 09/19). Proton beam therapy is reserved for small tumours with well-defined margins, such as; ependymoma, base of skull chondrosarcoma and base of skull and spinal chordoma (Brada *et al*., 2007; Crellin, 2018)

Proton beam therapy has also been shown to target glioma stem cells *in vitro*, generating high levels of oxidative stress, which causes irreversible DNA damage (Mitteer *et al*., 2015). However, proton beam therapy has also been shown to increase invasion of glioma cells *in vitro*, likely through SOX-2 mediated MMP-9 (Matrix metalloproteinase) upregulation (Park *et al*., 2006; Zaboronok *et al*., 2014). This is not unique to proton beam therapy as external beam X-irradiation has also been shown to increase glioma invasion through MMP-9 (Park *et al*., 2006).

1.3.2.1 Radiobiology

External beam radiotherapy is a treatment that uses a form of ionising radiation, such as X-rays to damage cells. X-rays are bundles of photons, between 0.1 and 10 nanometres in wavelength, which are absorbed by water within tissue, and it is through this absorption that the X-rays mediate damage. The majority of this damage is indirect DNA damage caused by the radiation absorbed by tissue interacting with water molecules. Ionisation of water molecules by the Compton Effect occurs in tissue where the radiation is absorbed. This is the process by which photons interact with a comparatively low energy or ‘free’ electron. The photon is then diverted and loses a significant portion of its energy, and the free electron becomes a fast-moving electron, which has the ability to generate free radicals by ionising other molecules, this is a form of indirect damage, and cleaving bonds in vital molecules, which is a form of direct damage (Dunne-Daly, 1999; Hall, 2000). This process is illustrated in Figure 1.5.

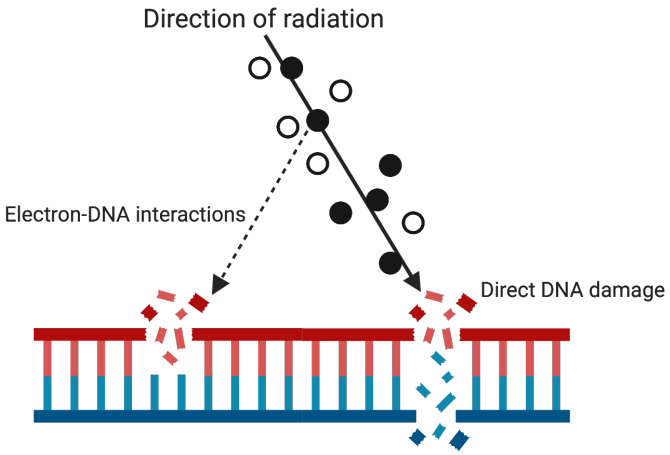

Figure 1.5: A simplified schematic of how radiation exerts damage on a strand of DNA. Radiation ionises intracellular molecules, particularly oxygen or water molecules, which results in free, fast moving electrons, which can damage DNA.

The Compton Effect tends to generate high or low energy electrons, which have different energy transfer values. About a third of these electrons are high energy, and as such feature a high linear energy transfer (LET) value, which means that the electrons travel for a further distance through the cell. These electrons tend to directly ionise DNA, and this form of damage can be difficult for the cell to repair as these electrons cause highly localised ionisation. Lower energy Compton electrons make up the remaining two thirds of the electrons generated by irradiation. These electrons generate more damage as they have a low LET, and ionise only sparsely on their path, which creates a high level of ionization throughout the cell. This is how the majority of free radicals are generated (Hall and Giaccia, 2012; Niemantsverdriet *et al*., 2012)

The highly reactive hydroxyl (OH^-) radical is the most toxic to DNA, as it scavenges hydrogen from the base thymine, and reacts with the double bonds of the bases and the deoxyribose that forms the backbone of the DNA helix (Cooke *et al*., 2003). This can result in both single and double stranded breaks in DNA. Following a standard single dose of 1-2Gy of radiation, there can be up to 1,000 single strand breaks, 40 double stranded breaks and many locally damaged sites in the DNA of an individual cell (McMillan *et al*., 2001; Vignard *et al*., 2013). These DNA breaks induce a DNA damage response preceding DNA replication during the cell cycle. Involving DNA damage repair proteins such as ATM, MGMT and BRCA (Jackson and Bartek, 2009). ATM-mediates

phosphorylation of p53 in response to irradiation causing arrest at the G_1, S and G_2 phases of the cell cycle, prior to the mitotic phase (Banin, 1998; Saito *et al*., 2002). At these checkpoints the cell attempts to repair the radiation induced damage. Single-stranded breaks can often be repaired, however DNA double stranded breaks are more problematic to repair, due to the lack of an intact template strand, which often to leads to the cell inducing p53 mediated apoptosis (Nelson and Kastan, 1994)

However, in cancer cells that have dysfunctional cell cycle checkpoints, aberrant cell cycle arrest takes place following irradiation leads to a form of cell death known as mitotic catastrophe. These cells enter a brief G_2 arrest, and prematurely enter mitosis, even though there is significant unrepaired damage to DNA (Vakifahmetoglu *et al*., 2008). Following mitosis, the cells will fail to divide, and re-enter G_1 phase with a tetraploid DNA level (Weaver and Cleveland, 2005). This results in large, multinucleated cells, which survive for several days, but eventually die through delayed apoptosis, necrosis or senescence (Eriksson and Stigbrand, 2010).

1.3.3 Chemotherapy

There are a large number of chemical agents that are designed specifically to target and kill cancer cells. These chemotherapeutic drugs target rapidly dividing cells, which provides the therapeutic differential for the majority of anti-cancer cytotoxic, as cancer cells divide at an accelerated rate compared to normal tissue.

There are many different classes of anti-cancer compounds, each with different mechanisms of action, including the DNA-damaging alkylating agents, the spindle poisoning taxols, and the growth-arresting anti-metabolites (McKnight, 2003). These drugs are almost always given in combination to increase their efficacy, which can enable a lower dose of each drug being prescribed reducing the total side effect profile and reducing the risk of resistance developing.

There is no established chemotherapy regime for glioma, but a regime comprising of procarbazine, lomustine and vincristine (PCV) being adopted, however this was never widely adopted as the gold standard therapy (Kappelle *et al*., 2001). Before the widespread usage of temozolomide, PCV therapy was used as a front-line treatment option, with temozolomide only being introduced following failure of that regime (Brandes

et al., 2001). This PCV therapy was shown to have an advantage over carmustine therapy (Newton *et al*., 1993). However, carmustine has been re-introduced to the clinic following development of local delivery systems (Perry *et al*., 2007).

1.3.3.1 Temozolomide

Temozolomide is the first line treatment for glioma, which has the added benefit of efficacy against the typically treatment refractory cancer stem cell population (Beier *et al*., 2008), and has significantly improved survival rates since its introduction (Perry *et al*., 2012). Temozolomide is an alkylating agent, and preferentially alkylates the N^7 or O^6 position of the base guanine, as well as the O^3 position of adenine (Friedman *et al*.). Methylation of these bases causes DNA aggregation, which may contribute to the cytotoxicity of temozolomide, as it does with other alkylating agents, but the main cytotoxic effects of temozolomide are believed to be caused by a failure of the DNA mismatch repair mechanism to find an appropriate complementary base for the methylated guanine.

During these mismatch repair attempts, methylated guanine can be paired incorrectly with thymine, which forces a re-entry of the cell into the mismatch repair system. This induces double stranded breaks (Sarkaria *et al*., 2008). These nicks in the DNA induce cell cycle arrest at the G_2/M stage (Barciszewska *et al*., 2015; D'Atri *et al*., 1998; Friedman *et al*.; Li, 2008). Following prolonged cell cycle arrest, and failure to repair the damaged DNA, the cell will then induce p53-mediated apoptosis (Hirose *et al*., 2001; Roos *et al*., 2007). This suggested mechanism is shown in Figure 1.6. Due to the need for a competent mismatch repair pathway, Deficiency in mismatch repair has been shown to contribute to temozolomide resistance (von Bueren *et al*., 2012; Cahill *et al*., 2007; Hunter *et al*., 2006).

The *MSH6* gene encodes the Guanine/Thymine binding protein, and is one of the mediators of mismatch repair, and mutations or hypermethylation of this gene has been shown to be a temozolomide resistance factor (Hunter *et al*., 2006; Xie *et al*., 2016). There is some evidence that the recurrence of treatment resistant glioblastoma is through clonal expansion of temozolomide treated cells, particularly through mismatch repair deficient cells (Hunter *et al*., 2006).

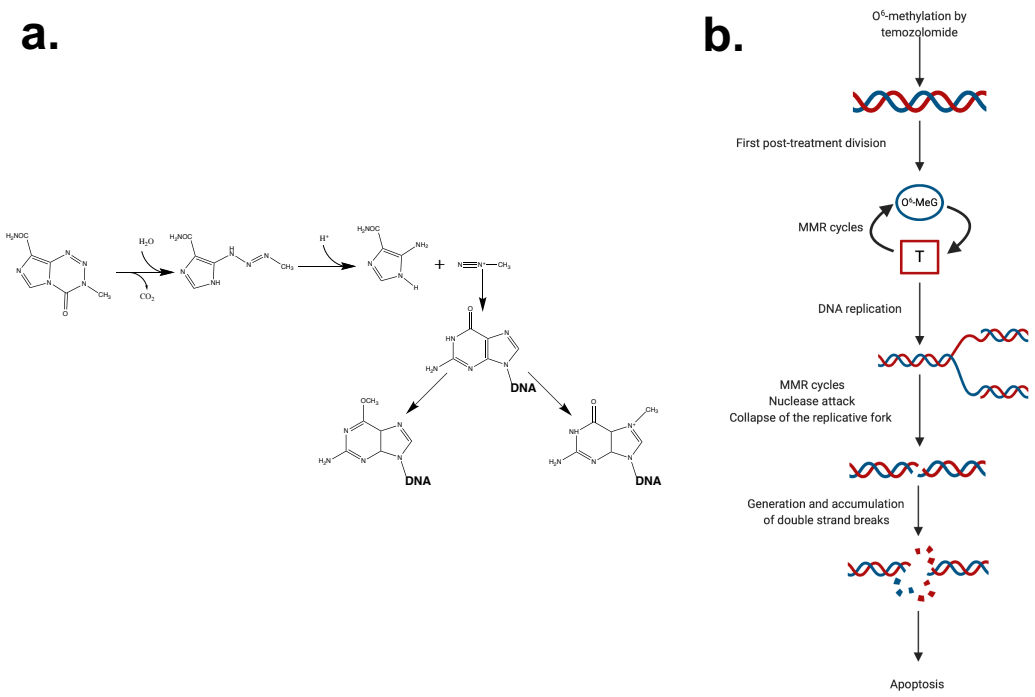

Figure 1.6: The suggested mechanism of action of temozolomide. **a.** the metabolism of temozolomide and subsequent O^6-methylation of guanine. **b.** the cellular response to temozolomide mediated damage. Mismatch repair attempts to incorrectly pair the O^6-methylated guanine (O^6-MeG) with the base thymine. This results in failure to successfully replicate DNA, leading to genomic stress and the induction of apoptosis inducing double strand breaks (Hirose *et al*., 2001; Roos *et al*., 2007)

It has been shown that in recurrent glioblastoma there is a significant loss of mismatch repair proficient cells, this indicates that first line treatment with temozolomide is positively selecting sensitive cells, and may lead to the recurrent tumour being treatment refractory (Felsberg *et al*., 2011)

One of the drawbacks of alkylating chemotherapy agents such as temozolomide is the induction of a DNA hypermethylation phenotype (Hunter *et al*., 2006; Kim *et al*., 2015). Increased mutagenicity following temozolomide treatment has been observed (Bodell *et al*., 2003), as well as increased silencing of *MSH6*, conferring increased chemoresistance. This is seen in approximately 25% of temozolomide treated patients (Hunter *et al*., 2006; Johannessen and Bjerkvig, 2012).

As well as mismatch repair deficiency, MGMT expression confers resistance to temozolomide in glioma, where MGMT status is used clinically to determine response of a patient to temozolomide therapy (Hermisson *et al*., 2006; Paz and Yaya-Tur, 2004). However in glioma, the MGMT promoter can be epigenetically silenced as discussed in Section 1.2.2.1, resulting in no expression of the protein, which results in a temozolomide sensitive tumour (Cabrini *et al*., 2015; Hegi *et al*., 2004). This translates to the clinic, where trials have shown that MGMT promoter methylation correlates to treatment efficacy (Hegi *et al*., 2005).

Due to MGMT mediated temozolomide resistance, there has been interest in developing an inhibitor of MGMT, and O^6-benzylguanine has been used clinically to increase the efficacy of temozolomide. However, in clinical trials O^6-benzylguanine was found to lower the levels of MGMT systemically, which resulted in a need for the dose of temozolomide to be lowered (Koch *et al*., 2007), which reduced response to temozolomide. A further separate clinical trial however demonstrated that there was no increase in sensitivity to temozolomide in resistant gliomas following administration of O^6-benzylguanine (Quinn *et al*., 2009). Before the introduction of temozolomide, O^6-benzylguanine was used in conjunction with the alkylating agent carmustine. This resulted in increased cytotoxicity of carmustine (Dolan *et al*., 1991).

Despite the prevalence of MGMT mediated chemoresistance, one of the major benefits of temozolomide is that it also can act as a radiosensitiser; significantly increasing the efficacy of radiotherapy, an effect which has been substantiated in the clinic as well as in *in vitro* studies (Grossman *et al*., 2010). It is believed that this increased cytotoxicity is caused by an increase in double strand breaks, or a failure in effective double strand break repair, which in turn causes an increase in the number of cells undergoing mitotic catastrophe (Kil *et al*., 2008). temozolomide is therefore given concomitantly and as an adjuvant to radiation as seen in Figure 1.4. This regime has significantly increased overall survival in glioblastoma patients (Stupp *et al*., 2005, 2007, 2009, 2010).

There is contradictory evidence as to whether MGMT status affects radiosensitisation, as different groups have published opposing result from studies using temozolomide as a radiosensitiser. One report demonstrated radiosensitising effects only in an orthotropic tumour model in mice when the MGMT gene was epigenetically silenced (Carlson *et al*., 2009). Others suggest that MGMT is not a dependent factor for radiosensitisation

(Bobola *et al*., 2010; van Nifterik *et al*., 2007). However, neither of the studies demonstrating that radiosensitisation is not dependent on MGMT used an *in vivo* model, which may limit their validity.

1.3.3.2 Carmustine

One of the treatment options for glioma utilised following surgical resection, is the local delivery of intracranial carmustine wafers (Perry *et al*., 2007). Similarly to temozolomide, the alkylating agent carmustine has been used as a front line glioma treatment (Engelhard, 2000).

Carmustine, also known as bis-chloroethylnitrosourea (BCNU), is an alkylating agent, which interferes with DNA repair and synthesis by forming inter-strand links on the DNA chain. Chloroethyl adducts at the O^6 position of guanine are formed, similarly to the mode of action of temozolomide. A chloride ion on the opposing DNA strand is displaced, and the combination of this chloroethylation and chlorine displacement causes the formation of an ethyl bridge across the DNA strand (Bota *et al*., 2007). This will prevent the DNA strands from unravelling which inhibits DNA replication, inducing apoptosis (Dronkert and Kanaar, 2001).

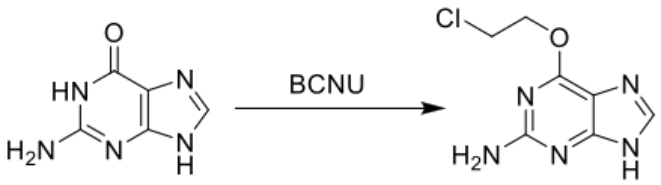

Figure 1.7: The chloroethylation of the O^6 position of the base guanine by BCNU (carmustine) this results in ethyl bridges being formed between DNA strands, preventing DNA helicase from unravelling the DNA helix, and apoptosis will be induced.

Carmustine mediated apoptosis occurs due to a collapse of the replicative fork, which causes double stranded breaks, resulting in a G_2/M cell cycle arrest (Roos and Kaina, 2006). Chloroethylating compounds such as carmustine are significantly more toxic to p53-mutated cells which have limited cell cycle arrest capability, meaning that there can be no repair of the double stranded breaks caused by the intrastrand links (Batista *et al*., 2007). Similarly to temozolomide, resistance to carmustine is mediated by MGMT (Friedman *et al*., 1998), and operates in an identical way, with MGMT removing the

chloroethyl adducts from the O^6-position of guanine (Esteller *et al*., 2000). As a result, silencing of the MGMT gene results in enhanced efficacy of carmustine, and inhibitors such as O^6-benzylguanine can be used to artificially deplete MGMT (Wedge and Newlands, 1996).

An attractive treatment option has been combining temozolomide and carmustine. This combination has been reported to be safe and efficacious (Barrié *et al*., 2005), and with increased use of carmustine implants, this combination was suggested to become the new first line treatment for glioma (McGirt and Brem, 2010). This has not been realised, and implant of carmustine wafers still occurs on a patient to patient basis (Bregy *et al*., 2013). The use of carmustine is predicated on careful selection of patient groups due to outcome depending on genes such as *TP53* and *MGMT* influencing treatment outcome (Batista *et al*., 2007; Hegi *et al*., 2005; Hirose *et al*., 2001).

1.3.3.3 Bevacizumab

As discussed in section 1.2.2.5, tumour vascularisation and sustained angiogenesis is a prominent feature of glioma. Over expression of vascular endothelial growth factor (VEGF) is associated with an increase in angiogenesis as well as increasing vascular permeability of the blood brain barrier. There is a level of cause and effect that exists in glioma regarding angiogenesis. In response to hypoxia and the production of HIF-1, large quantities of VEGF are produced, this leads to increased tumour vascularisation, as well as an increase in tumour growth (Jensen *et al*., 2006). However, as the tumour grows, the hypoxic fraction of the tumour will also increase in size, leading to further VEGF synthesis and action. In typical cancers, this increased vascularisation and vascular permeability is associated with metastasis, however, the production of VEGF in glioma is associated with growth and invasion through CXCR4 (C-X-C chemokine receptor type 4) signalling (Hong *et al*., 2006; Zagzag *et al*., 2006).

Vascular endothelial growth factor is viewed as the most potent mediator of angiogenesis in glioma, there are several strategies that have been deployed to target and inhibit VEGF. These include; VEGF-receptor inhibitors, VEGF trapping, inhibition of VEGF downstream signalling using multiple tyrosine kinase inhibitors (mTKIs) and direct inhibition of VEGF (Weathers and De Groot, 2015). Bevacizumab is a humanized monoclonal antibody that is targeted against vascular endothelial growth factor (VEGF),

and was the first anti-VEGF therapy to be approved by the European medical association (EMA) in 2005 for the treatment of breast, colorectal and lung cancers. In America, the FDA approved the use of bevacizumab for the treatment of glioblastoma multiforme in 2009 (Cohen *et al*., 2009) but has not been approved in Europe as of yet (08/2019).

However, Bevacizumab has not been reported to improve overall survival when combined with temozolomide and radiotherapy, but has shown an increased progression free survival in high grade glioma, albeit with a higher incidence of adverse events (Chinot *et al*., 2014; Gilbert *et al*., 2014). Interestingly, meta-analysis of 15 clinical trials has shown no dose escalating effect on survival benefit between administered doses of 5, 10 & 15 mg/kg of bevacizumab (Wong *et al*., 2011), potentially indicating that bevacizumab has a threshold effect on glioblastoma, and increasing concentration offers no significant survival benefit. It has also been shown that following bevacizumab treatment it is common to see a non-enhancing pattern on contrast-weighted MRI (Iwamoto *et al*., 2009; Norden *et al*., 2008), which is usually indicative of a lack of tumour invasion, a low grade cancer or, most likely, a decrease in tumour vascularisation (White *et al*., 2007). This decrease or lack of tumour enhancement has been seen using other anti-VEGF therapies (Batchelor *et al*., 2007), indicating that a decrease in enhancement may be due to a decrease in angiogenesis and vascularisation.

1.4 Repurposing of drugs for glioma

Due to a failure in the current treatment and the traditional drug discovery process, repurposing drugs for cancer is becoming an increasingly attractive prospect. The low output, time intensive drug discovery process is highly cost-inefficient and leads to very few pipeline compounds reaching clinical trials, and even fewer reaching the clinic setting (Moreno and Pearson, 2013; Neidle, 2011; Rishton, 2005; Slater, 2001; Waring *et al*., 2015).

Due to a lack of novel compounds reaching the clinic, there has been an influx of existing drugs that are being used in novel ways to increase the effect of existing therapies. In high-grade gliomas, this has been seen with the anti-malarial dihydroartemisinin and the anti-epileptic valproic acid, which have both been shown to increase the efficacy of temozolomide therapy (Chen *et al*., 2011; Huang *et al*., 2008). Existing compounds, including the alcohol-aversion compound disulfiram and the diabetes medication

metformin have also been demonstrated to target the treatment refractory cancer stem cell population (Hothi *et al*., 2012; Würth *et al*., 2014).

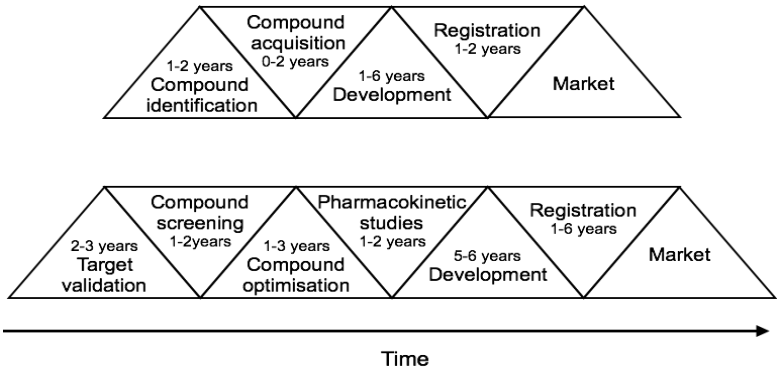

Figure 1.8: The differences in time and complexity between the drug repurposing process (top) and the *de novo* drug discovery process (bottom) (adapted from Ashburn and Thor, 2004).

1.4.1 Dimethyl fumarate

The thiol glutathione is the most common non-protein intracellular molecule and is found in virtually every cell, where it acts as a free radical and xenobiotic scavenger. Glutathione binds to potential toxins via its reactive sulfyhydryl moiety (Balendiran *et al*., 2004; Sies, 1999). Glutathione synthesis and recycling is accelerated in many cancers, conferring chemo- and radio-resistance by binding both reactive oxygen species and chemotherapeutic agents (Traverso *et al*., 2013). Expression of many of the enzymes related to glutathione metabolism are increased in glioma, and overexpression of these genes is correlated with poor response to treatment (Ali-Osman *et al*., 1997; Kogias *et al*., 2012; Townsend and Tew, 2003).

Dimethyl fumarate is used in the treatment of the autoimmune diseases multiple sclerosis and psoriasis, where it is has been demonstrated to reduce pro-inflammatory Th1 cytokine expression, and reduce the number of T-cells (Meissner *et al*., 2012). Fumaric acid derivatives such as dimethyl fumarate have also been shown to deplete intracellular glutathione (Schmidt and Dringen, 2010), the mechanism of which is shown in Figure 1.9. The depletion of intracellular glutathione is particularly important as glutathione is a free radical scavenger, and as discussed, the majority of the damage caused by clinical radiation can be attributed to free radicals (Bump *et al*., 1982; Sun *et*

al., 1998). Dimethyl fumarate has therefore been used as a radiosensitiser for hypoxic cells *in vitro*, which makes it a possible adjuvant to radiotherapy for glioma (Bump *et al*., 1982; Held *et al*., 1988). As a radiosensitiser, high concentrations of dimethyl fumarate were suggested to deplete intracellular glutathione levels, allowing for increased radiation induced reactive oxygen species levels which were able to interact with the DNA structure (Bump *et al*., 1982; Held and Hopcia, 1993; Held *et al*., 1988, 1991).

As well as acting as a potent radiosensitiser, dimethyl fumarate has been shown to be cytotoxic against glioma (Ghods *et al*., 2013). Furthermore, dimethyl fumarate has been demonstrated to prevent the expression and translocation of CD133 and NF-κB, which are both associated with poor patient outcome in glioma (Ghods *et al*., 2013; Kastrati *et al*., 2016). Inhibition of NF-κB is thought to occur due to direct interaction of dimethyl fumarate with p65 (Kastrati *et al*., 2016). p65 is necessary for nuclear translocation and transcription of NF-κB target genes (Pradère *et al*., 2016), and inhibition by dimethyl fumarate has been shown to decrease the ability of p65 to bind DNA and to reduce transcriptional activity by preventing nuclear translocation (Kastrati *et al*., 2016). This is likely to confer a therapeutic advantage in glioblastoma, where NF-κB signalling is frequently amplified due to EGFRvIII and AKT/PI3K signalling (An *et al*., 2018; Gray *et al*., 2014). NF-κB has been suggested to confer resistance to O^6-guanine alkylating agents such as temozolomide (Bredel *et al*., 2006) this likely occurs through an increase in anti-apoptotic signals such as Bcl-2 and p21 (Dolcet *et al*., 2005; Saile *et al*., 2001). In non-malignant cells, induction of the tumour suppressor gene p21 and cell cycle arrest by dimethyl fumarate has been reported (Valesky *et al*., 2016), and this may contribute to the growth inhibiting effects of dimethyl fumarate. This again should be of benefit in glioblastoma as p21 is known to inhibit apoptosis (Karimian *et al*., 2016) and p21 transfection has been shown to reduce tumorigenesis in *in vivo* models of glioblastoma (Hung *et al*., 2000; Wang *et al*., 2001). Temozolomide has been shown to induce senescence in a p21 dependent manner (Aasland *et al*., 2019), which was associated with repression of mismatch repair genes and increased temozolomide resistance (Aasland *et al*., 2019)

Dimethyl fumarate also has a number of indirect actions that make it attractive for glioma therapy. Glutathione depletion has been shown to increase the sensitivity of glioma cells to both temozolomide and cisplatin, which occurs through inhibition of glutathione binding and inactivation of the drugs (Rocha *et al*., 2014). The hypoxic associated

transcription factor, HIF-1α, is known to be a target that is inhibited by dimethyl fumarate (Koivunen *et al*., 2007; Zhao *et al*., 2014). Inhibition of HIF by dimethyl fumarate may translate to a decrease in hypoxia related genes such as *MDR1* (Comerford *et al*., 2002). which may help overcome the p-glycoprotein mediated chemoresistance associated with hypoxia (Wartenberg *et al*., 2003). It has also been hypothesized that inhibition of HIF by dimethyl fumarate may also decrease the tumorigenic capability of glioma stem cells (Bar *et al*., 2010; Li *et al*., 2009), and a decrease in breast cancer stemness has been shown using dimethyl fumarate (Kastrati *et al*., 2016).

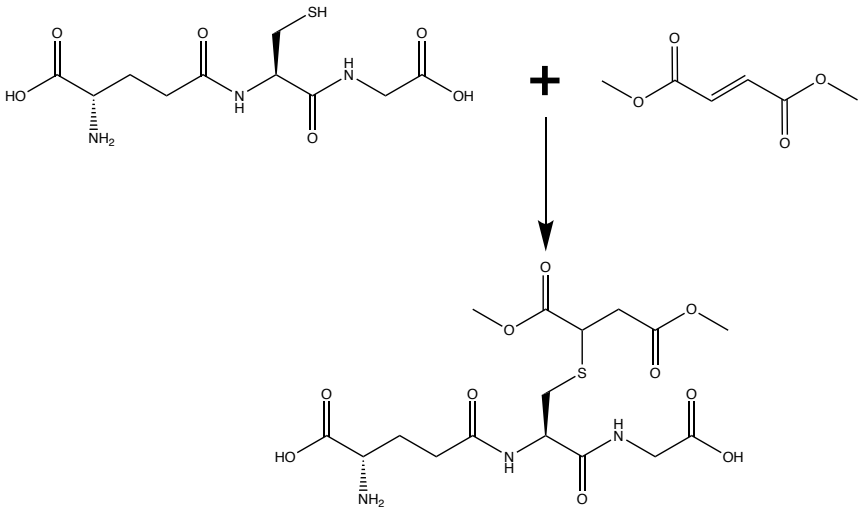

Figure 1.9: The inhibition of the sulfhydryl moiety of glutathione (left) by dimethyl fumarate (right) to form a thiosuccinic acid ester, dimethyl-2-(S-glutathionyl)-succinate (bottom). Glutathione conjugation to the electrophilic centre of dimethyl fumarate under normal cellular conditions would be further metabolised and detoxified by γ-glutamyltransferase, dipepdidase and cysteine-acetyltransferase leading to the final product, mercapturic acid derivatives (Schmidt *et al*., 2007).

1.4.1.1 NRF2

One of the suggested targets of dimethyl fumarate is the antioxidant transcription factor NRF2. Dimethyl fumarate is such a potent activator of NRF2 that it can be used as a biomarker for successful dimethyl fumarate treatment in relapsing-remitting multiple sclerosis (Hammer *et al*., 2018).

NRF2 is an essential anti-oxidant transcription factor, responsible for activation of over 15 target genes, including *IDH1*, glutathione-s-transferases (*GST)*, and haem-oxygenase 1 (*HMOX1*) (Kensler *et al*., 2007). In normal cells, NRF2 is bound to the regulatory protein KEAP-1, preventing continuous antioxidant gene transcription (Kansanen *et al*., 2013). Activation of NRF2 occurs through protein kinase-C mediated phosphorylation of the serine 40 residue of NRF2 which facilitates nuclear translocation (Chen *et al*., 2016; Huang *et al*., 2002; Jaiswal, 2004), although activation through different residue modification has also been reported (Bloom *et al*., 2002; He and Ma, 2009).

Structurally, KEAP-1 is cysteine rich, with 27 cysteine residues. Three of these residues, cysteines 151, 273 and 288, have a functional role by inducing a conformational change in Keap1 structure leading to the release and nuclear translocation of NRF2 (Kobayashi *et al*., 2006; Li *et al*., 2012a; Taguchi *et al*., 2011; Zhang, 2006). Release may instead occur through direct action of dimethyl fumarate with these cysteine residues. This has been shown by Brennan *et al*., (2015) with direct modifications of cysteine 151, 257 and 273 in response to dimethyl fumarate treatment (Brennan *et al*., 2015). All three of these cysteine residues have been shown to be amongst the most reactive residues in the KEAP-1 structure (Eggler *et al*., 2005; Kobayashi *et al*., 2006; Taguchi *et al*., 2011; Zhang, 2006).

As cancer cells have higher basal levels of oxidative stress (Pelicano *et al*., 2004), NRF2 is activated more frequently, or is constitutively active through KEAP-1 mutation (Hayes and McMahon, 2009) in some cancer cells. Due to the induction of the antioxidant response, NRF2 is known to be both chemo and radioprotective (Brennan *et al*., 2015; Hammer *et al*., 2018; Rocha *et al*., 2016; Saidu *et al*., 2017).

Dimethyl fumarate mediated activation of NRF2 has been shown to result in the constitutive transcription of antioxidant genes. This is detrimental to many treatment strategies such as radiotherapy (McDonald *et al*., 2010) and chemotherapy (Rocha *et al*., 2016; Sukumari-Ramesh *et al*., 2015), which generate reactive oxygen species as a key aspect of their mechanism of action. As a result, many anti-cancer therapies can also inadvertently upregulate NRF2, resulting in therapy resistance. Treatment-mediated NRF2 activation is a critical factor for cells surviving treatment-induced oxidative stress (Harvey *et al*., 2009). NRF2 is also associated with upregulation of HIF (Kim *et al*., 2011),

promoting the invasive phenotype of glioma, and maintaining the stem-cell population (Zhu *et al*., 2013). As a result of this, NRF2 expression strongly correlates to the grade of glioma, and is correlated with poor survival (Tsai *et al*., 2016).

1.5 Hypothesis

We hypothesis that dimethyl fumarate will deplete intracellular glutathione in human glioblastoma cells. When combined with temozolomide and external beam X-irradiation, we believe that dimethyl fumarate will allow for an increase in the anti-glioblastoma effects of these therapies. Our hypothesis states that an increase in the effects of both temozolomide and external beam X-irradiation will occur due to the depletion of glutathione by dimethyl fumarate. Depletion of glutathione will allow for higher intra-cellular concentrations of temozolomide or irradiation induced reactive oxygen stress, as well as allow for temozolomide to remain active within the cell for a sustained period of time. This will result in an increase in DNA damage, cell cycle arrest and subsequent induction of apoptosis compared to temozolomide or X-irradiation as a single agent. We aim to show that glutathione is a key chemoresistance factor in human glioblastoma cells, and that dimethyl fumarate mediated depletion of glutathione is a valid treatment modality for glioblastoma.

1.6 Aims and Objectives

This project aims to

- Determine combinations of temozolomide and dimethyl fumarate can exploit the distinctive changes seen in glioblastoma physiology, which will allow for greater anti-cancer activity while maintaining a low side effect profile.

- Show that the interaction between temozolomide and dimethyl fumarate increases cell kill, DNA damage, cell cycle arrest and subsequent induction of apoptosis compared to temozolomide as a single agent.

- Show that external beam X-irradiation interacts with the temozolomide-dimethyl fumarate combination in a synergistic manner.

- Investigate the use of the temozolomide-dimethyl fumarate combination and external beam X-irradiation in three-dimensional models of human glioblastoma.

- Investigate potential novel targets of dimethyl fumarate and how these novel targets influence temozolomide treatment.

Chapter 2:

Materials and Methods

2.1 Cell lines and routine cell maintenance

For the purpose of these studies two human glioblastoma cell lines were used. UVW human glioblastoma cells (Developed in house) (Mairs *et al.*, 2007) and T98g human glioblastoma cells (Sigma-Aldrich, UK) were cultured in MEM supplemented with 10% foetal bovine serum, 100μg/ml penicillin-streptomycin, 200mmol/L L-glutamine and 2μg/ml Fungizone. T98g cells were maintained with additional 1% (v/v) sodium pyruvate and 1% (v/v) non-essential amino acids (all Gibco, UK). Cells were incubated at 37°C in a 5% CO_2 environment.

Cells were sub-cultured as required 1-3 times per week when ~80% confluency had been reached. 80% confluent cells were washed in PBS to remove traces of serum and detached from the flask by addition of 0.05% (v/v) trypsin-ethylenediaminetetracetic acid (Gibco, UK). The cell suspension was neutralised by inactivation of trypsin in complete media and, if needed, disaggregated to a single cell suspension by passage through a 21-gauge needle. The cell suspension was then distributed between 75cm^2 flasks (ThermoFisher, UK), each containing 20ml of media.

2.2 Drug preparation and treatment

Temozolomide and dimethyl fumarate (Sigma-Aldrich, UK) were dissolved in 100% DMSO (Sigma-Aldrich, UK) to give a master stock, and stored at -20°C and freeze-thaw cycles avoided. Working stocks of each drug were prepared from each master stock and aliquoted to reduce freeze-thaw cycles and prevent contamination of the master stock. Working stocks were aliquoted and stored at -20°C and were discarded after each freeze-thaw cycle.

For drug treatment studies, UVW or T98g human glioblastoma cell lines were seeded at 1.5x10^5 cells in 25cm^2 flasks (ThermoFisher, UK) and incubated at 37°C in a 5% CO_2 environment for 24-72 hours until exponential growth phase was reached. Media was

removed from cells and replaced with fresh media containing appropriate concentrations of temozolomide or dimethyl fumarate.

2.3 Treatment of cells with X-ray radiation

For radiation treatment studies, UVW or T98g human glioblastoma cell lines were seeded at $1.5x10^5$ cells in $25cm^2$ flasks and incubated at 37°C in a 5% CO_2 environment for 24-72 hours until exponential growth phase was reached. Media was removed from cells and replaced with fresh media prior to X-ray exposure. X-ray exposure was performed with a X-RAD225KV X-ray cell irradiation cabinet (Precision X-ray, USA). Doses between 0-6Gy were delivered at a dose rate of 2.2Gy/min.

2.4 Treatment of cells with combination therapies

For studies using combinations of drugs and radiation, UVW or T98g human glioblastoma cell lines were seeded at $1.5x10^5$ cells in $25cm^2$ flasks incubated at 37°C in a 5% CO_2 environment for 24-72 hours until exponential growth phase was reached. Media was removed from cells and replaced with fresh media containing temozolomide, dimethyl fumarate or, the combination of these drugs. Cells were incubated for 2 hours with drug before X-ray exposure as described in Section 2.3.

IC_{50} values were calculated using non-linear regression analysis of single agent curves using GraphPad prism 8 software (version 8.12, Graphpad Software inc, USA). The doses for each combination used were determined by calculating the ratio of the IC_{50} of each drug. This ratio was then used to construct a dosing schedule, with the IC_{50} of each drug being the highest concentration used, with subsequent doses being constructed with the same ratio.

2.5 Clonogenic assay

Clonogenic assays were performed on both UVW and T98g cell lines to measure the clonogenic capacity of individual cells, a proxy for cell survival, following exposure to drugs, radiation or a combination of both as described above (Franken *et al*., 2006).

UVW or T98g human glioblastoma cell lines were seeded at $1.5x10^5$ cells in $25cm^2$ flasks and incubated at 37°C in a 5% CO_2 environment for 24-72 hours until exponential growth phase was reached (~70% confluency). Cells were treated as described in Section 2.2-2.4 and then incubated for 24 hours. Following 24-hour exposure, media containing drug was removed and the cells washed in PBS and detached from the flask using 0.05% (v/v) trypsin-ethylenediaminetetraacetic acid. The cell suspension was neutralised in complete media and disaggregated to a single cell suspension by passage through a 21-gauge needle. Cells were then counted using a haemocytometer (Jencons, UK). 200 UVW cells or 300 T98g cells were then seeded in triplicate in 60mm petri dishes (ThermoFisher, UK) with 5ml of complete media and incubated for 8-14 days until colonies of more than 50 cells were visible to the eye.

After 8-14 days, cell media was removed and colonies were washed in PBS and fixed in 100% methanol (ThermoFisher, UK) for 10-20 minutes. Fixed colonies were then stained with 10% (V/V) Giemsa solution (VWR, Germany) and washed with water. Visible colonies were counted by eye. Survival fraction was calculated as:

$$\text{Survival Fraction} = \frac{(\text{Number of colonies}/\text{number of colonies seeded})}{(\text{Number of control colonies}/\text{number of colonies seeded})}$$

Data reported was an average of three independent experiments.

2.6 Combination Index Analysis

In order to determine if combinations as described in section 2.4, were supra-additive or synergistic, a mathematical modelling approach known as combination index (CI) analysis was performed using Calcusyn software (Biosoft, UK) (Chou, 2006, 2010; Chou and Talalay, 1984). The median effect equation (below) was used to characterise the behaviour of biological systems in terms of the proportion of a population affected by treatment, and was calculated individually for each drug used in combination and the combination itself:

$$F_a/F_u = (D/IC50)^m$$

Where F_a is the fraction of the population affected, F_u is the fraction of the population unaffected by the dose; *D. m* is a Hill-equation type co-efficient which signifies the sigmoidicity of the curve. The median effect equation was linearised by transforming each side of the equation to the log to give the median effect plot:

$$\log F_a/F_u = m\log(D) - m\log(IC50)$$

From this equation, the dose of constituent drugs and the combination required to produce a set amount of toxicity was determined using:

$$D = IC50(F_a/F_u)^{\frac{1}{m}}$$

The median effect plot gives the slope of each line, the *m* value, and the intercept of the dose effect axis and the median-effect axis, which allows for an accurate IC_{50} measurement to be taken. The linear regression co-efficient of the median effect plot for each drug or combination determines the suitability of the use of combination index analysis, as if the median effect plot of the constituent drugs is parallel, it is assumed that the modes of action of the constituent drugs are mutually exclusive and the effect of the combination can be described using:

$$CI = \frac{(D)_1}{(D_x)_1} + \frac{(D)_2}{(D_x)_2}$$

Where *D* is the dose of each constituent drug used in combination required to inhibit *x* percentage of cells, and D_x is the dose of each constituent drug required to inhibit *x* percentage of cells as a single agent and CI is the combination index, a value that describes the nature of the combination. A CI value of >1 indicates infra-additivity, a value of 1 indicates additivity and a CI value < 1 indicates supra-additivity.

2.7 Cell cycle analysis

Cell cycle analysis was performed to determine the distribution of UVW or T98g cells exposed to various single or combination treatments throughout the phases of the cell cycle (Darzynkiewicz *et al*., 2017).

UVW or T98g human glioblastoma cell lines were seeded at $1.5x10^5$ cells in $25cm^2$ flasks and incubated at 37°C in a 5% CO_2 environment for 24-72 hours until exponential growth phase was reached (~70% confluency). Cells were treated as described in Section 2.2-2.4 for 4 or 24 hours. Following exposure, drug containing media was removed and the cells washed in PBS and detached from the flask using 0.05% (V/V) trypsin-ethylenediaminetetraacetic acid. The cell suspension was pelleted by centrifugation at 1400 rpm for 5 minutes and fixed in 70% (V/V) ice-cold ethanol. Following fixation, pellets were washed by resuspension in PBS and centrifugation at 1400rpm for 5 minutes prior to removal of supernatant.

Fixed pellets were incubated with 50μg/ml bovine ribonuclease A (Sigma-Aldrich, UK) to degrade and prevent unwanted staining of intracellular RNA. DNA content was stained with 10μg/ml propidium iodide (Sigma-Aldrich, UK). Stained samples were incubated at 4°C for at least an hour in a light-free environment prior to analysis.

Flow cytometry analysis of samples was performed using the BD FACSCanto analyser (Becton Dickinson Systems, UK), with 10,000 events per sample measured. Flow cytometry data was analysed using BD FACSDiva, V6.13 software. Data reported was an average of three independent experiments.

2.8 γ-H2a.X detection

DNA damage and repair was quantified through detection of Ser139 phosphorylated H2a.X, a histone phosphorylated in response to DNA damage (Burma *et al*., 2001; Zhao *et al*., 2019).

UVW or T98g human glioblastoma cell lines were seeded at $1.5x10^5$ cells in $25cm^2$ flasks and incubated at 37°C in a 5% CO_2 environment for 24-72 hours until exponential growth phase was reached (~70% confluency). Cells were treated as described in Sections 2.2-2.4 and incubated for 4 or 24 hours. Following exposure, drug containing media was removed and the cells washed in PBS and detached from the flask using 0.05% (v/v) trypsin-ethylenediaminetetraacetic acid.

The cell suspension was pelleted by centrifugation at 1400rpm for 5 minutes prior to removal of supernatant. Pellets were washed twice in PBS and fixed in 4% (V/V)

paraformaldehyde (ThermoFisher, UK) for 20 minutes. Fixed pellets were washed by resuspension in PBS and centrifugation at 1400rpm for 5 minutes. Samples were washed twice to remove fixative. Pellets were resuspended in 2ml of PBS and counted using a haemocytometer. Pellets were then permeabilised by resuspension at a density of $2x10^6$ cells/ml in 0.3% (V/V) Triton-X (Sigma-Aldrich, UK).

50μl of each sample was resuspended in a wash buffer containing 0.1% Triton (Sigma-Aldrich, UK) and 0.5% BSA (Sigma-Aldrich, UK) before addition of 100μg/ml FITC-conjugated anti-phospho-histone H2a.X (Ser139) (Millipore, UK). Stained samples were incubated on ice for 20 minutes. Excess antibody was removed by resuspension of the pellet in wash buffer and centrifugation at 1400rpm for 5 minutes and removal of the supernatant.

Samples were resuspended in 150μl of FACs buffer (1% bovine serum albumin in PBS) and flow cytometric analysis of samples was performed using the BD FACSCanto analyser (Becton Dickinson Systems, UK), with 10,000 events per sample measured. Flow cytometry data was analysed using BD FACSDiva, V6.13 software. Data reported was an average of three independent experiments.

2.9 Western blot analysis

Protein expression in UVW and T98g human glioblastoma cell lines was investigated using Western blot analysis.

UVW or T98g human glioblastoma cell lines were seeded at $1.5x10^5$ cells in $25cm^2$ flasks and incubated at 37°C in a 5% CO_2 environment for 24-72 hours until exponential growth phase was reached (~70% confluency). Media was then removed and the cells washed in PBS. Cells were lysed in Laemmli's sample buffer (63mM Tris-HCl pH6.8, 2mM $Na_4P_2O_7$, 5mM EDTA, 10% glycerol, 2% SDS, 50mM DTT, 0.007% bromophenol blue) (all Sigma-Aldrich, UK).

SDS-Polyacrylamide Gel Electrophoresis was performed using resolving gels containing 0.1% SDS, 0.375M Tris base (pH8.8), 3% glycerol, distilled water and the appropriate amount of 30% acrylamide/bisacrylamide stock depending on the size of the protein of interest, 10% ammonium persulfate and 0.05% TEMED (all Sigma-Aldrich, UK). Whole

cell lysates were ran in a tris-glycine gel at 135 volts for 90 minutes. Proteins were then transferred to a nitrocellulose membrane (GE healthcare, UK) at 300 milliamps for 105 minutes under wet conditions.

The membrane was the blocked in 5% Marvel-Tween for 60 minutes at room temperature. The membrane was then incubated in mouse anti-MGMT primary antibody (Millipore, UK) diluted 1:3000 in tween tris-buffered saline (TTBS) containing 3% BSA for 24-hours at 4^{o}C.

The membrane was then washed 3 times in TTBS and incubated with anti-mouse secondary HRP-conjugated antibody (Millipore, UK) 90 minutes at room temperature. The membrane was then washed 3 times in TTBS and developed using ECL (1:1 mixture of solution 1 [1M Tris pH8.5, 250mM luminol, 250mM p-cymuric acid and water] and solution 2 [1M Tris pH8.5, 0.19% H_2O_2 and water]) system (all Sigma-Aldrich, UK).

2.10 Apoptosis detection

Detection of the expression of apoptotic markers on UVW and T98g human glioblastoma cell lines was detected using an anti-annexin V FITC conjugate and propidium iodide, with each stain identifying the cellular population at different stages of the apoptotic cell death pathway. Early apoptotic cells were characterised as having an intact membrane and stained positively for annexin V which associates with membrane bound phosphatidylserine moieties, late apoptotic cells, which have a compromised membrane, were annexin V & propidium iodide positive. Necrotic cells were singly positive for propidium iodide and had a severely compromised membrane (Genderen *et al*., 2006). Time points 24-72 hours post-treatment cessation were chosen in order for cells to arrest and induce apoptosis (Ochs and Kaina, 2000; Roos *et al*., 2004, 2007).

UVW or T98g human glioblastoma cell lines were seeded at 1.5x10^5 cells in 25cm^2 flasks and incubated at 37°C in a 5% CO_2 environment for 24-72 hours until exponential growth phase was reached (~70% confluency). Cells were treated as described in Section 2.2-2.4. Following 24 hours of treatment, cells were washed in PBS and 1.5ml of drug free media was added. Cells were incubated for a further 24, 48 or 72 hours, after which the cells were washed in PBS and disassociated using accutase solution (Sigma Aldrich, UK) to prevent cleavage of membrane bound phosphatidylserine moieties.

Cells were then pelleted by centrifugation at 1400rpm for 5 minutes, washed in PBS and resuspended at a concentration of $2x10^6$ cells/ml in annexin V staining buffer (0.1M Hepes/NaOH (pH 7.4), 1.4M NaCl, 25mM $CaCl_2$). 100μl of each sample was transferred to a FACs tube (BD bioscience, UK) and incubated for at least 15 minutes at room temperature with 5μl of annexin V stain, 5μl of propidium iodide or both (all BD bioscience, UK).

Immediately before flow cytometry was performed, 400μl of annexin V staining buffer was added to each sample. FACs analysis of samples was performed using the BD FACSCanto analyser (Becton Dickinson Systems, UK), with 10,000 events per sample measured. Flow cytometry data was analysed using BD FACSDiva, V6.13 software. Data reported was an average of three independent experiments.

2.11 Measurement of intracellular glutathione contents

In order to assess the effects of dimethyl fumarate on intracellular glutathione levels, the reduction of DTNB to TNB was measured spectrophotometrically to give a quantifiable level of glutathione (Brennan *et al.*, 2015).

UVW or T98g human glioblastoma cell lines were seeded at $1.5x10^5$ cells in $25cm^2$ flasks and incubated at 37°C in a 5% CO_2 environment for 24-72 hours until exponential growth phase was reached (~70% confluency). Cells were treated with increasing doses of dimethyl fumarate between 0.3 and 25μM, as described in Section 2.2 for 30 minutes, 2, 4, 6, or 24-hours.

Following the designated treatment time, drug containing media was removed and the cells washed in PBS and detached from the flask using 0.05% (v/v) trypsin-ethylenediaminetetraacetic acid. The cell suspension was pelleted by centrifugation at 1400rpm for 5 minutes. Pellets were washed twice in PBS before being resuspended in PBS at a density of 10^8 cells/ml. Cells were then centrifuged at 600g for 5 minutes and pellets were washed in 3 volumes of 5% sulfosalicylic acid (Sigma-Aldrich, UK) and resuspended. The suspension was deproteinated by freeze-thawing using liquid nitrogen and water bath at 37°C three times before being incubated for 5-minutes at 4°C and then centrifuged at 10,000g for 10-minutes.

10μl of each sample was added in duplicate to a 96-well plate (TPP, Switzerland) with 150μl of working mixture (glutathione reductase (6 units/ml), DTNB (1.5mg/ml) and assay buffer (100mM potassium phosphate buffer, pH 7.0, with 1mM EDTA)) (All Sigma-Aldrich, UK). The reaction was started by addition of 50μl of 0.16 mg/ml NADPH to each well and read at 412nm using a FlexStation 3 (Molecular Devices, UK). Data reported was an average of three independent experiments.

2.12 Measurement of intracellular reactive oxygen species levels

To assess the effects of temozolomide on intracellular reactive oxygen species levels, temozolomide treated cells were stained with the fluorescent stain 2′,7′-dichlorodihydrofluorescein diacetate (DCFDA). Oxidative stress was then measured by the oxidation of DCFDA to the fluorescent molecule 2′,7′-dichlorofluorescein. Increasing fluorescent signal is indicative of increased intracellular oxidative stress (Eruslanov and Kusmartsev, 2010). Two known ROS scavengers, *N*-acetylcysteine and 4-hydroxy-tempo (Sigma-Aldrich, UK) were used in conjunction with temozolomide to measure ablation of temozolomide induced reactive oxygen species.

UVW or T98g human glioblastoma cell lines were seeded at $1.5x10^5$ cells in $25cm^2$ flasks and incubated at 37°C in a 5% CO_2 environment for 24-72 hours until exponential growth phase was reached (~70% confluency). Cells were treated with either 1mM *N*-acetylcysteine or 1mM 4-hydroxy-tempo (tempol) (both Sigma-Aldrich, UK) for 2 hours before addition of increasing doses of temozolomide as described in Section 2.2. After 24 hours of treatment, drug containing media was removed, and the cells washed in PBS and detached from the flask using 0.05% (v/v) trypsin-ethylenediaminetetraacetic acid. The cell suspension was pelleted by centrifugation at 1400rpm for 5 minutes prior to removal of supernatant.

The pellet was washed twice in PBS before being stained in 100μl of 50μM DCFDA (Sigma-Aldrich, UK) for 30 minutes at 37°C. Excess stain was washed off by resuspension of the pellet in FACs buffer (1% BSA in PBS) and centrifugation at 1400rpm for 5 minutes prior to removal of supernatant. Samples were resuspended in 150μl of FACs buffer (1% BSA in PBS) and flow cytometric analysis of samples was performed using the BD FACSCanto analyser (Becton Dickinson Systems, UK), with 10,000 events per sample measured. Flow cytometry data was analysed using BD

FACSDiva, V6.13 software. Data reported was an average of three independent experiments.

2.13 Fast activated cell-based ELISA for pNRF2

To quantify the phosphorylation of the anti-oxidant transcription factor NRF2 in response to dimethyl fumarate treatment, fast activated cell-based ELISAs (FACE) assays (Egorina *et al*., 2006) were performed using an anti-phospho-NRF2 (Ser-40) antibody (Boveia and Schutz-Geschwender, 2015).

5,000 UVW or T98g cells were seeded in each well of a 96 well plate (TPP, Switzerland) and incubated at 37°C in a 5% CO_2 environment for 24-48 hours until exponential growth phase was reached (~70% confluency).

Cells were treated with increasing doses of dimethyl fumarate, CDDO-imidazolide (Tocris, UK) or ML385 (Sigma-Aldrich, UK) for between 30 minutes and 24-hours. Following treatment, cells were washed twice in PBS and fixed in 4% paraformaldehyde for 20 minutes. Post-fixation, cells were washed three times in wash buffer (0.1% Tween in PBS) and permeabilised for 20 minutes with 0.3% triton. Cells were then washed twice in wash buffer before being blocked for 30 minutes with blocking buffer (0.1% Tween, 1% w/v BSA, 22.5mg/ml glycine in PBS) to prevent non-specific antibody binding. 20μl of antibody (detailed in Table 2.1) was added to each well in staining buffer (1% BSA, 0.1% triton in PBS) and the plate was incubated at 4°C overnight.

Antibody	Dilution	Source
Anti-NRF2	1:100	Abcam, UK
Anti-pSer40 NRF2	1:150	Abcam, UK

Table 2.1: Primary antibodies and dilutions used for detection of NRF2 and pNRF2 (Abcam, UK).

Primary antibody was removed and cells were washed twice in wash buffer before addition of secondary antibodies (Table 2.2) for 1 hour at room temperature. Cells were then washed twice in wash buffer and counterstained with 1μg/ml DAPI (Sigma-Aldrich,

UK) for 5 minutes. Cells were then washed, and the plate was read immediately at 355, 488 and 647nm using a FlexStation 3 (Molecular Devices, UK).

Antibody	Dilution	Source
Anti-Mouse Alexa Fluor 647	1:1000	Abcam, UK
Anti-Rabbit Alexa Fluor 488	1:1000	Abcam, UK

Table 2.2: Secondary antibodies and dilutions used for detection of NRF2 and pNRF2 (Abcam, UK).

Data was reported as normalised to absolute cell number as measured by DAPI. Data reported was an average of three independent experiments.

2.14 RNA extraction

To validate the results of FACE assays, RT-qPCR was performed on RNA extracted from cells treated with dimethyl fumarate to detect transcription of downstream targets of NRF2. RNA extraction was performed using the Qiagen RNeasy Mini kit (Qiagen, UK).

UVW or T98g human glioblastoma cell lines were seeded at $1.5x10^5$ cells in $25cm^2$ flasks and incubated at 37°C in a 5% CO_2 environment for 24-72 hours until exponential growth phase was reached (~70% confluency). Cells were treated with increasing doses of dimethyl fumarate, ML385 (Sigma-Aldrich, UK) or CDDO-imidazolide (Tocris, UK) for 2, 4 or 24-hours.

Following treatment, media was removed and the cells washed in PBS and detached from the flask using 0.05% (v/v) trypsin-ethylenediaminetetraacetic acid. The cell suspension was pelleted by centrifugation at 1400rpm for 5 min. The pellet was then resuspended in RNAlater (Sigma-Aldrich, UK). Samples were kept at 4ºC until RNA extraction could be performed. RNA extraction was performed using the Qiagen RNeasy Mini kit (Qiagen, UK).

The RNAlater cell suspension was pelleted by centrifugation at 1400rpm for 5 min. RNAlater was removed and cells were lysed by the addition of 350μL RLT buffer

containing 1% v/v β-mecarptoethanol (Sigma-Aldrich, UK) and agitation using a 21-gauge needle. 350μl of 70% ethanol was added to each lysed sample. 700μl of each sample was added to a spin column before the tube was centrifuged at >8000g for 15 seconds. Flow through from the spin column was discarded before addition of RW1 buffer to the spin column.

Samples were then centrifuged at >8000g for 15 seconds before the flow through was then again discarded. 500μl RPE buffer was added to the spin column before centrifugation at >8000g for 15 seconds. 500μl RPE buffer was added to the spin column before 500μl RPE buffer was added to the spin column before centrifugation at >8000g for 2 minutes. RNA was collected by addition of 50μl RNAase free water to the spin column membrane before centrifugation at >8000g for 1 minute. Samples were stored at -20^{o}C until qPCR could be performed.

2.14.1 RNA quantification

Prior to RT-qPCR being performed, RNA was quantified using a BioTek Epoch spectrophotometer (BioTek Instruments, USA). 1.5μl of each sample was added to each well of a 6-well microplate immediately prior to reading. The microplate was read at 260 and 280nm, and the ratio of each wavelength was analysed using BioTek Gen5 software (BioTek Industries, USA). A ratio of 2±0.1 was taken to indicate high fidelity RNA (Dell'Anno *et al*., 1998). The Beer-Lambert law allowed RNA to be quantified from the light absorbed by the RNA sample, with an absorbance of 1 at 260nm correlating to 40μg/ml (Peirson and Butler, 2007).

2.15 RT-qPCR

In order to validate the results of the FACE assays, reverse transcription real time polymerase chain reactions (RT-qPCR) for downstream targets of NRF2 was performed using a QuantiTect SYBR Green RT-PCR kit (Qiagen UK). RNA was extracted as described in Section 2.14.

A reaction mixture containing 25μl of 2x master mix (Qiagen, UK), 0.25μl of 100mM forward primer, 0.25μl of 100mM reverse primer (Sigma-Aldrich, UK), 0.5μl reverse

transcriptase mix (Qiagen, UK) and 24.25μl of RNAase free water (Qiagen, UK) was prepared for each individual primer pair and kept on ice.

Gene	Primer pair (5'-3')
HMOX1	CAACAAAGTGCAAGATTCTG TGCATTCACATGGCATAAAG
NQO1	AGTATCCACAATAGCTGACG TTTGTGGGTCTGTAGAAATG
ACTB	GACGACATGGAGAAAATCTG ATGATCTGGGTCATCTTCTC

Table 2.3: Predesigned forward (top) and reverse (bottom) primers for each gene used in the reactions described (all Sigma Aldrich, UK) (Brennan *et al*., 2015).

25μl of reaction mix was added to each well before addition of 200ng of template RNA. RNA was quantified as described above. Reactions were carried out in a Step-one plus (Applied biosystems, UK) under the conditions seem in Table 2.4, with 40 cycles being performed.

Step	Time	Temperature (^{o}C)
Reverse transcription	30 minutes	50
Activation	15 minutes	95
Denaturation	15 seconds	94
Annealing	30 seconds	50-60
Extension	30 seconds	72

Table 2.4: Reaction conditions used in the Applied biosystems Step-one plus.

Data was reported using the $2^{-\Delta\Delta CT}$ method (Livak and Schmittgen, 2001; Schmittgen and Livak, 2008). Data reported was an average of three independent experiments.

2.16 Measurement of cellular nitrite production

Dimethyl fumarate has been shown to be able to modulate nitrite levels in a number of systems (Wilms *et al*., 2010). Griess assays were performed on supernatant from cells treated with increasing concentrations of dimethyl fumarate for 2, 4 or 24 hours to determine the level of intracellular nitrites (Hensley *et al*., 2003).

5,000 UVW or T98g cells were seeded in each well of a 96 well plate (TPP, Switzerland) and incubated at 37°C in a 5% CO_2 environment for 24-48 hours until exponential growth phase was reached (~70% confluency). Cells were treated with increasing doses of dimethyl fumarate or *S*-nitrosoglutathione for between 30 minutes and 24-hours before the supernatant was removed and stored at -20°C until the assay could be performed.

0.1% napthylethylenediamine in deionised water and 1% sulphanilamide in 5% phosphoric acid (all Sigma-Aldrich, UK) were mixed in a 1:1 ratio to give the reaction mixture. To quantify nitrites levels, 100mM standard solution was prepared by dissolving sodium nitrite (Sigma-Aldrich, UK) in deionised water. The stock solution was serially diluted 1:2 in culture media. 50μl of each sample and 50μl of each concentration of standard solution was added in duplicate to a 96 well plate before addition of 50μl of the reaction mixture.

Nitrites in the supernatant or the sodium nitrite standard reacted with sulphanilamide to form a diazonium salt. The diazonium salt reacted with napthylethylenediamine to form an azo dye that could be quantified spectrophotometrically. The plate was then read at 540nm using a FlexStation 3 (Molecular Devices, UK). Data reported was an average of three independent experiments.

2.17 Spheroid formation and treatment

Spheroid models were established in order to assess the effects of both single agents and combination treatments as described in Section 2.2-2.4 on three-dimensional models of glioblastoma (Nath and Devi, 2016). 300 UVW or T98g cells were seeded in each well of a round-bottomed ultra-low attachment 96-well plate (Corning, USA) in 200μl of media. Plates were incubated at 37°C in a 5% CO_2 environment for 48-72 hours until spheroids formed. Spheroids were treated with combinations as described in Section 2.4.

Media was removed from each well, with care taken not to disrupt the spheroid, and 200μl media containing drug was added to each well. Each treatment was repeated in sextuplicate. Following 24 hours of treatment, media was removed and spheroids were washed in PBS before addition of 200μl of fresh media.

Spheroids were imaged immediately before treatment and subsequently imaged every 3-4 days for a period of three weeks using an EVOS FL auto system (Life Technologies, UK).

2.17.1 Spheroid analysis

Spheroid images were analysed using FIJI software (Version 2.0) (Schindelin *et al*., 2012). Image analysis was performed blind. For each spheroid, two orthogonal diameters, dmax and dmin (μm), were measured using FIJI. Spheroid volume (V) was calculated as described by Jensen (Jensen *et al*., 2008) using the equation*:*

$$V = \frac{1}{2}(d_{max} \times (d_{min})^2)$$

Change in spheroid volume (V/V_0) was calculated by dividing the spheroid volume (V) at each time point by the initial spheroid volume (V_0). Data was reported as V/V_0, as an average of three independent experiments ± standard error of the mean.

2.17.2 Determination of growth delay, doubling time and area under the curve

Growth kinetics of UVW and T98g human glioblastoma multicellular tumour spheroids were quantified following the growth delay assays described above. Treatment induced growth delay was quantified by τx, the time required for an x-fold increase in spheroid volume (Boyd *et al*., 2002).

Change in spheroid volume (V/V_0) was logarithmically transformed and linear regression analysis of $Log(V/V_0)$ against time (t) was performed using Graphpad prism (version 8) to give the equation:

$$\log(V/V_0) = mt + c$$

Where m is the slope and c is the point at which the line intercepts the y-axis. These values were then used to calculate the growth delay (τ2) for each treatment using the equation:

$$\tau_2 = \frac{\log 2 - c}{m}$$

The doubling time (DT), was defined as the time required for a two-fold increase in spheroid volume within the exponential growth phase of the spheroid growth curve. DT was calculated for each treatment using the equation:

$$DT = \log \frac{2}{m}$$

The area under the curve was calculated for Log(V/V0) against time using trapezoidal approximation using Graphpad prism (version 8) to evaluate the overall change in spheroid volume following each treatment.

2.18 Statistical analysis

All data reported was an average of at least three independent experiments. All data was analysed and graphed using GraphPad prism 8 software (version 8.12, Graphpad Software inc, USA).

One-way analysis of variance with Bonferroni post-tests were employed to control for evaluation of the degree of significance in groups measuring a single variable. p-values of less than 0.05 were taken as statistically significant.

Combination treatments and experiments with multiple groups were analysed using a two-way ANOVA with Bonferroni post-testing to allow for multiple comparisons between combination groups with single agents and controls. p-values of less than 0.05 were taken as statistically significant.

Data that was not normally distributed was analysed using Kruskal-Wallis analysis with Dunn's post hoc testing for multiple comparisons. p-values of less than 0.05 were taken as statistically significant.

Chapter 3

The effects of temozolomide and dimethyl fumarate in combination on human glioblastoma cells

3.1 Introduction

Glutathione is the most common intracellular non-peptide molecule, functioning to maintain genomic integrity by binding potential DNA-damaging xenobiotics and neutralising oxidative stress through a highly reactive thiol group that is capable of donating H^+ ions (Dringen *et al*., 2000; Forman *et al*., 2009). These ions are responsible for the neutralisation of reactive oxygen species and the reduction of disulphide bonds within potentially xenobiotic molecules. This thiol moiety can also bind DNA damaging xenobiotics to maintain genomic integrity (Balendiran *et al*., 2004; Held and Hopcia, 1993). Via this function, glutathione has been shown to be chemoprotective by binding chemotherapeutic agents and therefore lowering the intracellular concentration of active drug.

Depletion of glutathione has been demonstrated to be chemosensitising in a number of glioma cell lines, but these studies have been performed using the glutathione-s-transferase inhibitor BSO (Allalunis-Turner *et al*., 1991; Rocha *et al*., 2014; Townsend and Tew, 2003). To our knowledge, there has only been one study published using dimethyl fumarate to chemosensitise cancer cells to temozolomide (Booth *et al.,* 2014) but with no mechanistic interrogation of how dimethyl fumarate elicited these effects. We believe that this is the first mechanistic investigation into dimethyl fumarate induced temozolomide chemosensitisation.

We hypothesis that dimethyl fumarate will potentiate the effects of temozolomide, and hypothesis the most likely mechanism is via inhibition of glutathione. We further hypothesise that this potentiation will occur via a bimodal mechanism; the inhibition will

allow for higher intra-cellular concentrations of temozolomide, as well as allow for temozolomide to remain active within the cell for a sustained period of time.

3.2 Aims

The aims of this study were:

- To characterise the response of UVW and T98g human glioblastoma cells to a novel combination of temozolomide and dimethyl fumarate

- To elucidate potential mechanisms of action and targets for the combination of temozolomide and dimethyl fumarate

3.3 Materials and Methods

3.3.1 Cell lines and routine cell maintenance

All routine maintenance of cell lines was performed as described in Section 2.1.

3.3.2 Cell treatment

Temozolomide and dimethyl fumarate were prepared as described and treatment was performed as described in Section 2.2. The combination of temozolomide and dimethyl fumarate used were calculated as described in Sections 2.4 and 3.4.5.1 and seen below in Table 3.1.

UVW	
Dimethyl fumarate (μM)	Temozolomide (μM)
0.3	0.5
1	1.6
3	5
6	10
9	15

T98g	
Dimethyl fumarate (μM)	Temozolomide (μM)
3.125	50
6.25	100
12.5	200
18.75	300
25	400

Table 3.1: The combinations of temozolomide and dimethyl fumarate used throughout Chapter 3.

3.3.3 Clonogenic assay

Clonogenic assays were performed as described in Section 2.5.

3.3.4 Combination index analysis

Combination index analysis was performed using Calcusyn software as described as in Section 2.6.

3.3.5 Cell cycle analysis

Cell cycle analysis was performed as described in Section 2.7.

3.3.6 γ-H2Aa.X assays

γ-H2Aa.X assays were performed as described in Section 2.8.

3.3.7 Western blotting for MGMT

Western blotting was performed using an anti-MGMT mouse antibody (Millipore, UK) diluted at 1:3000 in TTBS as described in Section 2.9.

3.3.8 Apoptosis detection through annexin-V staining

Annexin V staining and detection was performed as described in Section 2.10.

3.4 Results

3.4.1 Design of the temozolomide-dimethyl fumarate combination based on single agent curves

When designing a drug-drug combination, a number of factors were required to be taken into consideration, such as the shape of each individual curve, the mechanism of action for each drug and how each drug would interact with any other drug in combination on a pharmacokinetic and pharmacodynamic level (Chou, 2006; Straetemans *et al*., 2005). In this study, each combination was designed to cover as broad a concentration range as possible for each drug, and also to take into account the unique shape of each curve. These factors were identified through the use of cell survival data derived from single agent clonogenic assays and literature searches to examine known or likely pharmacokinetic or pharmacodynamic issues arising from administering both temozolomide and dimethyl fumarate.

3.4.1.1 Cytotoxic effects of temozolomide treatment on UVW and T98g human glioblastoma cells

Figure 3.1 shows the response of UVW and T98g human glioblastoma cells to incubation with increasing concentrations of the alkylating agent temozolomide, as measured by assessing the clonogenic capacity of temozolomide treated cells.

As seen in Figure 3.1a, UVW cells were highly sensitive to the cytotoxic effects of temozolomide, showing statistically significant cytotoxicity following incubation with 5μM (p-value <0.05), relative to an untreated control, corresponding to approximately 25±9.11% cell kill. Temozolomide mediated cytotoxicity increased in a concentration-dependent manner, with 50% cell kill achieved after incubation with 15μM. At a concentration of 50μM, over 98±0.34% cell kill was achieved. Beyond this concentration 100% cell kill was achieved.

In contrast to the UVW cell line, T98g human glioblastoma cells were highly resistant to temozolomide, as demonstrated in Figure 3.1a. Incubation with 50μM of temozolomide resulted in 7±1.70% cell kill compared to UVW cells, where over 98% cell kill was achieved at this concentration. Significant cytotoxicity was induced from incubation with 200μM of temozolomide relative to an untreated control (p-value <0.001) where 32±2.4% cell kill was achieved. 50±8.79% cell kill occurred after incubation with 400μM of temozolomide and 78±8.43% cell kill was achieved at 800μM, the highest concentration of temozolomide used.

In order to examine this variable response to temozolomide between the T98g and UVW cell lines, Western blot analysis for the temozolomide resistance factor MGMT was performed. Figure 3.1b shows basal expression of MGMT protein in two separate T98g lysates as indicated by the distinct band at 21kDa, and no basal expression in two separate UVW lysates at the same molecular weight.

Using Graphpad Prism 8, a line of best fit of the data seen in Figure 3.1 was fitted to determine the IC_{50} of temozolomide in each cell line. The IC_{50} in UVW cells was 15.2μM (R^2 >0.9), and the IC_{50} in T98g cells was 400μM (R^2 >0.94) demonstrating that UVW cells are significantly more sensitive to temozolomide than the T98g cell line and that this increased resistance is likely due to expression of MGMT as seen in the T98g cell

line, but not the UVW cell line (Chalmers *et al*., 2009; Hegi *et al*., 2005; Montaldi and Sakamoto-Hojo, 2013).

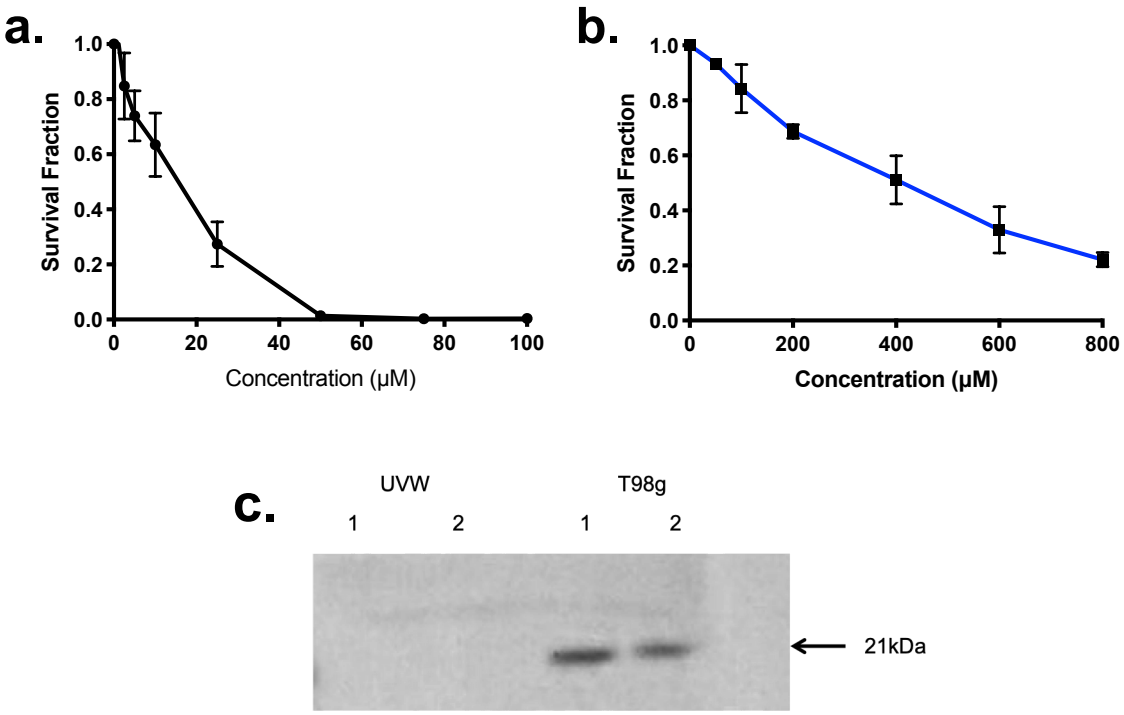

Figure 3.1: The impact of 24-hour temozolomide (0-800μM) exposure on the clonogenic capacity of UVW (**a.**) and T98g (**b.**) human glioblastoma cell lines, and Western blot analysis of UVW and T98g protein lysates showing MGMT expression (**c.**). Data shown is an average of at least three independent experiments ± standard deviation. A 1-way ANOVA with Bonferroni post testing was performed using Graphpad Prism 8 software, with p-values of <0.05 = *, <0.01=** and <0.001 = *** reported as significant.

3.4.1.2 Cytotoxicity of dimethyl fumarate on UVW and T98g human glioblastoma cell lines

In order to assess the cytotoxicity of dimethyl fumarate on UVW and T98g cells, both cell lines were incubated with increasing concentrations of dimethyl fumarate for 24 hours. Figure 3.2 shows the response of UVW and T98g cells to incubation with increasing concentrations of dimethyl fumarate, as measured by the clonogenic capacity of these cells following 24-hour exposure to the drug.

Both UVW and T98g cells displayed a distinct response to increasing concentrations of dimethyl fumarate as seen in Figure 3.2. Treatment of cells with concentrations of between 0-10μM of dimethyl fumarate causes a statistically significant increase in cell kill relative to an untreated control in both cell lines, with administration of 10μM dimethyl fumarate causing 55±10.42% cell kill (p-value <0.001) in the UVW cell line and 30±7.66% cell kill (p-value <0.001) in the T98g cell line.

As the concentration of drug administered was increased to 25μM, there was a decline in the steepness of the slope, and beyond this point there was a distinct plateau effect, with no significant changes in cytotoxicity in either cell line when drug concentration is increased from 10μM to 100μM as measured using the Bonferroni post-test. Due to this plateau effect, the maximum level of cell kill achieved with dimethyl fumarate was approximately 65±6.50% in the UVW cell line and 47±4.97% in the T98g cell line.

Using Graphpad Prism 8, line of best fit of the data seen in Figure 3.2 gave an IC_{50} of 9.1μM for the UW cell line (R^2 >0.9), but as the level of cell kill of dimethyl fumarate in the T98g cell line remained below 50%, it was not possible to calculate an IC_{50} based on the data generated.

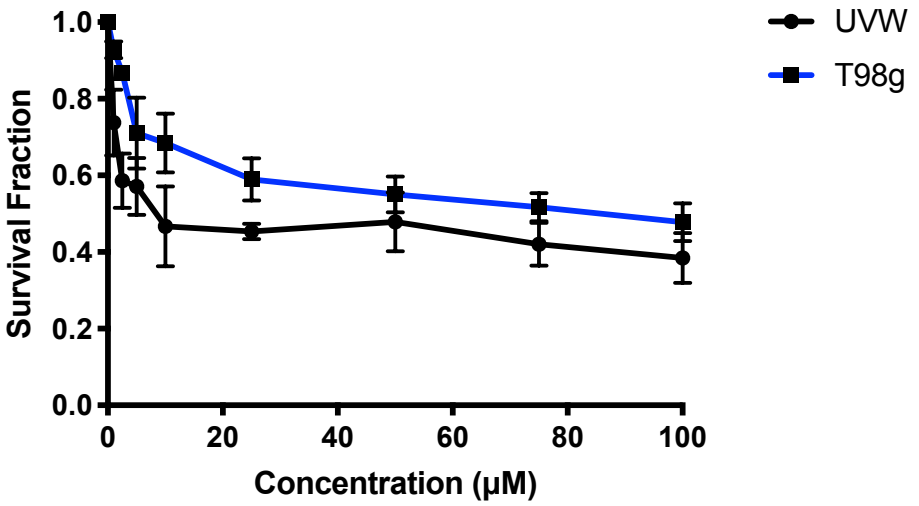

Figure 3.2: The impact of 24-hour dimethyl fumarate (0-100μM) exposure on the clonogenic capacity of UVW and T98g human glioblastoma cell lines. Data shown is an average of at least three independent experiments ± standard deviation. A 1-way ANOVA with Bonferroni post testing was performed using Graphpad Prism 8 software, with p-values of <0.05 = *, <0.01=** and <0.001 = *** reported as significant.

3.4.1.3 Design of the temozolomide-dimethyl fumarate combination

As demonstrated in Figures 3.1 and 3.2, the IC_{50} of temozolomide and dimethyl fumarate in the UVW cell line was determined to be 15μM and 9μM respectively. The ratio of the IC_{50} of dimethyl fumarate to temozolomide was simplified to 3:5, with the combinations of temozolomide and dimethyl fumarate used following this ratio, as seen in Table 3.1.

In the T98g line, the IC_{50} of temozolomide was 30 times higher than in the UVW cell line, at 400μM. However, as identified in Section 3.4.1.2, an IC_{50} for dimethyl fumarate was not calculable. Due to the distinct plateau of the curve seen in Figure 3.4, the highest concentration of dimethyl fumarate used was 25μM, the first point on the curve after which there was no further statistically significant increase in cell kill as determined using the Bonferroni post-test. This resulted in a ratio of 1:16 (dimethyl fumarate to temozolomide) being used, as seen in Table 3.1.

3.4.2 Effects of temozolomide and dimethyl fumarate in combination in UVW and T98g human glioblastoma cells

As discussed in Section 3.4.1, cell line specific combinations of temozolomide and dimethyl fumarate were generated based on the response of each cell line to each drug. This allowed for a combination unique to each cell line to be generated. For the purpose of these experiments, the MGMT positive T98g cell line and the MGMT negative UVW cell line were utilised in order to account for the clinical perspective, where up to 70% of patients present with MGMT mediated temozolomide resistance (Hegi *et al*., 2005).

3.4.2.1 Cytotoxicity of temozolomide and dimethyl fumarate as single agents and in combination in UVW and T98g human glioblastoma cells

In the temozolomide sensitive UVW cell line, administration of increasing concentration of temozolomide or dimethyl fumarate corresponded to a significant increase in cytotoxicity, as demonstrated in Figure 3.3a & b respectively. A statistically significant increase in cytotoxicity was observed at all concentrations of dimethyl fumarate (Figure 3.3b) compared to an untreated control (p-value <0.001), and at concentrations greater than 5μM of temozolomide (p-value <0.001) (Figure 3.3a). As these concentrations were determined from the IC_{50} of each drug, the highest concentration of each drug was expected to correspond to 50% toxicity, as predicted by the non-linear fit of data seen in Figures 3.1 & 3.2. The experimental data corresponds closely to this, with exposure to 15μM temozolomide and 9μM dimethyl fumarate resulting in 45±1.25% and 47±1.14% cytotoxicity respectively (Figure 3.3a & b).

When utilised in combination 0.5μM temozolomide and 0.3μM dimethyl fumarate resulted in 25±2.63% cell kill, which is significantly higher than either agent when used as monotherapy at the same concentrations (Figure 3.3c & d). This trend continued in a concentration-dependent fashion, with over 65±5.10% cell kill found at the highest concentration combination, compared to less than 50% cell kill observed at the corresponding concentrations of either single agent. The combination of temozolomide and dimethyl fumarate induced a significantly higher level of cytotoxicity compared to equivalent concentrations of temozolomide (p-value <0.001), however there was a lesser increase in cytotoxicity when comparing combinations to the equivalent concentrations of dimethyl fumarate, with a significant increase in cell kill observed at only combinations 1,2,4 & 5 (Figure 3.3d).

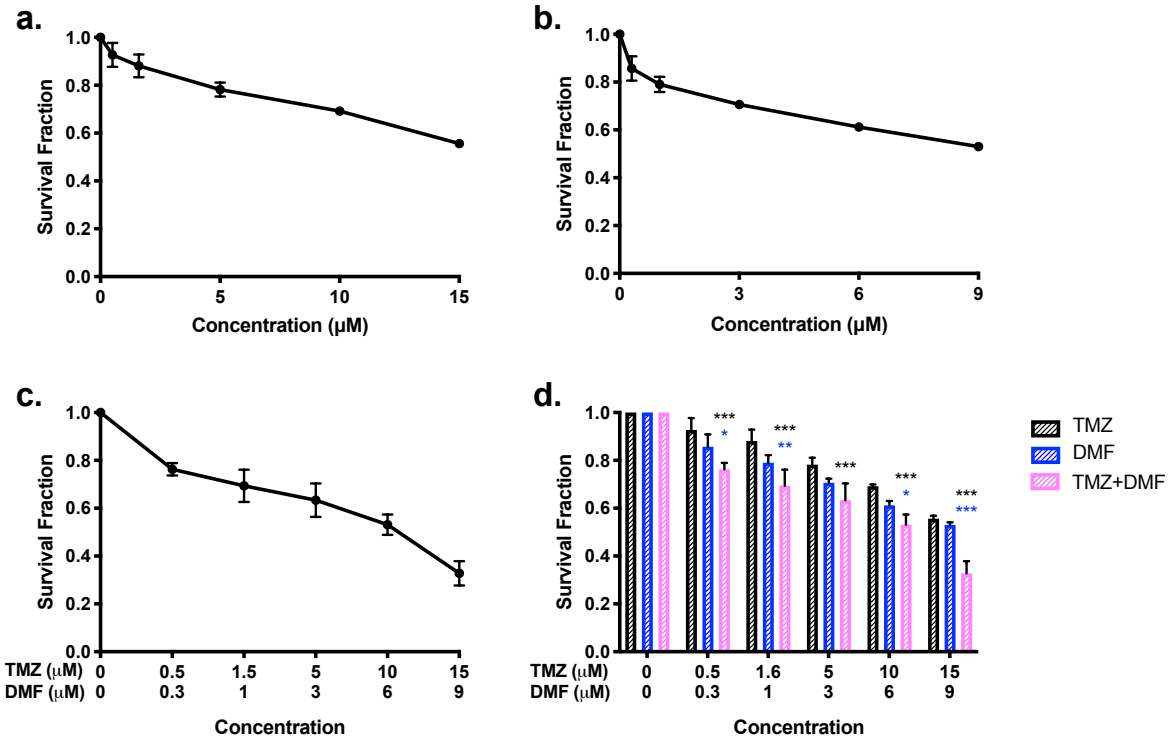

Figure 3.3: concentration response curves of the UVW cell line following 24-hour exposure to increasing concentrations of temozolomide (**a**), dimethyl fumarate (**b**) and a combination of temozolomide and dimethyl fumarate (**c**). The comparison between temozolomide and dimethyl fumarate and the combination of both drugs (**d**). Data shown is the average of three independent experiments ± standard deviation. A 1-Way ANOVA with Bonferroni post-test was performed on single agent curves, and a 2-Way ANOVA Bonferroni post-test was performed to compare single agents to the combination, with p-values of <0.05 = *, <0.01=** and <0.001 = *** reported as significant.

In the temozolomide resistant T98g cell line, temozolomide induced cytotoxicity in a concentration dependent manner (Figure 3.4a), with a statistically significant increase in cell kill observed from 200μM compared to an untreated control (p-value <0.001). 400μM, the highest concentration of temozolomide used, was expected to induce 50% cytotoxicity, as calculated from Figure 3.1b. Experimental data correlated closely with the predicted IC_{50}, as 400μM temozolomide exposure induced 49±0.99% cell kill. Dimethyl fumarate induced concentration-dependent cytotoxicity in the T98g cell line, with a statistically significant increase in cell kill compared to an untreated control observed from 6μM (p-value <0.05). As discussed in Section 3.4.1.3, it was not possible to generate an IC_{50} from data presented in Figure 3.2. However, exposure of the T98g cell line to 25μM dimethyl fumarate induced similar cytotoxicity in Figure 3.4b as in Figure 3.2, with 45±6.55% and 41±5.51% cell kill respectively. The temozolomide-dimethyl fumarate combination induced cytotoxicity in a concentration-dependent manner, with a significant increase in cell kill observed from the second concentration of the temozolomide-dimethyl fumarate combination, 100μM+5.25μM. At the highest concentration combination used, 400μM+25μM, 65±9.62% cell kill was observed.

When compared to each single agent, the temozolomide-dimethyl fumarate combination induced significantly increased cytotoxicity at some, but not all concentrations. The lowest combination used, 50μM+3.125μM, induced no significant increase in cytotoxicity compared to corresponding concentrations of single agent. A statistically significant increase in cell kill was observed compared to 100μM of temozolomide (p-value <0.001), but 6.25μM, the concentration of dimethyl fumarate that makes up this combination does not induce significantly more cytotoxicity as a single agent compared to the combination. As the concentrations of the combination increased, a significant increase in cytotoxicity compared to each single agent was observed at the 200μM+12.5μM combination (p-value <0.01 & 0.05 respectively). Significant increase in cytotoxicity compared to each single agent was observed at the 300μM+17.5μM combination (p-value <0.001 & 0.01 respectively). However, at the highest concentration of the combination used, 400μM+25μM, there was no increase in cytotoxicity compared to either single agent (Figure 3.4d).

This suggests that our hypothesis is correct, and that dimethyl fumarate appears to potentiate the effects of temozolomide in UVW and T98g human glioblastoma cell lines.

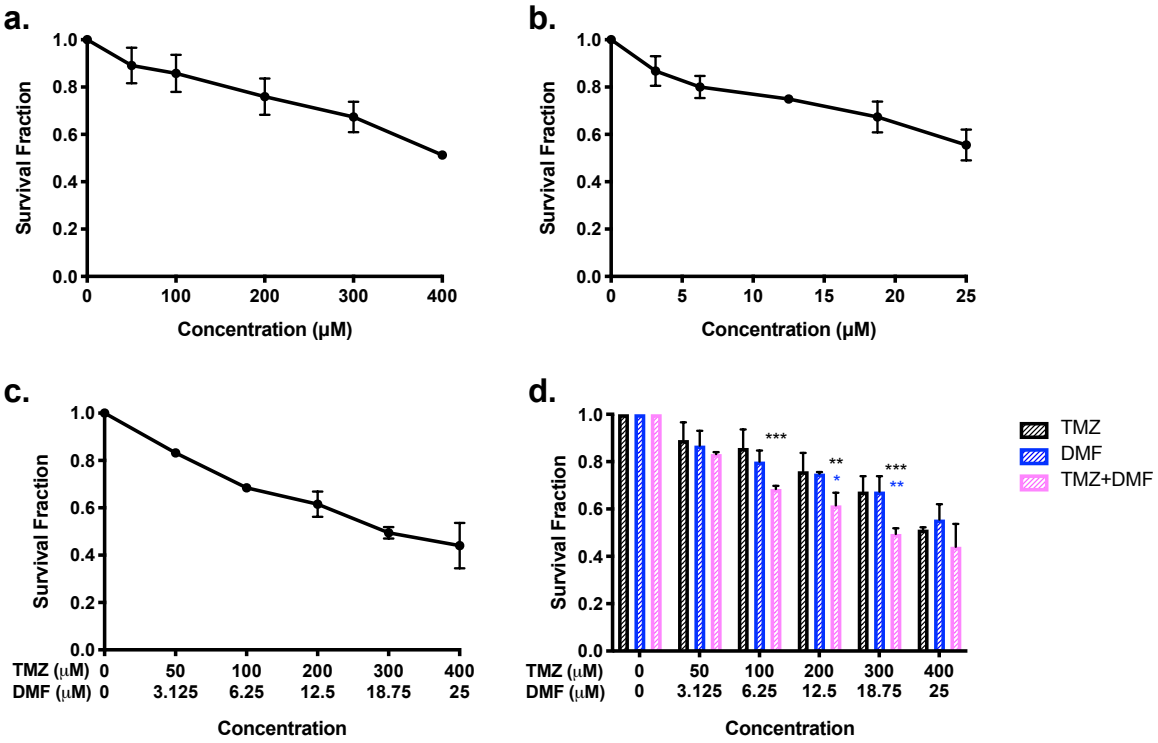

Figure 3.4: concentration response curves of the T98g cell line following 24-hour exposure to increasing concentrations of temozolomide (**a**), dimethyl fumarate (**b**) and a combination of temozolomide and dimethyl fumarate (**c**). The comparison between temozolomide and dimethyl fumarate and the combination of both drugs (**d**). Data shown is the average of three independent experiments ± standard deviation. A 1-Way ANOVA with Bonferroni post-test was performed on single agent curves, and a 2-Way ANOVA Bonferroni post-test was performed to compare single agents to the combination, with p-values of <0.05 = *, <0.01=** and <0.001 = *** reported as significant.

3.4.3 Combination index analysis of the temozolomide-dimethyl fumarate combination in UVW and T98g human glioblastoma cells

The use of combination index analysis allows for the relationship between two or more agents within a system to be defined in terms of their cytotoxicity. The relationship is defined as being either infra-additive (antagonistic), additive (neither antagonistic or synergistic) or supra-additive (synergistic, or better than the sum effect of each agent). Terms used throughout this section are taken from combination index analysis but have been contextualised to the results.

Combination index analysis modelling is highly dependent on the goodness of fit values (R^2 values) for the lines of best fit applied to the dose effect and median effect plots, as the model does not interpret generated data, but will interpolate data from the lines which the program fits. Due to the nature of combination index analysis, experimental data is shown (marked as symbols) as well as the line of fit calculated by Calcusyn software.

Combination index analysis of the temozolomide-dimethyl fumarate combination in UVW human glioblastoma cells was performed using Calcusyn software.

Figure 3.5 graphically represents the data shown in Figure 3.3 that has been analysed via combination index analysis using Calcusyn software (Section 2.6). Figure 3.5a shows the median effect plot (MEP). The MEP demonstrates that treatment with increasing dose of temozolomide, dimethyl fumarate or the temozolomide-dimethyl fumarate combination, increases the ratio of affected to unaffected cells (fa/fu). This is representative of the proportion of cells that have been affected by treatment, the effect measured and reported here is cell survival . R^2 values of the lines of best for are shown in Figure 3.5d, with the single agents having the highest R^2 values. Unfortunately, the temozolomide-dimethyl fumarate combination had a low R^2 value, meaning that the line fitted to the data was poor, which may limit the application of combination index analysis as a model.

Figure 3.5b shows the dose effect plot, showing that increasing doses of each single agent or the temozolomide-dimethyl fumarate combination increases the effect measured – in this case cell kill.

Figure 3.5c shows the combination index plot of the temozolomide-dimethyl fumarate combination, with each point representing the additivity of each fraction affected by increasing doses of the temozolomide-dimethyl fumarate combination. This data shows that all combinations are supra additive, meaning that there is a synergistic effect on cell kill when the temozolomide-dimethyl fumarate combination if used, except when cells were incubated with 5μM+3μM of the temozolomide-dimethyl fumarate combination, which is additive, meaning there is no synergy, but also no antagonism when the agents are used in combination. These CI values and corresponding fractions affected by each combination are seen in Figure 3.5e.

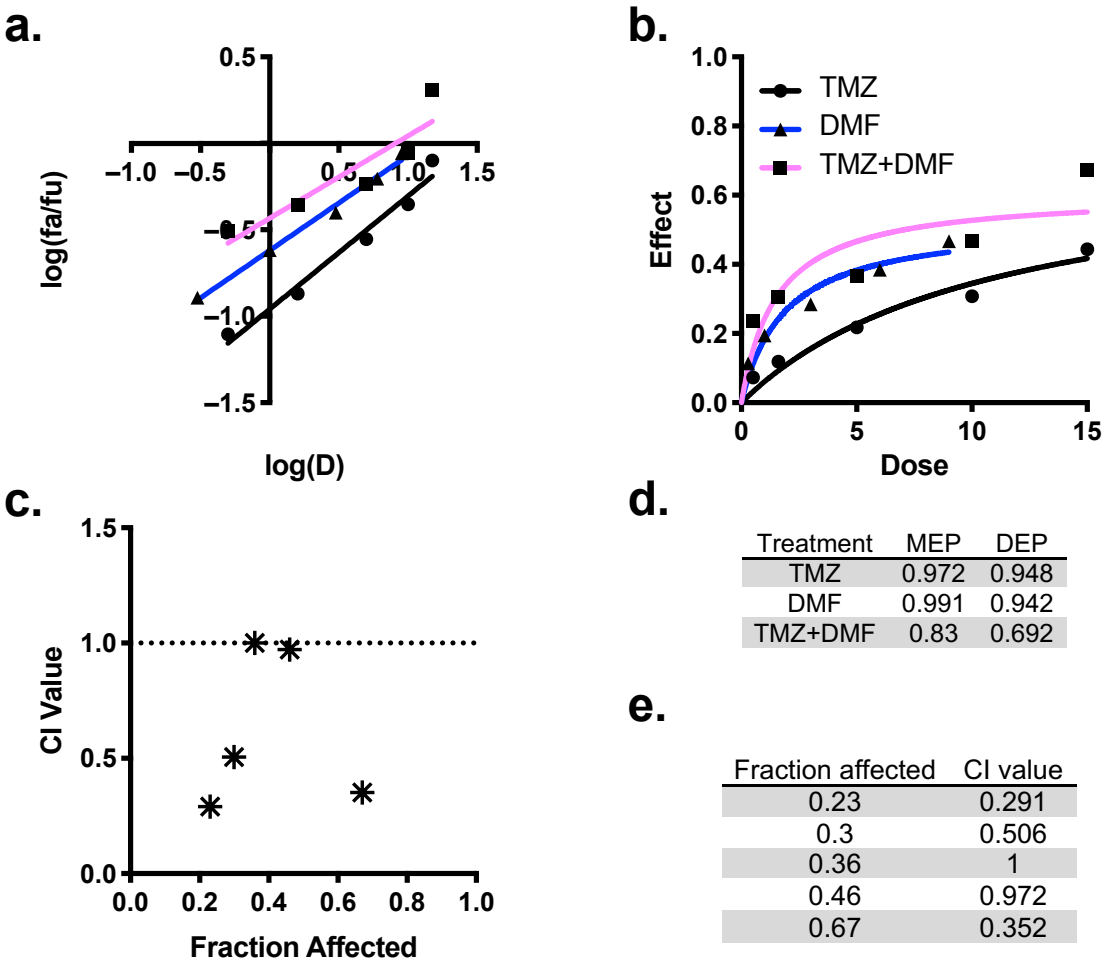

d.

Treatment	MEP	DEP
TMZ	0.972	0.948
DMF	0.991	0.942
TMZ+DMF	0.83	0.692

e.

Fraction affected	CI value
0.23	0.291
0.3	0.506
0.36	1
0.46	0.972
0.67	0.352

Figure 3.5: Combination index analysis of the temozolomide-dimethyl fumarate combination in UVW human glioblastoma cells **a.** increasing doses of temozolomide (●), dimethyl fumarate (▲) and the temozolomide-dimethyl fumarate combination (■) against the logarithmic ratio of the affected fraction to unaffected fraction with associated lines of best fit. **b.** the effects of increasing dose of temozolomide, dimethyl fumarate or the combination of temozolomide and dimethyl fumarate on the population analysed. **c.** the combination index value of each fraction affected for each dose of the temozolomide and dimethyl fumarate combination. **d.** the R^2 values for each line of best fit in the dose effect plot (DEP) and median effect plot (MEP) shown in Figure 3.5a & b. respectively **e.** the combination index values and associated fraction affected for each dose in the temozolomide-dimethyl fumarate combination.

Combination index analysis of the temozolomide-dimethyl fumarate combination in the T98g human glioblastoma cell line was performed using Calcusyn software. Figure 3.6 graphically represents the cytotoxicity data shown in Figure 3.4 following analysis via combination index analysis using Calcusyn software (Section 2.6).

Figure 3.6a shows the median effect plot (MEP). The MEP demonstrates that treatment with increasing dose of temozolomide, dimethyl fumarate or the temozolomide-dimethyl fumarate combination correlates strongly with an increase in the ratio of affected to unaffected cells (fa/fu). This is representative of the proportion of cells that have been affected by treatment, the effect measured and reported here is cell kill. R^2 values for the lines of best are shown in Figure 3.6d, showing that this correlation is strong (R^2 >0.9). Strong correlation and therefore high R^2 values are needed for high fidelity combination index analysis. This is due to the software used as the model does not interpret generated data, but will interpolate data from the lines which the program fits

Figure 3.6b shows the dose effect plot, showing that increasing doses of each single agent or the temozolomide-dimethyl fumarate combination correlates strongly (R^2 >0.9) with increase in the effect measured, in this case the effect measured was cell survival Figure 3.6c shows the combination index plot of the temozolomide-dimethyl fumarate combination, with each point representing the additivity of each fraction affected by increasing doses of the temozolomide-dimethyl fumarate combination of each fraction affected by the combination. These CI values and corresponding fractions affected by each combination are seen in Figure 3.6e.This data shows that two doses of the temozolomide-dimethyl fumarate combination, 50μM+3.125μM and 200μM+12.5μM, are infra-additive, with a combination index value greater than 1, which is indicative of an antagonistic effect at these doses. All other doses of the temozolomide-dimethyl fumarate combination in the T98g cell line are suggested to be synergistic as the CI value for fraction affected by these was concentrations of the temozolomide-dimethyl fumarate combination was less than 1.

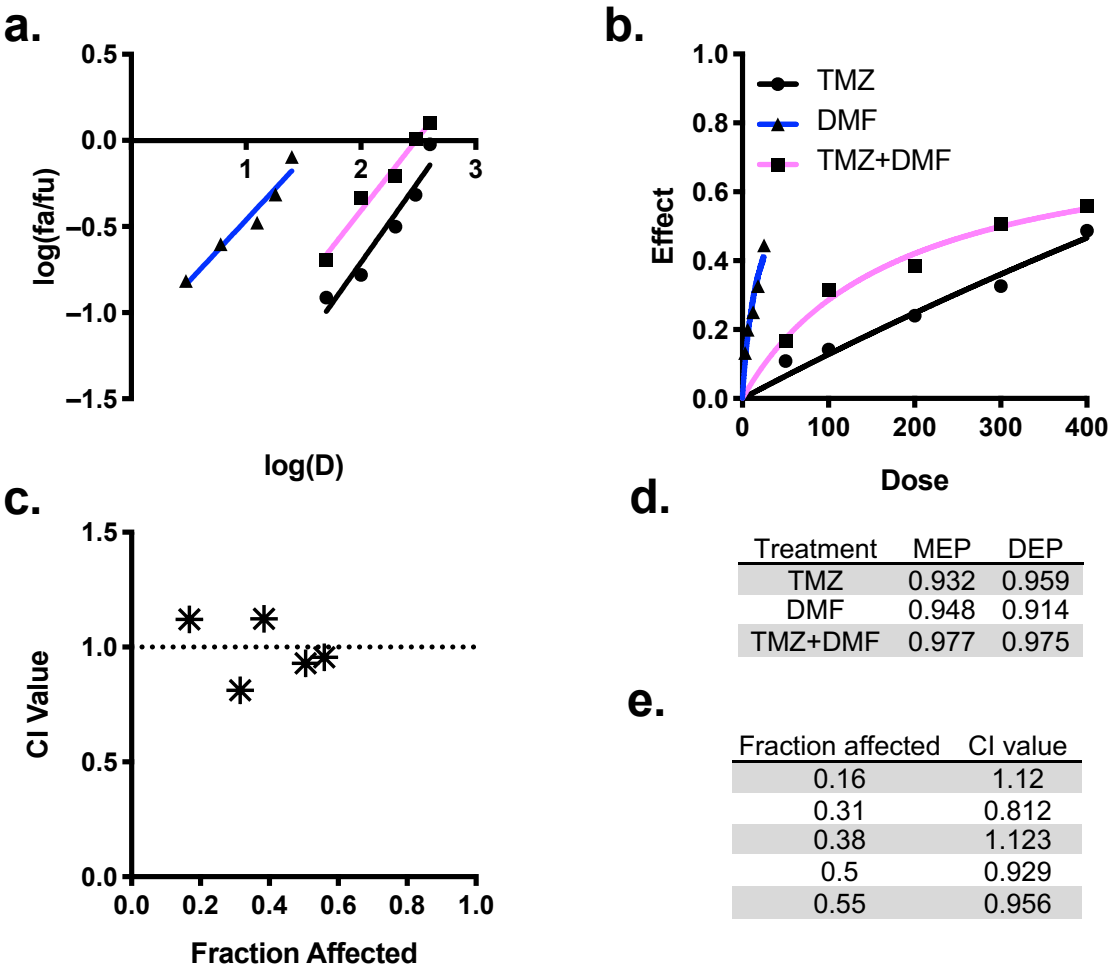

d.

Treatment	MEP	DEP
TMZ	0.932	0.959
DMF	0.948	0.914
TMZ+DMF	0.977	0.975

e.

Fraction affected	CI value
0.16	1.12
0.31	0.812
0.38	1.123
0.5	0.929
0.55	0.956

Figure 3.6: Combination index analysis of the temozolomide-dimethyl fumarate combination in T98g human glioblastoma cells. **a** increasing doses of temozolomide (●), dimethyl fumarate (▲) and the temozolomide and dimethyl fumarate combination (■) against the logarithmic ratio of the affected fraction to unaffected fraction with associated lines of best fit. **b** the effects of increasing dose of temozolomide, dimethyl fumarate or the combination of temozolomide and dimethyl fumarate on the population analysed. **c** the combination index value of each fraction affected for each dose of the temozolomide and dimethyl fumarate combination. **d.** the R^2 values for each line of best fit in the dose effect plot (DEP) and median effect plot (MEP) shown in Figure 3.6a & b. respectively. **d.** the combination index values and associated fraction affected for each dose in the temozolomide-dimethyl fumarate combination.

3.4.4 Quantification of DNA double stranded breaks in UVW and T98g human glioblastoma cells in response to treatment with temozolomide, dimethyl fumarate and the temozolomide-dimethyl fumarate combination

In order to assess the dynamics of DNA damage and repair, phosphorylation of Ser139-H2a.X was quantified by detection of a FITC-conjugated anti–Ser139 H2a.X antibody. H2a.X phosphorylation is a hallmark of double stranded breaks in DNA. Double stranded breaks recruit the ATM/ATR complex, which initiates a cascade that results in H2a.X phosphorylation and G_2/M arrest.

The temozolomide-dimethyl fumarate combination was hypothesised to induce a higher level of DNA damage, and therefore a greater level of γH2a.X than temozolomide or dimethyl fumarate as a single agent. It was further hypothesised that the level of γH2a.X induced by the temozolomide-dimethyl fumarate combination would persist due to temozolomide remaining active within the cell for an increased period of time. Cells were treated with combinations of temozolomide and dimethyl fumarate as previously described. Flow cytometric analysis was performed, with fold increase in γH2A.x levels compared to an untreated but stained control reported. Cells were treated for 4 or 24-hours to assess the dynamics of DNA damage and repair over time.

In UVW cells there was no significant increase in γH2a.X levels following 4 or 24-hours of dimethyl fumarate exposure, with a maximum 1.86±0.54-fold increase seen following 4-hour treatment (Figure 3.7a). This was not significant compared to the γH2a.X levels found in untreated cells (p-value >0.05) indicating that, as expected, dimethyl fumarate does not induce DNA damage. In contrast, 4-hour treatment with temozolomide induced a statistically significant 2.7±0.60-fold increase in γH2a.X levels (p-value <0.05), and 24-hour treatment induced a 3.8±0.51-fold increase in γH2a.X levels compared to an untreated control (p-value <0.05). This is suggestive that temozolomide induces DNA damage in the UVW cell line, in a manner that was dependent on treatment time, with 24-hour treatment inducing significantly higher levels of γH2a.X than 4-hour treatment (p-value <0.05).

The combination of temozolomide and dimethyl fumarate resulted in a statistically significant increase in γH2a.X levels relative to an untreated control following 4 and 24-hour treatment, with a 3.3±0.74 and 3.5±0.36-fold increase observed respectively (p-

value <0.01). Contrary to our hypothesis, the temozolomide-dimethyl fumarate combination did not increase the levels of DNA damage compared to temozolomide alone, although a trend of increased γH2a.X levels was seen in combination treated cells compared to cells treated with temozolomide alone, this was not statistically significant (p-value >0.05).

In the MGMT positive T98g cell line, no significant increase in γH2a.X levels was observed following 4 or 24-hours of dimethyl fumarate treatment, indicating no increase in the amount of double stranded breaks compared to an untreated control (p-value >0.05).

4-hour temozolomide treatment of T98g cells did not significantly increase γH2a.X levels, while 24-hour treatment induced a 3.5±1.02-fold increase in γH2a.X detection compared to an untreated control (p-value <0.05) (Figure 3.7b). This is suggestive that the temozolomide induced DNA damage is a time dependent event. This is in keeping with our knowledge of temozolomide. We believe that the expression of MGMT in the T98g cell line, but not the UVW cell line is responsible for the slower induction of γH2a.X in the T98g cell line.

Treatment for 4 hours with temozolomide and dimethyl fumarate resulted in a 2.9±1.17-fold increase in γH2a.X levels, however, following 24-hour treatment this increased to a 3.6±0.98-fold increase compared to an untreated control. This is not significantly higher than the levels of γH2a.X seen when equivalent concentrations of temozolomide were used as a single agent (p-value >0.05). This was contrary to our hypothesis that the temozolomide-dimethyl fumarate combination would increase levels of γH2a.X compared to temozolomide as a single agent.

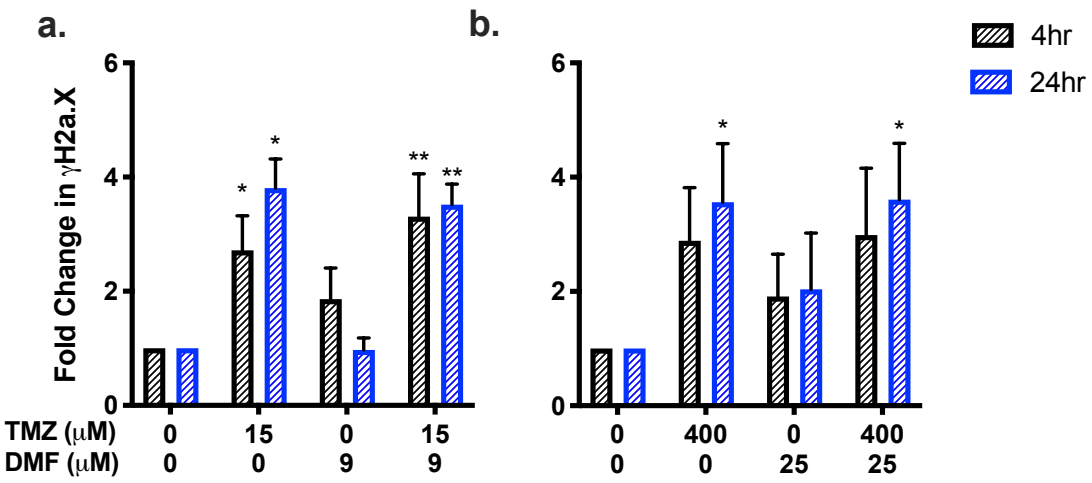

Figure 3.7: γH2a.X levels in UVW and T98g human glioblastoma cells. The fold change in γH2a.X levels in **a.** UVW or **b.** T98g cells in response to 4 or 24-hour treatment with temozolomide (15 or 400μM), dimethyl fumarate (9 or 25μM) or the equivalent concentrations that constitute the temozolomide-dimethyl fumarate combination. Data shown is an average of at least 3 independent experiments ± standard deviation. A 2-Way ANOVA with Bonferroni post-test was performed with p-values of <0.05 = *, <0.01=** and <0.001 = *** reported as significant.

3.4.5 Effects of temozolomide and dimethyl fumarate on cell cycle progression in UVW and T98g human glioblastoma cells

Cells were treated with combinations of temozolomide and dimethyl fumarate for 4 or 24-hours in order to examine effects of drug treatment on cell cycle distribution. Treatment for 4 or 24-hours was performed in order to examine when arrest and recovery was observed. In order to determine the distribution of a population of cells throughout the cell cycle, cellular DNA was stained with propidium iodide and flow cytometric analysis was performed, with distinction between the G_1, S, G_2 and M phases of the cell cycle made by assessing intracellular DNA content.

Following 4-hour exposure to 0.5 and 5μM of temozolomide there was no phase redistribution in UVW cells compared to an untreated control. Following treatment with 15μM of temozolomide, there was an accumulation of cells in the G_2 phase of the cell cycle, which is indicative of DNA damage. However, this was not found to be statistically significantly larger than the G_2 population of untreated cells (p-value >0.05). After 24-hour exposure, all concentrations of temozolomide induced a significant accumulation of cells in the G_2 phase of the cell cycle compared to an treated control (p-value <0.01), with 45.38±6.9% 15μM treated cells being found in the G_2 phase following compared to 23.74±3.63% in an untreated control. 24-hour treatment with all concentrations of temozolomide induced a significantly larger G_2 arrest than 4-hour treatment (p-value <0.001).

Accumulation in the G_2 phase of the cell cycle after 24-hour incubation with temozolomide compared to 4-hour indicates DNA damage, as cells arrest at this phase to repair DNA damage. This is in line with out γH2a.X data, which shows an increase in temozolomide mediated DNA damage after 4 and 24-hours. We believe we see accumulation after 24-hours, but not 4-hours as the cells have completed, or attempted to complete a full cycle by 24, but not 4-hours.

Exposure to increasing concentration of dimethyl fumarate for either 4 or 24 hours had no significant effect on the distribution of UVW cells throughout the cell cycle (p-value >0.05).

4-hour exposure to the temozolomide-dimethyl fumarate combination increased G_2 accumulation in a concentration dependent manner, however, this was not found to be statistically significantly larger than the G_2 population of untreated cells or cells treated with equivalent concentrationss of temozolomide or dimethyl fumarate as single agents (p-value >0.05).

Similarly to temozolomide as a single agent, following 24-hour exposure to the temozolomide-dimethyl fumarate combination there was a significant accumulation in cells in the G_2 phase of the cell cycle compared to an untreated control (p-value <0.01). This resulted in 42.96±2.3% of 15μM+9μM treated cells being found in the G_2 phase compared to 23.74±3.63% in an untreated control. 24-hour treatment with all concentrations of the temozolomide-dimethyl fumarate combination induced a significantly larger G_2 arrest than 4-hour treatment (p-value <0.001). The temozolomide-dimethyl fumarate combination did not induce cell cycle redistribution compared to temozolomide or dimethyl fumarate as single agents (p-value >0.05).

A larger G_2 accumulation was expected in cells treated with the temozolomide-dimethyl fumarate combination compared to temozolomide alone due to an increase in DNA damage. This was not realised, but is in keeping with our γH2a.X results.

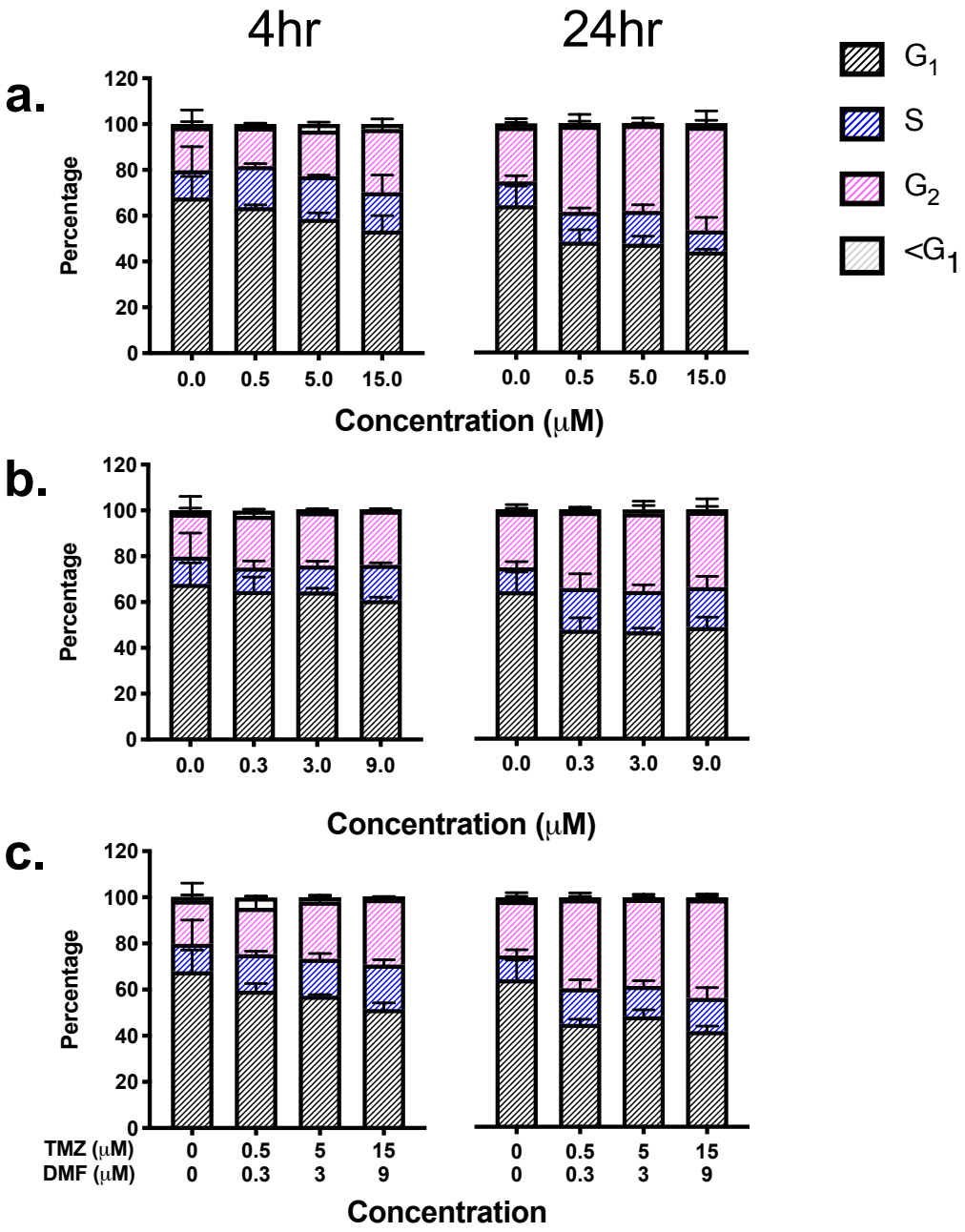

Figure 3.8: Cell cycle progression in UVW cells treated with temozolomide, dimethyl fumarate or the temozolomide-dimethyl fumarate combination. The cell cycle distribution of UVW cells in response to 4 or 24-hour exposure to increasing concentrations of temozolomide (**a.**) dimethyl fumarate (**b.**) or the temozolomide-dimethyl fumarate combination (**c.**). Data shown is an average of at least 3 independent experiments ± standard deviation. A 2-Way ANOVA with Bonferroni post-test was performed with p-values of <0.05 = *, <0.01=** and <0.001 = *** reported as significant. Statistics are reported in Appendix A1.

In T98g cells, there was no significant redistribution of cells following 4-hours of temozolomide treatment (p-value >0.05). Following 24-hour exposure to 400μM temozolomide, T98g cells accumulated in the G_2 phase of the cell cycle compared to an untreated, however this was not significant (p-value >0.05). No cell cycle redistribution was seen following 24-hour exposure to lower concentrations of temozolomide (p-value >0.05). This indicates that temozolomide does not induce a level of DNA damage that results in T98g cell cycle arrest.

Similarly to UVW cells, T98g cells showed no changes in cell cycle distribution following either 4 or 24-hour exposure to dimethyl fumarate compared to an untreated control (p-value >0.05).

Following 4-hour exposure, combinations of temozolomide and dimethyl fumarate caused cells to accumulate in the G_2/M phase in a concentration-dependent manner. Post 4-hour exposure to 400μM of temozolomide and 25μM of dimethyl fumarate, 45.43±8.54% of the population were found to be in the G_2/M phase of the cell cycle, significantly higher than the same population in untreated cells, 22.94±6.77% (p-value <0.05). a trend of increased G_2 accumulation was seen in combination treated cells compared to cells treated with temozolomide alone, however this was not statistically significant (p-value >0.05). 24-hour exposure to the temozolomide-dimethyl fumarate combination induced a concentration-dependent accumulation of cells in the G_2 phase of the cell cycle compared to an untreated control. only the arrest at the G_2 phase induced by 400μM+25μM of the temozolomide-dimethyl fumarate combination was significant compared to an untreated control (p-value <0.001). Again, this accumulation was larger, but not statistically significantly more so, than the accumulation induced by equivalent concentrations of temozolomide as a single agent (p-value >0.05).

Lack of G_2/M arrest indicates that a lack of DNA damage. This is likely due to the resistance to temozolomide in the T98g cell line.

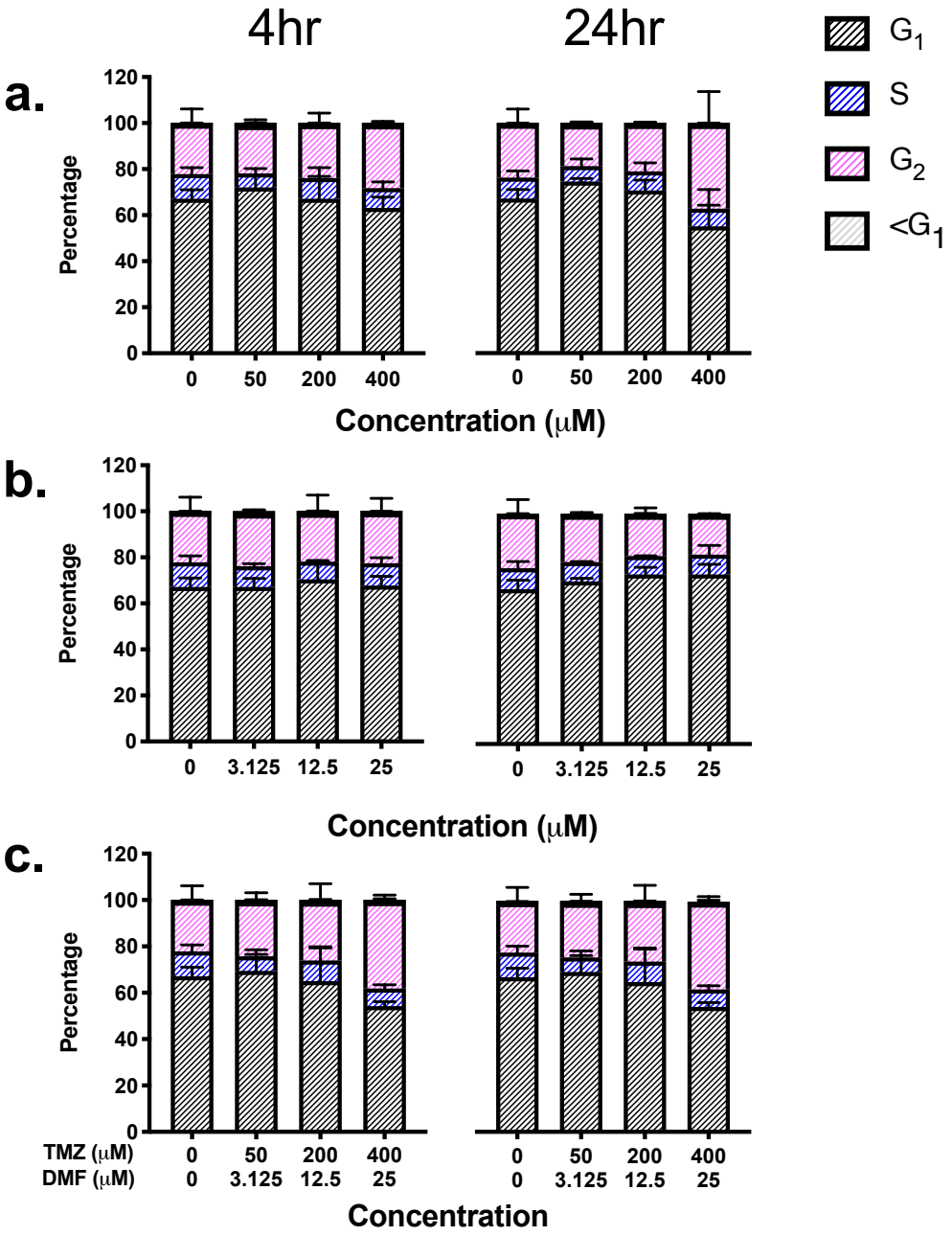

Figure 3.9: Cell cycle progression in T98g cells treated with temozolomide, dimethyl fumarate or the temozolomide-dimethyl fumarate combination. The cell cycle distribution of UVW cells in response to 4 or 24-hour exposure to increasing concentrations of temozolomide (**a.**) dimethyl fumarate (**b.**) or the temozolomide-dimethyl fumarate combination (**c.**). Data shown is an average of at least 3 independent experiments ± standard deviation. A 2-Way ANOVA with Bonferroni post-test was performed with p-values of <0.05 = *, <0.01=** and <0.001 = *** reported as significant. Statistics are reported in Appendix A2.

3.4.6 Apoptotic induction by temozolomide and dimethyl fumarate on UVW and T98g human glioblastoma cells

Apoptosis was detected using an anti-annexin V FITC conjugate and propidium iodide, with each stain identifying the cellular population at different stages of the apoptotic cell death pathway. Early apoptotic cells were characterised as having an intact membrane and stained positively for annexin V which associates with membrane bound phosphatidyl serine moieties, late apoptotic cells, which have a compromised membrane, were annexin V & propidium iodide positive. Necrotic cells were singly positive for propidium iodide and had a severely compromised membrane. Time points 24-72 hours post-treatment cessation were chosen in order for cells to arrest and induce apoptosis.

Time points 24-72 hours post-treatment cessation were chosen in order for cells to arrest and induce apoptosis following treatment. We believe that we have shown that DNA damage and cell cycle arrest in UVW cells treated with temozolomide do not occur until 24-hours of treatment. Following this mismatch repair cycles take place. Failed cycles of mismatch repair leads to DNA damage in the form of double stranded breaks (Kaina, 2003; Roos and Kaina, 2006; Roos *et al*., 2007), inductions of double stranded breaks has been shown to be necessary for induction of apoptosis (Ochs and Kaina, 2000), and induction of apoptosis as late as 120-hours post treatment has been shown to take place.

In UVW cells 12.9±0.99% of the population were found to basally express apoptotic markers. This population was broken down to show that 8.9±0.62% of this population were early apoptotic, meaning they were singly annexin V positive, and 4.9±0.38% of the population were late apoptotic, meaning they were doubly positive for propidium iodide and annexin V.

As seen in Figure 3.10a, treatment with temozolomide induced apoptosis in a concentration independent manner. 24-hours post-treatment cessation there was no significant increase in the size of the apoptotic population compared to an untreated control, and there was no significant difference in the size of the apoptotic population between each treatment group (p-value >0.05). The size of these populations increased, again in a concentration independent manner, 48-hours post-treatment cessation. This population was found to be approximately double that of an untreated control, with all

concentrations of temozolomide inducing apoptosis in approximately 25% of the analysed population (p-value >0.05). Between 48 and 72 hours, there was a significant increase in the size of the apoptotic population compared to 24 or 48-hour time points (p-value <0.01). This increase was found to correlate inversely with concentration. Following treatment with 0.5μM, 5μM or 15μM temozolomide, 79.9±5.41%, 72.6±11.50% and 66.9±6.67% of each population was found to be apoptotic respectively.

Figure 3.10b shows that there was no significant redistribution of cells between apoptotic phases following 24 or 48hr incubation post temozolomide treatment (p-value >0.05). 72-hours post-treatment there was a significant increase in the size of the late apoptotic (p-value <0.01) and necrotic (p-value <0.05) population, compared to an untreated control or cells incubated for 24 or 48-hours post-treatment. The increase in the size of the late apoptotic population was found to be inversely correlated with concentration, likely through cells cycling undergoing late apoptosis between 48 and 72-hours, resulting in the increased necrotic population at this time point. This increase in the size of the necrotic population was found to be concentration dependent, with the highest concentration of temozolomide inducing the highest level of necrosis. However, increasing temozolomide concentration appeared to have no effect on the size of the apoptotic population, with no significant difference at any time points (p-value >0.05).

Dimethyl fumarate induced apoptosis in a concentration dependent manner as seen in Figure 3.10c & d. 24-hours post treatment cessation there was no significant increase in the size of the apoptotic population at any concentration compared to an untreated control. The size of the apoptotic population increased in a concentration dependent manner 48 hours post-treatment cessation, with a statistically significant increase compared to 24-hour incubation observed at all concentrations (p-value <0.01). Treatment with 9μM dimethyl fumarate resulted in apoptosis being induced in 78.1±8.42% of the population, which is significantly higher than the size of the apoptotic population in cells treated with either 0.3μM (47.1±3.59% apoptotic) or 3μM (55.6±10.45% apoptotic) dimethyl fumarate (p-value <0.05). 72-hours post treatment cessation there was no significant difference between the size of the apoptotic population following treatment with any of the designated concentrations of dimethyl fumarate (p-value >0.05). The apoptotic population was significantly larger at 72-hours-post treatment compared to 24 or 48-hours following treatment with either 0.3μM or 3μM of dimethyl fumarate (p-value <0.05).

As seen in Figure 3.10d, there was no significant phase redistribution of the apoptotic population following 24-hour incubation after dimethyl fumarate treatment compared to an untreated control. Following 48-hour incubation there was a significant increase in the size of both the early (p-value <0.001) and late (p-value <0.05) apoptotic populations compared cells incubated for 24-hours. After 72-hour incubation there was further significant redistribution of the apoptotic population. At all concentrations of dimethyl fumarate there was a significant decrease in the early apoptotic population (p-value <0.01) and a significant increase in the late apoptotic population compared to 48-hour incubation (p-value <0.05). There was a significant increase in the size of the necrotic population at all concentrations of dimethyl fumarate used (p-value <0.05) compared to the same concentrations at 48-hours post treatment cessation.

The temozolomide-dimethyl fumarate combination induced apoptosis in a similar pattern to temozolomide as a single agent (Figure 3.10e & a respectively). There was no significant induction of apoptosis above basal levels 24-hours after treatment cessation, and no significant difference between each concentration of the temozolomide-dimethyl fumarate combination. There was also no statistically significant difference between the combination and corresponding concentration of each single agent. Similarly to temozolomide as a single agent, there was an increase in the size of the apoptotic population 48-hours post treatment cessation, which appeared to be concentration-dependent. There was no significant apoptotic induction at this time point compared to an untreated control (p-value >0.05), or compared to temozolomide as a single agent (p-value >0.05). The size of this population was significantly lower than the corresponding concentrations of dimethyl fumarate as a single agent (p-value <0.01). 72-hours post treatment cessation there was a significant increase in the size of the apoptotic population, with all concentrations of the temozolomide-dimethyl fumarate combination compared to the same concentrations at the 48-hour time point (p-value <0.01).

As seen in Figure 3.10f, there was no significant redistribution of apoptotic cells 24-hours post treatment cessation compared to the basal population or the congruent concentrations of each single agent. At the 48-hour time point, there was a significant increase in the proportion of early apoptotic cells compared to an untreated control (p-value <0.05), but this population was not significantly different from the correlating concentrations of temozolomide (Figure 3.10f & b). The early and late apoptotic

population detected following combination treatments were significantly smaller than the corresponding populations detected following treatment with dimethyl fumarate as a single agent (p-value <0.01 and <0.05 for early and late populations respectively) (Figure 3.10f & d). There was a significant, concentration-dependent increase in the size of the necrotic population in cells treated with the temozolomide-dimethyl fumarate combination compared to equivalent doses of temozolomide as a single agent 72-hours post treatment cessation (p-value <0.01).

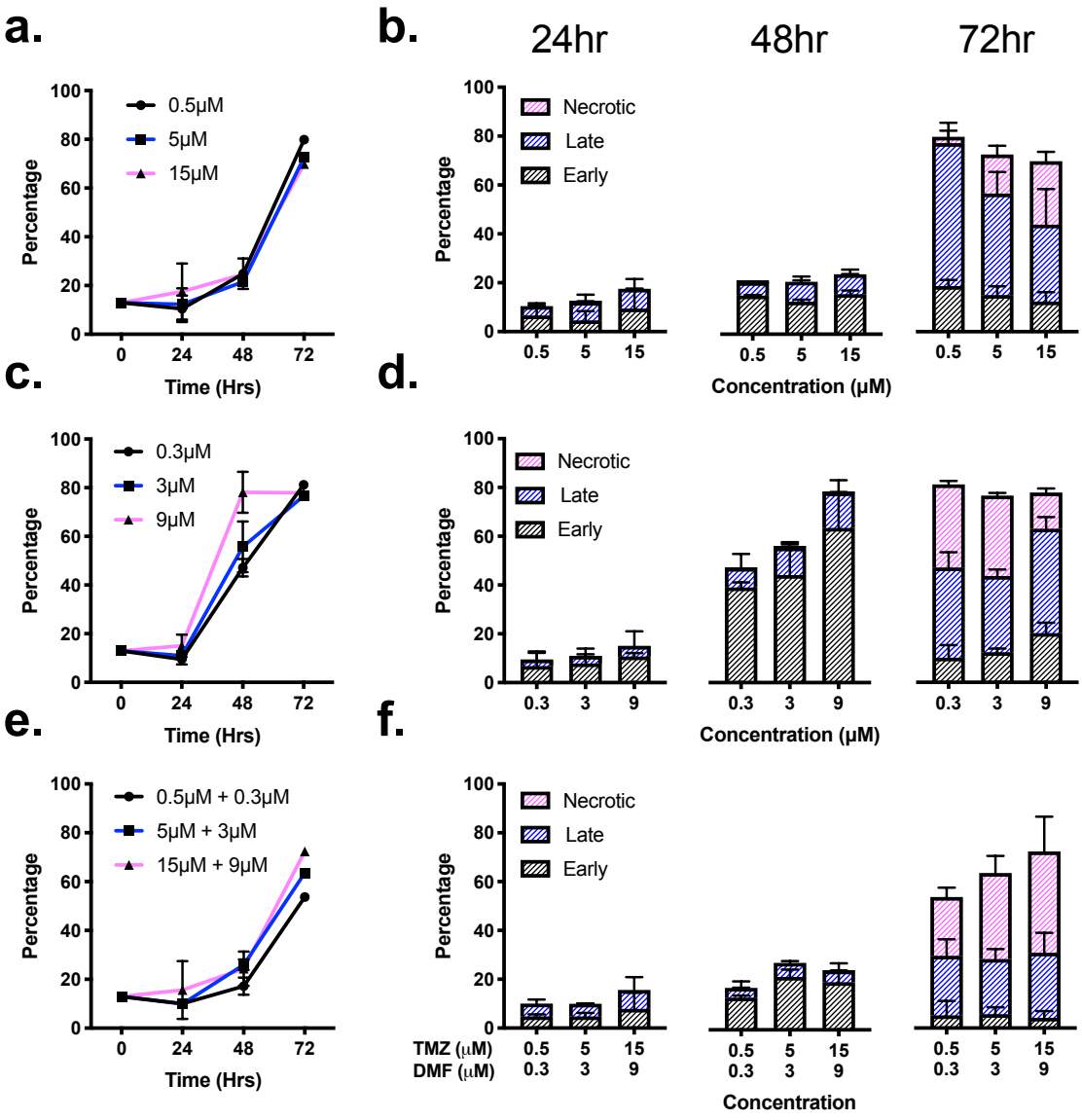

Figure 3.10: Induction of apoptosis in UVW cells by temozolomide, dimethyl fumarate and the temozolomide-dimethyl fumarate combination. Apoptotic induction in UVW cells in response to increasing concentrations of temozolomide (**a.**) dimethyl fumarate (**c.**) or the temozolomide-dimethyl fumarate combination (**e.**) and apoptotic phase redistribution in response to increasing concentrations of temozolomide (**b.**) dimethyl fumarate (**d.**) or the temozolomide-dimethyl fumarate combination (**f.**). Data shown is an average of at least 3 independent experiments ± standard deviation. A 2-Way ANOVA with Bonferroni post-test was performed with p-values of <0.05 = *, <0.01=** and <0.001 = *** reported as significant. Statistics are reported in Appendix B1.

As seen in Figure 3.11a, treatment with temozolomide induced expression of apoptotic markers in a concentration independent manner at concentrations greater than 50μM. 24-hours post-treatment cessation there was a significant increase in the size of the apoptotic population compared to an untreated control following treatment with 200 and 400μM of temozolomide (p-value <0.05). The size of these populations did significantly increase 48 or 72-hours post-treatment cessation. Treatment with 50μM of temozolomide induced significant expression of apoptotic markers at 72-hours post-treatment cessation compared to 24 or 48-hour time points (p-value <0.05)

Figure 3.11b shows that there was no significant redistribution of cells between apoptotic phases following 24 or 48-hour incubation post temozolomide treatment. 72-hours post-treatment there was a significant increase in the size of the late apoptotic population, compared to cells incubated for 24 or 48-hours post-treatment (p-value <0.05). This increase in the size of the late apoptotic population was found to be concentration independent.

Dimethyl fumarate induced apoptosis in a concentration independent manner as seen in Figure 3.11c & d. 24 and 48-hours post treatment cessation there was no significant increase in the size of the apoptotic population at any concentration compared to an untreated control. The size of the apoptotic population increased in a concentration independent manner 72-hours post-treatment cessation, with a statistically significant increase compared to 24 and 48-hour time points observed at all concentrations (p-value <0.01). 72-hours post treatment cessation there was no significant difference between the size of the apoptotic population following treatment with any of the designated concentrations of dimethyl fumarate, with all concentrations inducing apoptosis in ~70% of treated cells.

As seen in Figure 3.11d, there was no significant phase redistribution of the apoptotic population following 24 or 48-hour incubation after dimethyl fumarate treatment compared to an untreated control. Following 72-hour incubation there was a significant increase in the size of the late apoptotic populations compared to cells incubated for 24 or 48-hours (p-value <0.01). This increase correlated positively with concentration.

The temozolomide-dimethyl fumarate combination induced apoptosis in a similar pattern to temozolomide as a single agent (Figure 3.11e & a respectively). There was no

significant induction of apoptosis above basal levels 24 or 48-hours after treatment cessation, and no significant difference between each concentration of the temozolomide-dimethyl fumarate combination (p-value >0.05). The apoptotic population detected after treatment with the temozolomide-dimethyl fumarate combination was significantly smaller than the corresponding concentrations of dimethyl fumarate as a single agent at the 72-hour time point (p-value <0.05) (Figure 3.11c & e) but was not significantly different than anytime point or concentration of temozolomide (p-value >0.05) (Figure 3.11a & f).

As seen in Figure 3.11f, there was no significant redistribution of apoptotic cells 24 or 48-hours post treatment cessation compared to the basal population or the correspondent concentrations of each single agent (p-value >0.05). The late apoptotic population detected following combination treatment were significantly smaller than the corresponding populations detected following treatment with dimethyl fumarate as a single agent at the 72-hour timepoint (p-value <0.05) (Figure 3.11f & d). There was a no significant difference between apoptotic phases following treatment with the temozolomide-dimethyl fumarate combination and temozolomide as a single agent (p-value >0.05) (Figure 3.11b & f).

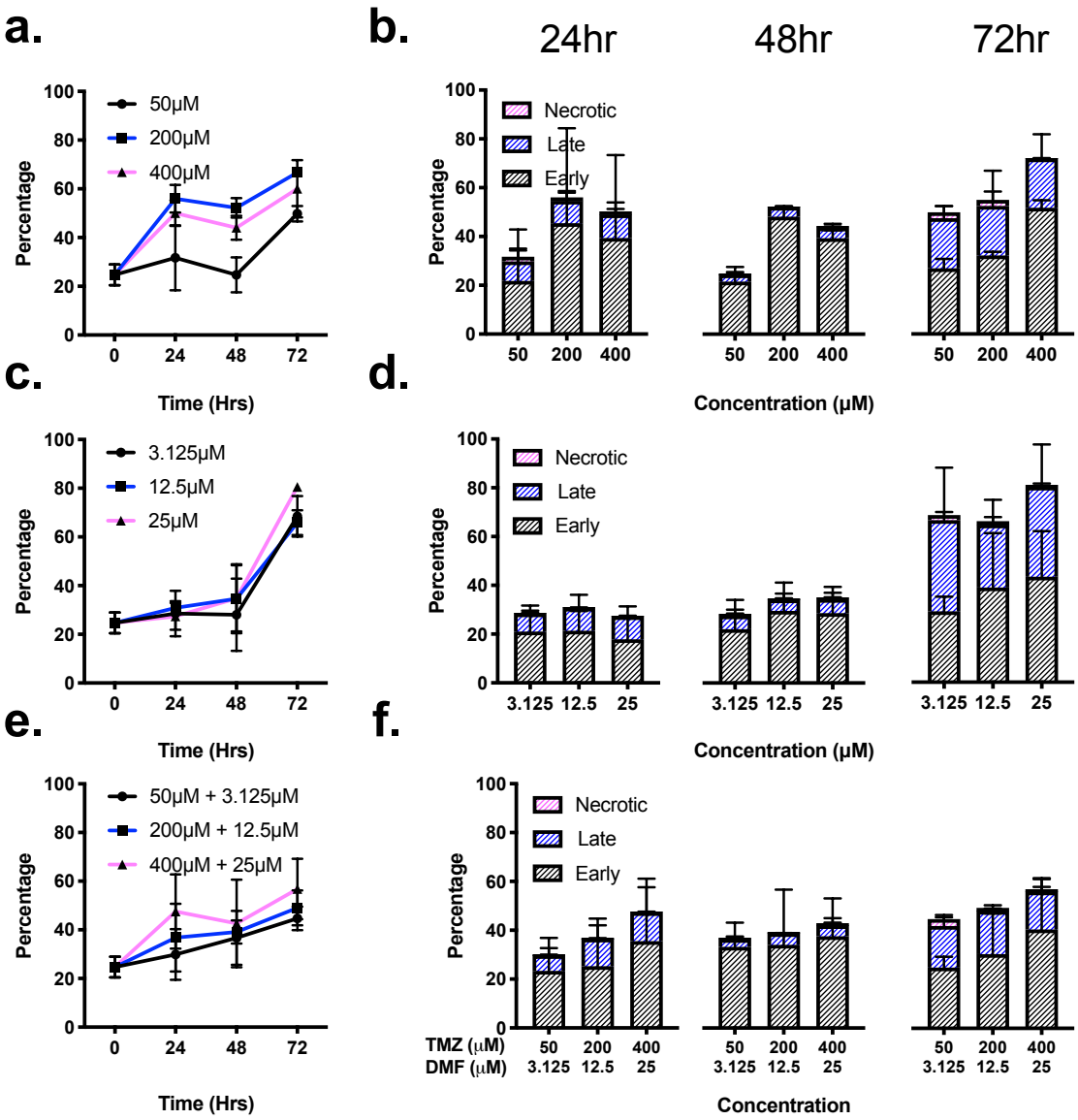

Figure 3.11: Induction of apoptosis in T98g cells by temozolomide, dimethyl fumarate and the temozolomide-dimethyl fumarate combination. Apoptotic induction in UVW cells in response to increasing concentrations of temozolomide (**a.**) dimethyl fumarate (**c.**) or the temozolomide-dimethyl fumarate combination (**e.**) and apoptotic phase redistribution in response to increasing concentrations of temozolomide (**b.**) dimethyl fumarate (**d.**) or the temozolomide-dimethyl fumarate combination (**f.**). Data shown is an average of at least 3 independent experiments ± standard deviation. A 2-Way ANOVA with Bonferroni post-test was performed with p-values of <0.05 = *, <0.01=** and <0.001 = *** reported as significant. Statistics are reported in Appendix B2.

3.5 Discussion

3.5.1 Generation and rationale of therapeutic combinations

Combining chemotherapeutic agents with radiotherapy and surgery is the current standard of curative care for the majority of cancers. These combinations tend to consist of two or more cytotoxic chemotherapeutic agents as well as adjuvant or concomitant radiotherapy for solid tumours, which can cause systemic side effects and can result in poor patient compliance and possible treatment withdrawal if side effects begin to outweigh potential benefit (Bassan *et al.,* 2014; Clarke *et al.,* 2015; DeSantis *et al.,* 2014)

Combinations of drugs that target different cellular pathways are particularly important in cancers such as high-grade glioma where acquired drug resistance is frequently seen. By targeting different pathways, the cell is found to be under greater stress as the cancer cannot rely on a single pathway for metabolism, DNA damage repair or cell division. This also allows for a potential lowering of doses of each agent in a regimen as there should be synergistic effects between each agent (Doroshow and Simon, 2017; Makin, 2018; Pritchard *et al*., 2013; Yardley, 2013). These combinations described below were designed with the aim of increasing anti-glioblastoma activity, with each designed to target a specific aspect of the specific biology unique to the cancer, dimethyl fumarate should have a greater tumour specificity as astrocytes, the cells that glioblastoma is composed of (Louis *et al*., 2016), have a higher level of both glutathione (Dringen *et al*., 2000) and glutathione synthesis enzymes (Ali-Osman *et al*., 1997; Okcu *et al*., 2004) than neurons.

Glutathione acts as a major chemoresistance factor, capable of binding and inhibiting a huge variety of chemotherapeutic agents, including alkylating agents, spindle poisons and platinum based agents (Rocha *et al*., 2014, 2016; Townsend and Tew, 2003). The large number of chemotherapy agents that can be inactivated by glutathione, makes glutathione depletion an attractive therapeutic strategy for increasing cancer cell chemosensitivity. Upregulation and overexpression of enzymes involved in glutathione metabolism and catabolism is a common feature of a number of cancers. The difference in expression levels of glutathione and its precursor enzymes between healthy and malignant tissues should allow for a significant therapeutic differential to be achieved. In order for glutathione to successfully eliminate xenobiotic threats against DNA integrity,

the enzyme glutathione-s-transferase (GST) catalyses the nucleophilic attack of glutathione against reactive centres of these xenobiotics (Zhang *et al.,* 2014). These xenobiotic threats can include chemotherapeutic agents, meaning that GST expression and activity can increase chemoresistance (Allalunis-Turner *et al*., 1991; Townsend and Tew, 2003).

GST is overexpressed in a large proportion of cancers, with approximately 40% of all brain cancers overexpressing the GSTπ isoform (Hayat, 2014). High basal expression of GSTπ in patients with glioma correlates with worse overall survival compared to low or moderate expression levels. When examined by grade, overall survival was worse in grade IV glioma patients who also had higher GSTπ levels. Interestingly, there was also significantly poorer survival in glioma patients whose biopsies showed the presence of nuclear GSTπ rather than only cytoplasmic GSTπ. This is likely due to increased glutathione activity in the nucleus preventing expected levels of DNA damage by agents such as temozolomide, which elicit the majority of their effects in the nucleus (Ali-Osman *et al*., 1997; Okcu *et al*., 2004).

Treatment with DNA damaging agents has also been shown to increase expression levels of GSTπ, and this is believed to confer acquired drug resistance to a number of cancers. For example, elevated levels of GSTs are associated with increased resistance to apoptosis in response to DNA damaging agents (Balendiran *et al*., 2004; Townsend and Tew, 2003) *in vitro* in colon, pancreatic and breast cancer as well as leukaemia, glioma and myeloma (Dorr *et al*., 1986; Schnelldorfer *et al*., 2000). This is hypothesised to be due to the higher intracellular levels of glutathione preventing the action of these DNA damage agents, as well as the GST family inhibiting the pro-apoptotic MAP-K pathway through the suppression of apoptosis signal-regulating kinase 1 (ASK1), a protein involved in both TNF-α/FAS-mediated and apoptotic cell death via JNK & p38 signalling (Cho *et al.,* 2001).

Glutathione depletion using buthionine sulphoximine (BSO) has been shown to be an effective chemosensitisation strategy using a number of alkylating agents in a number of cancers; this includes the glioma cell lines U87, U138MG & U251MG which were sensitised to temozolomide and cisplatin, patient derived high-grade glioma cells (WHO Grade III-IV) being sensitised to nitrogen mustard and carmustine, and neuroblastoma

being sensitised to melphalan (Allalunis-Turner *et al.,*1991; Rocha *et al.*, 2014; Balendiran *et al.,* 2004).

We believe that dimethyl fumarate is a more appropriate option for depleting glutathione over BSO. Dimethyl fumarate is already clinically available as Tecfidera, and has known safety, toxicity and pharmacokinetic profiles. When utilised clinically, dimethyl fumarate has a low toxicity profile, showing immunomodulatory effects, as seen when used against psoriasis and multiple sclerosis (Bomprezzi, 2015), but is not immunosuppressive which is beneficial as alkylating agents such as temozolomide often cause immunosuppression as a side effect (Grossman *et al*., 2011; Longbrake *et al*., 2018). Concentrations of dimethyl fumarate used in this combination are well tolerated across the population, as seen in those suffering from multiple sclerosis and psoriasis. These doses are easily clinically achievable and should be well tolerated as they are below what is widely regarded as a therapeutic dose (100μM) (Wilms *et al*., 2010). Doses of BSO used to deplete glutathione *in vitro* are between 50μM and 100mM. Doses in the millimolar range, when administered *in vivo,* proved toxic through the intraperitoneal route, but not the perioral route (Dorr *et al*., 1986). At comparable doses of BSO notable side effects were observed in mice, which include potentially mutagenic deletions of up to 70kB in foetal mouse DNA (Reliene and Schiestl, 2006).

As far as we are aware, there is only one published study using dimethyl fumarate to sensitise cancerous cells to alkylating agents (Booth *et al.,* 2014). This study used a single concentration of temozolomide and dimethyl fumarate in combination and featured no mechanistic interrogation of the action of these two drugs when used in combination. There is currently an ongoing clinical trial, scheduled to finish in November 2018 examining the effects of dimethyl fumarate in conjunction with temozolomide and radiotherapy (Shafer *et al.,* 2017; Trial NCT02337426). Recently published phase I results show that the addition of dimethyl fumarate to the current standard of care regimen yielded no increase in side-effects and no adverse reactions or safety concerns, allowing this trial to continue to phase II (Shafer *et al*., 2017).

As discussed in Section 3.4.1.3, combinations of temozolomide and dimethyl fumarate were designed with temozolomide in excess. This allowed for a clinically achievable dose of dimethyl fumarate being used at all concentrations of temozolomide – even doses of temozolomide greater than the accepted achievable plasma concentration of

~105μM (Patel *et al.,* 2003). The low toxicity of theses doses of dimethyl fumarate should allow for the full effects of glutathione depletion on temozolomide treated cells to be fully interrogated.

We hypothesised that a depletion in intracellular glutathione levels prior to temozolomide treatment would result in a temozolomide mediated increase in DNA damage, and through a cell cycle dependent mechanism, cell death will be induced (Rocha *et al.,* 2014). Furthermore, there is substantial evidence that both of these agents are potent radiosensitisers (Held *et al.,*1988; Kil *et al.,* 2008), and addition of radiation treatment to this combination is expected to enhance the hypothesised effects by increasing the overall amount of DNA damage induced, and also by dimethyl fumarate preventing glutathione mediated inhibition of reactive oxygen species, the major DNA damaging component of radiation.

3.5.2 Response of UVW and T98g human glioblastoma cells to single agents

Clonogenic assays were performed on the UVW and T98g cell lines treated with temozolomide and dimethyl fumarate to determine the effects of each of these agents on the sustained replicative ability and survival of each cell line. By examining the response of these cell lines to these agents, the experimental IC_{50} values of these agents could be compared to the literature IC_{50}, allowing us to validate future work using these cell lines. These values are also vital when designing combinations; ensuring appropriate concentrations of each drug are used. As the IC_{50} is a constant, responses to each drug in each cell line can be measured and compared, even when the values are massively different, this is of particular use when comparing two cell lines that have a different response to the same agent.

3.5.2.1 Temozolomide

The importance of the introduction of temozolomide as a treatment for glioma cannot be understated, the impact of the addition of temozolomide to the standard of care has led to an increase in 5-year survival from 1.9% to 9.8% in some patient groups (Perry *et al*., 2012). MGMT is the single biggest resistance factor to temozolomide, and MGMT promoter methylation is used clinically as a prognostic marker to predict the outcome of patient outcome to temozolomide therapy (Hegi *et al*., 2005; Perry *et al*., 2012).

There is a pronounced difference between UVW and T98g cells in response to treatment with temozolomide as seen in Figure 3.2a & b. UVW cells were highly sensitive to temozolomide, with just under 100% cell kill achieved after administration of 50μM of temozolomide. This is considerably lower than the average plasma concentration of temozolomide, measured at 104μM (Patel *et al.,* 2003) in the cerebrospinal fluid of non-human primates. We have also shown that UVW cells do not basally express the temozolomide resistance factor MGMT, explaining the sensitivity of these cells to temozolomide therapy (Figure 3.2c), this has been demonstrated previously (Chalmers *et al*., 2009). The IC_{50} of temozolomide in UVW cells was also similar to other temozolomide sensitive cell lines, where the IC_{50} which typically ranged from between 10 - 100μM (Hermisson *et al.,* 2006), although IC_{50} values of less than 10μm have been reported (van Nifterik *et al.,* 2007). It is likely that the UVW cell line has an epigenetically silenced MGMT promoter, resulting in the high level of temozolomide sensitivity we demonstrated in this cell line.

In contrast to the UVW cell line, T98g cells are highly resistant to temozolomide, with 50μM of temozolomide resulting in less than 7% cell kill, while the same concentration prevented virtually all colony formation in the UVW cell line. In agreement with other studies in the literature, we have shown that, that T98g cells basally express MGMT (Figure 3.2c), accounting for the high level of temozolomide resistance demonstrated in Figure 3.2b. The IC_{50} of temozolomide in the T98g cell of 400μM is significantly higher than an achievable intracranial concentration of temozolomide (Patel *et al*., 2003), meaning that temozolomide is ineffective in these cells, which translates to poor clinical outcome in these resistant patient groups (Dunn *et al.,* 2009; Hegi *et al.,* 2005). The literature IC_{50} for temozolomide in the T98g cell line varies hugely, with values from 250μM to concentrations greater than 3.5mM (Kislin *et al*., 2009; Lan *et al*., 2016; Lee, 2016; Montaldi and Sakamoto-Hojo, 2013; Zhang *et al*., 2015). Our experimental IC_{50} value of 400μM closely matched work performed by Yoshino *et al.,* (Yoshino *et al.,* 2010).

This difference in temozolomide induced cytotoxicity between the UVW and T98g cell lines in response to temozolomide is likely due to the ability of each cell line to repair DNA damage through MGMT (Hegi *et al*., 2005). Temozolomide is known to induce DNA damage in the form of O^6-methylguanine lesions (Friedman *et al*., 1998), and a failure to repair these lesions via activation of mismatch repair pathways leads to the formation

of double-stranded breaks (Li, 2008; Roos and Kaina, 2006). We have shown that T98g cells basally express MGMT, the protein that repairs these lesions, and that UVW cells do not. When the level of DNA damage was measured by detection of γH2a.X, a significant increase in damage was observed in UVW cells after 4 and 24 hours of treatment, but this was only observed after 24-hour treatment in the T98g cell line (Figure 3.8).

This level of DNA damage was expected to cause a G_2/M cell cycle arrest (Fragkos *et al*., 2009; Hirose *et al*., 2001) to prevent the cells from dividing with damaged or low-fidelity DNA (Friedman *et al*., 1998; Li, 2008). Consistent with the level of DNA damage, a concentration-dependent G_2/M arrest was seen following 4-hour temozolomide exposure in UVW cells and following 24-hour exposure there was no concentration dependency on the magnitude of the G_2/M arrest, indicating an accumulation of cells with damaged DNA. There was no significant arrest in the T98g cell line after 4-hour treatment in keeping with the non-significant increase in DNA damage levels seen at this time point. Following 24-hour exposure to temozolomide, there was only G_2/M arrest at the highest concentration used, 400μM. Again, this correlates to the level of DNA damage seen following the same exposure to temozolomide. This evidence leads us to suggest that temozolomide induced DNA damage is an important factor in the induction of G_2/M cell cycle arrest, as the presence of DNA damage can be correlated with G_2/M arrest following exposures to temozolomide.

Furthermore, induction of apoptosis following temozolomide exposure was significantly greater in the UVW cell line than in the T98g cell line. There was no significant apoptotic induction in UVW cells until 48-hours post-temozolomide exposure. This effect was concentration-independent, and by 72-hours post-treatment induction, ~70% of the population was found to express apoptotic markers. Between 48-72 hours there was also a significant increase in the size of the late apoptotic population, indicating that cells are still actively undergoing apoptosis.

There was a lower level of apoptotic induction following temozolomide exposure in the T98g cell line, but the size of the apoptotic population appeared to be concentration dependent, with 50μM temozolomide inducing significantly lower expression of apoptotic markers than 200 or 400μM at the 24 and 48-hour time points. However, when compared to the UVW cell line, there was a more rapid induction of apoptosis, with apoptotic cells

detected 24-hours after temozolomide exposure was halted. However, the size of this population did not significantly increase between 24-72 hours post-treatment cessation. By 72-hours post treatment cessation, the last time point measured, there was no significant difference in the size of the apoptotic population between the three concentrations of temozolomide used. When the composition of each apoptotic population was analysed, there was no significant necrotic population found, and even at 72-hours, the majority of apoptotic cells were in the early apoptotic phase. This in indicative of apoptosis resistance and may explain the smaller than expected apoptotic population.

Induction of apoptosis between 24-48 hours is in keeping with our knowledge of temozolomide, where apoptosis is induced following several aborted cycle of mismatch repair (Ochs and Kaina, 2000; Roos and Kaina, 2006; Roos *et al*., 2007; Sarkaria *et al*., 2008). Studies have shown that apoptosis can occur at time points earlier than 24-hours post-treatment. We believe that as we have shown that DNA damage and cell cycle arrest do not occur until 24-hours of treatment has been completed. Following this mismatch repair (MMR) cycles take place. These cycles take a significant amount of time to complete, and it is likely that between exposure and 48-hours post exposure, aborted MMR cycles are occurring, explaining the lack of apoptotic cells (Cahill *et al*., 2007; Friedman *et al*., 1998; Hunter *et al*., 2006; Roos and Kaina, 2006; Roos *et al*., 2007). Failed cycles of mismatch repair leads to DNA damage in the form of double stranded breaks (Kaina, 2003; Roos and Kaina, 2006; Roos *et al*., 2007), induction of double stranded breaks has been shown to be necessary for induction of temozolomide mediated apoptosis (Ochs and Kaina, 2000). This has been shown to take up to 120-hours (Ochs and Kaina, 2000). We believe that this indicates we have chosen appropriate time points for measuring induction of apoptosis. It has been suggested that both these cell lines have a high level of apoptotic resistance, likely through evasion of pro-apoptotic signals, a common motif in many cancers. This may go some way to explain how there is not an as large as expected apoptotic population, but significant cell kill is observed, these cells may be undergoing a different mode of cell death such as mitotic catastrophe or autophagy (Kanzawa *et al*., 2004). In an expansion of this, it may be a subpopulation of the UVW and T98g cell lines are apoptosis sensitive, and temozolomide may be targeting this population.

Temozolomide resistance is seen across the assays that have been performed, with T98g cells showing consistently less DNA damage, G_2/M cell cycle arrest and induction of apoptosis at significantly higher concentrations than the UVW cell line. This is consistent with our knowledge of the MGMT status of T98g and the formation of O^6-methylguanine lesions by temozolomide (Roos & Kaina, 2006). These assays combine to show how harmful MGMT is for high-grade glioma patients treated with temozolomide, as temozolomide has a negligible effect while the patients will still be open to the significant side effect profile of temozolomide.

3.5.2.2 Dimethyl fumarate

Glutathione is a hugely important intracellular peptide, protecting the cell from oxidative stress and xenobiotics (Forman *et al.,* 2009). In cancer, the role of glutathione is often more harmful, contributing to both chemo and radioresistance (Balendiran *et al.,* 2004). Dimethyl fumarate is a known inhibitor of glutathione (Lin *et al.,* 2011), which has the potential to make dimethyl fumarate a potent radio and chemosensitiser (Rocha *et al.,* 2014).

In both UVW and T98g cells dimethyl fumarate induces a biphasic response, with an initial increase in toxicity, before a distinct plateau phase. This may be due to a number of factors. Dimethyl fumarate may be binding intracellular glutathione, allowing for the higher levels of intracellular ROS associated with malignant tissue to damage the DNA beyond repair, resulting in toxicity (Schumacker, 2015; Sullivan *et al.,* 2013). There is also the possibility that dimethyl fumarate is saturating the cell and binding all available glutathione. This may result in a stress response, during which the cell induces cell death as a result of the glutathione depletion (De Nicola and Ghibelli, 2014).

A combination of these two proposed mechanisms has been shown using high concentrations of buthionine sulphoximine (BSO) in the PW B-cell lymphoma cell line (Armstrong *et al*., 2002). In this study, 1mM BSO treatment for between 24-72 hours critically depleted glutathione, causing an increase in intra-cellular reactive oxygen species (ROS). This intracellular ROS caused a translocation in cytochrome-C from the mitochondria, resulting in the cleavage of caspase-3, and the induction of apoptosis (Armstrong *et al*., 2002).

In the context of Figure 3.3, we hypothesise that there is dimethyl fumarate mediated glutathione depletion at all concentrations between 0-100μM, but maximal glutathione depletion is observed after administration of 25μM of dimethyl fumarate, explaining why there is no significant increase in cytotoxicity beyond 25μM in either cell line.

Another possible mechanism is through dimethyl fumarate mediated NRF2 activation. NRF2 is an antioxidant transcription factor, which induces the expression of a large number of chemo- and radioprotective target genes. It may be that concentrations of less than 10μM are able to bind glutathione, allowing for intracellular ROS to damage DNA and induce apoptosis, but at concentrations greater than 25μM, NRF2 is activated by dimethyl fumarate, resulting in a cascade of anti-oxidant genes being transcribed, and quenching the intracellular ROS (Brennan *et al.,* 2015; Wang *et al.,* 2008).

In our study there was no measurable DNA damage following 4 or 24-hour exposure to dimethyl fumarate in either UVW or T98g cell lines and no significant cell cycle arrest at the same time points in either cell line. This is in keeping with our limited knowledge of dimethyl fumarates mode of action, as no effects on the cell cycle or DNA damage have been reported in the literature. Dimethyl fumarate is, however, a potent inducer of apoptosis in both UVW and T98g cells. This effect appears to be concentration independent in both cell lines with ~80% and ~75% of all UVW and T98g cells expressing apoptotic markers 72-hours after treatment was halted. In UVW cells apoptosis was induced by 48-hours post treatment cessation, with the majority of the apoptotic population being in the early apoptotic phase. T98g cells demonstrated increased resistance to dimethyl fumarate induced apoptosis compared to UVW cells, with apoptotic induction occurring later following treatment cessation.

During previously reported studies, glutathione depletion induced apoptosis via cytochrome-C translocation and subsequent caspase-3 induction without DNA damage or cell cycle arrest (Armstrong *et al*., 2002; De Nicola and Ghibelli, 2014). As we were unable to detect any changes in cell cycle progression or any DNA damage, we propose that dimethyl fumarate is inducing apoptosis directly through glutathione depletion, independently of p53. This is supported by the lack of G_2/M arrest seen when UVW and T98g cells were treated with dimethyl fumarate, as p53 induced apoptosis is strongly correlated with a DNA damage induced G_2/M arrest (Agarwal *et al*., 1995; Hirose *et al*.,

2001; Kaina, 2003; Pietenpol and Stewart, 2002; Roos and Kaina, 2006). However further assays are needed to fully verify this hypothesis.

3.5.3 Response of UVW and T98g human glioblastoma cells to the temozolomide-dimethyl fumarate combination

It was hypothesised that the combination of temozolomide and dimethyl fumarate would potentiate the effects of temozolomide therapy UVW and T98g human glioblastoma cells. Assays were chosen to interrogate the hypothesised mechanism of action of temozolomide and show how dimethyl fumarate influenced these mechanisms. These assays were also chosen to observe the effects of dimethyl fumarate as a single agent, as the literature is lacking in information on dimethyl fumarate as an anti-cancer agent.

As discussed, the principle of glutathione depletion to sensitise cancer to chemotherapy has been well documented (Allalunis-Turner *et al*., 1991; Rocha *et al*., 2014). The single study using dimethyl fumarate in combination with temozolomide shows a significant increase in cell kill, but features no mechanistic interrogation of how this cell kill is occurring and no mention of glutathione as a target (Booth *et al*., 2014) .

We have shown that by combining temozolomide and dimethyl fumarate in a fixed ratio, we can significantly increase the level of cell kill compared to either single agent, and using a mathematical modelling approach, we can describe this combination in terms of both single agents at one time. Our data demonstrated that the combination of temozolomide and dimethyl fumarate is supra-additive in the UVW cell line, and supra-additive at the majority of combinations in the T98g cell line. We believe that this supports our hypothesis that the addition of dimethyl fumarate to temozolomide therapy increases cell kill in both temozolomide sensitive and temozolomide resistant cell lines.

However, our hypothesis that dimethyl fumarate will potentiate the effects of temozolomide has not been validated. It has previously been demonstrated by Rocha (2014) demonstrated that depleting glutathione in glioma cells prior to addition of a DNA damaging agent – either cisplatin or temozolomide – significantly increased the level of DNA damage inflicted by either drug as measured γH2a.X levels (Rocha *et al*., 2014). Congruently with our results, this study has shown that the addition of a glutathione inhibitor had no effect on DNA damage (Rocha *et al*., 2014). Our results also show no

significant increase in the level of DNA damage when glutathione depletion was combined with a DNA damaging agent. This increase was expected but not observed, perhaps due to a threshold in the detection of FITC-γH2a.X. by flow cytometry, or there may not have been an increase in DNA damage at all. Further assays using confocal microscopy for γH2a.X detection may be more sensitive and allow us to distinguish a difference between the level of γH2a.X between temozolomide and the temozolomide-dimethyl fumarate combination. Time constraints prevented these assays being performed during the course of this study.

An increase in the size of the temozolomide mediated G_2/M arrest was expected, as our hypothesis stated that there would be an increase in the intra-cellular concentrations of temozolomide, and temozolomide is known to induce a G_2/M arrest (Hirose *et al*., 2001). Similarly to our reported γH2a.X data, there was no significant increase in the size of the G_2/M population between the temozolomide and temozolomide-dimethyl fumarate combination treated groups. This agrees with our γH2a.X data, as a significant increase in DNA damage would induce a G_2/M arrest (Fragkos *et al*., 2009).

An increase in the size of the apoptotic population between the single agent and combination treated cells was also expected. Temozolomide and the temozolomide-dimethyl fumarate combination induced apoptosis in very similar patterns, with no discernible difference between these two groups. Dimethyl fumarate induced apoptosis in a distinct pattern from the combination. This is likely through dimethyl fumarate inducing apoptosis directly through glutathione depletion, which triggers apoptosis through the mitochondrial pathway (Armstrong *et al*., 2002; De Nicola and Ghibelli, 2014). Temozolomide induces apoptosis through p53 which is activated by O^6-methylguanine lesions (Roos and Kaina, 2006). This supports our hypothesis that dimethyl fumarate is potentiating the effects of temozolomide, as we believe the combination would be inducing apoptosis through p53, rather than through mitochondrial depolarisation. Although we see no significant difference between the size of the apoptotic population in temozolomide or temozolomide-dimethyl fumarate combination treated cells, there was a significantly larger necrotic population following combination treatment, indicating that these cells are undergoing cell death at a faster rate. This could be indicative of greater p53 activation caused by a greater number of O^6-methylguanine lesions in these cells. There is a discrepancy between the size of the apoptotic population and the level of cell kill achieved by equivalent concentrations of

temozolomide. This is likely due to differences in the sensitivity of the methods used, and presence of apoptotic markers is not always directly correspondent to the level of cell kill achieved by treatment. Further assays are needed to further explore if and how dimethyl fumarate mediated glutathione depletion can influence the standard of care therapy for high-grade glioma.

3.6 Conclusions

Temozolomide is a DNA damaging agent. This DNA damage takes the form of double stranded breaks in the DNA helix, which results in a G_2/M cell cycle arrest. Following several failed or aborted cycles of MMR, apoptosis will be induced.

It was hypothesised that adding the immunomodulatory drug dimethyl fumarate to systems treated with temozolomide would increase the effects of temozolomide, as dimethyl fumarate has been shown to decrease intracellular concentrations of the temozolomide resistance factor glutathione.

We have shown that addition of dimethyl fumarate to temozolomide therapy significantly increases cytotoxicity compared to cells treated with either drug as a single agent in a supra-additive manner. However, we have been unable to demonstrate an increase in the effects of temozolomide when cells were treated with the temozolomide-dimethyl fumarate combination. We believe that this is the first investigation into the mechanistics of dimethyl fumarate as an adjuvant therapy in glioma, and although we were unable to pinpoint a precise mechanism of action, our core hypothesis that the combination treatment would increase cell kill has been validated.

Chapter 4

The effects of temozolomide and dimethyl fumarate in combination with external beam X-irradiation on human glioblastoma cells

4.1 Introduction

Every patient diagnosed with high-grade glioma is treated with radiotherapy when appropriate to do so. On average, a patient will receive a total of 60Gy of external beam radiotherapy in fractions of 1.8-2Gy (Weller, 2011). The current standard of care for high-grade glioma is temozolomide therapy and radiotherapy (Dressler *et al*., 2019; Preusser *et al*., 2011; Stupp *et al*., 2009, 2010). Temozolomide is given as an adjuvant to radiotherapy (Stupp *et al*., 2005, 2010), but there is contradictory evidence as to whether or not temozolomide acts as a radiosensitiser (Kil *et al*., 2008; van Nifterik *et al*., 2007). There is also contradiction in the literature as to whether MGMT status effects potential temozolomide mediated radiosensitisation (Bobola *et al*., 2010; van Nifterik *et al*., 2007; Rivera *et al*., 2010; Sarkaria *et al*., 2006). MGMT status is also highly relevant as it has been suggested that methylation of the MGMT promoter results in improved response to radiation treatment (Bobola *et al*., 2010; Carlson *et al*., 2009; van Nifterik *et al*., 2007).

Temozolomide has been shown to radiosensitise primary glioblastoma cells and xenografts of the U87 glioma cell line by increasing DNA double strand breaks, overwhelming the capabilities of normal DNA damage repair mechanisms (Chakravarti *et al*., 2006). This has been shown to result in an increase in induction of mitotic catastrophe instead of induction of apoptotic pathways (Kil *et al*., 2008). The addition of bulky methyl groups to the DNA helix can also prevent DNA damage repair mechanisms from successfully interacting with the damaged site, leading to sustained DNA damage that cells struggle to repair.

Historically, there has been interest in the use of dimethyl fumarate as a radiosensitiser. Several studies have shown that dimethyl fumarate can act as potent hypoxic cell radiosensitiser (Held and Hopcia, 1993; Held *et al*., 1988). As external beam radiotherapy elicits the majority of its effects through generation of reactive oxygen species, hypoxic cells are known to be radioresistant due to the absence of ionisable oxygen, preventing DNA damage induced by reactive oxygen species (Dunne-Daly, 1999; Hall and Giaccia, 2012).

The precise mechanism of dimethyl fumarate mediated radiosensitisation has not been fully elucidated, but as it has been demonstrated that dimethyl fumarate inhibits glutathione, another acknowledged radioresistance factor, it is possible that dimethyl fumarate mediated inhibition of glutathione results in hypoxic cell radiosensitisation (Held *et al*., 1988). Glutathione elicits radiosensitisation by quenching free radical species (Dringen *et al*., 2000; Vos *et al*., 1986). It is therefore likely that in hypoxic tissue, which has lower levels of radiation-induced reactive oxygen species, glutathione will be able to more easily quench radiation induced oxidative stress, resulting in radioresistance (Harrison, 2002). We hypothesise that when dimethyl fumarate is added as an adjuvant to X-irradiation, glutathione is inhibited, there will be an increase in free reactive oxygen species (Xie *et al*., 2015), resulting in increased DNA damage and therefore increased radiosensitisation.

We further hypothesise that the combination of temozolomide and dimethyl fumarate will synergise with external beam X-irradiation. We believe that this will occur through dimethyl fumarate inhibiting intracellular glutathione resulting in higher intracellular temozolomide concentrations and higher ROS levels. This will increase DNA damage to a level greater than DNA damage response pathways could repair, resulting in increased cell death.

4.2 Aims and Objectives

The aims of this study were:

- To characterise the response of UVW and T98g human glioblastoma cells to external beam radiation delivered with the temozolomide-dimethyl fumarate combination

- To elucidate potential mechanisms of action and potential mechanisms of action and targets for the X-irradiated temozolomide-dimethyl fumarate combination

4.3 Materials and Methods

4.3.1 Cell lines and routine cell maintenance

All routine maintenance of cell lines was performed as described in Section 2.1.

4.3.2 Cell treatment

Temozolomide and dimethyl fumarate were prepared and treatment was performed as described in Section 2.2. The combination of temozolomide and dimethyl fumarate used was calculated as described in Sections 2.4 and 3.4.5.1 and seen below in Table 4.1. Experiments combining drug and radiation treatment were performed as described in Sections 2.3 and 2.4.

UVW	
Dimethyl fumarate (μM)	Temozolomide (μM)
0.3	0.5
3	5
9	15

T98g	
Dimethyl fumarate (μM)	Temozolomide (μM)
3.125	50
12.5	200
25	400

Table 4.1: The combinations of temozolomide and dimethyl fumarate used throughout Chapter 4. Design of this combination is described in Section 3.4.5.1

4.3.3 Clonogenic assay

Clonogenic assays were performed as described in Section 2.5.

4.3.4 Combination index analysis

Combination index analysis was performed using Calcusyn software as described as in Section 2.6.

4.3.5 Cell cycle analysis

Cell cycle analysis was performed as described in Section 2.7.

4.3.6 γH2a.X assays

γH2a.X assays were performed as described in Section 2.8.

4.3.7 Apoptosis detection through Annexin-V staining

Annexin V staining and detection was performed as described in Section 2.10

4.4 Results

4.4.1 Cytotoxicity of temozolomide and dimethyl fumarate as single agents in conjunction with external beam X-irradiation

Before assessing the effects of external beam X-irradiation in combination with the temozolomide-dimethyl fumarate combination, UVW and T98g cells were treated with temozolomide or dimethyl fumarate for 24-hours with exposure to either 1 or 3Gy of radiation occurring 2-hours after drug was added. This was undertaken to examine the response of each cell line to each single agent when combined with external beam radiotherapy.

4.4.1.1 Cytotoxic effects of X-irradiation as a single agent in UVW and T98g human glioblastoma cells

In order to assess the effects of external beam radiation on the survival of UVW and T98g cells, clonogenic assays were performed on each cell line following treatment with increasing doses of external beam X-irradiation. Figure 4.1 shows the response of UVW and T98g human glioblastoma cell lines to exposure to increasing doses of external beam X-irradiation, as measured by the clonogenic capacity of irradiated versus non-irradiated cells.

In response to exposure to increasing doses of external beam X-irradiation, UVW cells displayed a dose response relationship, best characterised using a linear quadratic model (R^2 >0.99). Statistically significant cytotoxicity, relative to an unirradiated control, was observed after exposure to 2Gy of external beam X-irradiation (p-value <0.05), corresponding to approximately 32±18.59% cell kill. Cell kill increased in a dose dependent manner, reaching 93±4.09% cell kill following exposure to 6Gy.

The T98g cell line also displayed a dose response relationship that is best characterised using a linear quadratic model in response to treatment with external beam radiation (R^2 >0.99). There was a statistically significantly increase in radiation induced cell kill after exposure of cells to 2Gy of external beam X-irradiation compared to an unirradiated control (p-value <0.05), corresponding to approximately 37±15.57% cell kill. Cell kill increased in a dose dependent manner, reaching approximately 72±9.52% cell kill at 6Gy. This is statistically significantly higher than the level of cell kill achieved by administration of the same radiation dose in the UVW cell line, showing that the T98g cell line displays increased radioresistance at higher radiation doses compared to the UVW cell line (p-value <0.05).

A line of best fit was applied using Graphpad Prism 8 Software to determine the IC_{50} of each cell line (UVW R^2 >0.9, T98g R^2 >0.9). The IC_{50} of UVW and T98g cell lines were 3.1 and 3.2Gy respectively.

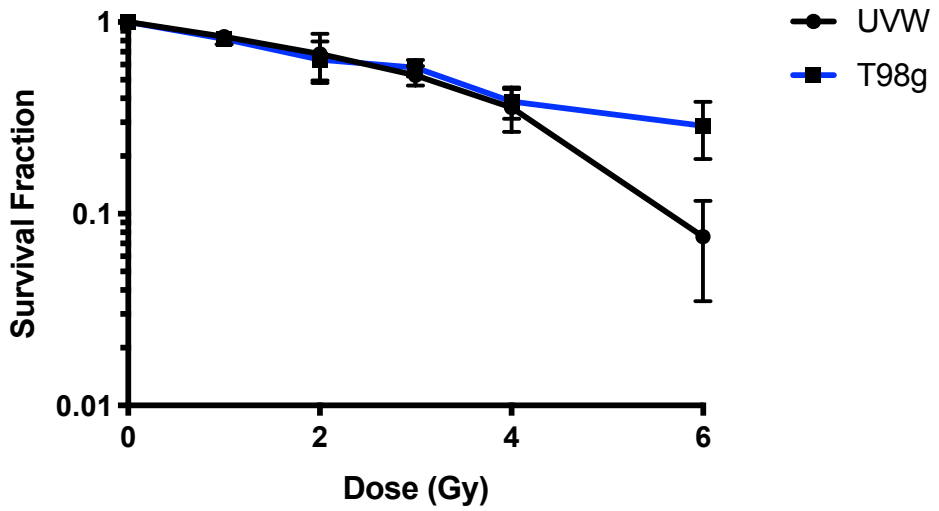

Figure 4.1: The effect of increasing doses of X-irradiation on the clonogenic capacity of UVW and T98g human glioblastoma cell lines. Data shown is an average of at least three independent experiments ± standard deviation. A 1-way ANOVA with Bonferroni post testing was performed using Graphpad Prism 8 software, with p-values of <0.05 = *, <0.01=** and <0.001 = *** reported as significant

4.4.1.2 Cytotoxicity of temozolomide and dimethyl fumarate in combination with external beam X-irradiation

In order to assess the effects of external beam X-irradiation in combination with temozolomide and dimethyl fumarate as single agents on the survival of UVW and T98g cells, clonogenic assays were performed on each cell line following treatment with increasing doses of temozolomide or dimethyl fumarate and exposure to 1 or 3Gy of external beam X-irradiation.

When compared to temozolomide as a single agent, temozolomide and external beam X-irradiation induced a significant increase in cell kill at all administered concentrations of temozolomide (significance represented by *).

Temozolomide mediated cell kill was significantly improved by addition of external beam X-irradiation from the lowest dose of temozolomide used, 0.5μM. Exposure to 1Gy of radiation induced a 30% increase in cell kill, with 37.5±6.03% cell kill being achieved (p-value <0.001) and 3Gy induced a 50% improvement in cell kill in 0.5μM treated cells, achieving 58.1±9.46% cell kill (p-value <0.001). As temozolomide concentration increased to 5μM, exposure to 1Gy of radiation induced cell kill in 53±4.29% of the population(p-value <0.001) and 3Gy induced cell kill in 65±14.8% of the population (p-value <0.001), compared to the cell kill induced by the same dose of temozolomide in non-irradiated cells.

At the highest concentration of temozolomide administered, 15μM, there was a similar increase in cytotoxicity following exposure to 1 or 3Gy of external beam X-irradiation, with cell kill increasing to 67±15.31% (p-value <0.01) and 86±3.87% (p-value <0.001) cell kill being achieved respectively compared to the cell kill induced by the same dose of temozolomide in non-irradiated cells.

As the administered concentration of temozolomide increased, X-irradiation appeared to have less radiosensitising effect as measured by percentage increase in cell kill (Figure 4.2a). However, the percentage change in cell kill compared to temozolomide treated but non-irradiated cells increased in a dose dependent manner, with a 32, 39 and 40% percentage increase in cell kill following 1Gy X-irradiation and a 55, 56 and 74% percentage increase following 3Gy of X-irradiation for each dose of temozolomide

respectively. This indicates that dose of both temozolomide and external beam X-irradiation are important for increased radiosensitisation.

When comparing X-irradiated cells to X-irradiated and temozolomide treated cells (significance represented by #), it was found that temozolomide and 1Gy induced significantly higher cell kill than 1Gy alone in a temozolomide dose dependent manner (p-value <0.05, <0.001, <0.001 respectively). However, temozolomide and 3Gy treatment did not induce significantly higher cell kill than 3Gy as a single agent at 0.5μM, the lowest dose of temozolomide administered (p-value >0.05). However 5μM and 15μM of temozolomide and 3Gy induced significantly higher cell kill than 3Gy alone (p-value <0.05 and <0.0001 respectively).

Figure 4.2c shows a summation of combination index analysis performed on data shown in Figure 4.2a. The data demonstrates that all concentrations of temozolomide in combination with 1 or 3Gy of external beam X-irradiation were supra-additive, indicating synergy between the two agents as the CI value was lower than 1. Taken together with the increase in cell kill when temozolomide was combined with external beam X-irradiation, we believe that this indicates that temozolomide is a radiosensitiser in the UVW cell line.

Dimethyl fumarate demonstrated less radiosensitising potential compared to temozolomide in the UVW cell line (Figure 4.2c). Increased cell kill appeared to be dependent on the administered dose of X-irradiation. Only concentrations of 3 and 9μM of dimethyl fumarate significantly increased the level of cell kill when combined with 1Gy of external beam radiation (p-value <0.01), but all concentrations of dimethyl fumarate significantly increased cell kill with 3Gy of X-irradiation compared to an untreated control.

When compared to dimethyl fumarate as a single agent, dimethyl fumarate in combination with 1Gy of external beam radiation only induced a significant increase in cytotoxicity after administration of 3μM of dimethyl fumarate (p-value <0.01). 3Gy in combination with dimethyl fumarate induced a greater level of cell kill compared to dimethyl fumarate as a single agent, with significance observed at each dose of dimethyl fumarate (p-value <0.001). At the highest concentration of dimethyl fumarate used, 9μM, there was an increase in cytotoxicity of only 9% when combined with 1Gy, but an increase of 19% was seen when combined with 3Gy.

Figure 4.2d shows a summation of combination index analysis performed on data shown in Figure 4.2b. Data shows that only the highest two concentrations of dimethyl fumarate in combination with 1Gy external beam X-irradiation were supra-additive and only 9μM of dimethyl fumarate in in combination with 3Gy external beam X-irradiation was supra-additive, indicating a lack of synergy between the two agents as the CI value was greater than 1. Taken with the lack of increase in cell kill when dimethyl fumarate was combined with external beam X-irradiation, we believe that this indicates that dimethyl fumarate is not capable of radiosensitisation in the UVW cell line

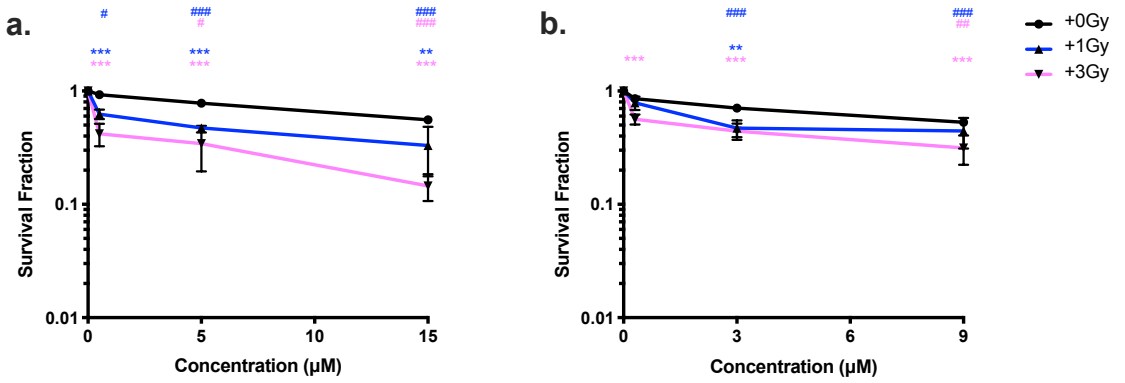

c.

	Fraction affected	CI value
0.5μM+1Gy	0.37	0.53
0.5μM+3Gy	0.58	1.01
5μM+1Gy	0.65	0.94
5μM+3Gy	0.52	0.53
15μM+1Gy	0.66	0.48
15μM+3Gy	0.85	0.55

d.

	Fraction affected	CI value
0.3μM+1Gy	0.21	1.04
0.3μM+3Gy	0.48	1.35
3μM+1Gy	0.52	0.53
3μM+3Gy	0.55	1.18
9μM+1Gy	0.55	0.75
9μM+3Gy	0.68	0.93

Figure 4.2: Dose response curves of the UVW human glioblastoma cell line to increasing doses of **a.** temozolomide or **b.** dimethyl fumarate with or without 1 or 3Gy external beam X-irradiation. Data shown is an average of at least three independent experiments ± standard deviation. The effects of X-irradiation on temozolomide and dimethyl fumarate as single agents was reported with p-values of <0.05 = *, <0.01=** and <0.001 = *** reported as significant. The effects of X-irradiation as a single agent compared to irradiated and drug treated cells was reported with p-values of <0.05 = #, <0.01=## and <0.001 = ### reported as significant.

In the MGMT positive T98g cell line, compared to temozolomide as a single agent, temozolomide in combination with 1Gy showed a significant improvement in cell kill from 50μM, with 73±6.83% cell kill being achieved (p-value <0.01). At 200μM there was a significant improvement in cell kill (p-value <0.01), with 40±2.65% cell kill being achieved. At 400μM+1Gy, there was no significant increase in cell kill compared to treatment with 400μM temozolomide alone (p-value >0.05) (Figure 4.3a).

In combination with 3Gy, temozolomide induced a significant improvement in cell kill at all doses used. At 50μM+3Gy, there was an improvement in cell kill compared to 3Gy alone (p-value <0.01). The largest increase in cell kill was seen after administration of 200μM of temozolomide, with treatment with this combination resulting in 49±12.86% cell kill (p-value <0.001). At 400μM, there was a significant increase in cell kill to 65±8.36 (p-value <0.05). This indicates that temozolomide can interact with external beam X-irradiation to improve cell kill.

In the T98g cell line, the combination of temozolomide and external beam X-irradiation induced no significant increase in cell kill compared to 1 or 3Gy of external beam X-irradiation as a single agent at the lowest concentration of temozolomide used, 50μM (p-value >0.05). Conversely, 200μM of temozolomide in combination with 1Gy significantly improved cell kill compared to 1Gy alone, (p-value <0.01). 200μM of temozolomide in combination with 3Gy of external beam X-irradiation offered no significant improvement in cell kill compared to 3Gy alone (p-value >0.05). In combination with external beam X-irradiation, 400μM of temozolomide showed a significant improvement in cell kill compared to 1 or 3Gy as single agents, with a 40±8.63 and 30±11.01% increase in cell kill respectively (p-value <0.001).

Figure 4.3c shows a summation of combination index analysis performed on data shown in Figure 4.3a. In combination with 1Gy of external beam X-irradiation, only 50 and 400μM of temozolomide resulted in a combination index value of less than 1, indicating synergy. Data shows that all concentrations of temozolomide in combination with 3Gy of external beam X-irradiation were not supra-additive, indicating a lack of synergy between the two agents as the CI value was greater than 1. Taken with the lack of increase in cell kill when temozolomide was combined with external beam X-irradiation, this indicates that temozolomide does not act as a radiosensitiser in the MGMT positive T98g cell line.

Compared to dimethyl fumarate as a single agent, the combination of dimethyl fumarate and 1Gy of external beam X-irradiation induced significantly higher cell kill only at 12.5μM, with a 20±3.21% increase in cell kill (p-value <0.01). All doses of dimethyl fumarate in combination with 3Gy induced significantly higher cell kill than dimethyl fumarate as a single agent, with an improvement in cell kill at 3.125, 12.5 and 25μM respectively (p-value <0.05, <0.001, <0.05), leading to 63±13.92% cell kill at the highest dose used (Figure 4.3b).

Dimethyl fumarate in combination with 1Gy induced significantly improved cell kill at concentrations of 12.5 and 25μM compared to 1Gy as a single agent (p-value <0.001). In combination with 3Gy, only 25μM dimethyl fumarate induced significantly higher cell kill than X-irradiation as a single agent, with an increase to 63±13.92% cell kill (p-value <0.01).

Figure 4.3d shows a summary of combination index analysis performed on data shown in Figure 4.3b. Data shows that only the highest two concentrations of dimethyl fumarate in combination with 1Gy external beam X-irradiation were supra-additive and no concentrations of dimethyl fumarate used in combination with 3Gy external beam X-irradiation were supra-additive, indicating a lack of synergy between the two agents as the CI value was greater than 1. Taken together with the lack of increase in cell kill when dimethyl fumarate was combined with external beam X-irradiation, we believe that this indicates that dimethyl fumarate does not act as a radiosensitiser in the T98g cell line.

Our data indicates that dimethyl fumarate does not act as a radiosensitiser in UVW or T98g human glioblastoma cell lines. Our data also indicates that MGMT status is a key factor that needs to be considered for temozolomide mediated radiosensitisation, as we have demonstrated temozolomide mediated radiosensitisation in only the MGMT negative UVW cell line.

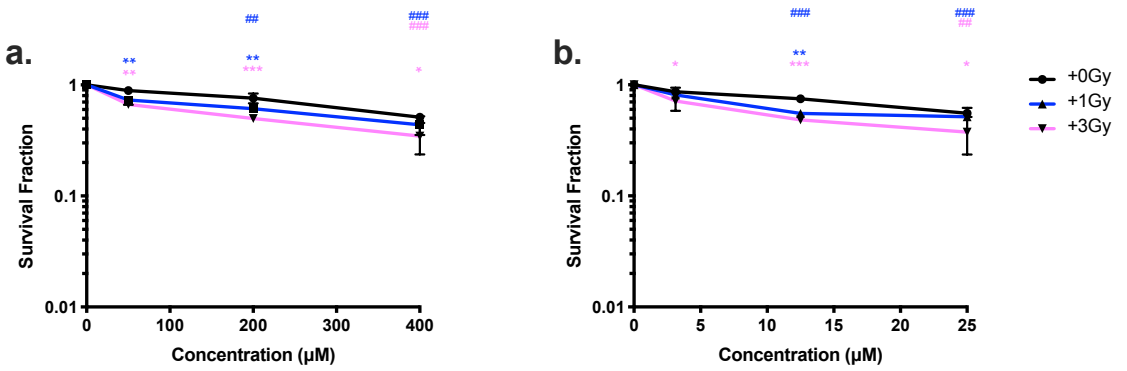

c.

	Fraction affected	CI value
50μM+1Gy	0.26	0.95
50μM+3Gy	0.33	1.81
200μM+1Gy	0.38	1.07
200μM+3Gy	0.50	1.34
400μM+1Gy	0.56	0.86
400μM+3Gy	0.65	0.99

d.

	Fraction affected	CI value
3.125μM+1Gy	0.18	1.46
3.125μM+3Gy	0..28	2.15
12.5μM+1Gy	0.51	0.58
12.5μM+3Gy	0.44	1.52
25μM+1Gy	0.62	0.53
25μM+3Gy	0.48	1.67

Figure 4.3: Dose response curves of the T98g human glioblastoma cell line to increasing doses of **a.** temozolomide or **b.** dimethyl fumarate with or without 1 or 3Gy external beam X-irradiation. Data shown is an average of at least three independent experiments ± standard deviation. The effects of X-irradiation on temozolomide and dimethyl fumarate as single agents was reported with p-values of <0.05 = *, <0.01=** and <0.001 = *** reported as significant. The effects of X-irradiation as a single agent compared to irradiated and drug treated cells was reported with p-values of <0.05 = #, <0.01=## and <0.001 = ### reported as significant.

4.4.2 Cytotoxic effects of the temozolomide-dimethyl fumarate combination in conjunction with external beam X-irradiation

Based on the results of combination index analysis in Figures 4.2 and 4.3, the temozolomide-dimethyl fumarate combination was taken forward to be used in combination with external beam X-irradiation. The effects of 1 or 3Gy of external beam X-irradiation in combination with the temozolomide-dimethyl fumarate combination on UVW and T98g human glioblastoma cell lines was investigated using clonogenic assays.

4.4.2.1 Cytotoxicity of the temozolomide-dimethyl fumarate combination with external beam X-irradiation

As seen in Figure 4.4a, the temozolomide-dimethyl fumarate combination significantly increased cell kill compared to X-irradiation as single agent (significance reported as #).

When temozolomide-dimethyl fumarate combination treated UVW cells were exposed to external beam X-irradiation, cell kill increased in a dose dependent manner. Following 1 or 3Gy X-irradiation, cell kill increased significantly compared to 1 or 3Gy as a single agent at all doses of temozolomide-dimethyl fumarate (p-value <0.001). There was no significant difference between 1 or 3Gy treated groups (p-value >0.05).

At the lowest dose of the temozolomide-dimethyl fumarate combination, which induced only 14±2.63% cell kill, 1Gy X-irradiation increased cell kill by 31% and 3Gy increased cell kill by 53%, with cell kill of 45±4.40% and 67±1.07% respectively compared to non-irradiated but temozolomide-dimethyl fumarate treated cells (p-value <0.01).

As the concentration of the temozolomide-dimethyl fumarate combination increased, cell kill also increased, with a 35 and 42% increase in cell kill following 1 or 3Gy X-irradiation, resulting in 65±2.26 and 72±1.03% cell kill respectively (p-value <0.001). The highest dose of the temozolomide-dimethyl fumarate combination increased cell kill by 33% and 46% following exposure with 1 and 3Gy respectively (p-value <0.001). This resulted in 80±7.39 and 93±3.90% cell kill being achieved with the temozolomide-dimethyl fumarate combination in combination with 1 or 3Gy of external beam X-irradiation.

Following exposure to 1Gy of external beam X-irradiation, all doses of the temozolomide-dimethyl fumarate induced higher levels of cell kill than the constitutive doses of temozolomide and dimethyl fumarate, however this increase was not significant (p-value >0.05) (Figure 4.4b). After exposure to 3Gy, the temozolomide-dimethyl fumarate combination induced significantly higher cell kill than 3 and 9μM dimethyl fumarate plus 3Gy (p-value <0.001). The temozolomide-dimethyl fumarate combination did not induce significantly higher cell kill compared to temozolomide following exposure to 3Gy of external beam X-irradiation (p-value >0.05).

This indicates that although the temozolomide-dimethyl fumarate combination appears to radiosensitise the UVW human glioblastoma cell, this radiosensitisation does not significantly improve cell kill compared to the combination of temozolomide and external beam X-irradiation.

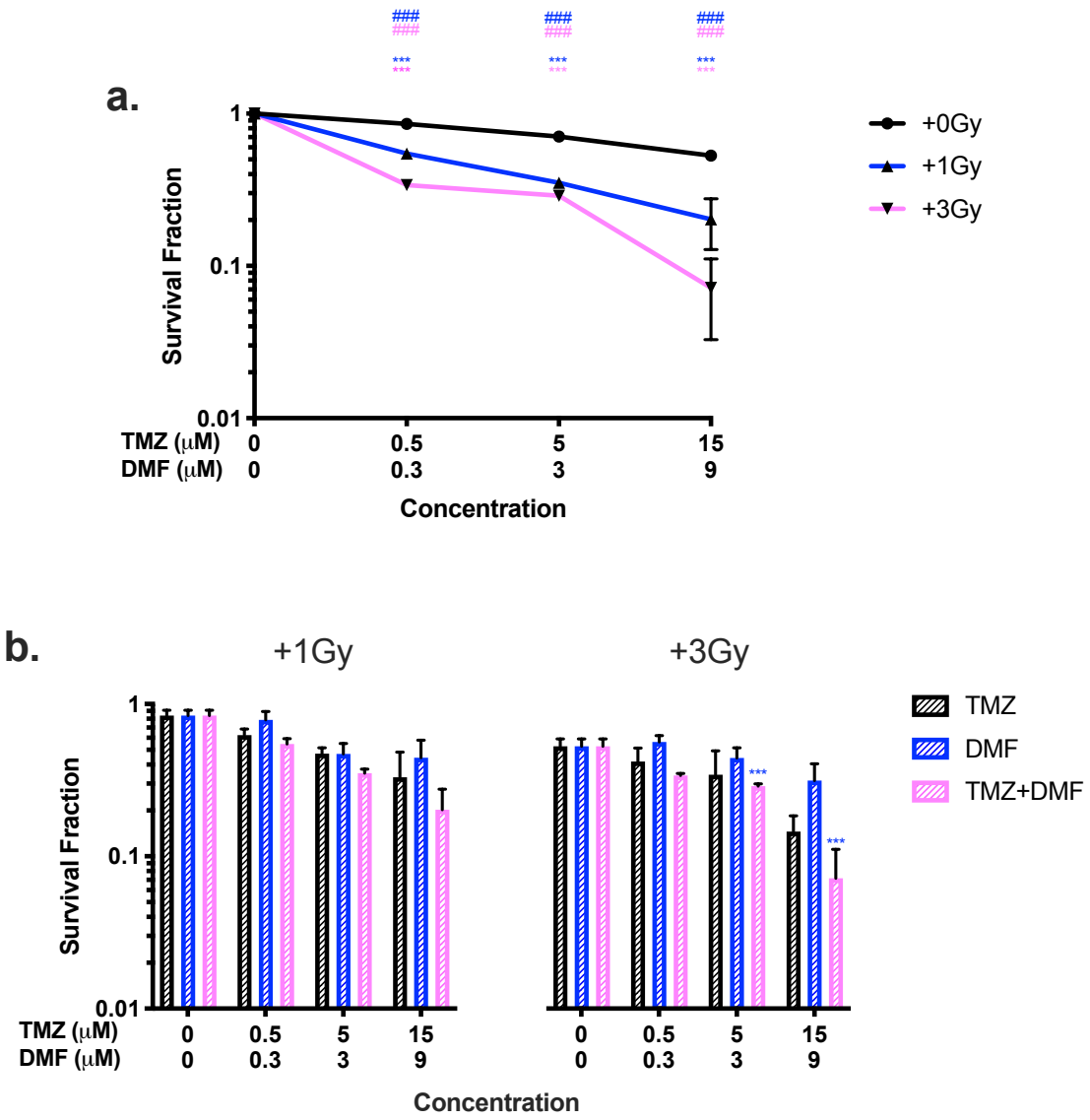

Figure 4.4: Dose response of the UVW human glioblastoma cell line to **a.** increasing doses of the temozolomide-dimethyl fumarate combination ± 1 or 3Gy external beam X-irradiation and **b.** the temozolomide-dimethyl fumarate combination ± 1 or 3Gy compared to temozolomide or dimethyl fumarate ± 1 or 3Gy of external beam X-irradiation. Data shown is an average of at least three independent experiments ± standard deviation. A 2-way ANOVA with Bonferroni multiple comparison was performed. The effects of X-irradiation on the temozolomide-dimethyl fumarate combination was reported with p-values of <0.05 = *, <0.01=** and <0.001 = *** reported as significant. The effects of X-irradiation as a single agent compared to irradiated and drug treated cells was reported with p-values of <0.05 = #, <0.01=## and <0.001 = ### reported as significant.

As seen in Figure 4.5a, the X-irradiated temozolomide-dimethyl fumarate combination displayed a significant increase in cell kill compared to X-irradiation as single agent (significance reported as #) in T98 human glioblastoma cells. Cell kill mediated by the X-irradiated temozolomide-dimethyl fumarate combination increased in a dose-dependent manner, but there was no significant difference in cell kill between 1Gy and 3Gy X-irradiated groups (p-value >0.05).

Cell kill in X-irradiated temozolomide-dimethyl fumarate combination treated groups was significantly higher than in non-irradiated temozolomide-dimethyl fumarate combination treated cells, with a 40% improvement in cell kill at the lowest combination used, 50μM+3.125μM, resulting in 55±3.99% cell kill when combined with 1Gy (p-value <0.001) and a 47% improvement in cell kill when the temozolomide-dimethyl fumarate combination was exposed to 3Gy of X-irradiation (p-value <0.001), giving 64±11.40% cell kill. This was significantly higher than the cell kill induced by 1Gy or 3Gy (p-value <0.001) as a single agent. All doses of the temozolomide-dimethyl fumarate combination induced significantly higher cell kill than X-irradiation as a single treatment (p-value <0.001).

The mesial dose of the temozolomide-dimethyl fumarate combination, 200μM+12.5μM, gave a 35% improvement in cell kill when combined with 1 or 3Gy external beam X-irradiation, resulting in 72±3.57 and 72±8.21% cell kill respectively (p-value <0.001) compared to the non-X-irradiated temozolomide-dimethyl fumarate combination. This level of cell kill was again higher than the cell kill induced by 1 or 3Gy of external beam X-irradiation as single agents (p-value <0.001). At the highest concentration of the temozolomide-dimethyl fumarate combination used, 400μM+25μM, there was a 32% and 37% increase in cell kill when drug treated cells were exposed to 1 or 3Gy of external beam x-irradiation respectively, resulting in 88±3.79 and 93±5.54% cell kill (p-value <0.01 & <0.001 respectively) compared to the non-X-irradiated temozolomide-dimethyl fumarate combination. This level of cell kill was again higher than the cell kill induced by 1 or 3Gy of external beam X-irradiation as single agents (p-value <0.001). This indicates that the temozolomide-dimethyl fumarate combination is capable of interacting with external beam X-irradiation in a synergistic manner.

As seen in Figure 4.5b, the X-irradiated temozolomide-dimethyl fumarate combination significantly improved cell kill compared to each single agent in combination with 1 or

3Gy of external beam X-irradiation. In combination with 1Gy, all doses of the temozolomide-dimethyl fumarate combination induced significantly higher cell kill than the constitutive doses temozolomide or dimethyl fumarate in combination with 1Gy (p-value <0.001). This trend was seen again with 3Gy. The temozolomide-dimethyl fumarate combination increased cell kill compared to 3Gy irradiated temozolomide or 3Gy irradiated dimethyl fumarate groups (p-value <0.001, <0.01 and <0.001 for each dose of the temozolomide-dimethyl fumarate combination respectively).

This data indicates that the temozolomide-dimethyl fumarate combination acts as a radiosensitiser in the T98g human glioblastoma cells despite neither temozolomide or dimethyl fumarate appearing to act as a radiosensitiser as single agents in this cell line.

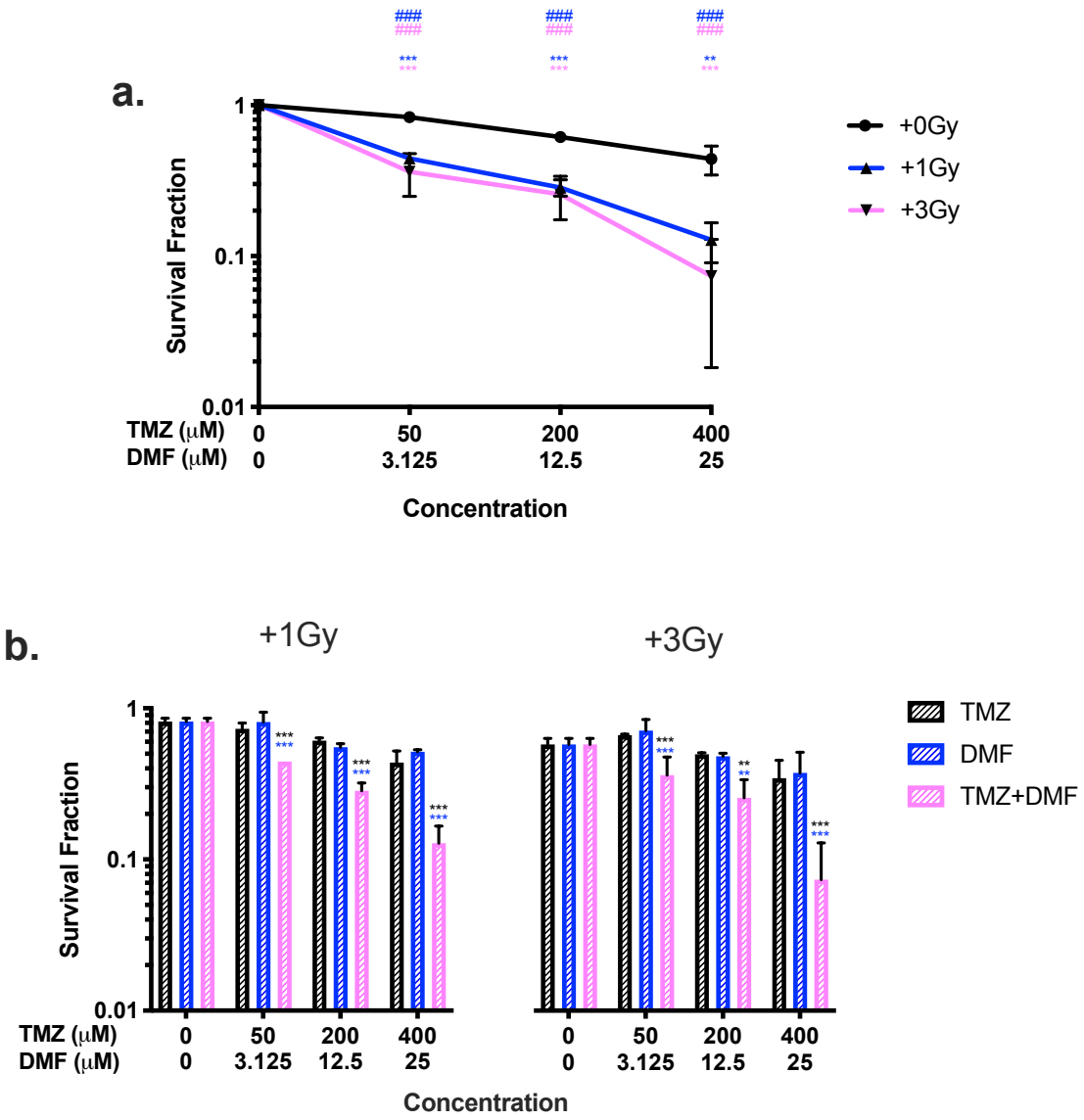

Figure 4.5: Dose response of the T98g human glioblastoma cell line to **a.** increasing doses of the temozolomide-dimethyl fumarate combination ± 1 or 3Gy external beam radiation and **b.** the temozolomide-dimethyl fumarate combination ± 1 or 3Gy compared to temozolomide or dimethyl fumarate ± 1 or 3Gy of external beam X-irradiation. Data shown is an average of at least three independent experiments ± standard deviation. A 2-way ANOVA with Bonferroni multiple comparison was performed. The effects of X-irradiation on the temozolomide-dimethyl fumarate combination was reported with p-values of <0.05 = *, <0.01=** and <0.001 = *** reported as significant. The effects of X-irradiation as a single agent compared to irradiated and drug treated cells was reported with p-values of <0.05 = #, <0.01=## and <0.001 = ### reported as significant.

4.4.3 Combination index analysis of the temozolomide-dimethyl fumarate combination and external beam radiation in UVW and T98g human glioblastoma cells

The use of combination index analysis allows for the relationship between two or more agents within a system to be defined in terms of infra-additivity, additivity or supra-additivity. Combination index analysis also allows for a combination that is considered supra-additive to be treated as a single agent. This allowed for the temozolomide-dimethyl fumarate combination to be considered a single agent. External beam X-irradiation was then used as a single agent, and combination index analysis performed defining the interaction between the temozolomide-dimethyl fumarate combination, external beam X-irradiation and the combination of both “single agents”. Due to the nature of combination index analysis, experimental data is shown (marked as symbols) as well as the line of fit calculated by calcusyn software. this is good

Combination index analysis of the X-irradiated temozolomide-dimethyl fumarate combination in UVW human glioblastoma cells was performed using Calcusyn software.

Figure 4.6 graphically represents the data shown in Figures 4.1 and Figure 4.4a that has been analysed using Caclusyn software (Section 2.6). Figure 4.6a shows the median effect plot (MEP). Data shows that increasing doses of the temozolomide-dimethyl fumarate combination increases the ratio of affected to unaffected cells. This is representative of the proportion of cells that have been affected by treatment, the effect measured and reported here is cell kill. The ratio, and therefore cell kill, increases when the temozolomide-dimethyl fumarate combination was irradiated, in a radiation-dose dose dependent manner. Radiation alone induced a dose-dependent increase on the ratio of affected to unaffected cells. R^2 values of the lines of best fit are shown in 4.6d.

Figure 4.6b shows the dose effect plot, showing that increasing dose of radiation, temozolomide-dimethyl fumarate combination or the temozolomide-dimethyl fumarate-radiation combination increases the effect measured – in this case cell kill. Due to the nature of combination index analysis, experimental data is shown (marked as symbols) as well as the line of fit calculated by calcusyn software. Increasing doses of radiation correlated linearly with effect, as did the temozolomide-dimethyl fumarate combination. When cells treated with the temozolomide-dimethyl fumarate combination were irradiated, there was a radiation dose dependent increase in the effect measured.

Figure 4.6c shows the combination index plot of the X-irradiated temozolomide-dimethyl fumarate combination, with each point representing the additivity of each fraction affected by the treatment This data shows that the effect of 1Gy of external beam X-irradiation and all doses of the temozolomide-fumarate combination used can be described as synergistic, as the combination index (CI) value for the effect of each treatment is less than 1.

Only 15μM+9μM, the highest dose of the temozolomide-dimethyl fumarate combination induced a synergistic effect when combined with 3Gy of X-irradiation as defined by the CI value being lower than 1. When exposed to 3Gy of X-irradiation the effect of the two lower doses of the temozolomide-dimethyl fumarate combination was infra-additive, having a CI value of greater than 1. However, the R^2 values of the 3Gy irradiated temozolomide-dimethyl fumarate combination were lower than typically required for high fidelity combination index analysis (Figure 4.6d). This can be seen in Figure 4.6 and b, with the central point outlying the line of fit (pink). This means that the output of the combination index analysis performed may be negatively affected and may not be an accurate representative of the data.

The CI values and corresponding fractions affected by each combination are seen in Figure 4.6e. This indicates the temozolomide-dimethyl fumarate combination is capable of radiosensitising UVW human glioblastoma cells to 1, but not 3Gy of external beam X-irradiation

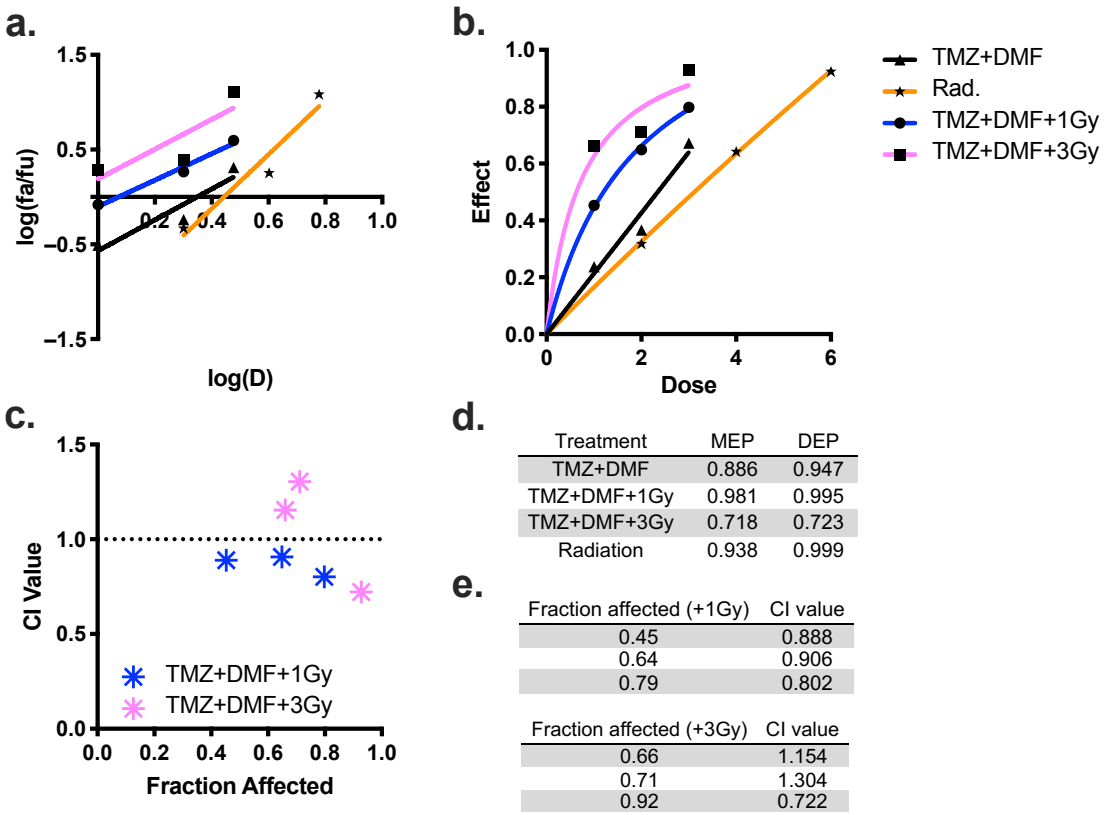

d.

Treatment	MEP	DEP
TMZ+DMF	0.886	0.947
TMZ+DMF+1Gy	0.981	0.995
TMZ+DMF+3Gy	0.718	0.723
Radiation	0.938	0.999

e.

Fraction affected (+1Gy)	CI value
0.45	0.888
0.64	0.906
0.79	0.802

Fraction affected (+3Gy)	CI value
0.66	1.154
0.71	1.304
0.92	0.722

Figure 4.6: Combination Index analysis of the X-irradiated temozolomide-dimethyl fumarate combination in UVW human glioblastoma cells. **a.** increasing doses of external beam X-irradiation (★), the temozolomide-dimethyl fumarate combination (▲), and the temozolomide-dimethyl fumarate combination +1Gy (●) or +3Gy (■) against the logarithmic ratio of the affected fraction to unaffected fraction with associated lines of best fit. **b.** the effects of increasing dose of external beam irradiation, the temozolomide-dimethyl fumarate combination ± 1 or 3Gy of external beam radiotherapy on the population analysed. **c** the combination index value of each fraction affected for each dose of the temozolomide dimethyl fumarate combination plus 1 or 3Gy of X-irradiation. **d.** the R^2 values for each line of best fit in Figure 4.6a & b. **e.** The combination index values and associated fraction affected for each dose in the temozolomide-dimethyl fumarate combination with 1 or 3Gy external beam X-irradiation.

Combination index analysis of the X-irradiated temozolomide-dimethyl fumarate combination in T98g human glioblastoma cells was performed using Calcusyn software.

Figure 4.7 graphically represents the data shown in Figures 4.1 and Figure 4.4a that has been analysed using Caclusyn software (Section 2.6). Figure 4.7a shows the median effect plot (MEP). The data suggests that increasing doses of the temozolomide-dimethyl fumarate combination increases the ratio of affected to unaffected cells. The ratio increases when the temozolomide-dimethyl fumarate combination was irradiated, in a radiation-dose dose dependent manner. Radiation alone induced a dose-dependent effect on the ratio of affected to unaffected cells. R^2 values of the lines of best fit are shown in 4.7d.

Figure 4.7b shows the dose effect plot, showing that increasing dose of radiation, temozolomide-dimethyl fumarate combination or the temozolomide-dimethyl fumarate-radiation combination increases the effect measured – in this case cell kill. Due to the nature of combination index analysis, experimental data is shown (marked as symbols) as well as the line of fit calculated by Calcusyn software. Increasing doses of radiation correlated linearly with effect, as did the temozolomide-dimethyl fumarate combination, indicating a strong dose response relationship. When the temozolomide-dimethyl fumarate combination was irradiated, there was a radiation dose dependent increase in the effect measured.

Figure 4.7c shows the combination index plot of the X-irradiated temozolomide-dimethyl fumarate combination, with each point representing the additivity of each fraction affected by the treatment This data shows that the effect of 1Gy and 3Gy of external beam X-irradiation and all doses of the temozolomide-fumarate combination used can be described as synergistic, as the combination index (CI) value for the effect of each treatment is less than 1.

The CI values and corresponding fractions affected by each combination are seen in Figure 4.7e. This indicates the temozolomide-dimethyl fumarate combination is capable of radiosensitising T98g human glioblastoma cells to 1 and 3Gy of external beam X-irradiation

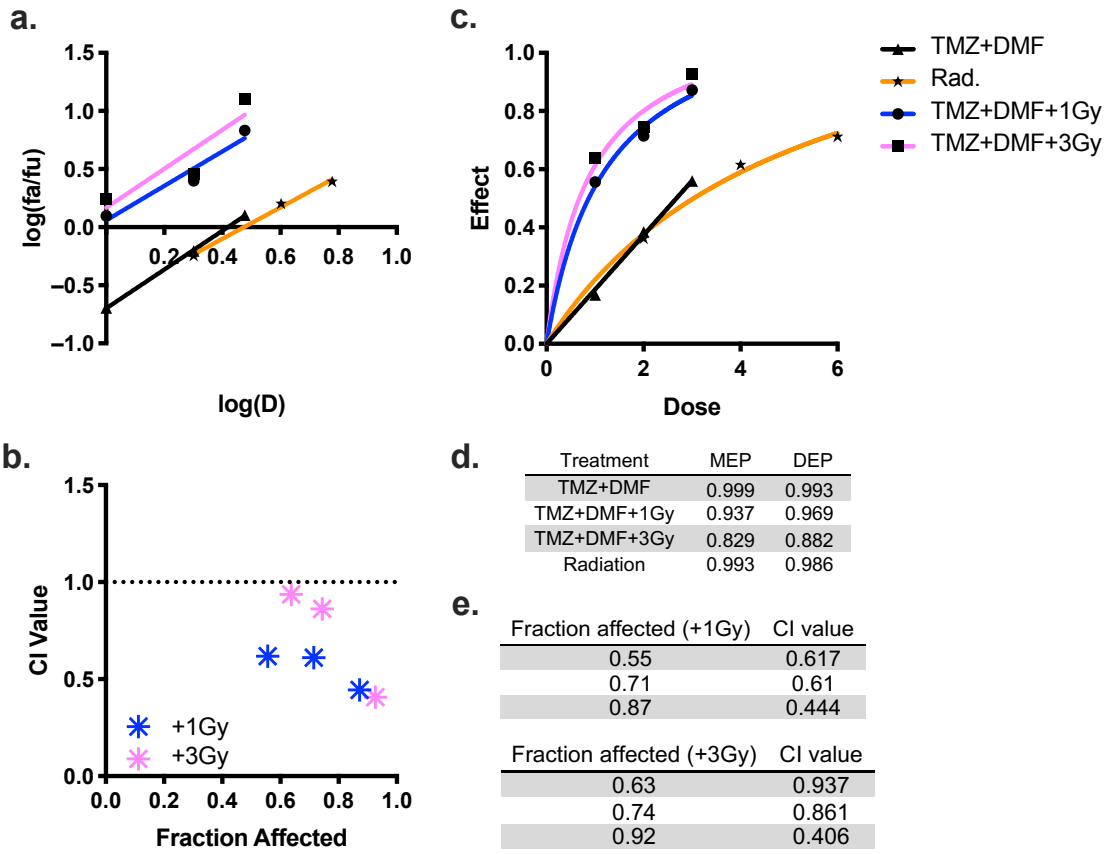

d.

Treatment	MEP	DEP
TMZ+DMF	0.999	0.993
TMZ+DMF+1Gy	0.937	0.969
TMZ+DMF+3Gy	0.829	0.882
Radiation	0.993	0.986

e.

Fraction affected (+1Gy)	CI value
0.55	0.617
0.71	0.61
0.87	0.444

Fraction affected (+3Gy)	CI value
0.63	0.937
0.74	0.861
0.92	0.406

Figure 4.7: Combination Index analysis of the X-irradiated temozolomide-dimethyl fumarate combination in T98g human glioblastoma cells. **a.** increasing doses of external beam X-irradiation (★), the temozolomide-dimethyl fumarate combination (▲), and the temozolomide-dimethyl fumarate combination +1Gy (●) or +3Gy (■) against the logarithmic ratio of the affected fraction to unaffected fraction with associated lines of best fit. **b.** the effects of increasing dose of external beam irradiation, the temozolomide-dimethyl fumarate combination ± 1 or 3Gy of external beam radiotherapy on the population analysed. **c** the combination index value of each fraction affected for each dose of the temozolomide dimethyl fumarate combination plus 1 or 3Gy of X-irradiation. **d.** the R^2 values for each line of best fit in Figure 4.7a & b. **e.** The combination index values and associated fraction affected for each dose in the temozolomide-dimethyl fumarate combination with 1 or 3Gy external beam X-irradiation.

4.4.4 Quantification of DNA double stranded breaks in UVW and T98g human glioblastoma cells in response to treatment with the X-irradiated temozolomide-dimethyl fumarate combination

In order to assess the dynamics of DNA damage and repair, phosphorylation of Ser139-H2a.X was quantified by detection of a FITC-conjugated anti–Ser139 H2A.x antibody. H2a.X phosphorylation is a hallmark of double stranded breaks in DNA. Double stranded breaks recruit the ATM/ATR complex, which initiates a cascade that results in H2a.X phosphorylation and G_2/M arrest.

Phosphorylation of H2a.X was quantified by detection of a FITC-conjugated anti–Ser139 γH2a.X antibody. Cells were treated with combinations of temozolomide and dimethyl fumarate with the addition of 1 or 3Gy of external beam x-irradiation. Flow cytometric analysis was performed, with fold increase in γH2a.X levels compared to untreated but stained control cells reported. Cells were treated for 4 or 24-hours to assess the dynamics of DNA damage and repair over time. An increase in double stranded breaks was expected to be seen with the X-irradiated temozolomide-dimethyl fumarate combination due to the increased cell kill seen in Figure 4.4 and 4.5

In UVW cells external beam X-irradiation induced a significant 3.6±0.81 and 5.2±0.74-fold increase in DNA damage 4 hours after treatment with 1 (p-value <0.01) or 3Gy (p-value <0.001) respectively. This level of DNA damage almost doubled 24-hours post exposure with 1 or 3Gy of external beam X-irradiation, with a 6.9±1.30 (p-value <0.05) and 8.6±2.38-fold (p-value <0.001) increase respectively. However, there was no statistically significant difference in γH2a.X levels between 1 or 3Gy irradiated groups at either time point, and no statistically significant variation in DNA damage between time points. This indicates that external beam X-irradiation increases DNA double stranded breaks in a dose dependent manner, in keeping with our knowledge of external beam X-irradiation and the DNA damage repair response, however, our data indicates that the expected resolution of DNA damage after 24-hours was not observed.

Temozolomide increased DNA damage in UVW cells, with a 2.7±0.60 and 3.8±0.51-fold increase in γH2a.X levels following 4 or 24-hour exposure. Following 4-hour temozolomide treatment and X-irradiation, there was a 4.4±1.99-fold increase in DNA damage with 1Gy of external beam X-irradiation and a 6.3±1.96-fold increase when

temozolomide was combined with 3Gy of external beam X-irradiation (p-value <0.001). After 24-hour temozolomide exposure, DNA damage increased 8.2±1.00 and 10.1±2.22-fold when combined with 1Gy or 3Gy of external beam X-irradiation respectively, however only the increase mediated by 15μM temozolomide and 3Gy was statistically significant (p-value <0.01) compared to 15μM of temozolomide alone. treated cells There was no statistically significant difference between 1 or 3Gy irradiated groups at either time point, and no statistically significant variation in DNA damage between time points. (p-value >0.05). This indicates that the combination of temozolomide and external beam X-irradiation increases DNA damage, but this is not greater than the level of DNA damage induced by external beam X-irradiation alone.

Increased DNA damage was seen in UVW cells treated with dimethyl fumarate and external beam X-irradiation compared to drug treated but non-irradiated cells. This increase was significant following 4-hour dimethyl fumarate treatment and exposure to 3Gy external beam X-irradiation, with a 5±0.62-fold increase in γH2a.X levels compared to dimethyl fumarate treated but non-irradiated cells (p-value <0.001). Following 24-hour treatment, there was a greater increase in γH2a.X levels with 1Gy and 3Gy increasing dimethyl fumarate induced γH2A.x levels 5.7±0.04-fold (p-value <0.05) and 7.1±0.07-fold (p-value <0.01) respectively.

Following 4-hour treatment, only the combination of dimethyl fumarate and 3Gy significantly increased γH2a.X levels compared to untreated cells (p-value <0.001). After 24-hour treatment, both 1Gy and 3Gy groups demonstrated a significant increase in γH2a.X levels compared to an untreated control (p-value <0.05 & <0.01 respectively). All γH2a.X levels induced by the dimethyl fumarate X-irradiation combination were equivalent to or lower than X-irradiation induced γH2a.X levels (p-value >0.05). This pattern of DNA damage indicates that dimethyl fumarate had no DNA damaging effect and therefore no effect on the DNA damage repair response in UVW human glioblastoma cells.

The temozolomide-dimethyl fumarate combination induced the highest level of DNA damage measured in the UVW cell line. When combined with external beam X-irradiation, DNA damage increased in a radiation dose dependent manner. Following 4-hour exposure to 15μM of temozolomide, 9μM of dimethyl fumarate and 1Gy of external beam X-irradiation, there was a 4.2±1.86-fold increase in γH2a.X levels. Unexpectedly,

this level of γH2a.X was not significantly higher than the level of γH2a.X that was induced by the non-irradiated temozolomide-dimethyl fumarate combination (p-value >0.05). Treatment with the temozolomide-dimethyl fumarate combination and 3Gy of external beam X-irradiation significantly increased the level of γH2a.X compared to the non-irradiated temozolomide-dimethyl fumarate combination, with a 7.3±2.14-fold increase (p-value <0.001). The X-irradiated temozolomide-dimethyl fumarate combination did not induce a significantly higher level of γH2a.X compared to temozolomide or dimethyl fumarate in combination with external beam X-irradiation.

Taken together, this data suggest that DNA damage was not significantly higher in temozolomide-dimethyl fumarate combination treated UVW cells than in UVW cells treated with temozolomide, dimethyl fumarate or X-irradiation as single agents. This was contrary to our hypothesis, as the increase in cell kill seen in Figures 4.4 and 4.5 was hypothesised to be due to an increase in DNA damage.

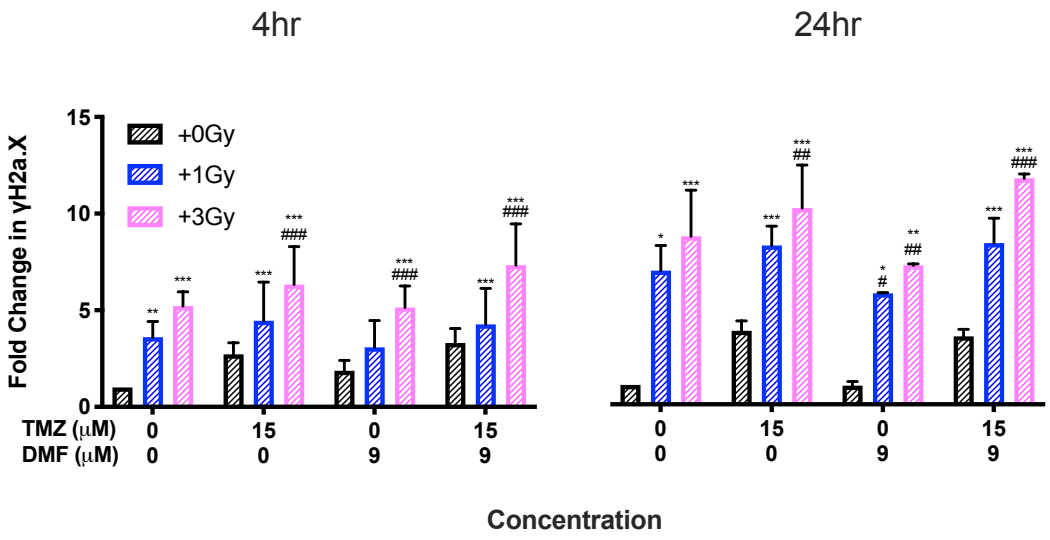

Figure 4.8: H2a.X phosphorylation in UVW human glioblastoma cells. The fold change in γH2a.X levels in response to treatment with temozolomide, dimethyl fumarate or the equivalent doses that constitute the temozolomide-dimethyl fumarate combination ± 1 or 3Gy of external beam X-irradiation. Data shown is an average of at least 3 independent experiments ± standard deviation. A 2-Way ANOVA with Bonferroni post-test was performed with p-values of <0.05 = *, <0.01 = ** and <0.001 = *** reported as significant compared to an untreated control and p-values of <0.05 = #, <0.01 = ## and <0.001 = ### reported as significant compared to drug treated, but non-irradiated treatment groups.

Conversely, in the T98g cell line, 4-hours after treatment with 1 or 3Gy of external beam X-irradiation as a single agent, there was an increase in γH2a.X levels of 3.3±0.59 and 4±0.52-fold respectively, however, only the increase induced by 3Gy was significantly increased compared to basal levels (p-value <0.05). Unexpectedly, there was no significant difference in the level of γH2a.X between increasing doses of X-irradiation in the T98g cell line (p-value >0.05). 24-hours post irradiation, there was a further significant increase in the level of γH2a.X detected within treated cells, with a 4.1±0.79 and 4.4±1.11-fold increase following treatment with 1 or 3Gy respectively compared to untreated cells (p-value <0.05 and <0.01), again there was no significant difference between treatments (p-value >0.05). There was no significant difference between the level of DNA damage induced by each dose of X-irradiation after 4 or 24-hour treatment. This suggests that the T98g cell line has increased DNA damage repair capacity compared to the UVW cell line, as the T98g cell line appears maintain DNA damage levels between 4 and 24-hour time points while the γH2a.X levels in the UVW cell line increased over the same time course.

Following 4-hour treatment with temozolomide and 1Gy of external beam X-irradiation, there was a significant increase in the level of γH2a.X compared to an untreated control (p-value <0.01), but not compared to 1Gy or 400μM as single agents (p-value >0.05), with a 4.8±1.26-fold increase in γH2a.X levels. When temozolomide was combined with 3Gy of external beam X-irradiation, there was a significant 6.1±1.16-fold increase in levels of γH2a.X. This was significant compared to an untreated control (p-value <0.01) and compared to 400μM temozolomide as a single agent (p-value <0.05), but not compared to 3Gy alone (p-value >0.05).

This trend was also seen following 24-hour treatment. 400μM of temozolomide in combination with 1Gy induced a significant 5±0.62-fold increase in γH2a.X levels compared to an untreated control (p-value <0.001), but this was not significantly higher than the level of DNA damage induced when temozolomide was used as a single agent (p-value >0.05). When combined with 3Gy, 400μM of temozolomide induced significantly higher levels of DNA damage than an untreated control (p-value <0.001) and temozolomide as a single agent (p-value <0.05). However, this 6.2±0.55-fold increase was not significantly higher than the level of γH2a.X induced by 3Gy alone (p-value >0.05). There was no difference in the level of γH2a.X between temozolomide plus 1 or

3Gy of external beam X-irradiation, and no significant difference between 4 and 24-hour treatments (p-value >0.05). The combination of temozolomide and external beam X-irradiation was expected to increase DNA damage levels in line with the level of DNA damage induced by temozolomide and external beam X-irradiation as single agents, as we have previously shown that temozolomide does not radiosensitise the MGMT positive T98g cell line.

Unsurprisingly, treatment with 25μM dimethyl fumarate for 4 or 24 hours did not induce significantly increased levels of γH2a.X compared to an untreated control. 4 or 24-hour treatment with 25μM dimethyl fumarate and 1Gy of external beam X-irradiation did not result in significantly increased levels of γH2a.X compared to an untreated control or dimethyl fumarate as a single agent (p-value >0.05). After 4-hour treatment, dimethyl fumarate and 3Gy external beam X-irradiation significantly increased DNA damage compared to an untreated control (p-value <0.05), but not compared to dimethyl fumarate or external beam X-irradiation as a single agent (p-value >0.05). This also occurred following 24-hour treatment, with 25μM of dimethyl fumarate and 3Gy of external beam X-irradiation increasing γH2a.X levels 4.2±0.38-fold compared to an untreated control. This was not significantly higher than dimethyl fumarate or external beam X-irradiation as single agent treatment (p-value >0.05). All dimethyl fumarate X-irradiation combination γH2a.X levels were equivalent to, or lower than X-irradiation induced γH2a.X levels (p-value >0.05). This was expected, as we have previously shown that there was no synergy between dimethyl fumarate and external beam X-irradiation in the T98g cell line and that dimethyl fumarate is not a DNA damaging agent (Figures 3.7 and 4.3).

Similarly to the UVW cell line, in T98g cells the temozolomide-dimethyl fumarate combination induced the highest level of γH2a.X foci. 4-hour treatment with the temozolomide-dimethyl fumarate combination and 1Gy of external beam X-irradiation increased γH2a.X levels 5.1±1.27-fold, however, this is not significantly higher than the level of γH2a.X induced by the temozolomide-dimethyl fumarate combination alone (p-value >0.05). In combination with 3Gy, the temozolomide-dimethyl fumarate combination increased 6.7±0.90-fold compared to an untreated control (p-value <0.01). This was significantly higher than the level of γH2a.X induced by the temozolomide-dimethyl

fumarate combination alone (p-value <0.01), therefore the enhancement of DNA damage was dependent on the dose of radiation administered.

Following 24-hour treatment, the temozolomide-dimethyl fumarate combination in combination with 1 and 3Gy significantly increased γH2a.X levels 6.6±1.28 and 6.6±0.74-fold compared to an untreated control. This was significantly higher than the unirradiated temozolomide-dimethyl fumarate combination (p-value <0.05). The combination of temozolomide-dimethyl fumarate and external beam X-irradiation did not significantly increase levels of γH2a.X above those seen with either external beam X-irradiation as a single agent, or the combination of temozolomide and external beam X-irradiation. Taken together, this is indicative of an inability of the T98g cell line to repair DNA damage induced by the temozolomide-dimethyl fumarate combination, due to an increase in DNA damage over time points.

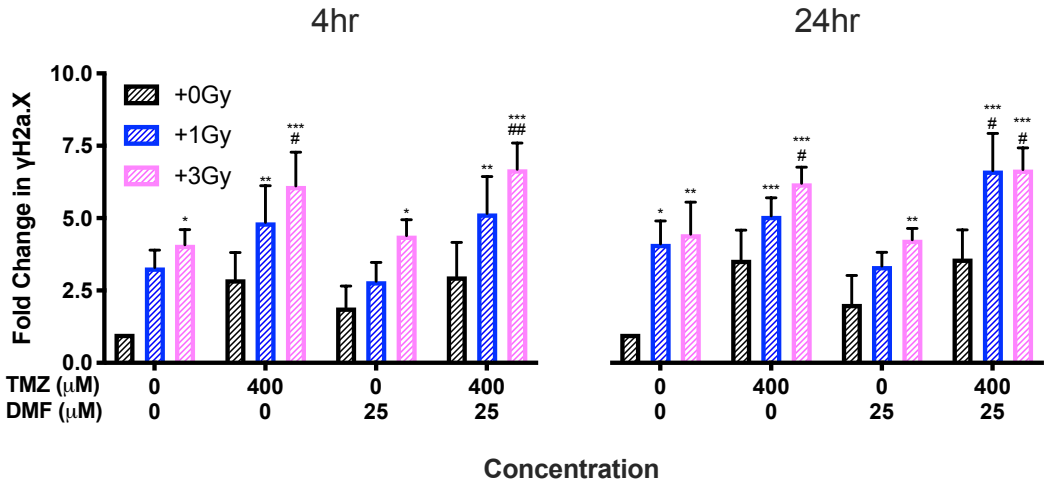

Figure 4.9: H2a.X phosphorylation in T98g human glioblastoma cells. The fold change in γH2a.X levels in response to treatment with temozolomide, dimethyl fumarate or the equivalent doses that constitute the temozolomide-dimethyl fumarate combination ± 1 or 3Gy of external beam X-irradiation. Data shown is an average of at least 3 independent experiments ± standard deviation. A 2-Way ANOVA with Bonferroni post-test was performed with p-values of <0.05 = *, <0.01 = ** and <0.001 = *** reported as significant compared to an untreated control and p-values of <0.05 = #, <0.01 = ## and <0.001 = ### reported as significant compared to drug treated, but non-irradiated treatment groups.

4.4.5 Cell cycle progression in UVW and T98g human glioblastoma cells exposed to the external beam X-irradiated temozolomide-dimethyl fumarate combination

In order to determine the distribution of a population of cells throughout the cell cycle, intracellular DNA was stained with propidium iodide and analysed by flow cytometry. Cells were treated for 24-hours with increasing doses of temozolomide, dimethyl fumarate or the temozolomide-dimethyl fumarate combination. 2-hours after drug treatment, cells were exposed to 1 or 3Gy of external beam X-irradiation in order to examine how progression through the cell cycle was affected by exposure to X-irradiated temozolomide-dimethyl fumarate combination. Flow cytometric analysis was performed, with distinction between the G_1, S, G_2 and M phases of the cell cycle made by quantification of intracellular DNA content. Cell cycle analysis was performed on cells treated for 24-hours due to the lack of effects seen after 4-hour treatment.

As a single agent, 1Gy and 3Gy of external beam X-irradiation induced a significant accumulation of UVW cells in the G_2 phase of the cell cycle, with 40.95±5.40 and 46.26±8.71% of the population accumulating in this phase (p-value <0.01). Accumulation in the G_2 phase of the cell cycle is indicative of DNA damage, as cells with DNA damage cannot progress beyond the G_2/M checkpoint with damaged DNA. This is in keeping with previous results, which show an increase in DNA damage as measured by γH2a.X levels.

When combined with 1Gy of external beam X-irradiation, temozolomide induced no variation in cell cycle accumulation compared to temozolomide or 1Gy of external beam X-irradiation as a single agent (p-value >0.05). When combined with 3Gy of external beam X-irradiation, 0.5, 5 and 15μM of temozolomide induced a significant accumulation of cells in the G_2/M phases of the cell cycle compared to each respective dose of temozolomide alone (p-value <0.05, <0.01 and <0.05 respectively).

Temozolomide in combination with 3Gy of external beam X-irradiation induced a significant G_2/M phase accumulation compared to temozolomide in combination with 1Gy of external beam x-irradiation at all doses of temozolomide used (p-value <0.01). Only 15μM of temozolomide in combination with 3Gy of external beam X-irradiation induced a significantly larger G_2/M accumulation than 3Gy as a single agent (p-value

<0.05). This G_2/M accumulation indicates that temozolomide in combination with 3Gy of external beam X-irradiation increases DNA damage.

Following treatment with increasing doses of dimethyl fumarate and external beam x-irradiation, there was no significant redistribution of the population throughout the cell cycle compared to dimethyl fumarate or external beam x-irradiation as a single agent (p-value >0.05).

As a combination therapy, the temozolomide-dimethyl fumarate combination induced a G_2/M phase arrest compared to an untreated control (p-value <0.01). This was not significantly higher than the arrest induced by temozolomide or dimethyl fumarate as single agents (p-value >0.05).

In combination with 1Gy of external beam X-irradiation, the temozolomide-dimethyl fumarate combination did not induce a significantly larger G_2/M phase arrest compared to 1Gy as a single agent or compared to the non-irradiated temozolomide-dimethyl fumarate combination (p-value >0.05). In combination with 3Gy of external beam X-irradiation, the two highest doses of the temozolomide-dimethyl fumarate combination induced a significantly larger G_2/M accumulation compared to 3Gy as a single agent, with 63.48±5.45 and 57.95±3.88% of the population accumulating at the G_2/M threshold (p-value <0.05).

As seen in Figure 4.10c, all doses of the 3Gy X-irradiated temozolomide-dimethyl fumarate combination induced a G_2/M accumulation which was significantly higher than the arrest induced by the non-irradiated temozolomide-dimethyl fumarate combination and the temozolomide-dimethyl fumarate combination in combination with 1Gy (p-value <0.01). This indicates that the exposure of UVW cells to the X-irradiated temozolomide-dimethyl fumarate combination increases DNA damage, as cells cannot progress beyond the G_2/M checkpoint with damaged DNA. This was suggested by the increase in γH2a.X levels as seen in Figure 4.8.

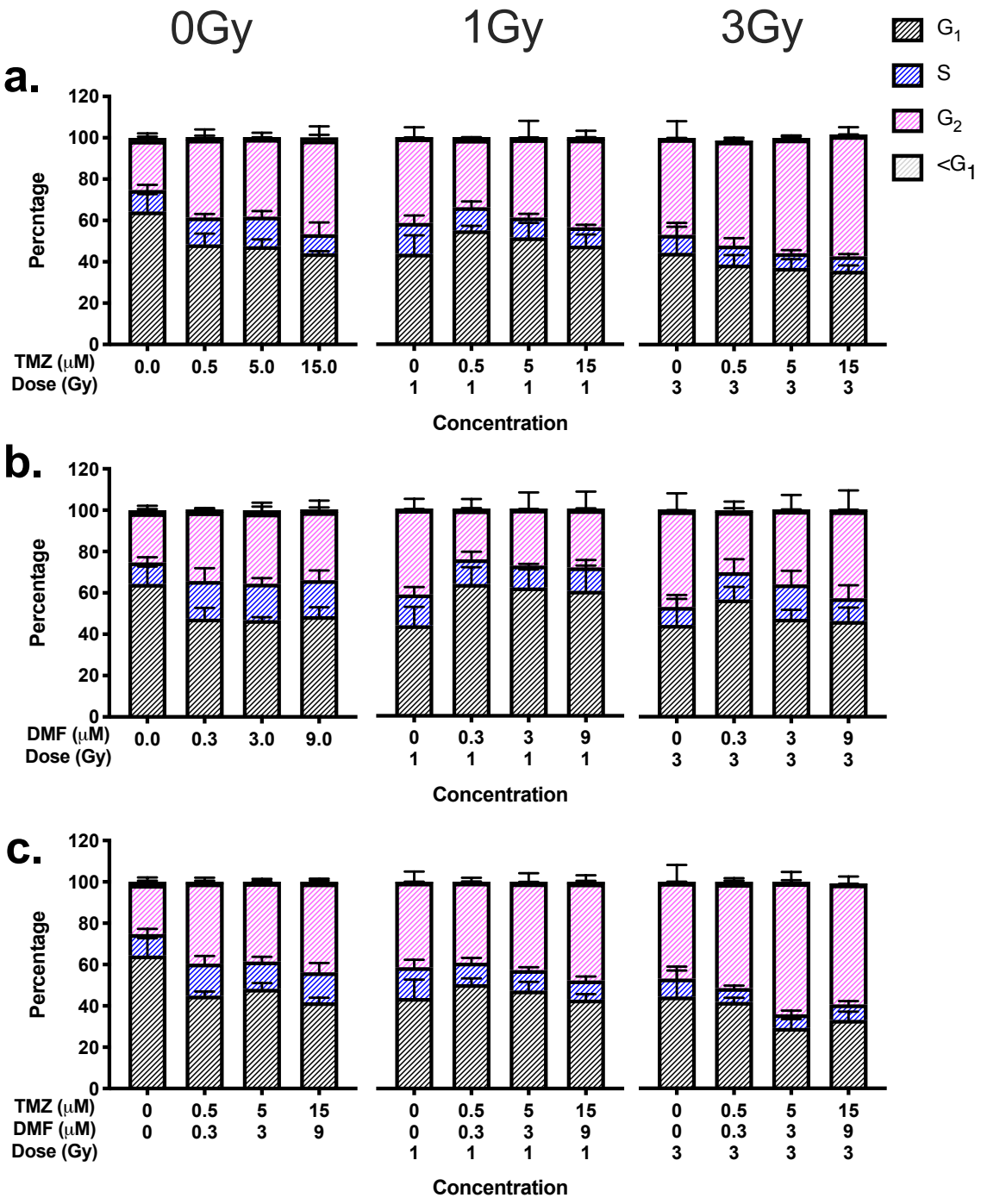

Figure 4.10: Cell cycle progression in UVW cells treated with **a.** temozolomide, **b.** dimethyl fumarate or **c.** the temozolomide-dimethyl fumarate combination ± 1 or 3Gy of external beam X-irradiation. Data shown is an average of at least 3 independent experiments ± standard deviation. A 2-Way ANOVA with Bonferroni post-test was performed with p-values of <0.05 = *, <0.01=** and <0.001 = *** reported as significant. Statistics are reported in Appendix C1.

In the MGMT positive T98g cell line, exposure to 3Gy of external beam X-irradiation induced a significant accumulation of cells in the G_2 phases of the cell cycle compared to non-irradiated cells, with 46.25±15.04% of the population being found in this phase (p-value <0.05). No phase redistribution of T98g cells was seen following exposure to 1Gy of external beam X-irradiation (p-value >0.05). This was expected due to the increase in γH2a.X seen following exposure to X-irradiation, as increased DNA damage is known to induce arrest at the G_2/M checkpoint.

Similarly to the UVW cell line, temozolomide induced a small G_2/M arrest at the highest concentration used in the T98g cell line (p-value >0.05). When combined with external beam X-irradiation, there was a significant increase in the size of G_2/M population following treatment with 400μM temozolomide and 1Gy or 3Gy of external beam X-irradiation compared to temozolomide alone (p-value <0.001), but not external beam X-irradiation as single agent. 50 and 200μM of temozolomide in combination with external beam X-irradiation had no significant effect on cell cycle phase distribution compared to temozolomide or external beam X-irradiation as single agents (p-value >0.05). This indicates that the T98g cell line, as hypothesised, has a greater ability to repair DNA damage than the UVW cell line, as only the highest dose of temozolomide is able to induce DNA damage associated arrest.

Following dimethyl fumarate treatment there was no significant redistribution of the population throughout the cell cycle (p-value >0.05). When combined with external beam X-irradiation, dimethyl fumarate treated T98g cells showed no difference in cell cycle distribution compared to cells treated with dimethyl fumarate or external beam X-irradiation as single agents (p-value >0.05).

This indicates that the combination of dimethyl fumarate and external beam X-irradiation has no effect on cell cycle distribution in the T98g cell line. This was suggested by γH2a.X results, which showed no increase in DNA damage compared to external beam X-irradiation as a single agent, and without this, no G_2 or G_1 accumulation was expected.

The temozolomide-dimethyl fumarate combination induced a G_2/M arrest when combined with external beam X-irradiation. This effect appeared to be independent of the dose of temozolomide-dimethyl fumarate. When combined with 1Gy, the temozolomide-dimethyl fumarate combination induced a significant increase in the G_2/M

arrest compared to 1Gy, temozolomide and dimethyl fumarate as single agents and the non-irradiated temozolomide-dimethyl fumarate combination (p-value <0.01). This resulted in over 50% of the population arresting at G_2/M phase. This was also seen with 3Gy, where the size of the G_2/M arrest increased by ~30% at all doses the temozolomide-dimethyl fumarate combination,, temozolomide and dimethyl fumarate as single agents (p-value <0.05), with over 70% of the population arresting at G_2/M phase.

This suggests a large amount of DNA damage is taking place across the T98g population, which was suggested by γH2a.X data, but was not found to be statistically significant. An arrest of this magnitude may suggest that the level of DNA damage is complex, and the population is overwhelmed in its repair capacity. We believe that this is particularly promising as we previously suggested that the T98g cell line has an increased DNA damage repair capacity. It was expected that an inability to repair the damage that resulted in this G_2/M arrest would lead to induction of apoptosis.

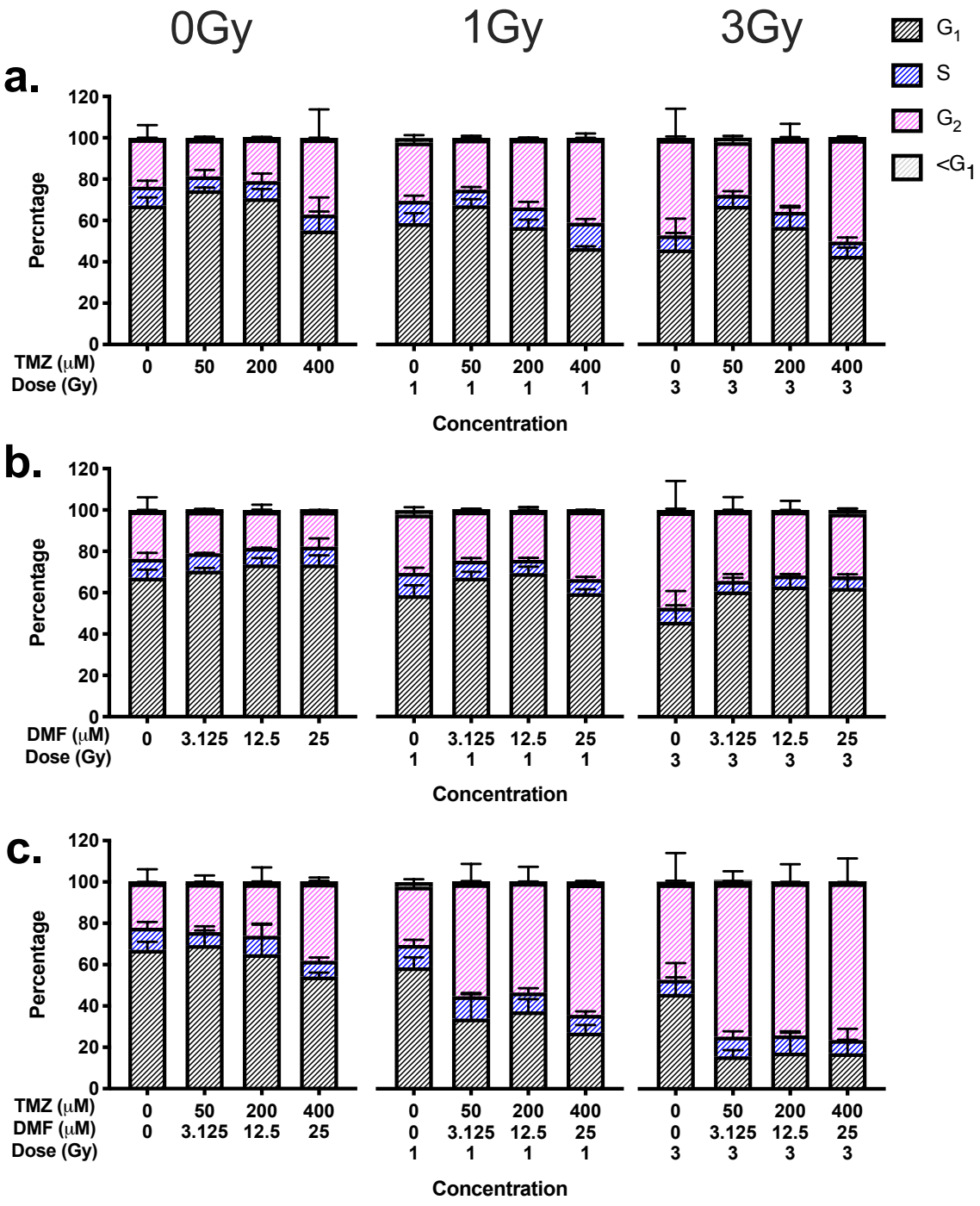

Figure 4.11: Cell cycle progression in T98g cells treated with **a.** temozolomide, **b.** dimethyl fumarate or **c.** the temozolomide-dimethyl fumarate combination ± 1 or 3Gy of external beam X-irradiation. Data shown is an average of at least 3 independent experiments ± standard deviation. A 2-Way ANOVA with Bonferroni post-test was performed with p-values of <0.05 = *, <0.01=** and <0.001 = *** reported as significant. Statistics are reported in Appendix C2.

4.4.6 Apoptotic induction by the temozolomide dimethyl combination and external beam X-irradiation in UVW and T98g human glioblastoma cells

Detection of the expression of apoptotic markers on UVW and T98g human glioblastoma cell lines was detected using an anti-annexin V FITC conjugate and propidium iodide, with each stain identifying the cellular population at different stages of the apoptotic cell death pathway. Early apoptotic cells were characterised as having an intact membrane and stained positively for annexin V which associates with membrane bound phosphatidyl serine moieties, late apoptotic cells, which have a compromised membrane, were annexin V & propidium iodide positive Necrotic cells were singly positive for propidium iodide and had a severely compromised membrane (Genderen *et al*., 2006). Cells were treated for 24-hours with increasing doses of temozolomide, dimethyl fumarate or the temozolomide-dimethyl fumarate combination. 2-hours after drug treatment, cells were exposed to 1 or 3Gy of external beam X-irradiation in order to examine how X-irradiation and drug treatment affected the expression of apoptotic markers and the progression of cells through the programmed cell death pathway. Media replacement 24-hour post irradiation was considered treatment cessation in X-irradiated only groups.

Time points 24-72 hours post-treatment cessation were chosen in order for cells to arrest and induce apoptosis following X-irradiation. We believe that we have shown that DNA damage and cell cycle arrest in UVW cells treated with temozolomide and external beam X-irradiation do not occur until 24-hours of treatment has been completed. Following this mismatch repair cycles take place. Failed cycles of mismatch repair leads to DNA damage in the form of double stranded breaks (Kaina, 2003; Roos and Kaina, 2006; Roos *et al*., 2007), inductions of double stranded breaks has been shown to be necessary for induction of apoptosis (Ochs and Kaina, 2000), and induction of apoptosis as late as 120-hours post treatment has been shown to take place.

4.4.6.1 Apoptotic induction by external beam X-irradiation

As a monotherapy, external beam X-irradiation induced apoptosis in a time dependent manner in the UVW human glioblastoma cell line (Figure 4.12a). Treatment with 3Gy of external beam X-irradiation induced a significant increase in the size of the apoptotic population 24-hour post-treatment cessation, with 46.05±11.04% of the population staining positively for apoptotic markers compared to a non-irradiated control (p-value <0.05). Exposure to 1Gy of external beam X-irradiation increased the apoptotic population at the same time point, however this was not significant (p-value >0.05). There was also no significant difference between the 1 and 3Gy treated groups at this time point. The increase in the size of the apoptotic population at this time point correlated to a significant increase in the size of the early apoptotic population in both 1Gy (25.03±8.54% positive, p-value <0.05) and 3Gy (41.36±2.65% positive, p-value <0.001) treatment groups. There was no significant increase in the size of the late apoptotic population, and no detectable necrotic population at this time point. This indicates that the times points chosen are appropriate as evidenced by the lack of cells that have progressed through the apoptotic cycle.

48-hours post treatment cessation, there was a further increase in the size of the apoptotic population compared to an unirradiated control. At this time point 51.70±17.99% of the 1Gy and 53.95±0.09% of the 3Gy exposed population was found to express apoptotic markers (p-value <0.05). There was no significant difference between these points (p-value >0.05). This correlated to an increase in the size of the early apoptotic population compared to a non-irradiated control (p-value <0.001), but not compared to the 24-hour population (p-value >0.05). This trend was seen at 72-hours post treatment cessation, with 54.94±12.79% of the 1Gy and 66.93±7.50% of the 3Gy exposed population was found to express apoptotic markers compared to an unirradiated control (p-value <0.01). Again, this correlated to an increase in the size of the early apoptotic population (p-value <0.001), but not the late or necrotic populations (p-value >0.05).

This indicates that cells did express early apoptotic markers following treatment with 1 or 3Gy of external beam X-irradiation, and expression of these moieties increased in a time dependent manner. However, cells exposed to external beam X-irradiation do not appear to be progressing through the programmed cell death pathway as expected. This

suggests that these cells may have initiated apoptosis but are resistant to progression through the programmed cell death pathway.

In the T98g cell line, apoptosis following external beam X-irradiation was induced in a dose-dependent manner. Exposure to 1 or 3Gy of external beam X-irradiation induced no change in the expression of apoptotic markers 24-hours post exposure (p-value >0.05). At this time point there was no redistribution of the apoptotic population compared to a non-irradiated control (p-value >0.05) (Figure 4.12d).

Treatment with 3Gy increased the apoptotic population to 47.05±5.57% 28-hours post treatment cessation, which was significantly larger than the basal apoptotic population (p-value <0.001). This correlated to a significantly larger early apoptotic population (p-value <0.05). 1Gy induced no significant increase in the apoptotic population 48-hours post exposure (p-value >0.05).

Both doses of external beam X-irradiation induced significant expression of apoptotic markers 72-hours post exposure compared to an unirradiated control. 1Gy increased the positively stained population to 44.29±3.54% (p-value <0.01) and 3Gy induced the positively stained population to 46.6±9.87% (p-value <0.001). This correlated to a significant increase in the size of the early apoptotic population compared to an untreated control (p-value <0.01). There was no significant difference between the size of the apoptotic population following treatment with 1 or 3Gy at any time point.

Both cell lines showed an increase in DNA damage and correlated G_2/M arrest in response to exposure to external beam X-irradiation. However, apoptosis is induced significantly smaller population in the T98g cell line than in the UVW cell line, we believe that that is indicative of the suggested ability of these cells to repair DNA damage.

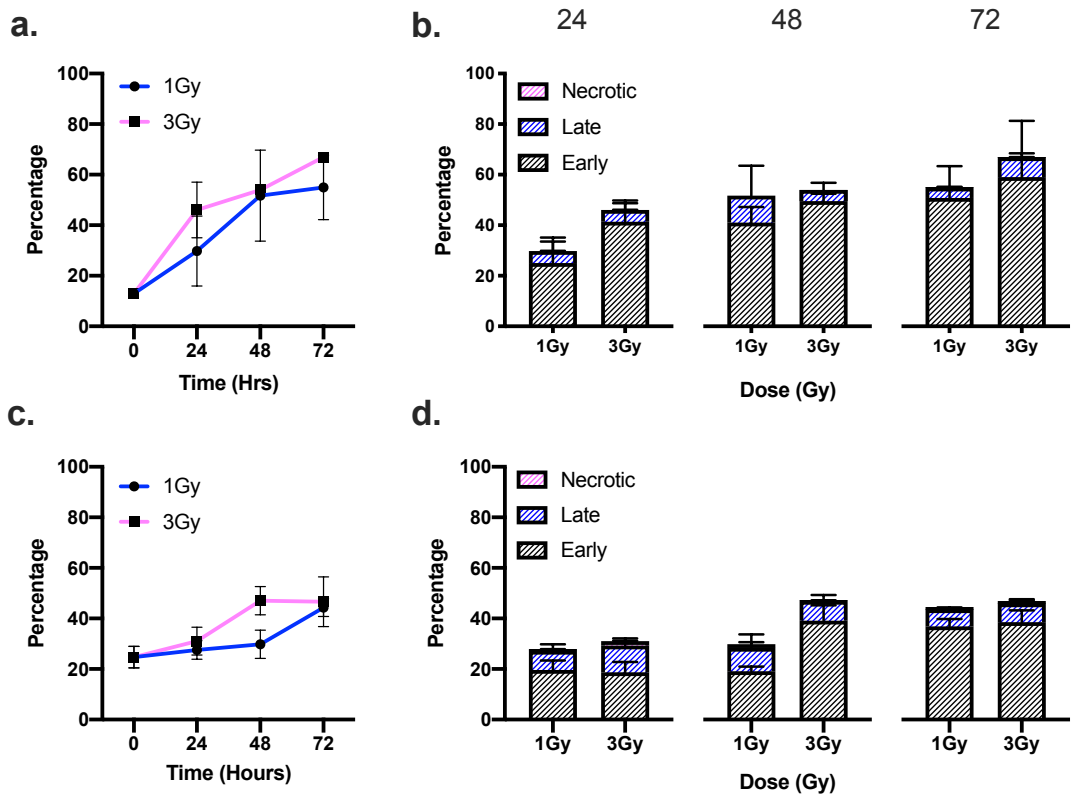

Figure 4.12: Induction of apoptosis in **a.** UVW and **c.** T98g cells following exposure to external beam X-irradiation. Apoptotic phase redistribution in response to increasing doses of X-irradiation in **b.** UVW and **d.** T98g cells is also shown. Data shown is an average of at least 3 independent experiments ± standard deviation. A 2-way ANOVA with Bonferroni post-test was performed with p-values of <0.05 = *, <0.01=** and <0.001 = *** reported as significant

4.4.6.2 Apoptotic induction by the temozolomide-dimethyl fumarate combination with external beam X-irradiation

As a single agent, temozolomide induced apoptosis in a dose independent manner 48 to 72-hours post treatment cessation (Section 3.4.6, Figure 3.11). By 72-hours after treatment cessation, ~75% of the UVW population were found to be stained positively for annexin V or propidium iodide, both of which are apoptotic markers. As seen in Figure 4.13b & c combining temozolomide with external beam X-irradiation significantly increased the speed at which apoptosis was induced but did not influence the final size of the apoptotic population.

When combined with 1Gy, 24-hours post treatment cessation temozolomide increased the size of the early apoptotic population following treatment with 0.5, 5 and 15μM of temozolomide, but not significantly (p-value >0.05) (Figure 5.13b). This increase was ~16% at both doses of temozolomide and increased the size of the apoptotic population to 28.96±7.32 and 33.96±15.17% for 5 and 15μM respectively. When combined with temozolomide, 3Gy increased the size of the early apoptotic population by ~20% at all 3 doses of temozolomide (p-value >0.05) (Figure 4.13c). 24-hours post treatment cessation there was no significant difference between increasing concentrations of temozolomide at either dose of X-irradiation, and no difference between either X-irradiation treatment in terms of both the size of the apoptotic population and the phase distribution of apoptotic cells (p-value >0.05).

48-hours after temozolomide treatment cessation, there was a further increase in the size of the early apoptotic population, but not the late or necrotic population when temozolomide was combined with both 1 or 3Gy of external beam X-irradiation. This was significantly larger than the apoptotic population induced by all concentrations of temozolomide as a single agent (p-value <0.05).

The final time point examined showed that there was no significant difference in the size of the apoptotic population between treatment with temozolomide as a single agent and the combination of temozolomide and external beam X-irradiation (p-value >0.05), with all treatment groups inducing apoptotic markers in ~70% of the population. However, in temozolomide treated cells there was significant accumulation of late apoptotic (p-value

<0.01) and necrotic cells (p-value <0.001) compared to when cells were treated with temozolomide and 1 or 3Gy of external beam X-irradiation.

No dose of temozolomide in combination with 1 or 3Gy of external beam X-irradiation induced a significant increase in the size of the apoptotic population greater than 1 or 3Gy of external beam X-irradiation as a single agent (p-value >0.05).

This data indicates the combination of temozolomide and external beam X-irradiation increases the speed at which cells enter into the apoptotic pathway, but the combination does not affect a larger population than temozolomide or external beam X-irradiation as single agents. The increased apoptotic marker expression at early time points is indicative of more severe DNA damage, as the cell has aborted or not attempted to repair the damage but has instead induced apoptosis. This was in keeping with our hypothesis, as well as all other data gathered showing synergy between temozolomide and external beam X-irradiation in the UVW cell line.

In the UVW cell line, dimethyl fumarate in combination with external beam X-irradiation induced apoptosis in a dose independent manner. In combination with 1Gy or 3Gy of external beam X-irradiation, all concentrations of dimethyl fumarate induced the expression of early apoptotic markers from 24-hours post treatment cessation (Figure 4.13e & f). Induction of apoptosis increased in a time dependent manner, but there was no significant difference in the expression of apoptotic markers between any treatments at any time points (p-value >0.05). There was no significant difference in the size of the apoptotic population between cells treated with dimethyl fumarate or external beam X-irradiation as single agents and cells treated with dimethyl fumarate and 1 or 3Gy of external beam X-irradiation at any time points (p-value >0.05). However, in dimethyl fumarate treated cells there was significant accumulation of late apoptotic (p-value <0.01) and necrotic cells (p-value <0.001) compared to when cells were treated with dimethyl fumarate and 1 or 3Gy of external beam X-irradiation.

All data taken together suggests that there is no benefit to external beam X-irradiation by the addition of dimethyl fumarate. We have shown no increase in DNA damage or cell cycle arrest when dimethyl fumarate is combined with external beam X-irradiation, and as such there is no increase in the rate or magnitude at which apoptosis is induced compared to external beam X-irradiation as a single agent.

When combined with 1Gy or 3Gy of external beam X-irradiation, all administered concentrations of the temozolomide-dimethyl fumarate combination significantly increased expression of markers compared to the temozolomide-dimethyl fumarate combination alone 24 (p-value <0.05) and 48-hours (p-value <0.01) post treatment cessation (Figure 4.13h & i). There was no significant difference in the size of the apoptotic population induced by the temozolomide-dimethyl fumarate combination and the 1Gy or 3Gy X-irradiated temozolomide-dimethyl fumarate combination 72-hours post treatment cessation (p-value >0.05). In X-irradiated temozolomide-dimethyl fumarate combination treated cells, there was significant accumulation of late apoptotic (p-value <0.05) 48-hours post treatment cessation.

There was no significant difference the size of the apoptotic population between the X-irradiated temozolomide-dimethyl fumarate combination and temozolomide or dimethyl fumarate in combination with external beam X-irradiation (p-value >0.05). However, in temozolomide-dimethyl fumarate combination treated cells, there was significant accumulation of late apoptotic (p-value <0.05) and necrotic cells (p-value <0.001) compared to when cells were treated with the temozolomide-dimethyl fumarate combination and 1 or 3Gy of external beam X-irradiation at 72-hours post-treatment cessation.

This indicates that the X-irradiated temozolomide-dimethyl fumarate combination increases the speed at which cells enter the apoptotic pathway, but the combination does not affect a larger population than temozolomide, dimethyl fumarate or external beam X-irradiation as single agents. The increased apoptotic marker expression at early time points is indicative of more severe DNA damage, as the cell has aborted or not attempted to repair the damage but has instead induced apoptosis. This was in keeping with our hypothesis, as well as all other data gathered showing synergy between the temozolomide-dimethyl fumarate combination and external beam X-irradiation in the UVW cell line.

Figure 4.13 (Facing): Induction of apoptosis in UVW cells by temozolomide, dimethyl fumarate and the temozolomide-dimethyl fumarate combination in combination with external beam X-irradiation. Apoptotic induction in UVW cells in response to increasing doses of **a.** temozolomide plus **b.** 1Gy and **c.** 3Gy of external beam X-irradiation, **d.** dimethyl fumarate temozolomide plus **e.** 1Gy and **f.** 3Gy of external beam X-irradiation, and **g.** the temozolomide-dimethyl fumarate combination plus **h.** 1Gy and **i.** 3Gy of external beam X-irradiation. Apoptotic phase distribution following each treatment is also shown. Data shown is an average of at least 3 independent experiments ± standard deviation. A 2-Way ANOVA with Bonferroni post-test was performed with p-values of <0.05 = *, <0.01=** and <0.001 = *** reported as significant. Statistics are reported in appendix D1.

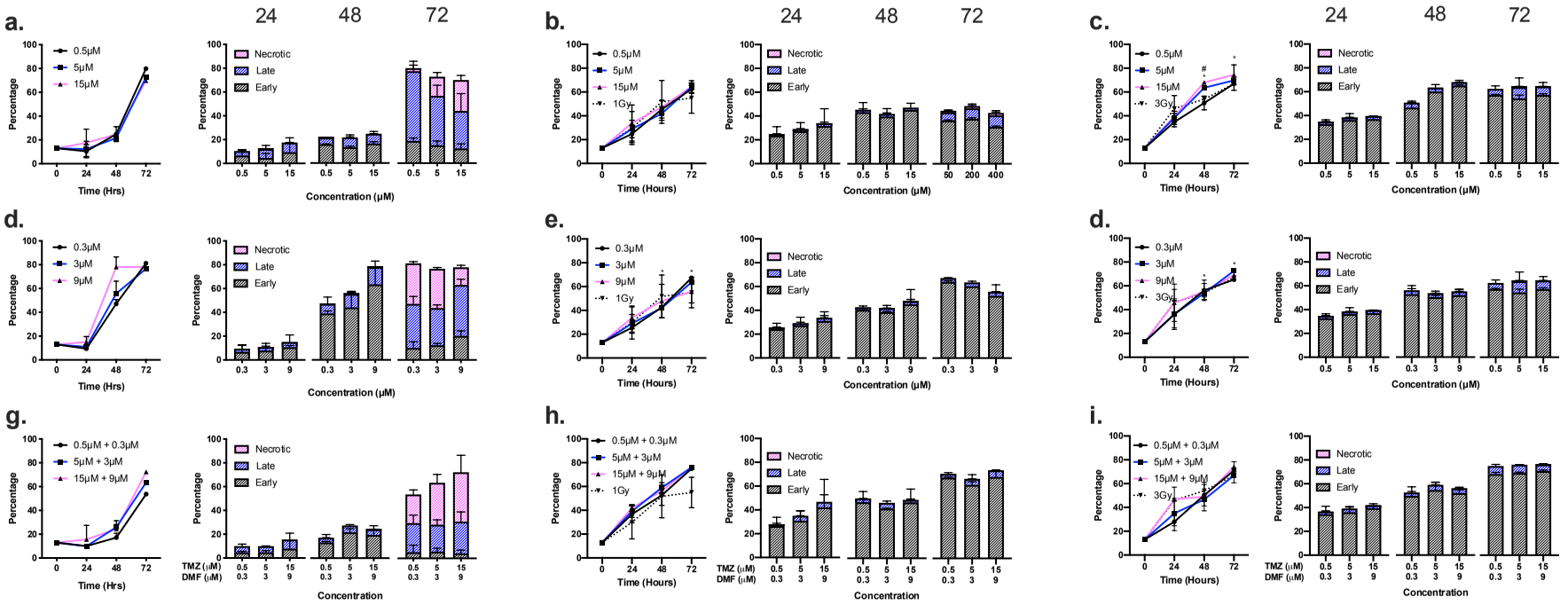
a.
b.
c.
d.
e.
d.
g.
h.
i.
24
48
72
0.5μM
5μM
15μM
1Gy
3Gy
0.3μM
3μM
9μM
0.5μM + 0.3μM
5μM + 3μM
15μM + 9μM
Necrotic
Late
Early
Percentage
Time (Hrs)
Time (Hours)
Concentration (μM)
Concentration
TMZ (μM)
DMF (μM)

In the T98g cell line, temozolomide in combination with external beam X-irradiation induced apoptosis in a dose dependent manner. In combination with 1Gy or 3Gy of external beam X-irradiation 200 and 400μM of temozolomide induced the expression of apoptotic markers from 24-hours post treatment cessation (p-value >0.05). This level increased at 48-hours, with a dose dependent increase in the expression of early apoptotic markers (Figure 4.14b & c,) indicating a failure of the T98g cell line to repair DNA damage induced by this combination and inducing apoptosis.

The percentage of cells expressing apoptotic markers following treatment with 50 or 200μM in combination of 1 or 3Gy of external beam X-irradiation increased at 72-hours post treatment exposure. At 72-hours post treatment, there was a decrease in the size of the apoptotic population following treatment with 400μM and external beam X-irradiation compared to previous time points. This decrease correlated with an increase in the size of the late apoptotic population (p-value >0.05) (Figure 4.14b & c). This decrease in the apoptotic population may be due to cell loss induced by this treatment, as we know that the combination of temozolomide and external beam X-irradiation can induce significant cell kill (Figure 4.3a).

There was no significant difference in the size of the apoptotic population or in apoptotic phase distribution between groups treated with temozolomide or cells treated with temozolomide and 1 or 3Gy of external beam X-irradiation (p-value >0.05). There was no significant difference between the size of the apoptotic population in cells treated with temozolomide and external beam X-irradiation and the apoptotic population in cells external beam X-irradiation as a single agent (p-value >0.05). This is indicative of a lack of synergy, which was expected, given the lack of synergy between these two agents as defined by combination index analysis presented in Figure 4.3b.

In the T98g cell line, dimethyl fumarate in combination with external beam X-irradiation induced apoptosis in a dose dependent manner. In combination with 1 or 3Gy of external beam X-irradiation, 12.5 and 25μM of dimethyl fumarate induced the expression of apoptotic markers from 48-hours post treatment cessation (Figure 4.14e &f). There was no significant difference in the expression of apoptotic markers between 12.5 and 25μM treatment groups at any time points. There was no increase in the expression of apoptotic markers following treatment with 3.125μM dimethyl fumarate until 72-hours post treatment cessation.

The percentage of cells expressing apoptotic markers following treatment with 12.5 or 25μM and 1 or 3Gy of external beam X-irradiation decreased at 72-hours post treatment exposure. At 72-hours, there was no difference in the size of the apoptotic population between treatment groups.

The final apoptotic population was significantly smaller at all concentrations when dimethyl fumarate was combined with 1Gy or 3Gy of external beam X-irradiation than when cells were treated with dimethyl fumarate as a single agent (p-value <0.01 and <0.05). This is due to a significantly larger late apoptotic (p-value <0.05) (positive for both annexin V and propidium iodide staining) when T98g cells were treated with dimethyl fumarate but not dimethyl fumarate and X-irradiation. This may be due to apoptotic cell loss at earlier time points when dimethyl fumarate is combined with external beam X-irradiation compared to dimethyl fumarate alone (Figure 4.14f).

There was no significant difference between the size of the apoptotic population in cells treated with dimethyl fumarate and external beam X-irradiation and the apoptotic population in cells exposed to external beam X-irradiation as a single agent (p-value >0.05). This indicates, as does all other data, that dimethyl fumarate has little effect when combined with external beam X-irradiation, and offers little benefit, with no synergistic increase in cell kill, no increase in DNA damage and no increase in cell cycle arrest.

In combination with 1 or 3Gy of external beam X-irradiation, the temozolomide-dimethyl fumarate combination induced expression of apoptotic markers from 24-hours post treatment cessation in a dose dependent manner (Figure 4.14h & i). This expression increased at 48-hours post treatment cessation and was significantly higher than the expression seen in an untreated control (p-value <0.05). Again, the percentage of cells expressing these markers decreased at 72-hours post treatment cessation following treatment with all doses of the 1 or 3Gy irradiated temozolomide-dimethyl fumarate combination. There was no significant variation in the size of the apoptotic population compared to the non-irradiated temozolomide-dimethyl fumarate combination or 1 or 3Gy as a single therapy (p-value >0.05).

There was no significant difference in the size of the apoptotic population or apoptotic phase distribution between the X-irradiated temozolomide-dimethyl fumarate

combination and temozolomide or dimethyl fumarate in combination with external beam X-irradiation (p-value >0.05).

Clonogenic data seen in Figure 4.5 had suggested that an increase in the size of the apoptotic population would be seen when T98g cells were treated with the X-irradiated temozolomide-dimethyl fumarate combination. An increase in cell kill, DNA damage and cell cycle arrest had previously been reported and led us to hypothesise that an increase in the size of the apoptotic population would be seen. This has not been realised. This may be due to the suggested increased DNA damage repair capacity of the T98g cell line.

Figure 4.14 (facing): Induction of apoptosis in T98g cells by temozolomide, dimethyl fumarate and the temozolomide-dimethyl fumarate combination in combination with external beam X-irradiation. Apoptotic induction in UVW cells in response to increasing doses of **a.** temozolomide plus **b.** 1Gy and **c.** 3Gy of external beam X-irradiation, **d.** dimethyl fumarate temozolomide plus **e.** 1Gy and **f.** 3Gy of external beam X-irradiation, and **g.** the temozolomide-dimethyl fumarate combination plus **h.** 1Gy and **i.** 3Gy of external beam X-irradiation. Apoptotic phase distribution following each treatment is also shown. Data shown is an average of at least 3 independent experiments ± standard deviation. A 2-Way ANOVA with Bonferroni post-test was performed with p-values of <0.05 = *, <0.01=** and <0.001 = *** reported as significant. Statistics are reported in appendix D2.

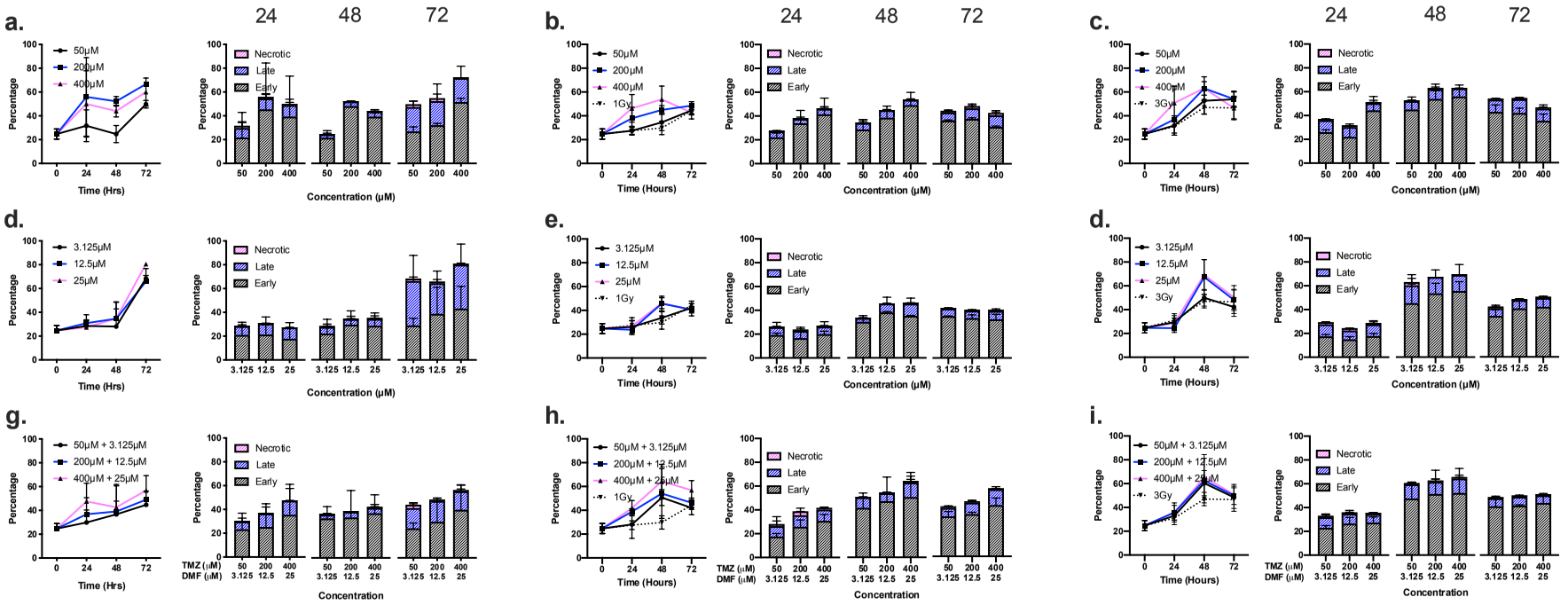
a.
b.
c.
d.
e.
d.
g.
h.
i.
24
48
72
50μM
200μM
400μM
1Gy
3Gy
3.125μM
12.5μM
25μM
50μM + 3.125μM
200μM + 12.5μM
400μM + 25μM
Necrotic
Late
Early
Percentage
Time (Hrs)
Time (Hours)
Concentration (μM)
Concentration
TMZ (μM)
DMF (μM)

4.5 Discussion

4.5.1 Cytotoxicity of temozolomide and dimethyl fumarate in combination with external beam radiation

Clonogenic assays were performed on the UVW and T98g cell lines treated with temozolomide and dimethyl fumarate to determine the effects of each of these agents on the sustained replicative ability and survival of each cell line. By examining the response of these cell lines to these treatments, the experimental IC_{50} values of these agents could be compared to the literature IC_{50}, allowing us to validate future work using these cell lines. These values are also vital when designing combinations; ensuring appropriate concentrations of each drug are used. As the IC_{50} is a constant, responses to each drug in each cell line can be measured and compared, even when the values are significantly different, this is of particular value when comparing two cell lines that have a different response to the same agent.

To fully examine the effects of external beam X-irradiation in combination with the previously described temozolomide-dimethyl fumarate combination in UVW and T98g human glioblastoma cells, the cytotoxic effects of external beam X-irradiation in combination with temozolomide and dimethyl fumarate as single agents were first examined.

4.5.1.1 External beam X-irradiation

Radiotherapy forms the backbone of the current standard of care for patients diagnosed with high grade glioma, with virtually every patient receiving radiotherapy (Grossman *et al*., 2010; Preusser *et al*., 2011). One of the main reasons for treatment failure for glioma is inherent radio-resistance (Kelley *et al*., 2016) . This is mediated by a number of different genetic and physiological factors, such as hypoxia (Bristow and Hill, 2008), the presence of radioresistant cancer stem cells (Rich, 2007) and ataxia telangiectasia mutated (ATM) activity (Bao *et al*., 2006).

In our study, a differential response in cell survival in UVW and T98g cells external beam X-irradiation was only evident at 6Gy. This difference in survival is indicative of the increased repair capacity displayed by T98g cells compared to UVW cells, which is likely

a result of the basal expression of MGMT seen in T98g cells, but not the UVW cell line (Figure 3.2c) (Chalmers *et al*., 2009; He *et al*., 2011; Preusser *et al*., 2011; Rivera *et al*., 2010).

In both UVW and T98g human glioblastoma cell lines, 3Gy of external beam X-irradiation induced a significant level of DNA damage from 4-hours after exposure, rising 24-hours after exposure. In the UVW cell line, this increase in γH2A.x levels was almost double the level seen after 4-hours exposure to 1 or 3Gy, indicating that the damage caused by external beam X-irradiation is a continuous process or the affected population are failing to repair the damage or induce early apoptosis and are instead locked in cell cycle arrest while still failing to resolve the DNA damage that resulted in the arrest. This continued increase in DNA damage is also indicative that the UVW cell line does not have a high level of DNA damage repair capacity compared to the T98g cell line. The increase in γH2A.x levels between 4 and 24-hours was much more subtle in the T98g cell line, with less than a 1-fold increase across time points.

We hypothesise that this data is suggestive of T98g cells displaying a high intrinsic capability for DNA damage repair. Taken with the basal expression of MGMT in T98g shown in Figure 3.2c, but not UVW cells, we believe that this can partly explain the difference in both DNA damage, and overall response to external beam X-irradiation. This effect has been well documented, with numerous studies validating the hypothesis that MGMT promoter methylation and therefore null MGMT activity increases radiosensitivity (Hermisson *et al*., 2006; Rivera *et al*., 2010; Roos *et al*., 2004).

We have found increased levels of γH2A.x does not to translate to the level of G_2/M cell cycle arrest seen in both UVW and T98g cell lines after exposure to external beam X-irradiation. There was a dose dependent increase in the size of the G_2/M arrest 4 or 24-hours after exposure to 1 or 3Gy of external beam X-irradiation. However, there was no time dependent increase in G_2/M arrest despite increase in γH2A.x levels. We believe that this indicates that there is a threshold effect occurring during the cellular response to external beam X-irradiation; DNA damage induced by exposure to external beam X-irradiation appears to induce the same level of G_2/M arrest 4 or 24-hours post-treatment.

Our hypothesis that the T98g cell line displays a high DNA damage repair capacity is evident in the induction of apoptosis following X-irradiation. Both cell lines induced a

comparable G_2/M arrest, which is indicative of DNA damage (Fragkos *et al*., 2009), however, only the UVW cell line showed a larger increase in apoptosis in response to X-irradiation. We believe that during the G_2/M arrest, the T98g cell line has the capacity to repair the X-irradiation induced damage or maintain cells in the cell cycle checkpoint but the UVW cell line does not. We believe that this may be due to the basal expression of MGMT in the T98g cell line (Figure 3.2c). Further work should be used to test this hypothesis using the MGMT inhibitor, O^6-benyzlguanine (Quinn *et al*., 2009)

4.5.1.2 Temozolomide

The literature surrounding temozolomide as a radiosensitiser is broad and contradictory, however it is important to remember that concomitant temozolomide and external beam radiotherapy remains the standard of care for high-grade glioma (Preusser *et al*., 2011; Stupp *et al*., 2005, 2010). Therefore, the interaction between the two treatments must be beneficial, or at the very least, not detrimental. In this study, radiosensitisation was defined as supra-additivity using combination index analysis. We demonstrated that temozolomide radiosensitises only the MGMT negative UVW cell line. This is in line with other studies using cells with a methylated MGMT promoter and has been validated clinically (Hegi *et al*., 2004; Stupp *et al*., 2005, 2009).

Radiosensitisation in MGMT negative glioblastoma has been demonstrated using patient derived samples stereotactically injected into mouse brains (Carlson *et al*., 2009; Sarkaria *et al*., 2006). These reported studies showed an increase in the survival ratio for MGMT negative, but not MGMT expressing samples, and suggests that temozolomide is a radiosensitiser due to an increased survival ratio when temozolomide is given concurrently with radiation compared to adjuvantly (Carlson *et al*., 2009). Radiosensitisation was also seen with concurrent, but not adjuvant temozolomide therapy in primary glioblastoma cells (Chakravarti *et al*., 2006), again this occurred in an MGMT dependent manner. Reversal of radioresistance in MGMT positive tumours was seen when the MGMT inhibitor O^6-benzylguanine was used (Chakravarti *et al*., 2006). We have shown that the T98g cell line basally express MGMT (Figure 3.2c), and when treated with temozolomide and external beam X-irradiation, no radiosensitisation was seen (Figure 4.3a & c).

The precise mechanism of temozolomide mediated radiosensitisation is disputed. It is agreed that the combination of temozolomide and external beam X-irradiation increased DNA damage compared to each constituent agent (Carlson *et al*., 2009; Chakravarti *et al*., 2006; Kil *et al*., 2008), an effect we have successfully replicated.. Specifically, we have shown that the combination of temozolomide and external beam X-irradiation increases recruitment of γH2a.X, which associates exclusively with double stranded breaks (Burma *et al*., 2001; Fragkos *et al*., 2009; Momota *et al*., 2003). Double stranded breaks in the DNA helix are induced by temozolomide and X-radiation as single agents (Hirose *et al*., 2001; Roos *et al*., 2004; Vignard *et al*., 2013) and are the most challenging DNA lesion to repair.

By using two agents that are capable of inducing double stranded breaks, the level of DNA damage is increased, leading to a higher level of cell kill (Chakravarti *et al*., 2006). We believe that the increase in DNA damage demonstrated in our study results in a G_2/M cell cycle arrest. Our data suggest that the increased levels of DNA damage is irreparable, given the subsequent G_2/M arrest and the induction of apoptosis (Hirose *et al*., 2001; Roos *et al*., 2004, 2007). Inhibition of MGMT using O^6-benzylguanine has been shown to increase the induction of apoptosis following DNA damage, suggesting that MGMT is a key radioresistance factor in glioblastoma (Chakravarti *et al*., 2006). This is supported by our data from the MGMT expressing T98g cell line, which showed no significant increase in apoptosis when treated with temozolomide and external beam X-irradiation compared to temozolomide alone.

However, Kil *et al*., (2008) also reported no G_2/M arrest, and no induction of apoptosis *in vivo* in the MGMT negative U251 human glioma cell line and in the brain seeking variant of the MDA-MB231 breast cancer cell line, instead suggesting that the combination of temozolomide and γ-radiation induces mitotic catastrophe (Kil *et al*., 2008). However, this is contradictory to what our data demonstrates. We have shown a dose dependent increase in the magnitude of the G_2/M cell cycle arrest and an increase in apoptotic induction. The combination of temozolomide and external beam X-irradiation did not increase the expression of apoptotic markers compared to external beam X-irradiation alone in the MGMT negative UVW cell line. Time points chosen for detection of apoptotic markers closely match previous work and were chosen due to the late G_2/M arrest and the requirement for temozolomide treated cells to undergo cycle of mismatch repair before apoptosis is induced (Caporali *et al*., 2004; Chakravarti *et al*., 2006; D'Atri

et al., 1998). The mitotic catastrophe induced by temozolomide and γ-irradiation in the Kil (2008) study may have occurred as there was no G_2/M cell cycle arrest, and arrest at this time point is required for induction of apoptosis (Fragkos *et al*., 2009; Roos *et al*., 2004)

Interestingly, both UVW and T98g cells treated with the combination of temozolomide and X-irradiation did not appear to progress through the apoptotic cell death pathway as expected. Similarly to cell treated with radiation alone, temozolomide and X-irradiated cells appeared to only enter early apoptosis, characterised by expression of phosphatidylserine moieties only (Genderen *et al*., 2006). Radiation is suggested to induce mitotic catastrophe over apoptosis (Eriksson and Stigbrand, 2010; Firat *et al*., 2011), a mode of cell death associated with aneuploidy following unsuccessful or aberrant mitosis (Castedo *et al*., 2004). Cells undergoing mitotic catastrophe can still die through caspase dependent mechanisms (Firat *et al*., 2011; Mansilla *et al*., 2006; Portugal *et al*., 2010), suggesting that expression of phosphatidylserine moieties may still occur during mitotic catastrophe (Firat *et al*., 2011; Mansilla *et al*., 2006). Our data is inconclusive to this fact; confirmation should be carried out using confocal imaging, with DAPI staining and scoring for mitotic catastrophe being correlated with expression of phosphatidylserine moieties (Genderen *et al*., 2006). There is also a possibility that cells exposed to temozolomide and external beam al-irradiation may be undergoing a prolonged cell cycle arrest. This would prevent induction of mitotic catastrophe, as mitotic catastrophe requires cell to continue to grow and divide (Castedo *et al*., 2004). This should be confirmed by a broad range of time points being used to examine cell cycle distribution of treated cells and should be correlated with expression of classical cell cycle arrest markers such as CHK2 and Wee1 (Bartek and Lukas, 2003; Matheson *et al*., 2016; Squatrito *et al*., 2010) .

4.5.1.3 Dimethyl fumarate

As mentioned, there has been significant interest in using dimethyl fumarate as a hypoxic cell radiosensitiser in a number of cancers (Held *et al*., 1988, 1991), as the radioresistance factor glutathione can be depleted by dimethyl fumarate (Held and Hopcia, 1993; Held *et al*., 1991). We hypothesise that there would be an increase in DNA damage, cell cycle arrest and cytotoxicity when dimethyl fumarate was used in combination with external beam X-irradiation.

However, contrary to out hypothesis we have not been able to increase the effects of external beam X-irradiation with dimethyl fumarate in the UVW and T98g human glioblastoma cell lines. However, the concentrations of dimethyl fumarate used in these studies were between 0.3 and 25μM, whereas the Held study, which demonstrated hypoxic and minimal normoxic cell radiosensitisation, used a significantly higher concentration of 5mM (Held *et al*., 1988).

The hypothesis that glutathione is a radioresistance factor has been well discussed and is commonly accepted (Bump *et al*., 1982). It was hypothesised that dimethyl fumarate would deplete intracellular glutathione levels, allowing for increased intracellular oxidative stress, through which radiation elicits most cytotoxicity (Hall and Giaccia, 2012). However in our studies, the combination of dimethyl fumarate and external beam X-irradiation did not increase levels of DNA damage above the level induced by X-irradiation as a single agent as measured by γH2A.x. γH2A.x is needed for G_1 and G_2/M cell cycle arrest following DNA damage via p21 and p53 stabilisation (Fragkos *et al*., 2009). Without increased DNA damage and therefore cell cycle arrest, we believe that dimethyl fumarate is unlikely to function as a radiosensitiser.

The failure of dimethyl fumarate to induce the hypothesised increase in DNA damage and cell kill may occur due to the levels of intracellular ionisable oxygen. Normoxic cells or tissue may have excess oxygen species, so that the level of oxygen species quenched by glutathione is negligible, meaning that dimethyl fumarate has a minimal effect (Bump *et al*., 1982; Held and Hopcia, 1993; Held *et al*., 1988).

Future studies should therefore be performed using a cell permeable dye that is capable of detecting reactive oxygen species, such as 2′,7′-dichlorodihydrofluorescein diacetate (DCFDA) (Eruslanov and Kusmartsev, 2010) to detect whether the concentrations of dimethyl fumarate in combination with external beam X-irradiation are capable of inducing the hypothesised increase in reactive oxygen species. This should be trialled in cells grown in both hypoxic and normoxic conditions, verification of hypoxia should be performed using markers such as hypoxia inducible factor-1 (HIF-1α).

4.5.2 Effects of the temozolomide-dimethyl fumarate combination in combination with external beam X-irradiation

We have shown that the combination of temozolomide and dimethyl fumarate is synergistic in UVW and T98g human glioblastoma cell lines. As discussed, the standard of care for glioblastoma is radiotherapy with concomitant and adjuvant temozolomide (Stupp *et al*., 2005, 2009, 2010). In order to determine how radiotherapy could influence the temozolomide-dimethyl fumarate combination, an assay cascade similar to Chapter 3 was performed with the addition of 1 or 3Gy of external beam X-irradiation – above and below a patient clinical fraction (Preusser *et al*., 2011).

We believe that this is the first combination of temozolomide and external beam X-irradiation in combination with any form of glutathione inhibition.

It was hypothesised that the temozolomide-dimethyl fumarate combination would synergise with external beam X-irradiation through two mechanisms: dimethyl fumarate will inhibit intracellular glutathione resulting in both higher intracellular temozolomide concentrations and higher reactive oxygen species levels, resulting in an increase in DNA damage to a level greater than DNA damage response pathways can repair, resulting in increased cell death.

Our hypothesis that the temozolomide-dimethyl fumarate combination will increase cell kill in combination with external beam X-irradiation has been validated. Unfortunately, we have not been able to discern a mechanism of action of this radiosensitisation. An increase in the DNA-damaging abilities of temozolomide and external beam X-irradiation was expected to occur, this was hypothesised to increase G2/M cell cycle arrest with a correspondent increase in apoptotic induction. However, these effects were not seen.

Significantly increased cell kill was seen when the temozolomide-dimethyl fumarate combination was combined with 1 or 3Gy of external beam X-irradiation compared to the non-irradiated temozolomide-dimethyl fumarate combination. Based on the use of combination index analysis, synergy between X-irradiation and the temozolomide-dimethyl fumarate combination was described. Disappointingly, only 1Gy of external beam of external beam X-irradiation showed a synergistic interaction with the temozolomide-dimethyl fumarate combination in the UVW cell line. Both doses of

external beam X-irradiation synergised with the temozolomide-dimethyl fumarate combination in the T98g cell line. This suggests that the temozolomide-dimethyl fumarate combination should have synergistic interaction with a patient clinical fraction of 2Gy (Weller, 2011), but also suggests that the same cell kill may be achieved using a lower radiation dose. We have shown no significant difference between the 1 or 3Gy X-irradiated temozolomide-dimethyl fumarate combination, and clinically, a lower dose of X-irradiation which achieves the same level of cell kill is likely to be beneficial to the patient.

The increase in cell kill was correlated with a significant increase in DNA damage compared to external beam X-irradiation as a single agent. However, the level of γH2A.x induced by the X-irradiated temozolomide-dimethyl fumarate combination was not significantly higher than the level induced by the combination of temozolomide and X-irradiation. Although the same level of DNA damage was detected in temozolomide and temozolomide-dimethyl fumarate combination X-irradiated samples, the damage caused by the combination may be more complex, meaning the cell cannot effectively repair the damage. Further work should be performed using confocal microscopy to detect individual H2A.x foci within the nucleus. This will allow for more precise quantification of DNA lesions to quantified. Confocal microscopy should be coupled with a broader range of time points, as well as experiments in which drug is removed, and the resolution of DNA damage measured.

Despite no significant increase in DNA damage, the X-irradiated temozolomide-dimethyl fumarate combination significantly increased the size of magnitude of the G_2/M cell cycle arrest in both UVW and T98g cells. We believe that this arrest is suggestive of increased temozolomide activity as dimethyl fumarate has no significant effect on the cell cycle alone or in combination with external beam X-irradiation. An increase in G_2/M arrest could be indicative of increased DNA damage as arrest at the G_2/M checkpoint occurs to prevent the cells from dividing with damaged or low-fidelity DNA (Friedman *et al*., 1998; Li, 2008). Again, γH2Ax foci detection through confocal microscopy may give a more precise quantification of DNA damage that correlates more closely with cell cycle data.

There was no significant increase in the size of the apoptotic population despite the increased G_2/M arrest. Cells arrested at the G_2/M checkpoint are faced with two options

following DNA damage; repair the damage or apoptosis will be induced (Kastan and Bartek, 2004). We have previously shown that the temozolomide-dimethyl fumarate combination induces apoptosis in a similar pattern to temozolomide as a single agent (Figure 3.11 & 3.12). Given that the X-irradiated temozolomide-dimethyl fumarate combination induced a larger cell cycle arrest than the combination of temozolomide and X-irradiation, it was expected that there would be a larger apoptotic population. This was not validated, with all apoptotic populations reaching the same final size.

Recovery from G_2/M arrest should be investigated using flow cytometry on cells that have been treated, and had drug removed at a time point at which cells are known to arrest. Significant decrease in the size of the G_2/M arrest following treatment removal would indicate a reparable level of DNA damage. This should be correlated with confocal microscopy data examining γH2a.X resolution. This would potentially inform on how the X-irradiated temozolomide-dimethyl fumarate combination influences DNA damage, cell cycle progression and overall cell fate following treatment.

4.6 Conclusions

Temozolomide and external beam radiotherapy remains the current standard of care for high-grade glioma. We have shown, for the first time, that dimethyl fumarate in combination with the standard of care for glioblastoma has the potential to significantly increase treatment efficacy. This synergy occurred in spite of either single agent being a strong radiosensitiser.

We believe that this increase in cell kill occurs through an increase in DNA damage. This increase in DNA damage is matched with an increase in G_2/M cell cycle arrest. Arrest at this stage of the cell cycle is associated with one of two options; DNA damage repair or induction of apoptosis. Our hypothesis states that the level of DNA damage that the X-irradiated temozolomide-dimethyl fumarate combination induced is high enough as to that cells will be incapable of successful DNA damage repair, and as such, apoptosis will be induced. However, we have not been able to successfully validate this hypothesis. Our data suggets that our hypothesis may be correct, but without further experimentation we cannot definitively state how the X-irradiated temozolomide-dimethyl fumarate combination induces cell kill to a greater extent that temozolomide or dimethyl fumarate in combination with external beam X-irradiation.

Our data suggests that dimethyl fumarate is a very promising drug repurposing candidate for high-grade glioma when combined with the current standard of care, however, more work is required to elucidate a precise mechanism of action

Chapter 5

Interrogation of the molecular and genetic targets of dimethyl fumarate, and the influence on temozolomide therapy in human glioblastoma cells

5.1 Introduction

Dimethyl fumarate is commonly used as an immunomodulatory agent to treat the auto-immune diseases psoriasis and multiple sclerosis (MS) (Xu *et al*., 2015). There is very little known about the precise mechanism of action of dimethyl fumarate in these diseases, however a number of mechanistic targets have been suggested. These targets include inhibition of glutathione, nitric oxide, activation of the anti-oxidant transcription factor NRF2 and stimulation of a number of cytokines such as IL-1β, IL-6 and TNF-α (Wilms *et al*., 2010). Table 5.1 shows the role of these factors in cancer.

Suggested dimethyl fumarate target	Effect of dimethyl fumarate	Effect of target on cancer	Ref.
IL-1β	Inhibition	Increased stemness	Li *et al.,* 2012
		Increased invasion and angiogenesis	Apte *et al.,* 2006
IL-6	Inhibition	Pro-survival and anti-apoptotic effects	Kumari *et al*., 2016
		Increased invasion, metastasis and angiogenesis	
NRF2	Upregulation	Increased chemoresistance	Wang *et al.,* 2008
		Required for self-renewal of stem cells	Zhu *et al.,* 2013
TNF-α	Inhibition	Increased growth and proliferation	Wang & Lin, 2012
		Increased invasion, metastasis and angiogenesis	

Table 5.1: Suggested targets for the effects of dimethyl fumarate taken from Wilms (Wilms *et al*., 2010), the effects of dimethyl fumarate on this target, and the link of the target to the cancer.

Many of the targets and pathways which dimethyl fumarate target overlap with pathways commonly overexpressed in cancer, and as such dimethyl fumarate may have potential as an anti-cancer agent beyond its suggested role as a glutathione inhibitor (Ghods *et al*., 2013; Rocha *et al*., 2016). As seen in Table 5.1, dimethyl fumarate inhibits the cytokines IL-1β, IL-6 and TNF-α (Wilms *et al*., 2010), all of which have are known to be found at high levels in the tumour micro-environment, and inhibition of all of which has been shown to have an anti-cancer effect.

Dimethyl fumarate has been reported to be a potent activator of the antioxidant transcription factor NRF2 which is known to be both chemo and radioprotective (Brennan *et al*., 2015; Hammer *et al*., 2018; Rocha *et al*., 2016; Saidu *et al*., 2017). NRF2 expression strongly correlates to the grade of glioma, and high expression appears to be correlated with poor survival (Tsai *et al*., 2016). Dimethyl fumarate is such a potent activator of NRF2 that it can be used as a biomarker for successful dimethyl fumarate treatment in relapsing-remitting multiple sclerosis (Hammer *et al*., 2018).

We hypothesise that dimethyl fumarate will decrease glutathione levels and modulate intracellular levels of nitrites to increase glioblastoma cell chemosensitivity. We also hypothesise that the concentrations of dimethyl fumarate used will not influence the antioxidant transcription factor NRF2.

5.2 Aims and Objectives

The aims of this study were:

- To elucidate the underpinning mechanism molecular and genetic targets that dimethyl fumarate is capable of influencing in human glioblastoma cells

- To understand how glutathione, nitrites and NRF2 affect temozolomide mediated cell kill in UVW and T98g human glioblastoma cells.

5.3 Materials and Methods

5.3.1 Cell lines and routine cell maintenance

All routine maintenance of cell lines was performed as described in Section 2.1.

5.3.2 Drug preparation and treatment

Temozolomide and dimethyl fumarate were prepared and treatment was performed as described in Section 2.2. The administered concentrations of temozolomide and dimethyl fumarate used were calculated as described in Sections 2.4 and 3.4.5.1.

Pretreatment UVW and T98g human glioblastoma cells was carried out with 1mM of the antioxidants *N*-acetylcysteine and 5-hydroxy-tempo, 50μM of the nitric oxide donor *S*-nitrosoglutathione, and 5μM of the NRF2 inhibitor ML385 (all Sigma Aldrich, UK), or 100nM of the NRF2 stimulator CDDO-im (Tocris, UK) of the NRF2 modulators for 2 hours prior to addition of temozolomide.

5.3.3 Clonogenic Assay

Clonogenic assays were performed as described in Section 2.5

5.3.4 Measurement of intracellular glutathione contents

Glutathione assays were performed as described in Section 2.11.

5.3.5 Measurement of intracellular reactive oxygen species levels

Detection of intracellular oxidative stress was performed as described in Section 2.12.

5.3.6 Fast activated cell-based ELISA

Face assays were performed as described in Section 2.13 using primary anti-NRF and anti-serine 40 pNRF2 antibodies as described in Table 2.2 (Abcam, UK).

5.3.7 RNA extraction

RNA extraction was performed as described in Section 2.14 using a Qiagen RNeasy Mini kit (Qiagen, UK)

5.3.8 RT-qPCR

RT-qPCR was performed as described in Section 2.15. Target gene transcription was performed using predesigned primers for *ACTB*, *HMOX1* and *NQO1* as described in Table 2.3 (Sigma Aldrich, UK) (Brennan *et al*., 2015) and a QuantiTect SYBR Green RT-PCR kit (Qiagen UK).

5.3.9 Griess assays

Cellular nitrite production was performed by Griess assay as described in Section 2.16.

5.4 Results

5.4.1 Modulation of intracellular glutathione levels by dimethyl fumarate and the impact on temozolomide mediated cell kill in UVW and T98g human glioblastoma cells

An assay cascade was designed that allowed for the hypothesis that glutathione is a resistance factor in UVW and T98g human glioblastoma cell lines to be tested and for the examination of the effects of dimethyl fumarate on glutathione levels in these cell lines.

Dimethyl fumarate was chosen for use in combination with temozolomide as it has been shown to modulate intracellular glutathione levels, an important chemoresistance factor in many cancers including glioblastoma (Rocha *et al*., 2014).

The assay cascade designed allowed for quantification of intracellular glutathione levels following dimethyl fumarate treatment, the effect of increased glutathione levels on temozolomide induced cell kill as measured by clonogenic assay and the modulation and effect of reactive oxygen species by and on temozolomide therapy.

5.4.1.1 Inhibition of intracellular glutathione by dimethyl fumarate

In order to assess the effects of dimethyl fumarate on intracellular glutathione levels, the reduction of DTNB to TNB was measured spectrophotometrically to give a quantifiable level of glutathione.

Dimethyl fumarate induced a rapid, dose independent decrease in intracellular glutathione levels in both UVW and T98g cells (Figure 5.1a and c respectively). In both cell lines this decrease occurred following 30-minute incubation with dimethyl fumarate and resulted in an approximately 50% decrease in intracellular glutathione levels in UVW cells (p-value <0.001) and a ~60% decrease in T98g cells (p-value <0.001) compared to an untreated control. There was a slight increase in glutathione levels following 2, 4 or 6 hours of 3 or 9μM dimethyl fumarate treatment in UVW cells compared to 30-minute treatment (p-value >.05).

There was a significant rebound in glutathione levels in both UVW and T98g cell lines following 24-hour dimethyl fumarate treatment, with glutathione levels returning to control levels in UVW cells and ~85% of control levels in T98g cell lines. Rebound levels of glutathione in both cell lines were not significantly lower than control levels (p-value >0.05), but were significantly higher than glutathione levels at all other time points (p-value <0.0001).

Increasing concentrations of dimethyl fumarate did not significantly affect glutathione levels. There was no significant difference in glutathione levels between each concentration of dimethyl fumarate used in either cell line (p-value >0.05). Area under the curve analysis shows this, with no significant difference in AUC for each concentration of dimethyl fumarate administered (p-value >0.05) (Figure 5.1b &d).

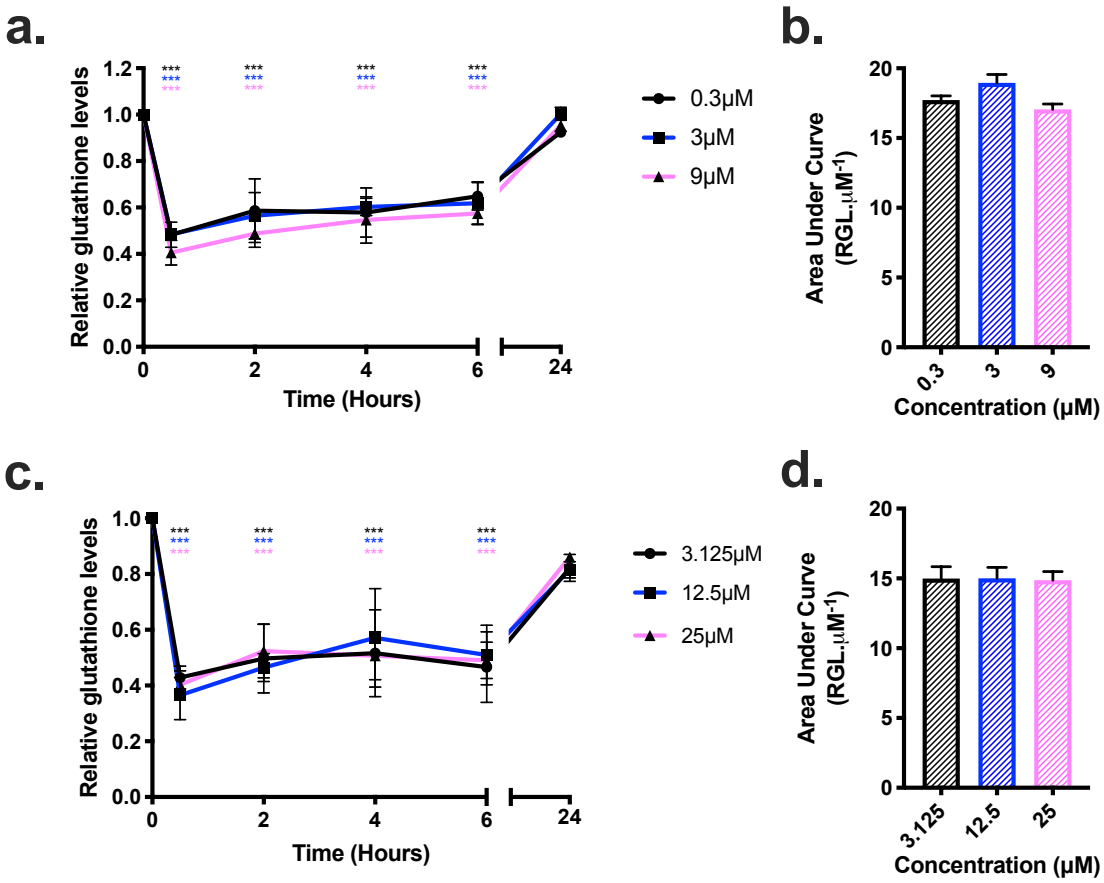

Figure 5.1: The impact of increasing concentrations of dimethyl fumarate on normalised intracellular glutathione content of **a.** UVW or **c.** T98g human glioblastoma cell lines over time. **b.** and **d.** show the area under the curve for each concentration of dimethyl fumarate. Data shown is an average of at least three independent experiments ± standard deviation. A 2-way ANOVA with Bonferroni post testing was performed using Graphpad Prism 8 software, with p-values of <0.05 = *, <0.01=** and <0.001 = *** reported as significant.

5.4.1.2 Assessment of increased glutathione levels on temozolomide mediated cell kill

N-acetylcysteine (NAC) is widely used as a reactive oxygen species scavenger. NAC is as prodrug, which spontaneously donates cysteine within the cytoplasm. Cysteine is then metabolised to increase intracellular glutathione levels, as the conjugation of cysteine is the rate limiting step of glutathione synthesis (Lu, 2013). Clonogenic assays were performed on cells pretreated with 1mM of NAC for two hours, and then treated with increasing doses of temozolomide to measure the effect of glutathione on temozolomide mediated cell kill. Glutathione assays were performed on NAC treated cells to confirm an increase in glutathione levels.

There was no significant decrease in temozolomide mediated cytotoxicity in UVW cell cells after treatment with 0.5 or 5μM of temozolomide when pretreated with 1mM *N*-acetylcysteine, however there was a significant decrease in cytotoxicity after administration of 15μM of temozolomide (p-value <0.001), with an increase in cell survival of 12%±0.04 in pretreated cells (Figure 5.2a) relative to cells treated with the same concentration of temozolomide, but not NAC. Furthermore, a 2-hour treatment of UVW cells with NAC significantly increased intracellular glutathione levels by 26%±0.02 (p-value <0.001) (Figure 5.2b), indicating that increased glutathione levels is correlated with increase temozolomide resistance in the UVW cell line. 1mM of NAC induced no significant cytotoxicity as single agent (p-value >0.05) (Figure 5.2c).

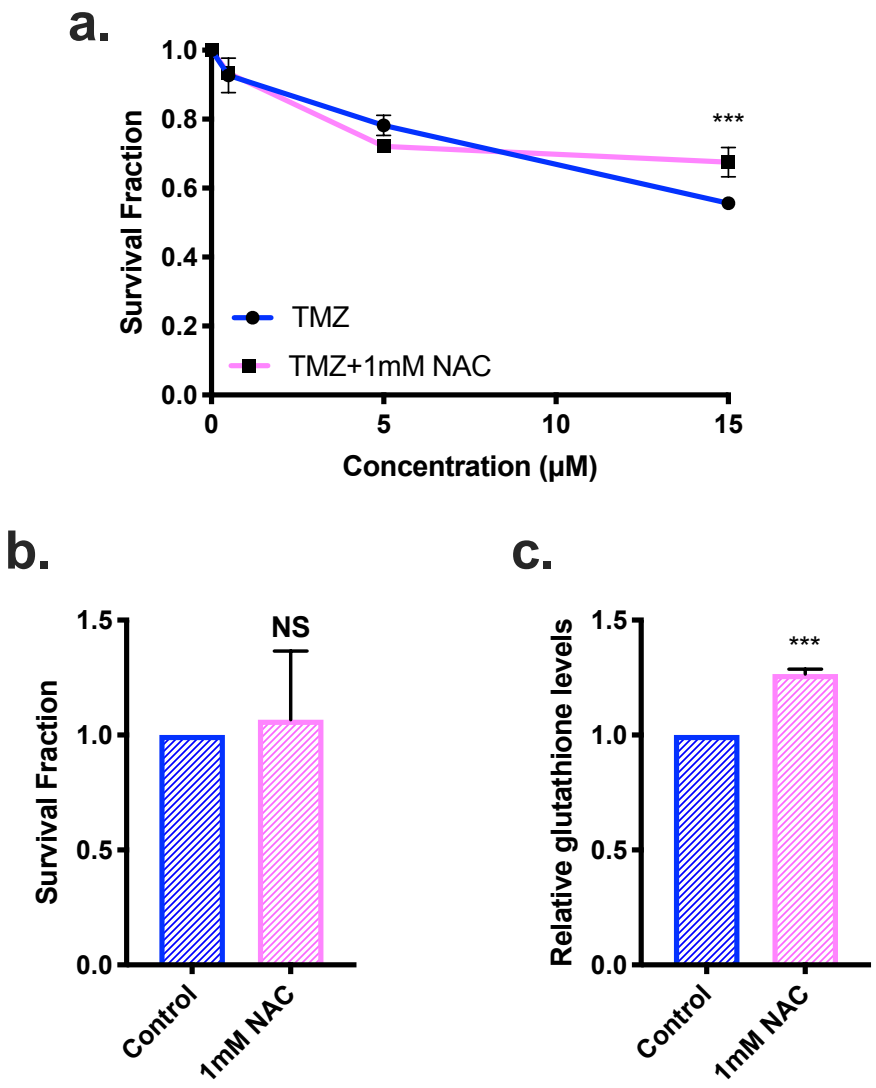

Figure 5.2: The effects of the glutathione prodrug *N*-acetylcysteine (NAC) on **a.** temozolomide mediated cell kill and **b.** the effects of NAC on intracellular glutathione levels in UVW cells. The effect of NAC as a single agent on cell kill is also shown (**c.**). A 1-way ANOVA with Bonferroni post testing was performed using Graphpad Prism 8 software, with p-values of <0.05 = *, <0.01=** and <0.001 = *** reported as significant.

Similarly to the UVW cell line, administration of 1mM of *N*-acetylcysteine to the T98g human glioblastoma cell line induced no significant cytotoxicity (p-value >0.05) (Figure 5.3c). Also similarly to the UVW cell line, NAC pretreatment did not significantly decrease the level of cell kill in temozolomide treated cells at the lowest two concentrations of temozolomide used, 50 and 200μM. *N*-acetylcysteine conferred significant resistance to temozolomide after administration of 400μM of temozolomide (p-value <0.01), with a 21%±0.07 reduction in cell kill (Figure 5.3a) compared to cells treated with the same concentration of temozolomide. 2-hour treatment of T98g cells with NAC significantly increased intracellular glutathione levels by 12%±0.04 (p-value <0.01) (Figure 5.3b).

We believe that this demonstrates that glutathione is a resistance factor to temozolomide in both UVW and T98g human glioblastoma cell lines as measured by the decrease in temozolomide mediated cell kill following *N*-acetylcysteine pretreatment, which we have shown significantly increases intracellular glutathione levels.

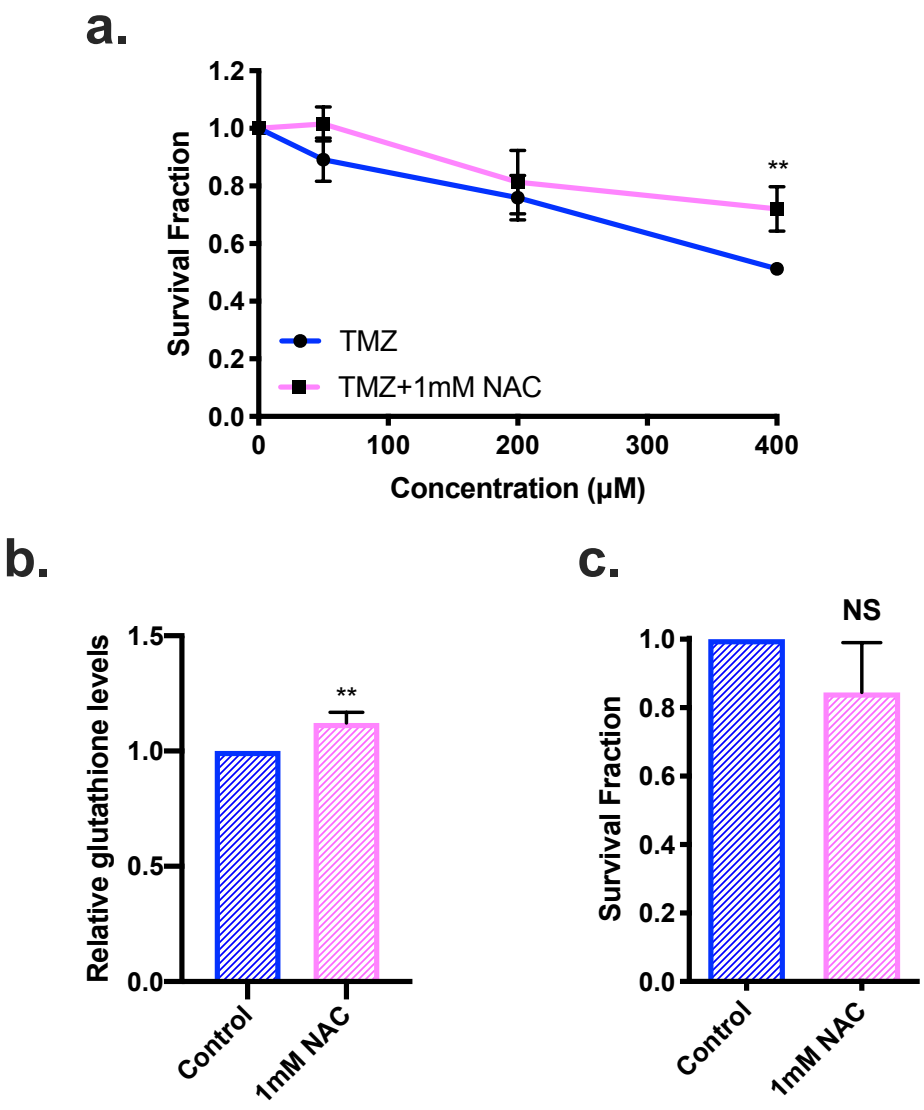

Figure 5.3: The effects of the glutathione prodrug *N*-acetylcysteine (NAC) on **a.** temozolomide mediated cell kill and **b.** the effects of NAC on intracellular glutathione levels in T98g cells. The effect of NAC as a single agent on cell kill is also shown (**c.**). A 1-way ANOVA with Bonferroni post testing was performed using Graphpad Prism 8 software, with p-values of <0.05 = *, <0.01=** and <0.001 = *** reported as significant.

5.4.1.3 Assessment of dimethyl fumarate pretreatment on temozolomide mediated cell kill

As dimethyl fumarate reduces intracellular glutathione levels, and glutathione has been shown to be a chemoresistance factor in UVW and T98g human glioblastoma cells, a time course study was performed. Cells were pretreated for between 30-minutes and 4-hours with increasing concentrations of dimethyl fumarate to deplete intracellular glutathione levels before addition of temozolomide. Concentrations of temozolomide used were the same as described in Section 3.4.1.3.

In UVW cells, increasing dimethyl fumarate pretreatment time correlated to increased cell kill at the lowest dose of dimethyl fumarate used, 0.3μM. This resulted in a 10±0.002, 15±0.04 and 20±0.03% reduction in cell survival compared to simultaneous treatment following 30-minutes, 2-hour or 4-hour pretreatment respectively. This improvement in cell kill was significant following 2-hour pretreatment (p-value <0.05) and 4-hour pretreatment (p-value <0.01) compared to a simultaneous treatment. This trend of decreased cell survival in relation to dimethyl fumarate pretreatment was observed again after administration of 3μM dimethyl fumarate, with a 5±0.11, 10±0.04 and 18±0.05% reduction in cell survival in response to increasing pretreatment time. However, only the reduction in cell survival following 4-hour pretreatment was significant (p-value <0.01),

At the highest dose of dimethyl fumarate administered, 9μM, no significant difference in cell kill between dimethyl fumarate pretreatment prior to addition of temozolomide and simultaneous treatment with the temozolomide-dimethyl fumarate combination was observed (Figure 5.3a). As seen in Figure 5.3b, there was a significant decrease in the area under the curve for the 2 and 4-hour pretreatment groups (p-value <0.05), indicating that dimethyl fumarate pretreatment does increase temozolomide mediated cell kill.

Similarly to the UVW cell line, dimethyl fumarate pretreatment in the T98g cell line showed increased cell kill compared to simultaneous treatment with temozolomide and dimethyl fumarate. Compared to simultaneous temozolomide and dimethyl fumarate treatment, pretreatment with 3.125μM of dimethyl fumarate prior to addition of temozolomide significantly increased cell kill by 15±0.04, 20±0.01 and 25±0.03% following 30-minutes (p-value <0.05), 2-hour (p-value <0.01) or 4-hour (p-value <0.01) pretreatment respectively.

As the concentration of dimethyl fumarate used for pretreatment increased to 12.5 and 25μM, there was no significant increase in cell compared to cells simultaneously with temozolomide and dimethyl fumarate (p-value >0.05).

There was a significant decrease in the area under the curve for the 4-hour pretreatment group (p-value <0.05) (Figure 5.3d), indicating that dimethyl fumarate pretreatment may give an overall increase temozolomide mediated cell kill.

Our hypothesis that dimethyl fumarate pretreatment would increase temozolomide mediated cell kill was not shown when cells were pretreated with dimethyl fumarate. Concentration of dimethyl fumarate did not appear to have an effect on the increase in cell kill.

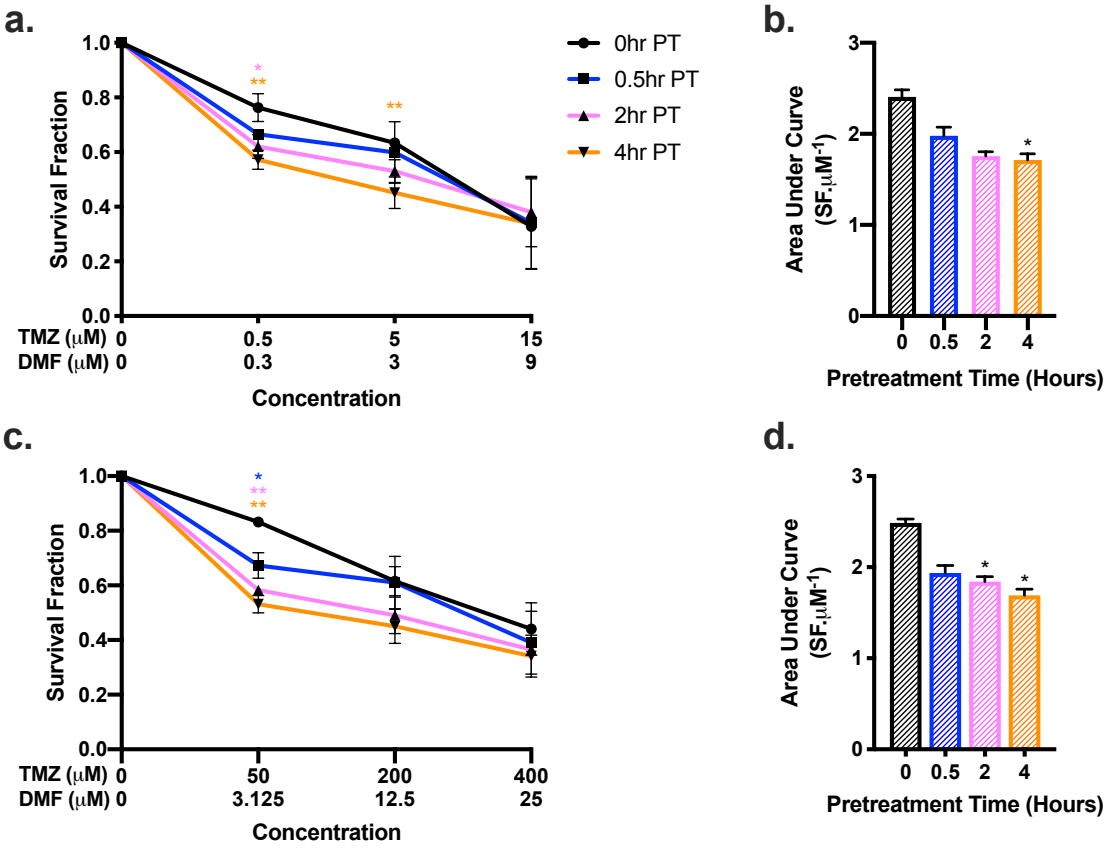

Figure 5.4: The impact of increasing concentrations of the temozolomide-dimethyl fumarate combination on the clonogenic capacity of **a.** UVW and **c.** T98g human glioblastoma cell lines following dimethyl fumarate pretreatment for between 4-hours and 30-minutes. The area under the curve for each data set is also shown in figures **b.** and **d.** for UVW and T98g human glioblastoma cell lines respectively. Data shown is an average of at least three independent experiments ± standard deviation. A 2-way ANOVA with Bonferroni post testing was performed using Graphpad Prism 8 software, with p-values of <0.05 = *, <0.01=** and <0.001 = *** reported as significant. Colours refer to significance compared to simultaneous treatment.

5.4.1.4 Assessment of reactive oxygen species scavengers on temozolomide mediated cell kill

N-acetylcysteine is used primarily as a reactive oxygen species scavenger. To show that increase in glutathione levels, but not ROS scavenging was the mechanism of NAC mediated chemoresistance, a glutathione independent reactive oxygen species scavenger was used. 5-hydroxy-tempo or tempol, is a superoxide dismutase mimetic that is capable of reactive oxygen species scavenging without increasing glutathione levels (Bernardy *et al*., 2017; Yamada *et al*., 2003). Clonogenic assays were performed on cells pretreated with 1mM of tempol for two hours, and then treated with increasing doses of temozolomide to measure the effect of a glutathione independent ROS scavenger on temozolomide mediated cell kill.

As demonstrated in Figure 5.5a, there was no significant alteration in UVW cell kill induced by temozolomide in UVW cells pretreated with 1mM tempol. Pretreatment with tempol prior to the addition of temozolomide has no significant effect on cell kill compared to treatment with temozolomide as a single agent (p-value >0.05). In the UVW cell line, tempol induced no significant increase in cytotoxicity compared to an untreated control, with a 5±0.008% decrease in cell survival respectively as seen in Figure 5.5c (p-value >0.05).

Tempol is suggested to scavenge ROS by acting as a superoxide dismutase mimetic, independently of glutathione. In order to rule out the role of glutathione in tempol mediated ROS scavenging, glutathione assays were performed on cells treated with 1mM tempol. In UVW cells there was a non-significant increase in glutathione levels (p-value >0.05) (Figure 5.5b).

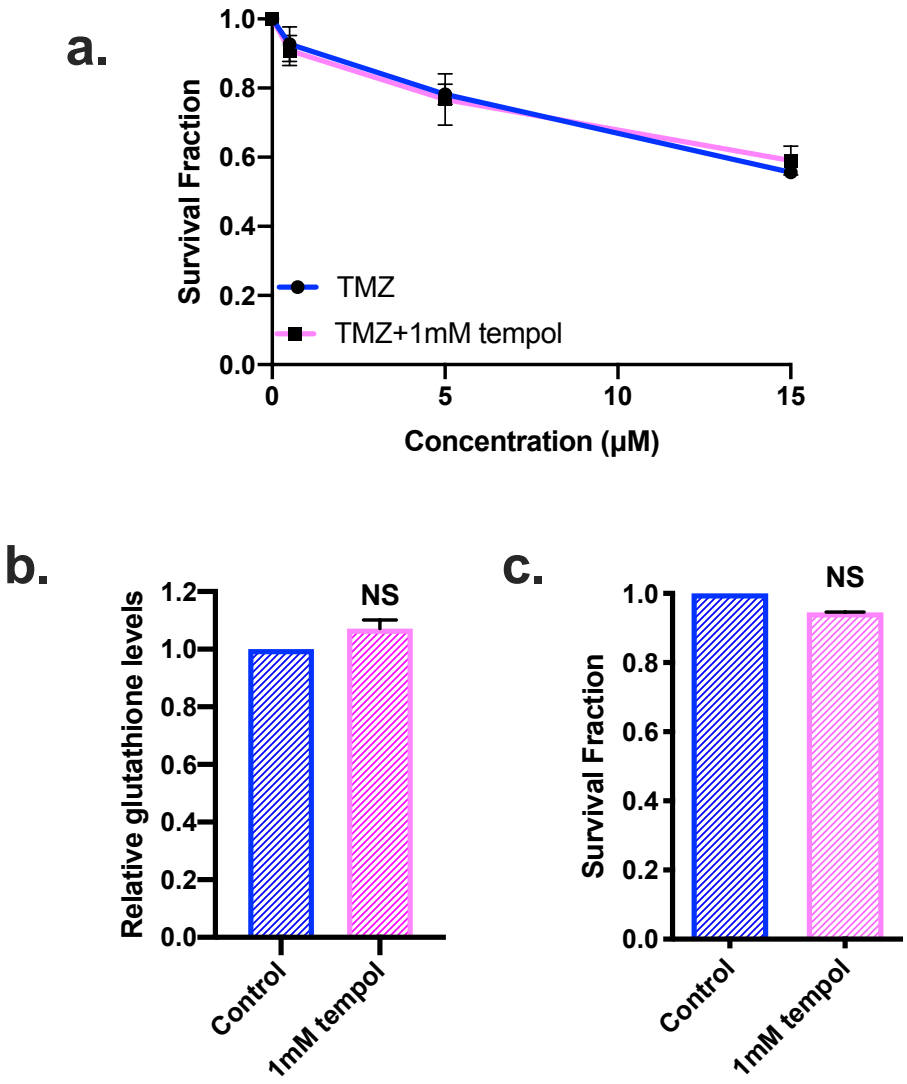

Figure 5.5: The effects of 1mM of the SOD mimetic tempol on **a.** temozolomide mediated cell kill and **b.** intracellular glutathione levels in UVW cells. The effect of tempol as a single agent on cell kill in UVW human glioblastoma cell is also shown (**c.**). A 1-way ANOVA with Bonferroni post testing was performed using Graphpad Prism 8 software, with p-values of <0.05 = *, <0.01=** and <0.001 = *** reported as significant.

Similarly to UVW cells, Figure 5.6a shows that there was no significant alteration in cell kill induced by temozolomide in T98g cells pretreated with 1mM tempol. Pretreatment with tempol prior to the addition of temozolomide has no significant effect on cell kill compared to treatment with temozolomide as a single agent (p-value >0.05) (Figure 5.6a). In the T98g cell line, tempol induced no significant increase in cytotoxicity compared to an untreated control, with a 7±0.08% decrease in cell survival respectively as seen in Figure 5.6c (p-value >0.05).

Tempol is suggested to scavenge ROS by acting as a superoxide dismutase mimetic, independently of glutathione. In order to rule out the role of glutathione in tempol mediated ROS scavenging, glutathione assays were performed on cells treated with 1mM tempol. In T98g cells there was a non-significant increase in glutathione levels (p-value >0.05) (Figure 5.6b).

This leads us to believe that *N*-acetylcysteine mediated increase in glutathione levels, and not reactive oxygen species scavenging, is the mechanism through which NAC is decreasing temozolomide mediated cell kill. We suggest this as tempol, a ROS scavenger that we have shown has no effect on glutathione levels, has no effect on temozolomide mediated cell kill in UVW and T98g human glioblastoma cell lines.

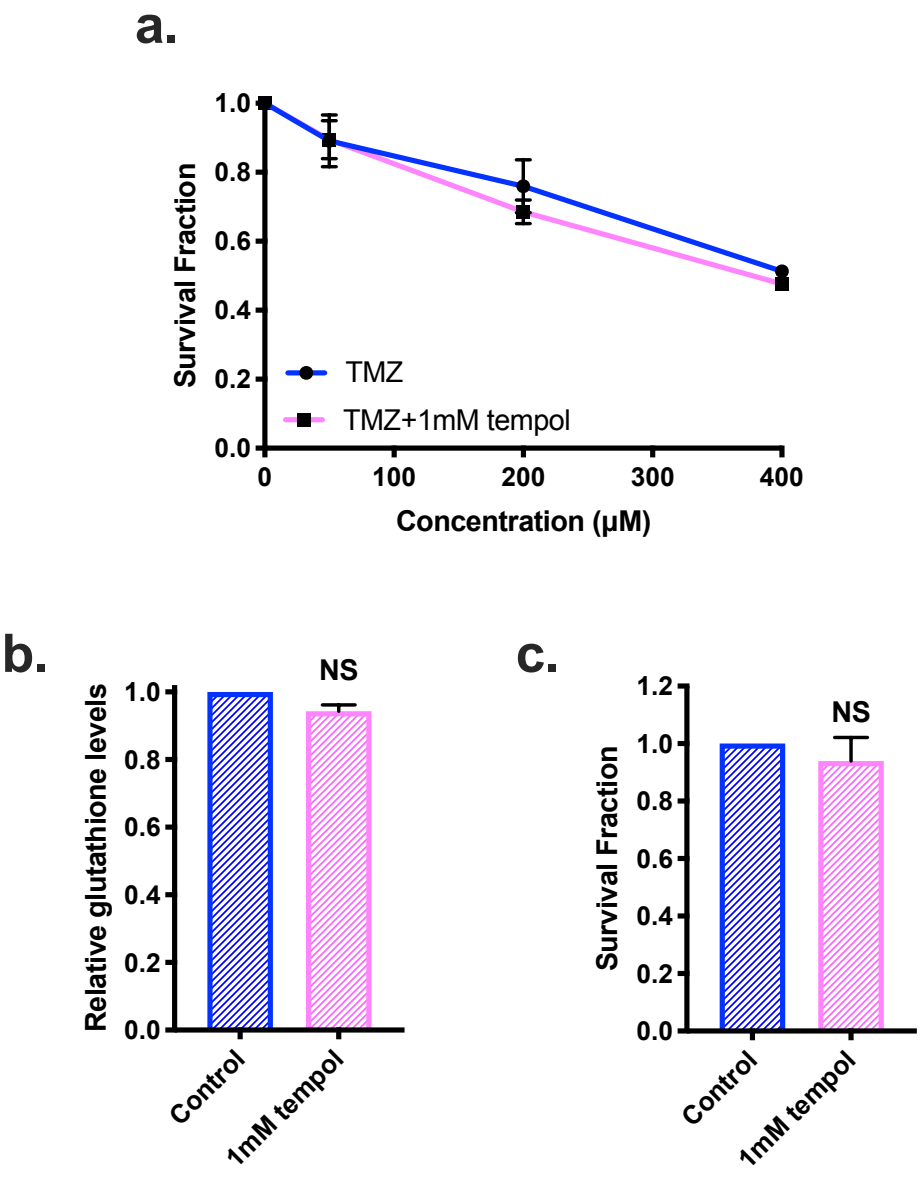

Figure 5.5: The effects of the SOD mimetic tempol on **a.** temozolomide mediated cell kill and **b.** intracellular glutathione levels in T98g cells. The effect of tempol as a single agent on cell kill in T98g human glioblastoma cell is also shown (**c.**). A 1-way ANOVA with Bonferroni post testing was performed using Graphpad Prism 8 software, with p-values of <0.05 = *, <0.01=** and <0.001 = *** reported as significant.

5.4.1.5 Assessment of N-acetylcysteine and tempol on temozolomide induced reactive oxygen species levels

In order to determine if temozolomide treatment induces the generation of reactive oxygen species, UVW and T98g human glioblastoma cells were incubated with increasing doses of temozolomide as a single agent, or in the presence 1mM of *N*-acetylcysteine or 1mM tempol. Oxidative stress was then measured by the oxidation of 2′,7′-dichlorodihydrofluorescein diacetate (DCFDA) to the fluorescent molecule 2′,7′-dichlorofluorescein (Eruslanov and Kusmartsev, 2010). Increasing fluorescent signal is indicative of increased intracellular oxidative stress. Data was quantified using flow cytometry.

In response to 24-hour temozolomide treatment, there was an increase in oxidative stress at all concentrations of temozolomide in UVW cells, with a 1.1±0.11, 1.2±0.10 and 2±0.26-fold increase in fluorescence at 0.5, 5 and 15μM respectively (Figure 5.7a). Only the increase in oxidative stress following 15μM temozolomide treatment was significantly higher than basal levels of oxidative stress (p-value <0.01).

When UVW cells were pretreated with either *N*-acetylcysteine or tempol the increase in oxidative stress was ablated to control level at all doses of temozolomide used. Only the reduction in oxidative stress after administration of 15μM of temozolomide was significant compared to temozolomide as a single agent (p-value <0.01), but this reduction was not significantly different than a NAC or tempol treated control (Figure 5.7a).

In response to 24-hour temozolomide treatment, there was a significant increase in oxidative stress at all administered concentrations of temozolomide in T98g cells, with a 1.3±0.15, 1.5±0.10 and 1.5±0.28-fold increase in fluorescence at 50 (p-value <0.01), 200 and 400μM respectively (p-value <0.001).

As demonstrated in Figure 5.7b, when T98g cells were pretreated with either *N*-acetylcysteine or tempol, the increase in oxidative stress was significantly ablated to control level at all doses of temozolomide administered (p-value <0.001). The reduction in oxidative stress by tempol after treatment with 200μM of temozolomide was

significantly lower than control levels (p-value <0.05), as was the reduction at 400μM of temozolomide (p-value <0.01).

Taken with previous data, we believe that we have shown that reactive oxygen species does not play a role in temozolomide mediated chemoresistance. We have shown that pretreatment with the reactive oxygen species scavenger NAC, but not tempol, is capable of decreasing temozolomide mediated cell kill. We believe that this is due to the ability of NAC to increase intracellular glutathione levels

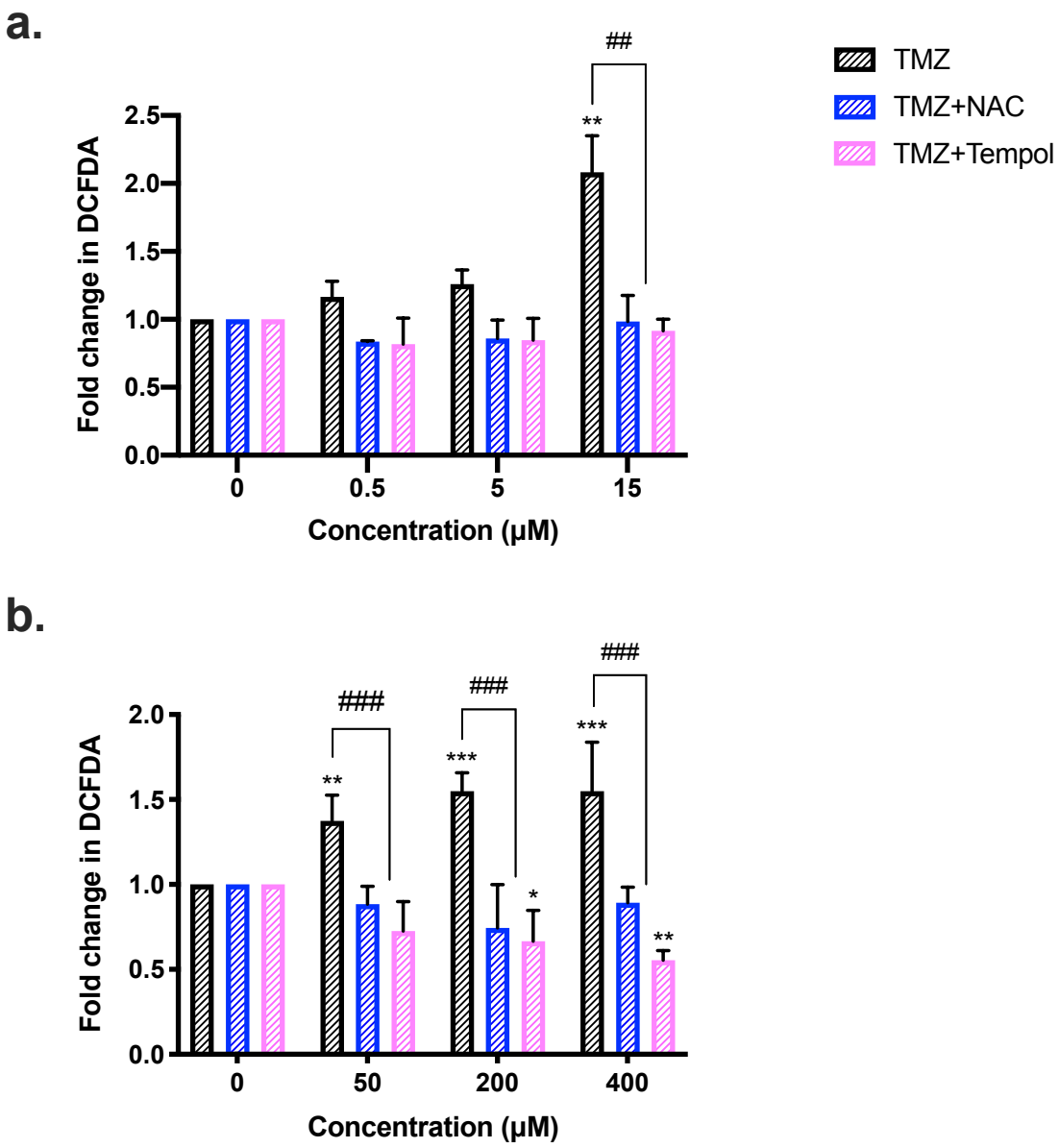

Figure 5.7: The impact of increasing doses of temozolomide on intracellular oxidative stress in **a.** UVW or **b.** T98g human glioblastoma cell lines following 24-hour treatment. Data also shows the effects of 2-hour pretreatment following either 1mM NAC or 1mM tempol on temozolomide induced oxidative stress. Data shown is an average of at least three independent experiments ± standard deviation. A 2-way ANOVA with Bonferroni post testing was performed using Graphpad Prism 8 software, with p-values of <0.05 = *, <0.01=** and <0.001 = *** reported as significant compared to an untreated, NAC or Tempol treated control and p-values of <0.05 = #, <0.01=## and <0.001= ### reported as significant compared to temozolomide treated cells.

5.4.2 Modulation of NRF2 by dimethyl fumarate and the effect on temozolomide therapy in UVW and T98g human glioblastoma cells

Dimethyl fumarate has been shown to activate NRF2, a transcription factor that is capable of activating a number of reactive oxygen scavenging genes. Using fast activated cell based ELISAs (FACE assays), activation of NRF2 was measured by phosphorylation of the serine-40 residue of NRF2 and confirmed by RT-qPCR for downstream targets of NRF2.

A known inducer of NRF2, the synthetic triterpenoid CDDO-im, was used to stimulate NRF2 activation in UVW and T98g human glioblastoma cell lines prior to temozolomide treatment. This allowed for temozolomide mediated cell kill following NRF2 activation in these cell lines to be measured.

5.4.2.1 Modulation of the activation of the antioxidant transcription factor NRF2 by dimethyl fumarate

FACE assays for quantification of ser40-pNRF2 were performed on dimethyl fumarate treated UVW and T98g human glioblastoma cell lines. To validate the results of FACE assays, RT-qPCR was performed on RNA extracted from cells treated with dimethyl fumarate to detect transcription of downstream targets of NRF2, *HMOX1* and *NQO1.*

Figure 5.8a shows the effects of administration of increasing doses of dimethyl fumarate on NRF2 phosphorylation over time. There was a rapid, dose independent increase in the level of pNRF2 following 2-hours of dimethyl fumarate treatment, with a 20±0.32% increase in the level of phosphorylated NRF2, however this was not significant compared to basal levels or the pNRF2 levels at any other time point (p-value >0.05). pNRF2 levels returned to basal levels after 4 hours of dimethyl fumarate treatment in a dose independent manner. This level of pNRF2 levels was maintained across the remaining time points.

The increase in pNRF2 levels was matched by a significant increase in transcription of *HMOX1* and *NQO1* (Figure 5.8b), with a relative increase in expression of 5.1±1.55 (p-value <0.01) and 6.1±1.29 (p-value <0.001) respectively. Expression of both genes declined rapidly after 4 and 24-hour treatment. Levels of *HMOX1* reduced to control levels after 4 and 24-hour treatment, however, levels of *NQO1* remained raised compared to a control (p-value <0.05). The decrease in *HMOX1* and *NQO1* levels at 4 and 24-hour time points post-dimethyl fumarate treated was significantly lower than peak expression levels (p-value <0.01 & 0.05 for each gene respectively).

In contrast, T98g cells displayed a markedly different response to dimethyl fumarate mediated NRF2 activation compared to the UVW cell line. Figure 5.8c shows that from 1-hour treatment with dimethyl fumarate, pNRF2 levels increased slowly in a dose dependent manner. The level of pNRF2 peaked after 6-hour dimethyl fumarate treatment, with 3.125μM, 12.5μM and 25μM inducing a 10±2.9, 25±3.1 and 30±3.2% increase respectively. However, this was not significant compared to basal levels of pNRF2 (p-value >0.05). Following this peak at 6-hours, there was a rapid decrease in pNRF2 levels to 15±3.03% below basal levels at 8-hour treatment. pNRF2 levels returned to basal levels by 24-hours.

Transcription of both *HMOX1* and *NQO1* approximately doubled after 4 and 24-hour treatment with 25μM dimethyl fumarate in the T98g cell line (Figure 5.8d), however this increase was not significant compared to basal expression levels (p-value >0.05). Levels of *HMOX1* remained raised, but not significantly so, compared to basal levels after 24-hour treatment, but transcription of *NQO1* increased 5±0.86 fold compared to a control expression (p-value <0.01). At this time point levels of *NQO1* were found to be significantly higher than 2 and 4-hour expression levels (p-value <0.01).

This data suggests that the concentrations of dimethyl fumarate used in in the temozolomide-dimethyl fumarate combination are capable of activating the transcription factor NRF2 as measured by the increase in target gene expression.

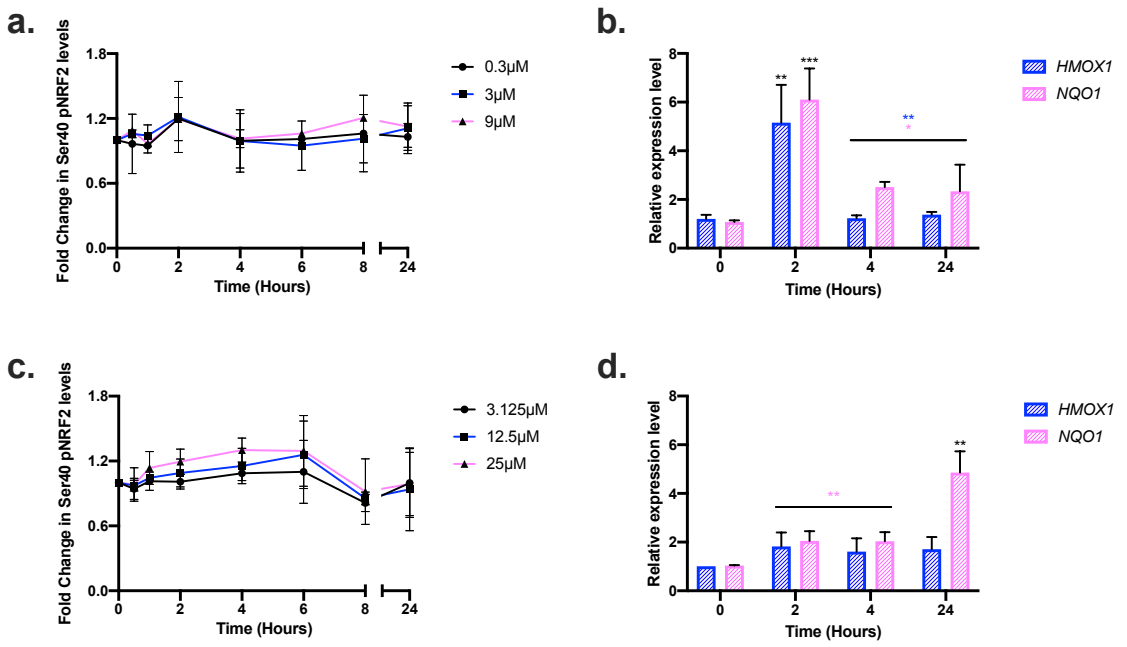

Figure 5.8: The impact of dimethyl fumarate on levels of serine-40 phosphorylated NRF2 in **a.** UVW or **c.** T98g human glioblastoma cell lines over time as quantified by FACE assay. NRF2 target gene activation following treatment with 9μM or 25μM dimethyl fumarate in **b.** UVW or **d.** T98g human glioblastoma cell lines over time as quantified by RT-qPCR. Data shown is an average of at least three independent experiments ± standard deviation. A 2-way ANOVA with Bonferroni post testing was performed using Graphpad Prism 8 software, with p-values of <0.05 = *, <0.01=**, and <0.001 = *** reported as significant compared to a control.

5.4.2.2 Modulation of temozolomide mediated cell kill by NRF2 activity

The triterpenoid CDDO-imidazolide is an activator of NRF2 via activation of antioxidant response elements and cyclic AMP response promoter elements. ML385 is a first in class synthetic NRF2 inhibitor that prevents NRF2 transcriptional activity by binding to the NEH1 domain of the protein which is required for DNA binding (Singh *et al*., 2016). UVW and T98g human glioblastoma cells were treated with 100nM of CDDO-im or 5μM ML385 for 2 hours to observe the effect of these compounds on serine-40 phosphorylated NRF2 levels and the levels of two downstream targets of NRF2, *HMOX1* and *NQO1*. The effects of pretreatment with each agent, and therefore NRF2 activity, on temozolomide mediated cell kill was also examined by clonogenic assay.

As demonstrated in Figure 5.9a, 2-hour treatment with 100nM CDDO-im increased levels of NRF2 with a phosphorylated serine-40 residue 1.9±0.44-fold (p-value <0.05) compared to an untreated control in UVW human glioblastoma cells. This translated to activation of NRF2 target genes, as seen in Figure 5.9b. Transcription of both *HMOX1* and *NQO1* increased over 2.64±1.2 and 2.782±1.33-fold respectively in relation to β-actin in response to treatment with 100nM CDDO-im (p-value <0.01).

ML385 induced a 1.2±0.27-fold increase in the level of pNRF2 (p-value >0.05) (Figure 5.9a). Furthermore, there was no increase in transcription of *HMOX1* or *NQO1*. Treatment with 5μM ML385 reduced *HMOX1* or *NQO1* transcription below control level in UVW cells, with a relative expression of 0.71±0.19 and 0.78±0.21 respectively. This was not significantly lower than basal gene expression levels in ML385 treated cells (p-value >0.05) (Figure 5.9b).

100nM CDDO-im treatment induced no significant toxicity as a single agent (p-value >0.05) (Figure 5.9d) but did induce a significant 1.9±0.44-fold increase in the level of phosphorylated NRF2. When combined with temozolomide, CDDO-im treatment reduced temozolomide mediated cell kill at all concentrations used, with a 5±2.30, 10±0.8 and 30±0.05% reduction in cell kill at 0.5, 5 and 15μM respectively. However, only the reduction in cell kill at 15μM of temozolomide was significant (p-value <0.01) (Figure 5.9c).

Despite having no effect on pNRF2 levels and no significant effect on cell kill (p-value >0.05), ML385 was able to increase temozolomide mediated cell kill at 5 and 15μM, with a 35±13 and 40±6% improvement in cell kill respectively (p-value <0.001 & <0.001). ML385 treatment caused no significant cell kill as a single agent in the UVW cell line (Figure 5.9d).

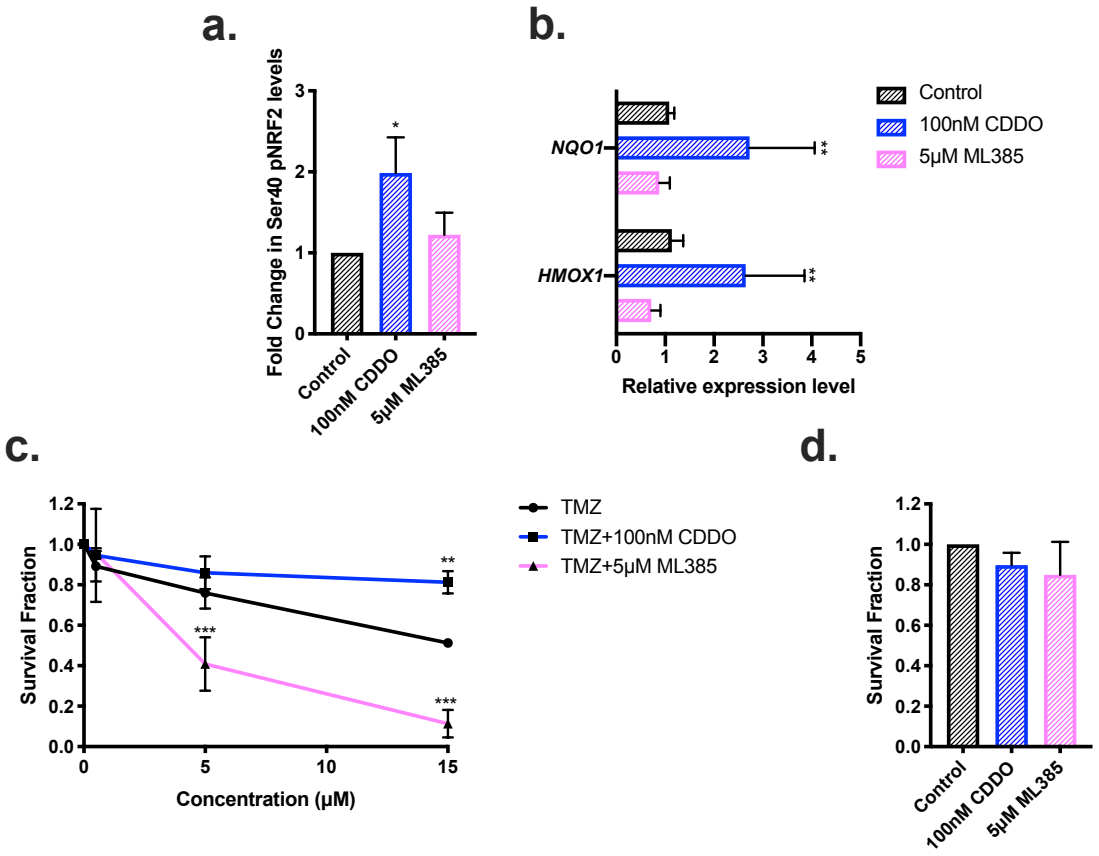

Figure 5.9: The effects of NRF2 modulation on temozolomide mediated cell kill in the UVW human glioblastoma cell line. The effects of CDDO-im and ML385 on **a.** pNRF2 levels and **b.** downstream targets of NRF2 in UVW cells. The effect of the NRF2 inducer CDDO-im and NRF2 inhibitor ML385 **c.** on temozolomide mediated cell kill is also shown, as is the effect of **d.** CDDO-im and ML385 as single agents. A 1-way ANOVA with Bonferroni post testing was performed using Graphpad Prism 8 software, with p-values of <0.05 = *, <0.01=** and <0.001 = *** reported as significant.

Figure 5.10a demonstrated that, similarly to the UVW cell line, treatment with 100nM CDDO-im significantly increased levels of serine 40 phosphorylated NRF2 1.5±0.25-fold (p-value <0.05) in the T98g cell line. This correlated to a significant increase in both *NQO1* and *HMOX1*, with a 3.6±0.78 and 2.6±0.55-fold increase in relative expression respectively (p-value <0.05). 5μM ML385 induced no significant increase in levels of pNRF2 but did significantly lower levels of *NQO1* below basal levels (p-value <0.01). There was no difference between expression of *HMOX1* in cells treated with 5μM ML385 and untreated cells (Figure 5.10b).

Treatment with 100nM CDDO-im induced no significant cytotoxicity as a single agent (p-value >0.05) (Figure 5.10d), but increased chemoresistance to temozolomide in T98g cells following treatment with 50 and 400μM. There was a significant 14±10.8 (p-value <0.05) and 15±4.09% (p-value <0.01) reduction in cell kill at 50μM and 400μM respectively, but no significant reduction in cell kill at 200μM (Figure 5.10c).

Pretreatment with 5μM ML385 increased chemosensitivity at all administered concentrations of temozolomide (Figure 5.10c). This increase in chemosensitivity was significantly higher than temozolomide alone at 200μM, with a 25±7.03% improvement in cell kill (p-value <0.001) and at 400μM, with an 18±7.71% improvement in cell kill (p-value <0.01). As a single agent, 5μM ML385 induced 15±10.1% cell kill, which was significantly greater than an untreated control (p-value <0.01) (Figure 5.10d).

Figures 5.9 and 5.10 show that activation of NRF2 significantly increases chemoresistance to temozolomide. This was confirmed pharmacologically using a positive and negative regulator of NRF2. Taken with Figure 5.8, we believe that dimethyl fumarate mediated activation of NRF2 may significantly inhibit the efficacy of the temozolomide-dimethyl fumarate combination.

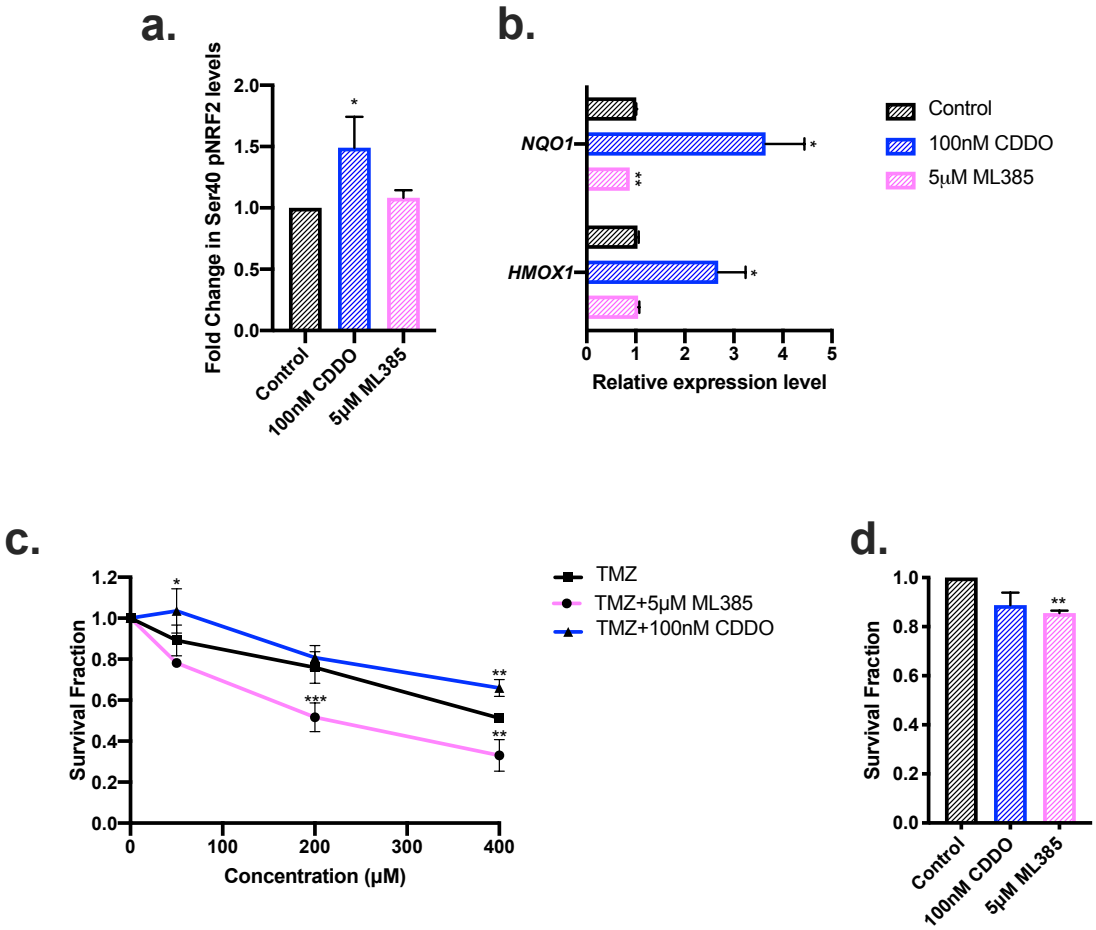

Figure 5.10: The effects of NRF2 modulation on temozolomide mediated cell kill in the T98g human glioblastoma cell line. The effects of the NRF2 inducer CDDO-im and NRF2 inhibitor ML385 on **a.** pNRF2 levels and **b.** downstream targets of NRF2 in T98g cells. The effect of CDDO-im and ML385 **c.** on temozolomide mediated cell kill is also shown, as is the effect of **d.** CDDO-im and ML385 as a single agent. A 1-way ANOVA with Bonferroni post testing was performed using Graphpad Prism 8 software, with p-values of <0.05 = *, <0.01=** and <0.001 = *** reported as significant.

5.4.3. Modulation of nitric oxide by dimethyl fumarate

Dimethyl fumarate has a large number of suggested targets, one of which is nitric oxide. Previous studies have shown that dimethyl fumarate decreased nitrite levels in a number of systems (Wilms *et al*., 2010). In order to determine how the concentrations of dimethyl fumarate that constitute the temozolomide-dimethyl fumarate combination affect nitric oxide levels, Griess assays were performed on supernatant from dimethyl fumarate treated cells. In order to determine how nitrites effect temozolomide cell kill, the nitric oxide donor S-nitrosoglutathione (GSNO) was used to increase nitrite levels in both UVW and T98g human glioblastoma cells. Clonogenic assays were performed using temozolomide and GSNO pretreatment.

5.4.3.1 Quantification of nitrite levels following dimethyl fumarate treatment

Dimethyl fumarate has been shown to modulate nitrite levels in a number of systems (Wilms *et al*., 2010). Nitrites have a broad range of actions in cancers, some of which are anti-neoplastic and some of which are pro-neoplastic (Eyler *et al*., 2011; Morbidelli *et al*., 2004). Griess assays were performed on supernatant from cells treated with increasing concentrations of dimethyl fumarate for 2, 4 or 24 hours.

In UVW cells, basal levels of nitrites were found to be 3.12±0.15μM at all time points. Dimethyl fumarate had no significant effect on levels of nitrites after 2, 4 or 24-hour treatment. There was no significant difference in nitrite levels between any of the time points examined (Figure 5.11a).

In the T98g cell line, increasing concentrations of dimethyl fumarate had no effect on nitrite levels at any time point. There was no significant change in nitrite levels following 2, 4, or 24-hour treatment with increasing concentrations of dimethyl fumarate in T98g cells. Again, there was no significant difference in nitrite levels between any of the time points examined (Figure 5.11b).

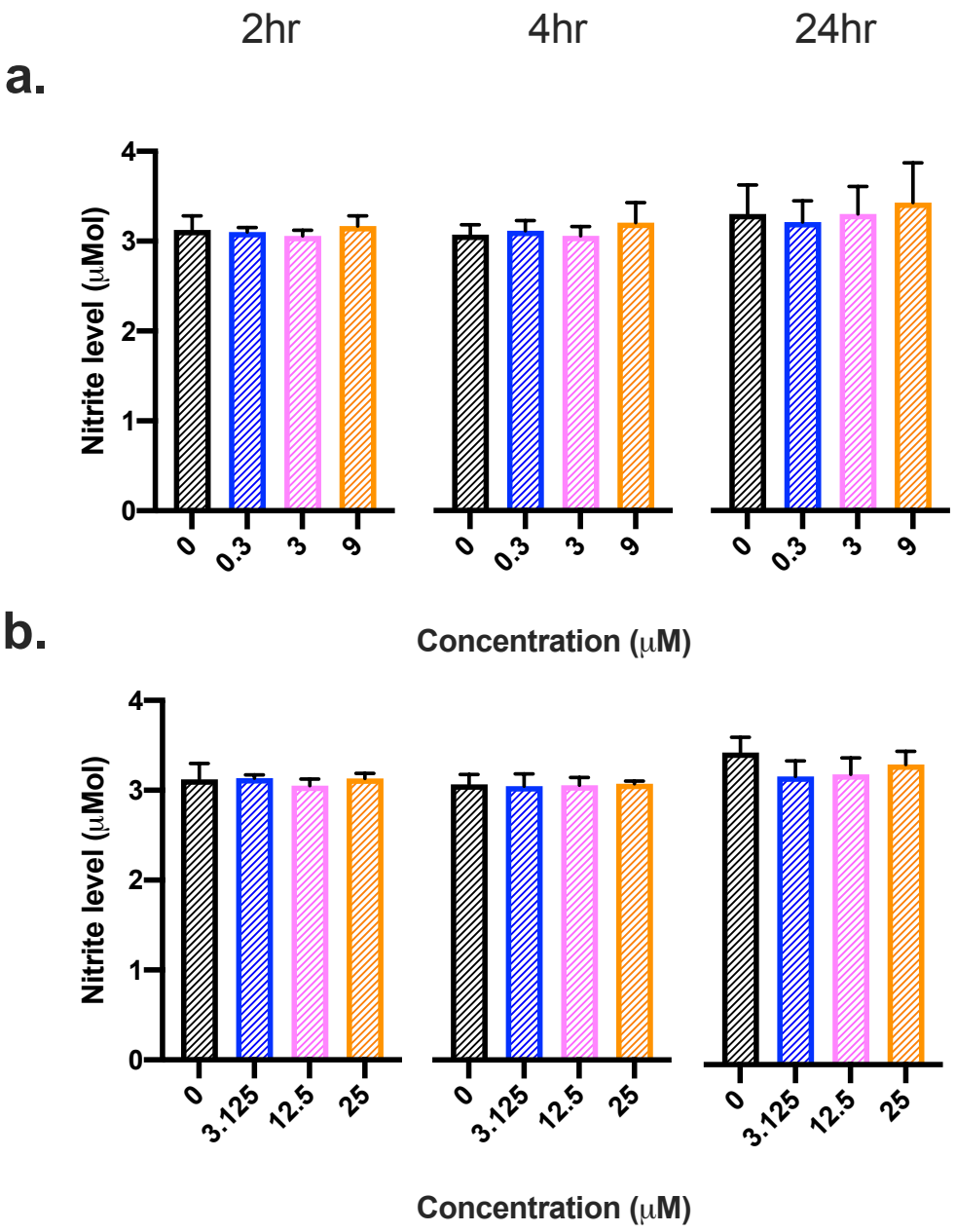

Figure 5.11: The effects of dimethyl treatment on nitrite levels in **a.** UVW and **b.** T98g human glioblastoma cell lines. Cells were treated with increasing concentrations of dimethyl fumarate for 2, 4 or 24 hours before supernatant was collected and nitrite level analysed using the Griess assay. Data shown is an average of 3 independent experiments ± standard deviation. A 2-way ANOVA with Bonferroni post testing was performed using Graphpad Prism 8 software, with p-values of <0.05 = *, <0.01=**, and <0.001 = *** reported as significant.

5.4.3.2 Assessment of S-nitrosoglutathione on temozolomide mediated cell kill

S-nitrosoglutathione (GSNO) is an endogenous nitric oxide donor that spontaneously releases nitric oxide under physiological conditions. GSNO is also used experimentally to increase nitric oxide levels in *in vitro* systems. Clonogenic assays were performed on cells pretreated with 50μM of GSNO for two hours, and then treated with increasing doses of temozolomide to measure the effect of nitric oxide on temozolomide mediated cell kill.

As seen in Figure 5.12a, treatment with 50μM *S*-nitrosoglutathione significantly increased basal nitrite levels from 3.1±0.15μM to 4.7±0.44μM (p-value <0.01). The same concentration of *S*-nitrosoglutathione did not significantly increase the levels of intracellular glutathione in UVW cells (Figure 5.10b).

The UVW cell line showed no significant decrease in temozolomide mediated cytotoxicity at any concentration of temozolomide when pretreated with 50μM GSNO, but a non-significant increase in survival was observed at each concentration of temozolomide used (p-value >0.05) (Figure 5.12c). 50μM of GNSO induced no significant cytotoxicity as single agent (p-value >0.05) (Figure 5.12d).

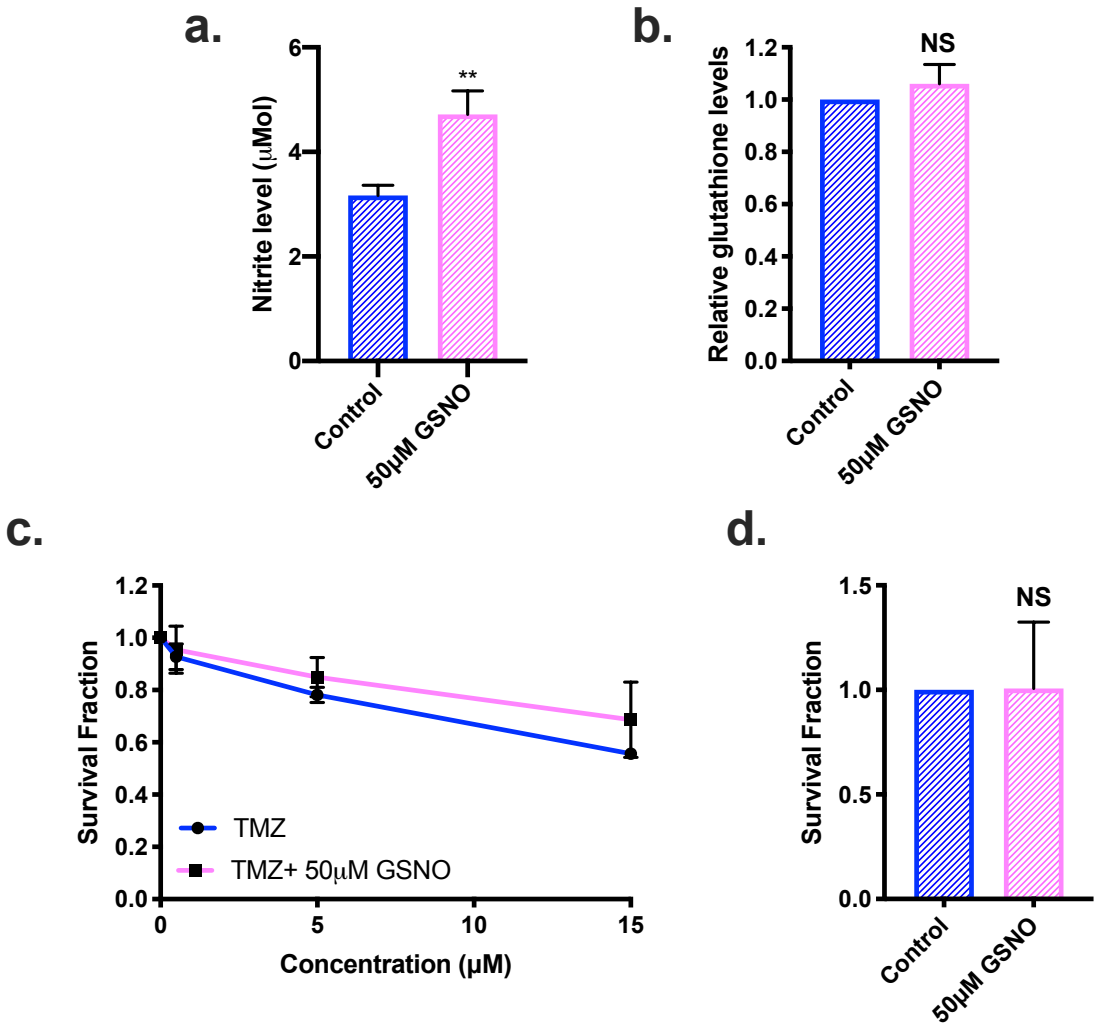

Figure 5.12: The effects of nitric oxide modulation by S-nitrosoglutathione (GSNO) on temozolomide mediated cell kill in the UVW human glioblastoma cell line. The effects of GSNO on **a.** nitric oxide and **b.** glutathione levels is shown as is the effect on survival of **c.** GSNO pretreatment on temozolomide mediated cell kill and **d.** GSNO as a single agent. A 1-way ANOVA with Bonferroni post testing was performed using Graphpad Prism 8 software, with p-values of <0.05 = *, <0.01=** and <0.001 = *** reported as significant.

In the T98g cell line, treatment with 50μM *S*-nitrosoglutathione (GSNO) significantly increased basal nitrite levels from 3.2±0.04μM to 5.2±1.02μM (p-value <0.05) (Figure 5.13a). Similarly to the UVW cell line, the same concentration of *S*-nitrosoglutathione did not significantly increase the levels of intracellular glutathione in T98g cells (Figure 5.13b).

GSNO pretreatment in temozolomide treated T98g cells showed no effect, with 50 and 200μM temozolomide treatment inducing the same level of cell kill with or without GSNO pretreatment (p-value >0.05) (Figure 5.13c).

Following treatment with 400μM temozolomide, approximately 51±0.9% cell kill was achieved. However, when cells were pretreated with 50μM GSNO, the same concentration of temozolomide caused a 30±7% cell kill, a 20% reduction (p-value <0.001) (Figure 5.13c). Again, 50μM of GNSO induced no significant cytotoxicity as single agent (p-value >0.05) (Figure 5.13d).

Our data indicates that nitric oxide has little effect on temozolomide mediated cell kill.

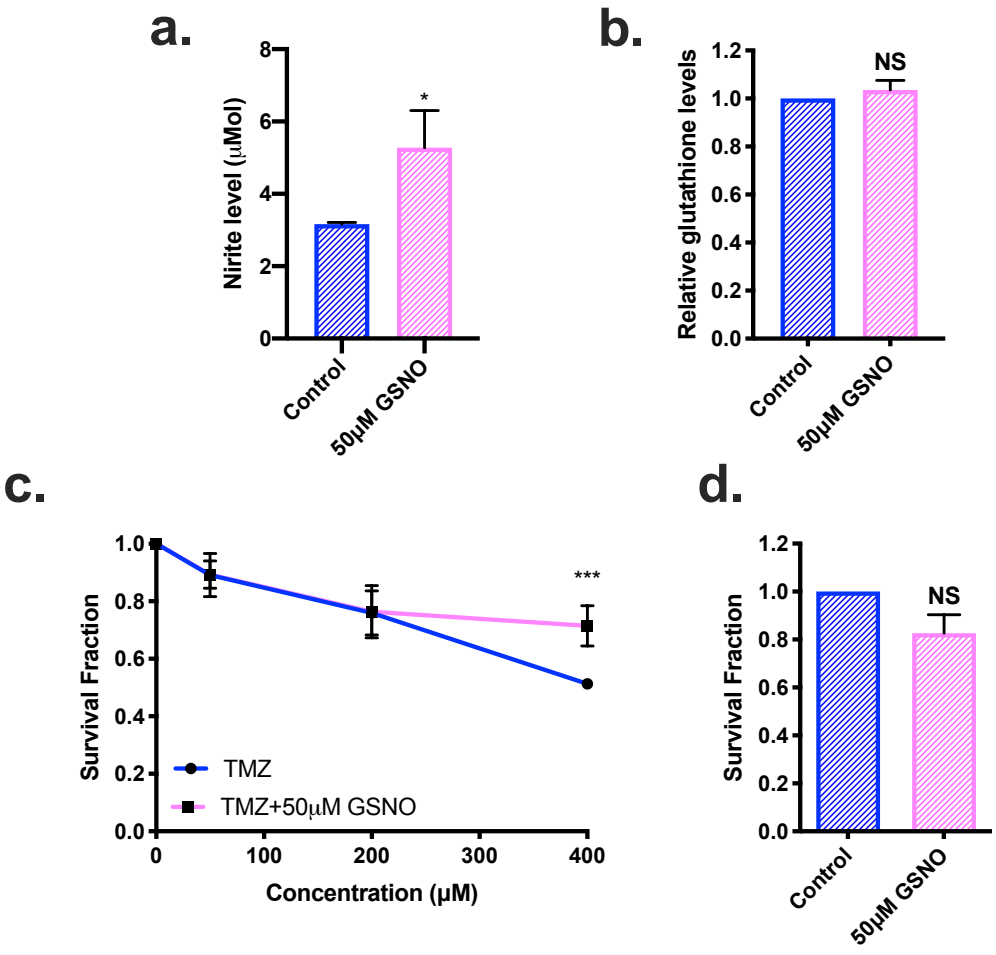

Figure 5.13: The effects of nitric oxide modulation by S-nitrosoglutathione (GSNO) on temozolomide mediated cell kill in the T98g human glioblastoma cell line. The effects of GSNO on a. nitric oxide and b. glutathione levels is shown as is the effect on survival of c. GSNO pretreatment on temozolomide mediated cell kill and d. GSNO as a single agent. A 1-way ANOVA with Bonferroni post testing was performed using Graphpad Prism 8 software, with p-values of <0.05 = *, <0.01=** and <0.001 = *** reported as significant.

5.5 Discussion

5.5.1 Glutathione as a chemoresistance factor in human glioblastoma cells

The effects of dimethyl fumarate on the intracellular glutathione levels were interrogated, and the effects of glutathione on temozolomide mediated cell kill on UVW and T98g human glioblastoma cells was also examined.

Dimethyl fumarate was initially proposed for use in cancer as a hypoxic cell radiosensitiser, where it was used at millimolar concentrations, with no significant mechanistic interrogation being performed beyond the suggestion of glutathione depletion (Bump *et al*., 1982; Held and Hopcia, 1993; Held *et al*., 1988, 1991). As discussed in Chapter 3, glutathione is a major chemo and radio-resistance factor (Rocha *et al*., 2014, 2016) with increased expression and nuclear localisation of the glutathione conjugating enzyme glutathione-s-transferase π (GSTπ) correlating with poorer patient outcome in glioma (Ali-Osman *et al*., 1997; Okcu *et al*., 2004; Zhu *et al*., 2018).

The concept of glutathione depletion has been widely used in cancer to enhance chemotherapy and radiotherapy. Buthionine sulphoximine has been previously used in a number of studies to deplete glutathione via inhibition of the glutathione precursor enzyme, γ-glutamylcysteine synthetase (Allalunis-Turner *et al*., 1991; Dorr *et al*., 1986; Lu, 2013). The millimolar range that BSO has been administered at has however been shown to induce deletions in foetal DNA (Reliene and Schiestl, 2006). Dimethyl fumarate is safe, efficacious and already clinically available, with doses of 480mg being well tolerated in humans (Phillips and Fox, 2013; Xu *et al*., 2015).

We have demonstrated that dimethyl fumarate induced a rapid depletion of intracellular glutathione (Figure 5.1). However, we have shown that this depletion appears to be both concentration and time independent, with glutathione levels decreasing below 50% within 30 minutes of dimethyl fumarate treatment in both UVW and T98g human glioblastoma cells. The dose independent effect of dimethyl fumarate on glutathione levels has been reported previously, but only at concentrations of dimethyl fumarate at far higher concentrations than those used in the temozolomide-dimethyl fumarate combination (Schmidt and Dringen, 2010). Rapid depletion of glutathione similar to our

results has been indicated to be pro-apoptotic (De Nicola and Ghibelli, 2014), correlating with data seen in Chapter 3, Figures 3.10 & 3.11.

Studies utilising dimethyl fumarate at concentrations comparable to our own have shown both a time and concentration dependency on the effects of dimethyl fumarate mediated glutathione depletion (Brennan *et al*., 2015; Lin *et al*., 2011). However, the work by Brennan *et al*., (2015), showed similar trends to those reported in Figure 5.1, with no significant variation in glutathione levels, beyond the initial decrease. This occurs across the first 6 hours of dimethyl fumarate treatment, but with the greatest decrease in dimethyl fumarate levels occurring after 30 minutes. This indicates that our study is in line with previous studies utilising dimethyl fumarate to inhibit glutathione.

There has been reports of a rebound in glutathione levels after 12 and 24 hours of dimethyl fumarate treatment (Brennan *et al*., 2015; Lin *et al*., 2011). This occurs though the activation of NRF2 and the subsequent transcription of a number of glutathione related enzymes such as glutathione S-transferase (GST), glutathione reductase, γ-glutamylcysteine ligase and glucose-6-phosphate dehydrogenase (Loboda *et al*., 2016; Saidu *et al*., 2017), a phenomenon that we have been able to replicate. This has been associated with glutathione depletion over a longer time period (De Nicola and Ghibelli, 2014). NRF2 transcription of the glutathione “recycling” enzyme GST is thought to be a vital mechanism in aiding cell survival during times of oxidative stress (Harvey *et al*., 2009), including oxidative stress induced by depletion of glutathione (Mytilineou *et al*., 2002).

As dimethyl fumarate was shown to deplete glutathione, it was hypothesised that pretreatment of UVW and T98g human glioblastoma cells with dimethyl fumarate would increase temozolomide mediated cell kill. This hypothesis was not however supported by the data. The hypothesised increase in cell kill was only seen at the lowest administered doses of dimethyl fumarate, although a trend in increased cell kill relative to pretreatment length was observed. This lack of increased cell kill was potentially due to the mechanism discussed above, with dimethyl fumarate depleting glutathione as expected, but also inducing NRF2 expression which prevents full realisation of the effects of glutathione depletion on temozolomide mediated cell kill (Brennan *et al*., 2015; Lin *et al*., 2011; Loboda *et al*., 2016; Saidu *et al*., 2017).

In order to interrogate the effects of increased glutathione on temozolomide induced cell kill, assays using the glutathione prodrug *N*-acetylcysteine were performed. However, *N*-acetylcysteine is most widely used and known as a reactive oxygen species scavenger, with literature tending to reference NAC as a ROS scavenger without mention of glutathione (Halasi *et al*., 2013; Zhitkovich, 2019). To account for this, assays using a separate, glutathione independent reactive oxygen species scavenger tempol were performed. Tempol is a non-thiol superoxide dismutase (SOD) mimetic (Yamada *et al*., 2003) and has been used previously in the literature to decrease ROS in models of inflammatory pain (Bernardy *et al*., 2017) and mouse models of chemotherapy induced nephrotoxicity (Ahmed *et al*., 2014).

Pretreatment with NAC significantly ameliorated temozolomide mediated cell kill in both UVW and T98g cell lines following administration of 15μM and 400μM of temozolomide respectively, the highest dose of temozolomide used in each cell line. The effects of NAC on temozolomide mediated cell kill are unfortunately under-reported in the literature. Analysis of DNA damage levels and cell cycle progression of U87 human glioblastoma cells treated with temozolomide and NAC has suggested that there is a decrease in the level of γH2a.X phosphorylation and a decrease in the size of $<G_1$ population in these cells compared to cells treated with temozolomide alone (Rocha *et al*., 2014). This is indicative of chemoprotection by NAC, although the Rocha study showed no cytotoxicity data for the pretreatment of U87 human glioblastoma cells with NAC (Rocha *et al*., 2014).

The decrease in DNA damage reported by Rocha is hypothesised to occur through the mechanism discussed below; NAC increases levels of glutathione, and as discussed in Chapter 3, the increased level of glutathione prevents temozolomide mediated DNA damage. Other studies have shown a direct decrease in temozolomide mediated cytotoxicity or cell viability when human glioblastoma cells are pretreated with comparable doses of NAC, with a decreased apoptotic induction in these cells (Zhang *et al*., 2010).

There is even less supporting evidence regarding the effect of tempol in conjunction with temozolomide. As a single agent, tempol has been reported to be significantly cytotoxic against C6 glioma cells following 24-hour exposure (Gariboldi *et al*., 2003), an effect we were unable to replicate, as we found 1mM tempol caused only 6% cytotoxicity in both UVW and T98g human glioblastoma cells. Another study using the U87 and U3737

glioma cell lines has shown that tempol synergizes with temozolomide to significantly increase cell kill in a glutathione dependent manner (Ravizza *et al*., 2004). We have not been able to replicate this cytotoxicity or the effects of tempol on glutathione levels, and studies show that nitroxides such as tempol are unreactive towards glutathione *in vitro* (Głębska *et al*., 2003). Our results suggest instead that that there is no increase in cell survival when cells were pretreated with tempol prior to addition of temozolomide, indicating that SOD has no effect on temozolomide mediated cell kill. However, SOD has been suggested as a resistance marker in glioblastoma in a study using both patient derived glioblastoma cell lines and the U87 glioma cell line (Chang *et al*., 2017).

We have also shown that temozolomide induces a significant increase in reactive oxygen species levels at the highest concentration used in UVW cells (15μM) and at all concentrations of temozolomide utilised in the T98g cell line. The induction of reactive oxygen species by temozolomide has been previously suggested by Barciszewska *et al.,* (2015) and has been shown previously (Barciszewska *et al*., 2015; Zhang *et al*., 2010), as has the induction of oxidative stress by alkylating agents (Conklin, 2004). Reactive oxygen species generation by temozolomide has been suggested to be due to mitochondrial DNA methylation (Rocha *et al*., 2016). We have shown that both NAC and tempol reduce temozolomide induced reactive oxygen species at the concentrations of NAC and tempol used. In the UVW cell line, there was a significant reduction of reactive oxygen species levels after administration of 15μM temozolomide when cells were pretreated with either NAC or tempol. In the T98g cell line, both tempol and NAC significantly decreased temozolomide induced reactive oxygen species at all doses of temozolomide used. No significance between either ROS scavenger was seen.

When these results are taken in conjunction with cytotoxicity assays, it is indicative that reactive oxygen species play no significant role in temozolomide mediated cell kill at the concentrations utilised in the UVW and T98g cell lines. Both the lack of temozolomide mediated ROS induction as measured by change in DCFDA levels in the temozolomide sensitive UVW cell line, and the lack of chemoprotection conferred by tempol indicate that there was no role for reactive oxygen species in the mechanism of action of temozolomide. As reactive oxygen species as a potential mode of action in temozolomide cell kill has been ruled out, the increase in cell survival seen when both UVW and T98g cells were pretreated with NAC is unlikely to be due to the reactive oxygen species scavenging properties of NAC.

As we have shown that NAC decreases temozolomide mediated cell kill and given what is known about the metabolism of NAC and the biosynthesis of glutathione, we hypothesise that the increase in cell survival is due to the increased biosynthesis of glutathione. As mentioned, NAC is a prodrug, operating through the deacetylation of *N*-acetylcysteine to cysteine (Zhitkovich, 2019), with the cysteine then being metabolised into glutathione. This is an effect we have been able to replicate (Figure 5.2 & 5.3). This is of particular importance as cysteine is found at levels seventy times lower than glutamate and glycine (~5μM compared to ~350μM in human erythrocytes), the other two amino acids in the glutathione tripeptide (Whillier *et al*., 2009). As a result of this concentration discrepancy, the atypical conjugation of cysteine and glutamate by γ-glutamylcysteine ligase is the rate limiting step in glutathione biosynthesis (Lu, 2013).

To fully consolidate these results, levels of glutathione in NAC and tempol treated cells was assayed. These results show that although NAC and tempol reducing temozolomide mediated reactive oxygen species, only NAC increases intracellular glutathione levels. This suggests that the chemoresistance mediated by NAC is likely to be mediated through an increase in glutathione levels, validating the hypothesis that glutathione is a chemoresistance mediator in glioblastoma.

We have shown that pretreatment with *N*-acetylcysteine, but not tempol, increased chemoresistance in both UVW and T98g human glioma cells towards the alkylating agent temozolomide. This is in keeping with our knowledge that glutathione is a major chemoresistance factor in glioma cells (Rocha *et al*., 2014, 2016). Given that dimethyl fumarate is able to significantly decrease glutathione levels and has been shown to have minimal effects on γH2a.X levels and cell cycle progression, we hypothesise that the chemosensitising effects of dimethyl fumarate are, as far as we are able to infer, are due to glutathione depletion.

5.5.2 The effects of dimethyl fumarate on NRF2 activation in human glioblastoma cells

NRF2 is a potent antioxidant transcription factor, responsible for cellular defence against increases in oxidative stress. As a transcription factor, NRF2 binds to areas of DNA known as antioxidant response elements (AREs), which allows transcription of genes vital to restoring the homeostatic redox environment of the cell (Loboda *et al*., 2016). These genes include the gene family responsible for increased glutathione activity,

turnover and clearance (Loboda *et al*., 2016) as well as the antioxidant genes *HMOX1* and *SOD1* (Jaiswal, 2004).

Due to this increase in transcription of protective and pro-survival genes, NRF2 is known as a chemo and radioresistance factor (Harvey *et al*., 2009; Kensler *et al*., 2007; Rocha *et al*., 2016; Sukumari-Ramesh *et al*., 2015). Both temozolomide and radiation are known to activate NRF2, which corresponds to increased chemo- and radioresistance (Cong *et al*., 2014; McDonald *et al*., 2010).

Activation of NRF2 occurs through protein kinase-C mediated phosphorylation of the serine 40 residue NRF2 which facilitates nuclear translocation (Chen *et al*., 2016; Huang *et al*., 2002; Jaiswal, 2004), although activation through different residue modification has also been reported (Bloom *et al*., 2002; He and Ma, 2009). Nuclear translocation of ser40 phospho-NRF2 has been shown occur in as little as 5-minutes after phosphorylation by protein kinase C (Huang *et al*., 2002). However, it has been demonstrated that NRF2 nuclear accumulation has been shown to occur after 6-hours in T98g cells (Mimura *et al*., 2011). pNRF2 will then bind to AREs allowing for the transcription of the genes described above. Unfortunately, dimethyl fumarate is known to be an activator of NRF2 (Brennan *et al*., 2015; Foresti *et al*., 2013; Jing *et al*., 2015; To *et al*., 2015), even being used as a positive control in assays measuring NRF2 activity (Marcotte *et al*., 2013). Clinically, NRF2 has been suggested as a biomarker for successful dimethyl fumarate treatment in multiple sclerosis (Hammer *et al*., 2018).

Dimethyl fumarate mediated activation of NRF2 has been widely reported (Hammer *et al*., 2018; To *et al*., 2015). The transcription of NRF2 activated genes has been demonstrated after administration of from 20μM of dimethyl fumarate to microglia cells (Foresti *et al*., 2013), 5μM lower than the highest concentration used in T98g cells in this study. 6-hour dimethyl fumarate treatment has also been shown to increase nuclear levels of NRF2 in a dose dependent manner (Brennan *et al*., 2015). Foresti *et al*., (2013) showed similar results as measured by induction of *HMOX1*, a downstream target of NRF2, with a significant increase in gene levels following 6-hour exposure to 20μM dimethyl fumarate (Foresti *et al*., 2013).

In order to be aware of the effects of dimethyl fumarate on NRF2 in human glioblastoma cells, FACE assays for serine-40 phosphorylated NRF2 were carried out with validation

by RT-qPCR for downstream targets of activated NRF2. The effects of NRF2 activation by the triterpenoid CDDO-imidazolide on temozolomide mediated cell kill were also assayed using clonogenic assays.

Concentrations of dimethyl fumarate used in the temozolomide-dimethyl fumarate combination appear to be capable of inducing NRF2 activation. UVW and T98g human glioblastoma cells display a markedly different trend in response to dimethyl fumarate. pNRF2 levels increased rapidly in T98g cells in a dose dependent manner, peaking after 6-hours of dimethyl treatment, before falling below basal levels after 8-hours of treatment. NRF2 target gene expression was raised after 2 and 4-hour treatment with 25μM dimethyl fumarate, but after 24-hour treatment levels of *NQO1* increased massively, indicating a slower activation of target genes as indicated by FACE data. NRF2 phosphorylation in UVW cells occurred differentially to T98g cells. In UVW cells, there is dose independent phosphorylation of NRF2 after 2 hours, before a decrease to basal levels after 4 hours treatment. This correlated closely with RT-qPCR data, with 9μM dimethyl fumarate inducing significant transcription of both *HMOX1* and *NQO1* after 2-hour treatment. Levels of *NQO1* remained raised after 4 and 24-hour treatment, but *HMOX1* levels did not. This is of interest as *NQO1* appeared to be more responsive to dimethyl fumarate treatment in both UVW and T98g cell lines. There was no difference in transcription of *HMOX1* or *NQO1* in response to CDDO-im treatment in either cell line.

The data showing dimethyl fumarate activation of *NQO1* potentially suggests that *NQO1* transcription is one of the key mechanisms of action of dimethyl fumarate. As mentioned, dimethyl fumarate is used as a treatment for the inflammatory diseases psoriasis and multiple sclerosis (Meissner *et al*., 2012; Phillips and Fox, 2013; Xu *et al*., 2015). Raised levels of *NQO1* have been found in severe multiple sclerosis lesions, indicating that induction of *NQO1* is an attempt by cells to ameliorate the damage caused by chronic demyelination (van Horssen *et al*., 2006), again suggesting that *NQO1* activation may be a key role in the action of dimethyl fumarate.

Activation of *NQO1* by 10μM dimethyl fumarate has been shown in primary cortical cultures and hippocampal HT22 cells (Albrecht *et al*., 2012). This study linked dimethyl fumarate induced NRF2 activation with glutathione recycling. In cancer, it has been shown that high concentrations of dimethyl fumarate (100μM) appear to be cytotoxic, but low concentrations (0.25-5μM) are chemoprotective via induction of NRF2. Dimethyl

fumarate chemoprotection was induced via NRF2 mediated increase in glutathione levels (Saidu *et al*., 2017).

The decrease in pNRF2 levels at 8-hours in T98g cells and 4 hours in UVW cells is indicative of a compensatory decrease upon induction of the antioxidant response following NRF2 phosphorylation by dimethyl fumarate. This is supported by our data, with a large increase in NRF2 target gene expression at time points overlapping with increases of pNRF2 levels. Nuclear export of activated NRF2 occurs through phosphorylation by a number of unknown kinases and GSK3 α/β before βTrCP mediated ubiquitination and subsequent proteasomal degradation (Cuadrado, 2015; Joo *et al*., 2016), this mechanism may be redox sensitive (Li *et al*., 2006; Velichkova and Hasson, 2005). The precise export mechanism has been muddied by a number of manuscript retractions based on the GSKβ/Fyn/NRF2-tyrosine568 phosphorylation hypothesis.

There is very little separating UVW and T98g cells in response to dimethyl fumarate, both cell lines displayed very similar dose response curves, radiosensitising potential and effects on cell cycle progression. Both cell lines used in these studies also show similar effects with respect to intracellular glutathione levels. The first quantifiable difference between UVW and T98g cells was the phosphorylation of NRF2 and subsequent gene transcription in response to dimethyl fumarate.

We suggest that this difference may be due to alterations or mutations in KEAP-1 cysteine residues in one of the cell lines, more likely T98g cells. T98g cells display a slower increase in pNRF2 and subsequent antioxidant gene expression compared to UVW cells. We suggest that this may be due to alteration in KEAP-1 cysteine residues, leading to slower release of NRF2 from the KEAP-1-NRF2 complex. KEAP-1 is the main regulator of NRF2, and binding of NRF2 to KEAP-1 induces proteasomal degradation of NRF2 (Kobayashi *et al*., 2006). Further work using mass spectrometry as described by Brennan could be used to validate this hypothesis (Brennan *et al*., 2015)

Structurally, KEAP-1 is cysteine rich, with 27 cysteine residues. Three of these residues, cysteines 151, 273 and 288, have a functional role by inducing a conformational change in Keap1 structure leading to the release and nuclear translocation of NRF2 (Kobayashi *et al*., 2006; Li *et al*., 2012a; Taguchi *et al*., 2011; Zhang, 2006). If the release of NRF2 is glutathione independent, release may instead occur through direct action of dimethyl

fumarate with these cysteine residues. This has been shown by Brennan *et al*., (2015) with direct modifications of cysteine 151, 257 and 273 in response to dimethyl fumarate treatment (Brennan *et al*., 2015). All three of these cysteine residues have been shown to be amongst the most reactive residues in the KEAP-1 structure (Eggler *et al*., 2005; Kobayashi *et al*., 2006; Taguchi *et al*., 2011; Zhang, 2006).

Impaired or slower NRF2 release may occur through dimethyl fumarate interacting with KEAP-1 residues other than cysteiene-151, such as cysteine-257 or 273, which have been shown to interact with dimethyl fumarate, but to a lesser degree than cysteine-151 (Brennan *et al*., 2015). Similarly to the effect of dose on pNRF2 levels in the T98g cell line, this effect has shown to be dose dependent (Brennan *et al*., 2015).

Our hypothesis has shortfalls, mainly that modification of cysteine residues, particularly cysteine 151, has been shown to have no effect on the release kinetics of NRF2 from KEAP-1 (Eggler *et al*., 2005). However, Eggler *et al*., (2005) also acknowledge that the main techniques used, the electrophoretic mobility shift assay, may not be sensitive enough to detect this change (Eggler *et al*., 2005). Although mutations in cysteine 151 may not be enough to alter the release kinetics of NRF2 from KEAP-1, it has been shown that substitution for the reactive cysteine-151 for a non-reactive alanine prevents full activation of NRF2 (Yamamoto *et al*., 2008), interestingly this study has also shown that cysteine-151 modification allows KEAP1 to retain the ability to bind NRF2. One of the main strengths of this theory is that Singh showed that ML385 was cytotoxic only towards KEAP-1 mutant cells (Singh *et al*., 2016), similarly to what we have shown in Figure 5.10d. This suggest that the T98g cell line has a mutant KEAP-1.

This leads us to maintain this as our working hypothesis for the differential activity of pNRF2 in UVW and T98g cells in response to dimethyl fumarate.

Due to the increased transcription of protective and pro-survival genes, NRF2 is known as a chemo and radioresistance factor (Harvey *et al*., 2009; Kensler *et al*., 2007; Rocha *et al*., 2016; Sukumari-Ramesh *et al*., 2015). This is shown in Figure 5.8. The synthetic triterpenoid CDDO-im (To *et al*., 2015) was used to induce NRF2 phosphorylation in UVW and T98g cells. CDDO-im significantly increased the level of serine-40 phosphorylated NRF2 in these cells with a correspondent increase in NRF2 related gene expression, however this was to a lower level than previously reported (To *et al*., 2015).

Our data agrees with what has been shown about the effects of NRF2 activity on temozolomide therapy (Cong *et al*., 2014, 2014; Ma *et al*., 2015b; Zhang and Wang, 2017). In UVW cells, there was almost complete ablation of temozolomide mediated cell kill following CDDO-im mediated induction of NRF2, with a 30% decrease in cell kill following administration of 15μM of temozolomide, the IC_{50} of temozolomide in these cells. There was a smaller effect in the T98g cell line, with a 15% amelioration of cell kill at the IC_{50}, 400μM, possibly due to the high DNA damage repair capacity of these cells proposed in Sections 3.5.2.1 and 4.5.1 meaning that MGMT is a more vital resistance factor than NRF2 for temozolomide in MGMT positive glioblastoma.

We believe that this is the first reported combination of temozolomide and ML385, the NRF2 inhibitor used for this study. ML385 prevents transcription of NRF2 target genes by binding Neh1, the cap'n'collar domain of the NRF2 protein (Singh *et al*., 2016). The Neh1 domain of NRF2 is required for DNA binding and dimerization (McMahon *et al*., 2004; Nioi *et al*., 2005). By preventing transcription of target genes, ML385 significantly improves temozolomide mediated cell kill in both UVW and T98g glioblastoma cell lines. We have shown that, as hypothesised, ML385 lowers gene expression to below control levels, but only significantly for *NQO1* in the T98g cell line. This occurs through the mechanism above; prevention of the transcription factor interacting with the antioxidant response elements needed for gene transcription. The improvement in temozolomide mediated cell kill likely occurs through the prevention of transcription of glutathione cycling enzymes (Loboda *et al*., 2016). Further interrogation of this mechanism of action should be performed as NRF2 inhibition is likely to be beneficial to a number of cancers (Ma *et al*., 2015b; Singh *et al*., 2016; To *et al*., 2015).

We suggest that the mechanism for dimethyl fumarate inducing NRF2 may be glutathione independent, as both cell lines were depleted of glutathione in a dose independent manner after just 30 minutes exposure. If NRF2 activation was glutathione mediated, we believe that there would similar phosphorylation and transcription activity in both cell lines. Glutathione depletion has been suggested as a mechanism of NRF2 release and phosphorylation (Chia *et al*., 2010; Limón-Pacheco *et al*., 2007), but our data does not support this. The increase in dimethyl fumarate levels following 24-hour exposure is likely to occur though the activation of NRF2 and a subsequent increase in glutathione metabolism genes (Loboda *et al*., 2016; Saidu *et al*., 2017). This aids cell

survival under oxidative stress (Harvey *et al*., 2009), including oxidative stress induced by depletion of glutathione (Mytilineou *et al*., 2002).

This data highlights the danger of NRF2 activation in glioblastoma cells. As discussed dimethyl fumarate is known to activate NRF2 (Brennan *et al*., 2015; Foresti *et al*., 2013), and it appears, that the temozolomide-dimethyl fumarate combination activates NRF2, leading us to conclude that care must be taken if using dimethyl fumarate clinically.

5.5.3 The effects of dimethyl fumarate on nitrite production in human glioblastoma cells

As a final, exploratory mechanistic investigation, the effects of dimethyl fumarate on nitrite levels were investigated using Griess assays.

The role of nitric oxide is incredibly diverse. In many cancers, high concentrations of nitric oxide have been shown to be cytotoxic to tumours, and nitric oxide donors have been suggested as anti-neoplastic agents. However, low concentrations of nitric oxide have been shown to have anti-apoptotic effects via mutation of p53 and direct inhibition of the proapoptotic caspase family (Zech *et al*., 2003). Nitric oxide has also been shown to increase tumour growth and metastasis via increased angiogenesis and vascularisation. Dimethyl fumarate has been previously shown to decrease levels of nitrites in microglia and astrocytes in response to interferon-γ and lipopolysaccharide (LPS) stimulation (Foresti *et al*., 2013; Wilms *et al*., 2010) as well as in astrocytes and C6 rat glioma cells (Lin *et al*., 2011).

Our data suggests that the effects of dimethyl fumarate on nitric oxide in cancer are negligible. Our data shows that there is no effect on nitric oxide levels following dimethyl treatment. studies showing that dimethyl fumarate reduces nitrite levels had stimulated dimethyl fumarate treated cells using interferon-γ to increase nitrite production (Foresti *et al*., 2013; Lin *et al*., 2011; Wilms *et al*., 2010). Although our data does not show a change in nitrite levels, translation of dimethyl fumarate to *in situ* is likely to have an effect on nitrite levels. This is due to the tumour microenvironment.

The tumour microenvironment describes the niche in the body that a tumour occupies, and the interaction of the tumour with the stroma, the immune and circulatory systems (Liotta and Kohn, 2001). Due to the level of immune infiltration observed in glioblastoma

(Beier *et al*., 2012; Doucette *et al*., 2013; Rutledge *et al*., 2013), it is likely that there will be an increase in tumoral nitric oxide levels. Immune cells are able to induce one of the three isoforms of the nitric oxide synthesis enzyme, inducible nitric oxide synthetase (iNOS/NOS2) (Lowenstein and Padalko, 2004). This could potentially increase levels of nitric oxide within tumour cells. In glioblastoma, this increase can lead to increased angiogenesis, tumour growth and stemness (Baker *et al*., 2014; Eyler *et al*., 2011).

We suggest that because of this likely increase in nitric oxide levels, the effects of dimethyl fumarate on nitrite levels may be more pronounced in patients. This is made more relevant as dimethyl fumarate has been shown to inhibit transcription of iNOS and subsequent nitric oxide production in astrocytes and microglia (Wilms *et al*., 2010). Because of this, the effects of increased nitric oxide levels on temozolomide mediated cell kill were investigated.

S-nitrosoglutathione is a nitric oxide donor that spontaneously releases nitric oxide under physiological conditions (Singh *et al*., 1996). GSNO has been shown to significantly increase nitric oxide levels in human blood cells (Macphail *et al*., 2003). We have shown that, as expected, GSNO significantly increased nitric oxide levels in both UVW and T98g human glioblastoma cells as measured using Griess assays. This increase was to a similar level as previously reported in C6 glioma cells (Yang *et al*., 2004).

As its name suggests, *S*-nitrosoglutathione is also a source of glutathione, and decomposition of GSNO has been shown to produce glutathione (Singh *et al*., 1996). We have shown that GSNO treatment does not significantly increase intracellular glutathione levels in UVW or T98g human glioblastoma cells, ruling out a role for glutathione in GSNO mediated chemomodulation. From this data and our understanding of GSNO metabolism, we hypothesise that the effects of GSNO pretreatment on temozolomide mediated cell kill occur through the actions of nitric oxide.

We have shown that pretreatment with GSNO is capable of significantly reducing temozolomide cell kill only at the highest concentration of temozolomide used in the T98g cell line. Chemoresistance mediated by GSNO has been previously been shown using the carbamoylating drug carmustine (Yang *et al*., 2004). This resistance occurred similarly to resistance mediated by iNOS, suggesting that iNOS may induce chemoresistance through the action of GSNO (Yang *et al*., 2004). Interestingly this study

only showed an increase in chemoresistance towards carbamoylating agents, but not alkylating agents such as temozolomide. As dimethyl fumarate has been shown to inhibit transcription of iNOS (Wilms *et al*., 2010), it stands to reason that dimethyl fumarate treatment may increase chemosensitivity of glioblastoma towards carmustine.

However, given that we have presented limited evidence to suggest that GSNO is a resistance factor and there is limited evidence in the literature suggesting iNOS acts as a chemoresistance factor for temozolomide (Yang *et al*., 2004), the impact of dimethyl fumarate on iNOS and subsequent chemosensitivity is likely to be limited.

This does not mean the action of dimethyl fumarate on nitrite levels in cancer may not be beneficial. As discussed, the production of nitrites is associated with increased angiogenesis (Cooke and Losordo, 2002; Kostourou *et al*., 2011; Morbidelli *et al*., 2003, 2004). Glioblastoma is known to be a highly vascularised tumour, with sustained angiogenesis contributing to disease progression and invasion (Baker *et al*., 2014; Popescu *et al*., 2016; Ricci-Vitiani *et al*., 2010). Dimethyl fumarate could therefore have a potential anti-angiogenic activity.

Further investigations should be performed to examine the effects of dimethyl fumarate on tumour vascularisation, and the effects of dimethyl fumarate in cancers with active iNOS. This would be best suited to models that are able to retain features of the tumour microenvironment.

5.6 Conclusions

Glutathione is well established as a chemoresistance factor in a number of cancers, and dimethyl fumarate has been shown to deplete intracellular glutathione levels. Our work confirms this. We have shown that the concentrations of dimethyl fumarate used in the temozolomide-dimethyl fumarate combination are capable of rapidly reducing intracellular glutathione levels in both UVW and T98g human glioblastoma cell lines. Expanding on this, we have shown that the glutathione prodrug and reactive oxygen species scavenger *N*-acetylcysteine is able to ameliorate temozolomide mediated cell kill. We have also shown that this reduction in cell kill is unlikely to be through ROS scavenging, leading us to maintain our hypothesis that dimethyl fumarate is capable of synergy with temozolomide by inhibiting glutathione.

Dimethyl fumarate is also known to be an activator of the antioxidant transcription factor NRF2. By measuring the intracellular levels of serine-40 phosphorylated NRF2 and determining NRF2 transcriptional activity with RT-qPCR for *NQO1* and *HMOX1*, we have shown that, unfortunately, concentrations of dimethyl fumarate that constitute the temozolomide-dimethyl fumarate combination are capable of activating NRF2. The NRF2 stimulator, CDDO-im, was able to significantly decrease temozolomide mediated cell kill. We have also shown that an NRF2 inhibitor, ML385, is able to significantly increase temozolomide mediated cell kill.

We conclude that nitric oxide has a minimal effect on chemomodulation, and that dimethyl fumarate may only affect nitrite levels in stimulated cells. We, however, do not rule out the role dimethyl fumarate may play in different models of glioblastoma.

This leads us to conclude that although dimethyl fumarate is a potent glutathione inhibitor, care should be taken to prevent activation of NRF2, and this NRF2 related activity may limit future clinical deployment.

Chapter 6

The effects of temozolomide and dimethyl fumarate in combination on three-dimensional models of human glioblastoma

6.1 Introduction

In vitro models are useful tools in drug discovery and development, offering a platform to screen and deconvolute the mode of actions of treatments in a rapid, economically viable manner. However, despite intensive *in vitro* research few of these screened compounds will translate to a clinical setting (Moreno and Pearson, 2013; Neidle, 2011; Rishton, 2005; Slater, 2001; Waring *et al*., 2015). This is in part due to the over utilisation of two-dimensional culture models, as these models often suggest translational potential, but fail to be representative of the *in vivo* or clinical environment leading to a low rate of clinical advancement of candidate drug molecules.

Similarly, *in vivo* techniques such as xenografts, orthotopic injection, and genetically modified animal models such as those using the CRISPR/Cas9 and Cre-Lox systems have a high running cost, ethical challenges and are low throughput for drug discovery compared to two-dimensional culture (Candolfi *et al*., 2007; Cekanova and Rathore, 2014; Cheon and Orsulic, 2011; Lampreht Tratar *et al*., 2018; Simons and Brayton, 2017). Furthermore, drug discovery data from animal models overwhelmingly fail to translate to the clinic, with an attrition rate of over 90% (Mak *et al*., 2014).

Multicellular tumour spheroids (MCTS; spheroids) are an important transitional model in the cancer therapeutics development pipeline, bridging the gap between 2D tissue culture and animal models (Kunz-Schughart, 1999). Spheroids better mimic several aspects of tumour biology that are difficult to capture with traditional *in vitro* cell culture techniques (Cui *et al*., 2017; Hirschhaeuser *et al*., 2010; Jamieson *et al*., 2015).

As seen in Figure 6.1, spheroid models consist of three distinct regions, a rapidly proliferating outer rim, a quiescent inner region and a necrotic core. As these regions do not have the same exposure to growth media, there is a decrease in nutrient and oxygen levels towards the core of the spheroid, and an increase in metabolic waste, carbon dioxide and lactate. This mirrors *in situ* tumour biology, where tissue distant from blood vessels receives limited nutrients and accumulates metabolic waste (Baker *et al.*, 2014; Ricci-Vitiani *et al.*, 2010).

The difference in oxygen and nutrient availability throughout the spheroid leads to three key phenomena not typically seen in monolayer culture of immortalised cell lines; heterogeneous cell phenotypes, asynchronous cellular growth and genetic mosaicism. Varied cell growth rates and genetic heterogeneity are features seen in tumour tissue and can result in increased treatment resistance compared to two-dimensional culture.

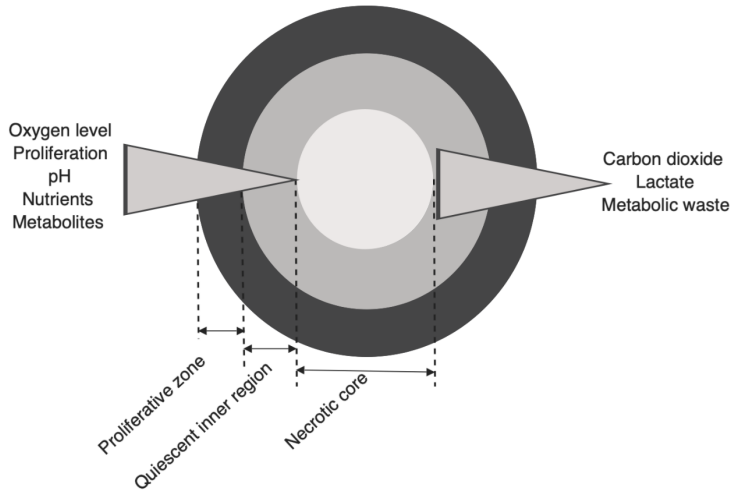

Figure 6.1: Schematic representation of a spheroid with the three main regions highlighted as well as relevant gradients. Adapted from (Hirschhaeuser *et al.*, 2010; Sant and Johnston, 2017)

We hypothesise that, based on results from Chapters 3 & 4, the supra-additive temozolomide-dimethyl fumarate combination will delay spheroid growth to a greater degree than temozolomide or dimethyl fumarate as single agents. We believe that the varied cell growth rates and phenotypic and genetic mosaicism, as well as the increased hypoxic cell fraction in spheroids, will offer a more robust challenge to the efficacy of temozolomide-dimethyl fumarate combination. This will allow us to reduce the animal

impact of this research by choosing only the most synergistic combinations to carry forward into *in vivo* models.

6.2 Aims and objectives

The aims of this study were:

- To determine the impact on spheroid growth of the temozolomide-dimethyl fumarate combinations when used to treat three-dimensional cultures of UVW and T98g human glioblastoma cells

6.3 Materials and Methods

6.3.1 Cell lines and routine cell maintenance

All routine maintenance of cell lines was performed as described in Section 2.1.

6.3.2 Spheroid Formation and treatment

Spheroids were formed and treated as described in Section 2.17

6.3.2.1 Spheroid analysis

Spheroids were analysed as described in Section 2.17.1 and 2.17.2

$\tau 2$ was defined as the time required for a 2-fold increase in spheroid volume following treatment, which represents a measure of the growth delay and doubling time (DT) was defined as the time required for a two-fold increase in spheroid volume within the exponential growth phase of the spheroid growth curve (McGinely, 2015).

6.4 Results

6.4.1 Effects of temozolomide, dimethyl fumarate and the temozolomide-dimethyl fumarate combination on UVW and T98g spheroid growth

The same concentrations of the temozolomide-dimethyl fumarate combination used throughout this project which resulted in supra-additivity were used in multicellular tumour spheroid models. Following treatment administration, spheroids were imaged and volumes measured over a period of three weeks. Growth kinetics following treatment were reported as τ_2 and doubling time (DT), which quantify growth delay and growth rate following treatment respectively. This allowed for the growth and spheroid regrowth delay of three-dimensional tumour models to the temozolomide-dimethyl fumarate combination to be measured.

6.4.1.1 Effects of temozolomide, dimethyl fumarate, and the temozolomide-dimethyl fumarate combination on UVW and T98g spheroid growth

In UVW multicellular spheroids, increasing concentrations of temozolomide from 0.5μM to 15μM had no effect on spheroid volume compared to an untreated control (Figure 6.2a & b). Overall, temozolomide treated spheroids increased in volume similarly to untreated control spheroids as measured by τ2, DT, final V/V_0 and area under the curve values (Figure 6.2c & d), with no significant difference between temozolomide treated and untreated groups (p-value >0.05). There was no significant difference in the τ_2, DT and area under the curve values between 0.5, 5 and 15μM temozolomide treated groups (p-value >0.05). This indicates that temozolomide had no effect on UVW spheroid growth in this administered concentration range. This was unexpected, given the response of UVW cells to temozolomide in two-dimensional culture (Figure 3.2a)

Similarly to temozolomide, dimethyl fumarate had no inhibitory effect on UVW spheroid growth (Figure 6.2e & f). Dimethyl fumarate treated spheroids increased in volume similarly to untreated spheroids as measured by τ2, DT and area under the curve values, with no significant difference between dimethyl fumarate treated and untreated groups (p-value >0.05) (Figure 6.2g & h). There was no significant difference in the τ_2, DT and area under the curve values between 0.3, 3 and 9μM dimethyl fumarate treated groups (p-value >0.05).

Conversely, the temozolomide-dimethyl fumarate combination had a dose-dependent inihibitory effect on UVW spheroid growth. There was inhibition of UVW spheroid growth at the highest concentration administered, 15μM+9μM of the temozolomide-dimethyl fumarate combination, but not at the two lower doses of the combination utilised in this study (Figure 6.2i & j). This is seen when comparing τ_2, DT and area under the curve values for spheroids treated with the temozolomide-dimethyl fumarate combination, with a dose dependent increase in growth delay and doubling time (p-value >0.05) (Figure 6.2l). Exposure of UVW spheroids to 15μM+9μM of the temozolomide-dimethyl fumarate combination resulted in a significant decrease in the AUC, where the calculated AUC value decreased from 16.55±2.57 in untreated control spheroids to 12.59±1.82 (p-value <0.05) in drug treated spheroids (Figure 6.2k).

Spheroid volume was significantly reduced compared to untreated control spheroids from 14 days after exposure to 15μM+9μM of the temozolomide-dimethyl fumarate combination (p-value <0.05). This combination reduced spheroid volume significantly below control volume at all remaining time points.

The highest dose of the temozolomide-dimethyl fumarate combination, 15μM+9μM, reduced spheroid growth compared to 15μM temozolomide and 9μM dimethyl fumarate as single agents as measured by τ_2 and DT values. This resulted in a significantly smaller V/V_0 at day 21 in spheroids treated with 15μM+9μM temozolomide-dimethyl fumarate combination compared to each constituent dose as a single agent (p-value <0.05).

Figure 6.2 (facing): Growth curves of UVW human glioblastoma spheroids in response to increasing doses of **a.** temozolomide, **e.** dimethyl fumarate or **i.** the temozolomide-dimethyl fumarate combination over a period of 3 weeks. Log transformed data for each treatment is shown in **b., f.,** and **j.** respectively. Growth kinetics for each treatment are shown in **d., h.,** and **l.,** respectively. Area under the curve for each treatment was calculated and is shown in Figure 6.2 **c., g.,** and **k.** Data shown is the average of three independent experiments ± standard error of the mean (SEM). Kruskal-Wallis analysis with Dunn's post hoc testing for multiple comparisons was performed using Graphpad Prism 8 software, with p-values of <0.05 = *, <0.01=** and 0.001 = *** reported as significant.

a.

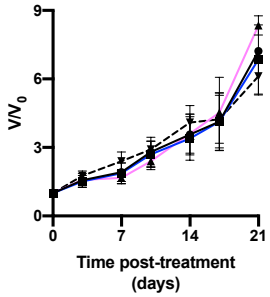

b.

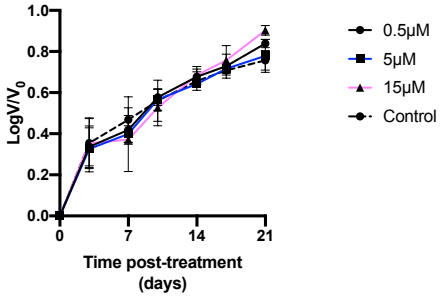

c.

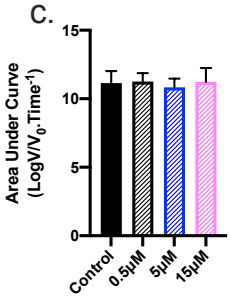

d.

Concentration (μM)	τ_2	DT	V/V_0 (Day 21)
0	8.26±0.47	9.77±1.40	6.11±0.81
0.5	7.46±0.15	8.40±0.55	7.21±0.12
5	8.06±0.66	9.15±1.24	6.85±1.51
15	7.15±0.34	8.02±0.99	8.3±0.41

e.

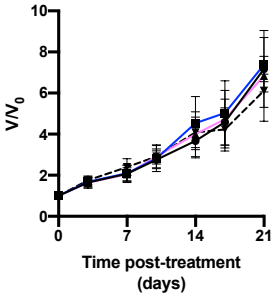

f.

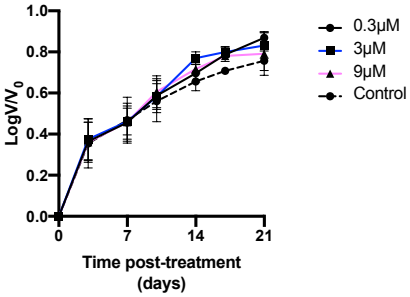

g.

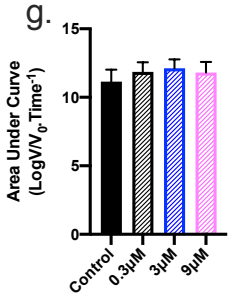

h.

Concentration (μM)	τ_2	DT	V/V_0 (Day 21)
0	8.26±0.47	9.77±1.40	6.11±0.81
0.3	7.10±0.20	8.05±0.24	7.16±0.61
3	7.19±0.39	8.35±0.98	7.37±1.32
9	7.54±0.47	8.77±0.95	6.83±1.20

i.

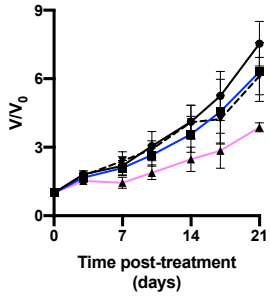

j.

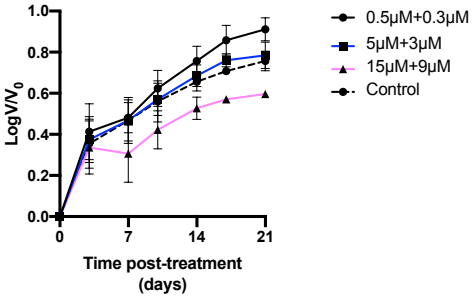

k.

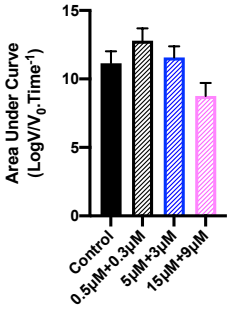

l.

Concentration (TMZ (μM)+DMF (μM))	τ_2	DT	V/V_0 (Day 21)
0	8.26±0.47	9.77±1.40	6.11±0.81
0.5+0.3	6.62±0.0.42	7.63±0.20	7.53±0.97
5+3	7.78±0.45	9.09±0.95	6.29±1.29
15+9	10.89±0.65	12.49+1.71	3.38±0.19

In T98g multicellular spheroids, increasing doses of temozolomide had a dose-dependent effect on spheroid volume compared to an untreated control (Figure 6.3a & b), as measured by $\tau 2$, DT and area under the curve values, with a dose dependent increase in both growth delay and doubling time in treated spheroids compared to untreated controls. This was not statistically significant (p-value >0.05) (Figure 6.3d). Treatment of T98g spheroids with 200 or 400μM temozolomide however resulted in a significant decrease in the AUC (Figure 6.3c), where the calculated AUC value decreased from 20.3±5.93 in untreated control spheroids to 13.36±3.71 (p-value <0.05) in spheroids treated with 200μM temozolomide and to 11.35±2.33 (p-value <0.05) in spheroids treated with 400μM of temozolomide. The final volume for T98g spheroids treated with 400μM of temozolomide was significantly smaller than the volume of untreated spheroids, decreasing from 7.05±0.93 to 4.18±0.35 (p-value <0.01). This is indicative of temozolomide having a dose dependent effect on T98g spheroid volume (Figure 6.3a & b).

Dimethyl fumarate had no inhibitory effect on T98g spheroid growth (Figure 6.3e & f). Dimethyl fumarate treated spheroids increased in volume at a similar rate to untreated spheroids as measured by $\tau 2$, DT and area under the curve values, with no significant difference between dimethyl fumarate treated and untreated groups (p-value >0.05) (Figure 6.3g). There was no significant difference in the τ_2, DT and area under the curve values between 3.125, 12.5 and 25μM dimethyl fumarate treated groups (p-value >0.05) (Figure 6.3h).

The temozolomide-dimethyl fumarate combination had a dose-dependent effect on T98g spheroid volume (Figure 6.3i & j), as measured by $\tau 2$, DT and area under the curve values, with a dose dependent increase in both growth delay and doubling time compared to untreated controls (Figure 6.3l). The area under the curve for spheroids treated with the temozolomide-dimethyl fumarate combination decreased from a volume of 20.3±5.93 in untreated control spheroids to 12.97±3.56 (p-value <0.05) following treatment with 200μM+12.5μM and to 10.13±1.52 (p-value <0.05) following treatment with 400μM+25μM of the temozolomide-dimethyl fumarate combination (Figure 6.3k) .

However, the temozolomide-dimethyl fumarate combination did not significantly inhibit T98g spheroid growth compared to temozolomide and dimethyl fumarate as single

agents as measured by $\tau 2$, DT and area under the curve values, with no significant difference between combination and single agent treated groups (p-value >0.05). This indicates that despite high efficacy in two-dimensional, the temozolomide-dimethyl fumarate combination does not translate as effectively to three-dimensional models of glioblastoma.

Figure 6.3 (facing): Growth curves of T98g human glioblastoma spheroids in response to increasing doses of **a.** temozolomide, **e.** dimethyl fumarate or **i.** the temozolomide-dimethyl fumarate combination over a period of 3 weeks. Log transformed data for each treatment is shown in **b., f.,** and **j.** respectively. Growth kinetics for each treatment are shown in **d., h.,** and **l.,** respectively. Area under the curve for each treatment was calculated and is shown in Figure 6.2 **c., g.,** and **k.** Data shown is the average of three independent experiments ± standard error of the mean (SEM). Kruskal-Wallis analysis with Dunn's post hoc testing for multiple comparisons was performed using Graphpad Prism 8 software, with p-values of <0.05 = *, <0.01=** and 0.001 = *** reported as significant.

a.

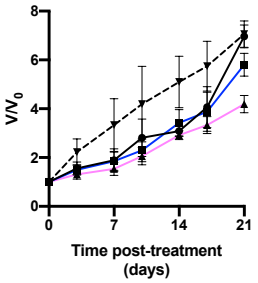

b.

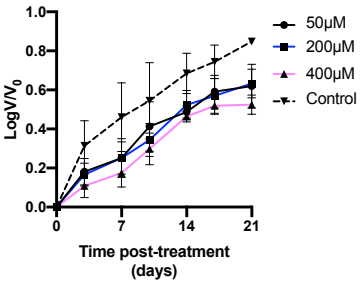

c.

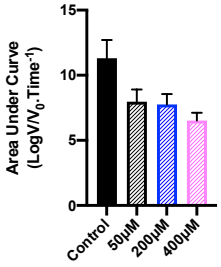

d.

Concentration (μM)	τ_2	DT	V/V_0 (Day 21)
0	7.26±0.34	8.20±0.42	7.05±0.93
50	9.83±1.20	10.12±1.03	6.96±0.46
200	9.97±1.18	10.37±0.97	5.80±0.46
400	10.91±0.56	11.05±0.35	4.18±0.35

e.

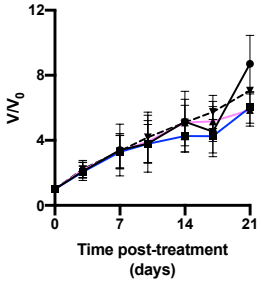

f.

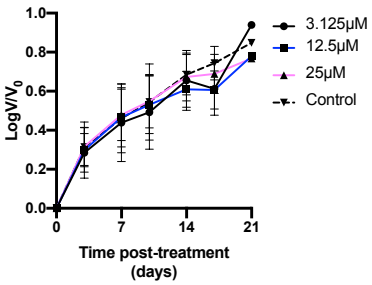

g.

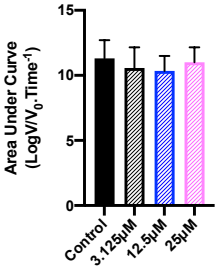

h.

Concentration (μM)	τ_2	DT	V/V_0 (Day 21)
0	7.26±0.34	8.20±0.42	7.05±0.93
3.125	7.41±0.82	8.09±0.70	8.70±1.75
12.5	8.52±0.67	9.65±0.76	6.02±0.96
25	8.12±0.81	9.29±0.89	5.86±0.98

i.

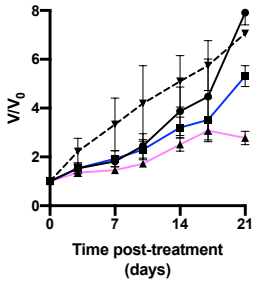

j.

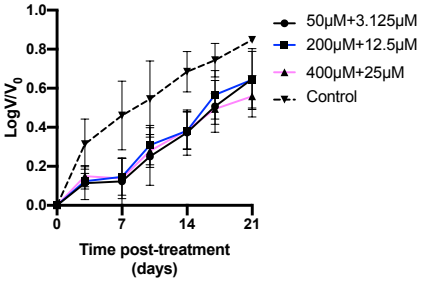

k.

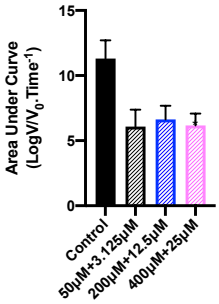

l.

Concentration (TMZ (μM)+DMF (μM))	τ_2	DT	V/V_0 (Day 21)
0	7.26±0.34	8.20±0.42	7.05±0.93
50+3.125	7.72±0.64	7.73±0.44	7.91±0.50
200+12.5	9.30±0.58	9.57±0.48	5.31±0.42
400+25	12.79±0.32	13.04±0.32	2.77±0.27

6.4.2. Effects of temozolomide and dimethyl fumarate in combination with external beam X-irradiation on UVW and T98g spheroid growth

In order to examine the effects of temozolomide and dimethyl fumarate in combination with external beam X-irradiation, UVW and T98g spheroids were treated with increasing doses of each agent prior to irradiation with 1or 3Gy. Spheroid growth was measured over a period of three weeks and changes in growth kinetics following treatment were reported as τ_2 and doubling time (DT), which quantify growth delay and growth rate following treatment respectively were compared to X-irradiation as a single agent.

6.4.2.1 Effects of external beam X-irradiation on UVW and T98g spheroid growth

As a single agent, external beam X-irradiation significantly inhibited UVW multicellular spheroid growth in a dose dependent manner compared to untreated spheroids (Figure 6.4a & b). UVW multicellular spheroids grew rapidly, significantly increasing in size after 10-days with a 2.9±0.37 increase in spheroid volume (p-value <0.01) compared to day 0 measurements. This increase in spheroid volume continued in a time dependent manner, with untreated spheroids reaching 6.1±0.81 times larger than initial measurements after 21 days (p-value <0.001).

1Gy irradiated spheroids showed delayed growth as measured by change in volume, τ_2, DT and area under the curve values, with a dose dependent increase in both growth delay and doubling time compared to untreated controls (Figure 6.4d). Exposure to 1Gy significantly decreased UVW spheroid growth after 10 days compared to an untreated control (p-value <0.05). Significantly reduced spheroid volume was observed from 14 days post exposure (p-value <0.01) compared to an untreated control, but not at 17 days (p-value >0.05). 21 days post X-irradiation, 1Gy irradiated spheroids had a significantly reduced volume compared to a non-irradiated control, with a final change in volume of 3.46 (±0.86) compared to 6.11 (±0.81) (p-value <0.01). UVW spheroids treated with 1Gy had an increased growth delay and doubling time compared to an untreated control (Figure 6.4d), however this was not found to be significant (p-value >0.05).

3Gy induced significant spheroid growth inhibition after 10 days post-irradiation compared to an untreated control (p-value <0.05) (Figure 6.4a & b), however the volume of 3Gy treated spheroids was not significantly different than the volume of 1Gy irradiated spheroids. Spheroids treated with 3Gy had a significantly lower increase in volume compared to non-irradiated spheroids at all remaining time points, with a final change in volume of 2.88 (±0.26) compared to 6.11 (±0.81) (p-value <0.001). Treatment with 3Gy significantly increased the τ_2 value from 8.26±047 in untreated spheroids to 19.13±2.65 (p-value <0.05). Doubling time increased from 9.77±1.40 in untreated UVW spheroids to 19.74±1.94 following exposure to 3Gy of external beam X-irradiation (p-value <0.05) (Figure 6.4d).

Area under the curve (AUC) was calculated for each treatment group over time, with 1Gy and 3Gy reducing the AUC compared to untreated controls. The area under the curve

for decreased from 16.55±2.57 in untreated UVW spheroids to 10.78±2.04 (p-value <0.05) following treatment with 3Gy of external beam X-irradiation. This is indicative of external beam X-irradiation having a dose dependent inhibitory effect on UVW spheroid growth (Figure 6.4c).

As demonstrated in Figure 6.4e, treatment with 1 or 3Gy of external beam X-irradiation did not significantly affect T98g spheroid growth kinetics as measured by change in volume, τ_2, DT and area under the curve values. The τ_2, DT and area under the curve values for T98g spheroids treated with both 1 and 3Gy of external beam X-irradiation were comparable to those of non-irradiated spheroids (Figure 6.4h).

This data highlights the differential radiosensitivity of UVW and T98g human glioblastoma cell lines as quantified by changes in growth kinetics following X-irradiation, as reported as τ_2 and doubling time (DT), which quantify growth delay and growth rate following treatment respectively,

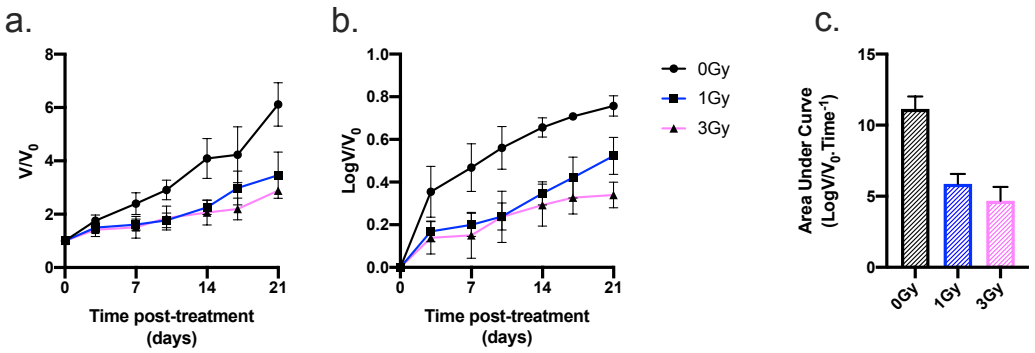

d.

Dose (Gy)	τ_2	DT	V/V_0 (Day 21)
0	8.26±0.47	9.77±1.40	6.11±0.81
1	13.93±1.81	14.42±1.66	3.46±0.86
3	19.13±2.65	19.74±1.94	2.88±0.25

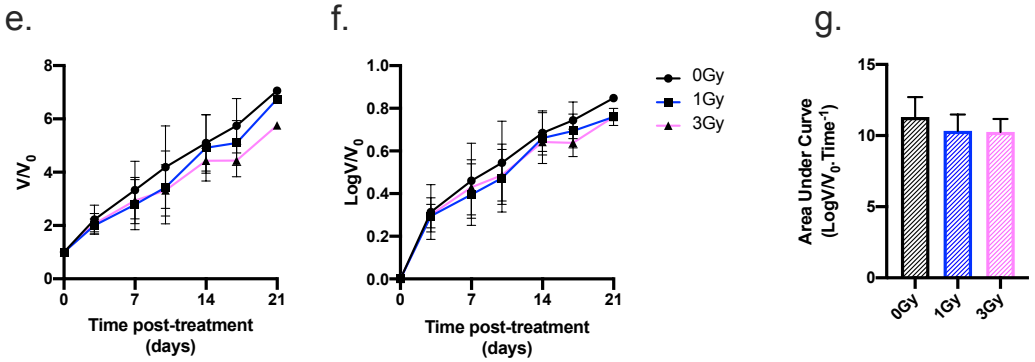

h.

Dose (Gy)	τ_2	DT	V/V_0 (Day 21)
0	7.26±0.34	8.20±0.42	7.05±0.93
1	8.28±0.63	9.13±1.16	6.74±0.84
3	8.40±0.35	9.45±0.71	5.75±0.60

Figure 6.4: Growth curves of **a.** UVW, **e.** T98g human glioblastoma spheroids in response to exposure to 1 or 3Gy of external beam X-irradiation over a period of 3 weeks. Log transformed data for each cell line is shown in **b.** and **f.** respectively. Growth kinetics for each treatment are shown in **d.** and **h.** respectively. Area under the curve for each treatment was calculated and is shown in Figure 6.4 **c.** and **g.** Data shown is the average of three independent experiments ± standard error of the mean (SEM). Kruskal-Wallis analysis with Dunn's post hoc testing for multiple comparisons was performed using Graphpad Prism 8 software, with p-values of <0.05 = *, <0.01=** and <0.001 = *** reported as significant.

6.4.2.2 Effects of temozolomide and dimethyl fumarate in combination with external beam X-irradiation on UVW and T98g spheroid growth

The combination of temozolomide and external beam X-irradiation inhibited UVW spheroid growth in a dose independent manner compared to untreated spheroids (Figure 6.5a & b) as measured by change in volume, τ_2, DT and area under the curve values, with a dose independent increase in both growth delay and doubling time compared to untreated controls. These increases were not found to be statistically significant (p-value >0.05).

When compared to temozolomide as a single agent, the combination of temozolomide and external beam X-irradiation inhibited UVW spheroid growth in a dose independent manner as measured by change in volume, τ_2, DT and area under the curve values, with a dose independent increase in both growth delay and doubling time compared to untreated controls. These increases were not found to be statistically significant (p-value >0.05) (Figure 6.5d & h).

The area under the curve values for the combination of temozolomide and external beam X-irradiation were reduced compared to temozolomide as a single agent (p-value >0.05). This reduction occurred in a radiation dose dependent manner (Figure 6.5c & g). This indicates that there was a decrease in the overall growth of UVW spheroids following combination treatment compared to spheroids treated with temozolomide alone, but no alteration in growth kinetics.

When compared to X-irradiation as a single agent, the combination of temozolomide and external beam X-irradiation did not inhibit UVW spheroid growth. The calculated values for τ_2 and DT were comparable to those in UVW spheroids exposed to external beam X-irradiation alone (Figure 6.4d), indicating that the combination of temozolomide and external beam X-radiation did not significantly affect the kinetics of spheroid growth, compared to the effects of external beam X-radiation exposure alone.

There was no significant variation between τ_2, DT and AUC values in UVW spheroids treated with temozolomide and 1Gy of external beam X-irradiation compared to UVW spheroids treated with temozolomide and 3Gy of external beam X-irradiation.

The combination of dimethyl fumarate and external beam X-irradiation had no effect on UVW spheroid growth compared to untreated spheroids as measured by change in volume, τ_2, DT and area under the curve values. There was found to be no variation in either growth delay or doubling time compared to untreated controls (p-value >0.05).

When compared to dimethyl fumarate as a single agent, the combination of dimethyl fumarate and external beam X-irradiation inhibited UVW spheroid growth in a dose independent manner as measured by change in volume, τ_2, DT and area under the curve values, with a dose independent increase in both growth delay and doubling time compared to untreated controls. These increases were not found to be statistically significant (p-value >0.05) (Figure 6.5l & p).

The area under the curve values for the combination of dimethyl fumarate and external beam X-irradiation was reduced compared to dimethyl fumarate as a single agent. This reduction occurred in a radiation dose dependent manner. This indicates that there was a decrease in the overall growth of UVW spheroids following combination treatment compared to spheroids treated with dimethyl fumarate alone, but no alteration in growth kinetics (Figure 6.5k & o).

When compared to X-irradiation as a single agent, the combination of dimethyl fumarate and external beam X-irradiation did not inhibit UVW spheroid growth. The calculated values for τ_2 and DT were comparable to those of non-irradiated UVW spheroids (Figure 6.4d), indicating that the combination of dimethyl fumarate and external beam X-radiation did not significantly affect the kinetics of spheroid growth, compared to untreated spheroids.

Figure 6.5 (facing): Growth curves of UVW human glioblastoma spheroids in response to increasing doses of temozolomide, plus 1Gy (**a.**) or 3Gy (**e.**) of external beam X-irradiation. Log transformed data is shown for 1 and 3Gy treated UVW spheroids is shown in **b.** and **f.** respectively. Growth kinetics for each treatment are shown in **d.** and **h.** respectively. Area under the curve for each treatment was calculated and is shown in Figure 6.5 **c.**, and **g.** **(Continued).**

a.

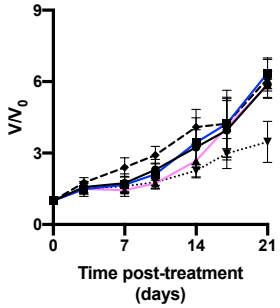

b.

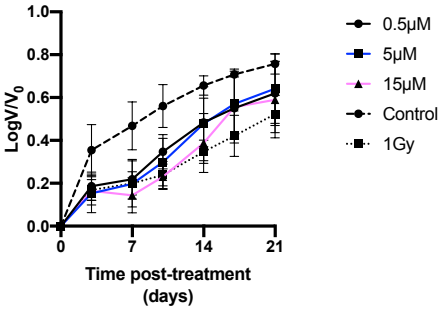

c.

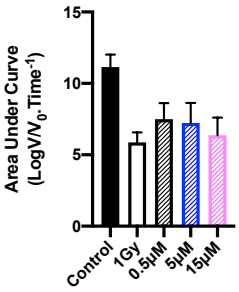

d.

Concentration	τ_2	DT	V/V_0 (Day 21)
0	8.26±0.47	9.77±1.40	6.11±0.81
1Gy	13.93±1.81	14.42±1.66	3.46±0.86
0.5μM	11.74±3.64	11.99±3.51	5.88±0.54
5μM	11.27±3.65	11.22+3.28	6.35±0.64
15μM	13.97±5.80	13.95±5.69	5.85±0.24

e.

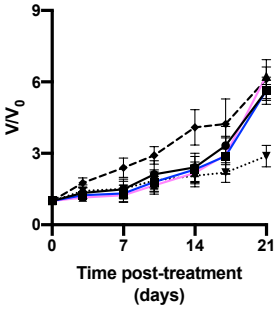

f.

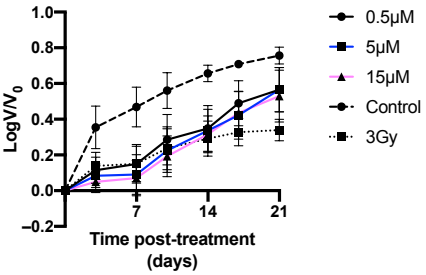

g.

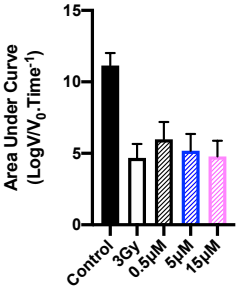

h.

Concentration	τ_2	DT	V/V_0 (Day 21)
0	8.26±0.47	9.77±1.40	6.11±0.81
3Gy	19.13±2.65	19.74±1.94	2.88±0.25
0.5μM	12.71±3.69	12.58±3.31	5.62±0.57
5μM	12.86±3.45	12.44±2.99	5.64±0.42
15μM	13.23±3.51	12.71±3.18	5.25±0.36

Continued.

Figure 6.5 (continued, facing): Growth curves of UVW human glioblastoma spheroids in response to increasing doses of dimethyl fumarate, plus 1Gy (**i.**) or 3Gy (**m.**) of external beam X-irradiation. Log transformed data is shown for 1 and 3Gy treated UVW spheroids is shown in **j.** and **n.** respectively. Growth kinetics for each treatment are shown in **l.** and **p.** respectively. Area under the curve for each treatment was calculated and is shown in Figure 6.5 **k.,** and **o.** Data shown is the average of three independent experiments ± standard error of the mean (SEM). Kruskal-Wallis analysis with Dunn's post hoc testing for multiple comparisons was performed using Graphpad Prism 8 software, with p-values of <0.05 = *, <0.01=** and 0.001 = *** reported as significant.

i.

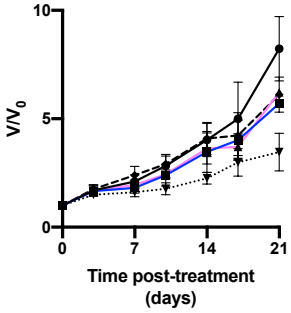

j.

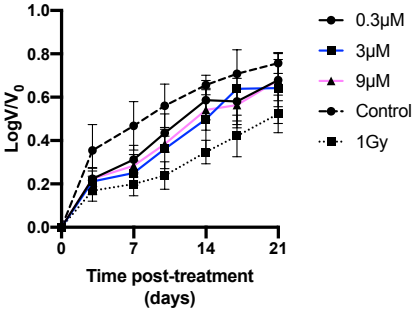

k.

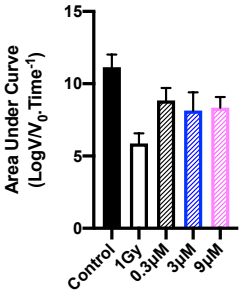

l.

Concentration	τ_2	DT	V/V_0 (Day 21)
0	8.26±0.47	9.77±1.40	6.11±0.81
1Gy	13.93±1.81	14.42±1.66	3.46±0.86
0.3μM	9.65±1.76	10.25±1.67	8.22±1.48
3μM	11.65±4.19	12.09±4.29	5.70±0.19
9μM	10.12+2.08	10.67±2.16	6.22±0.08

m.

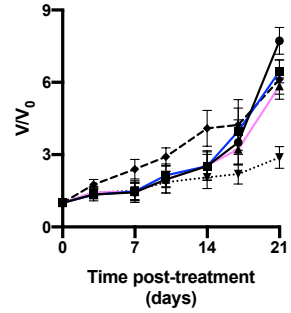

n.

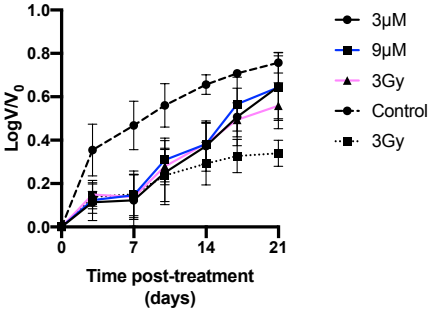

o.

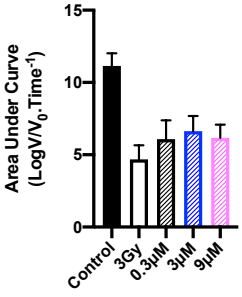

p.

Concentration	τ_2	DT	V/V_0 (Day 21)
0	8.26±0.47	9.77±1.40	6.11±0.81
3Gy	19.13±2.65	19.74±1.94	2.88±0.25
0.3μM	11.26±3.02	10.93±2.61	7.71±0.55
3μM	11.04±3.04	10.93±2.90	6.45±0.47
9μM	11.72±1.72	11.76±1.49	5.84±0.34

The combination of temozolomide and external beam X-irradiation delayed T98g spheroid growth in a dose dependent manner compared to untreated spheroids as measured by change in volume, τ_2, DT and area under the curve values, with a dose independent increase in both growth delay and doubling time compared to untreated controls. These increases were not found to be statistically significant (p-value >0.05) (Figure 6.6d & h).

When compared to temozolomide as a single agent, the combination of temozolomide and external beam X-irradiation did not affect T98g spheroid growth kinetics as measured by change in volume, τ_2, DT and area under the curve values (Figure 6.6c, d, g & h). The calculated values for τ2 and DT were comparable to those in spheroids exposed to temozolomide alone (Figure 6.3d), indicating that the combination of temozolomide and external beam X-irradiation did not significantly affect the kinetics of spheroid growth, compared to the effects of temozolomide treatment alone. This indicates that, as far as we can conclude, temozolomide is not a radiosensitiser in the T98g cell line.

When compared to X-irradiation as a single agent, the combination of temozolomide and external beam X-irradiation did inhibit T98g spheroid growth. The calculated values for τ_2 and DT were larger than those in UVW spheroids exposed to external beam X-irradiation alone (p-value >0.05) (Figure 6.4d), indicating that the combination of temozolomide and external beam X-radiation did affect the kinetics of spheroid growth, compared to external beam X-radiation exposure alone.

The combination of dimethyl fumarate and external beam X-irradiation had no effect on T98g spheroid growth compared to untreated spheroids as measured by change in volume, τ_2, DT and area under the curve values. There was no variation in either growth delay or doubling time compared to untreated controls (p-value >0.05).

When compared to dimethyl fumarate as a single agent, the combination of dimethyl fumarate and 3Gy, but not 1Gy, of external beam X-irradiation inhibited T98g spheroid growth in a dose independent manner as measured by change in volume, τ_2, DT and area under the curve values. These increases were not found to be statistically significant (p-value >0.05) (Figure 6.6p).

The area under the curve values for the combination of dimethyl fumarate and external beam X-irradiation was not reduced compared to dimethyl fumarate as a single agent (p-value >0.05) (Figure 6.6k & o).

When compared to X-irradiation as a single agent, the combination of dimethyl fumarate and external beam X-irradiation did not inhibit T98g spheroid growth. The calculated values for τ_2 and DT were comparable to those of non-irradiated T98g spheroids (Figure 6.3h), indicating that the combination of dimethyl fumarate and external beam X-radiation did not significantly affect the kinetics of spheroid growth compared to untreated spheroids.

Figure 6.6 (facing): Growth curves of T98g human glioblastoma spheroids in response to increasing doses of temozolomide, plus 1Gy (**a.**) or 3Gy (**e.**) of external beam X-irradiation. Log transformed data is shown for 1 and 3Gy treated UVW spheroids is shown in **b.** and **f.** respectively. Growth kinetics for each treatment are shown in **d.** and **h.** respectively. Area under the curve for each treatment was calculated and is shown in Figure 6.6 **c.**, and **g.** **(Continued).**

a.

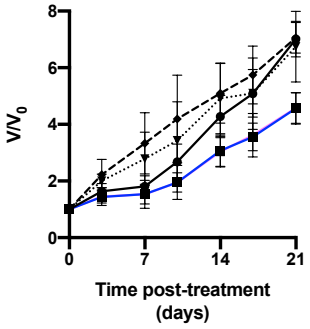

b.

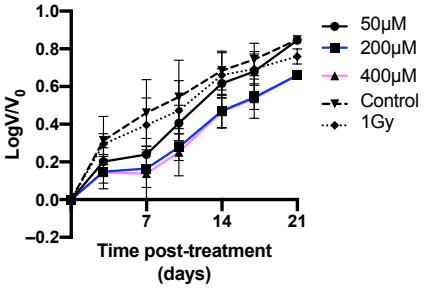

c.

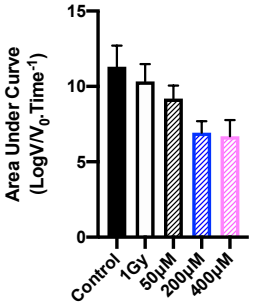

d.

Concentration (μM)	τ_2	DT	V/V_0 (Day 21)
0	7.26±0.34	8.20±0.42	7.05±0.93
1Gy	8.28±0.63	9.13±1.16	6.74±0.84
50μM	7.55±0.53	7.69±0.49	7.011±0.62
200μM	9.64±0.52	9.68±0.522	4.56±0.55
400μM	10.68±0.47	9.71±0.87	4.57±0.53

e.

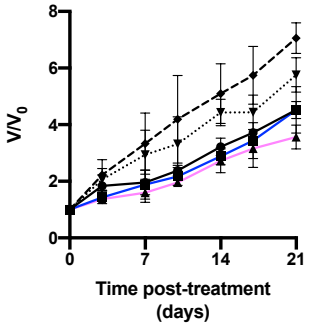

f.

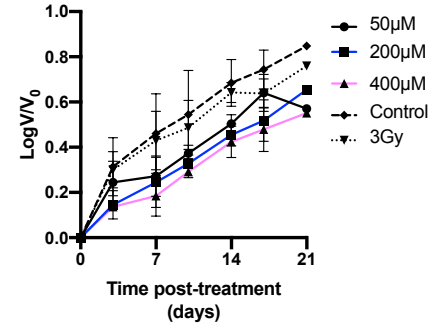

g.

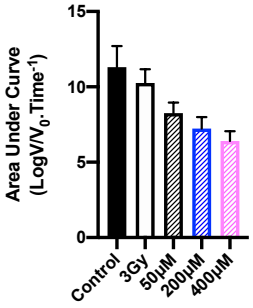

h.

Concentration	τ_2	DT	V/V_0 (Day 21)
0	7.26±0.34	8.20±0.42	7.05±0.93
3Gy	8.40±0.35	9.45±0.71	5.75±0.60
50μM	10.44±0.95	11.31±1.49	4.52±0.82
200μM	9.90±0.53	10.21±0.71	4.51±0.30
400μM	11.43±1.00	11.65±1.00	3.56±0.42

Continued.

Figure 6.6 (continued, facing): Growth curves of T98g human glioblastoma spheroids in response to increasing doses of dimethyl fumarate, plus 1Gy (**i.**) or 3Gy (**m.**) of external beam X-irradiation. Log transformed data is shown for 1 and 3Gy treated UVW spheroids is shown in **j.** and **n.** respectively. Growth kinetics for each treatment are shown in **l.** and **p.** respectively. Area under the curve for each treatment was calculated and is shown in Figure 6.2 **k.,** and **o.** Data shown is the average of three independent experiments ± standard error of the mean (SEM). Kruskal-Wallis analysis with Dunn's post hoc testing for multiple comparisons was performed using Graphpad Prism 8 software, with p-values of <0.05 = *, <0.01=** and 0.001 = *** reported as significant.

i.

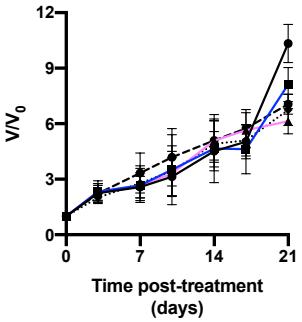

j.

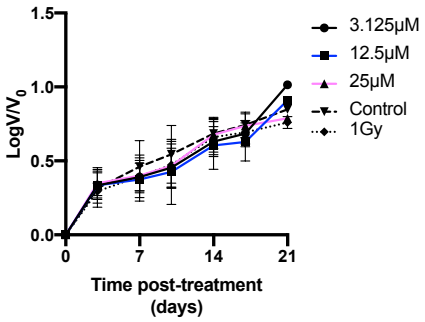

k.

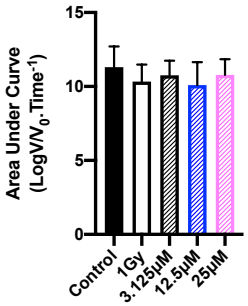

l.

Concentration	τ_2	DT	V/V_0 (Day 21)
0	7.26±0.34	8.20±0.42	7.05±0.93
1Gy	8.28±0.63	9.13±1.16	6.74±0.84
3.125µM	6.99±0.53	7.49±0.56	10.33±1.03
12.5µM	7.86±0.98	8.51±0.91	8.11±0.92
25µM	7.87±0.70	8.78+0.69	6.13±0.67

m.

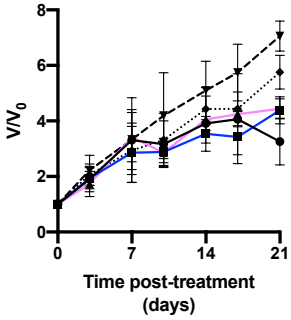

n.

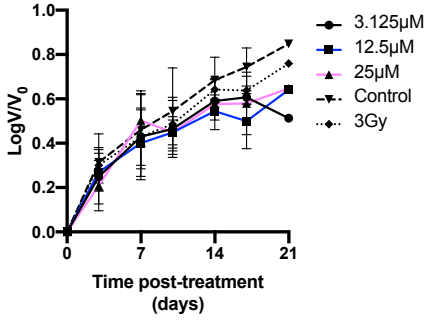

o.

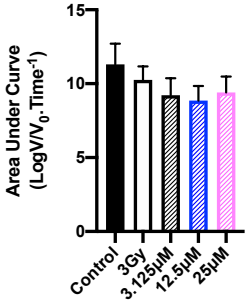

p.

Concentration	τ_2	DT	V/V_0 (Day 21)
0	7.26±0.34	8.20±0.42	7.05±0.93
3Gy	8.40±0.35	9.45±0.71	5.75±0.60
3.125µM	11.30±1.20	13.39+2.77	3.25±0.84
12.5µM	10.98±1.32	12.52±2.11	4.38±0.48
25µM	10.24±1.59	11.58±2.30	4.43±0.35

6.4.2.3 Effects of the temozolomide-dimethyl fumarate combination in combination with external beam radiation on UVW and T98g spheroid growth

When combined with external beam X-irradiation, the temozolomide-dimethyl fumarate combination delayed UVW spheroid growth in a dose dependent manner compared to untreated spheroids as measured by change in volume, τ_2, DT and area under the curve values, with a dose independent increase in both growth delay and doubling time compared to untreated controls. However, none of these increases were found to be significant (p-value >0.05) (Figure 6.7d & h).

When compared to external beam X-irradiation as a single agent, the X-irradiated temozolomide-dimethyl fumarate combination did not significantly affect UVW spheroid growth kinetics as measured by τ_2, DT and area under the curve values. This is indicative of the X-irradiated temozolomide-dimethyl fumarate combination not being more effective at altering UVW spheroid growth kinetics compared to X-irradiation as a single treatment.

The addition of X-irradiation to the temozolomide-dimethyl fumarate combination increased the growth delay and doubling time of UVW spheroids compared to spheroids treated with the temozolomide-dimethyl fumarate combination alone (Figure 6.2l), however this was not found to be statistically significant. As dose of external beam X-irradiation increased, there was a dose dependent decrease in the area under the curve values of UVW spheroids treated with the temozolomide-dimethyl fumarate combination, indicating that while the X-irradiated temozolomide-dimethyl fumarate combination does not alter UVW spheroid growth kinetics, but appears to have an inhibitory effect on overall spheroid growth compared to spheroids treated with the temozolomide-dimethyl fumarate combination alone (Figure 6.7c & g).

Compared to the combinations of temozolomide and external beam X-irradiation and dimethyl fumarate and external beam X-irradiation, the X-irradiated temozolomide-dimethyl fumarate combination did not significantly affect UVW spheroid growth kinetics as measured by τ_2, DT and area under the curve values. This is indicative of the X-irradiated temozolomide-dimethyl fumarate combination not being more effective at altering UVW spheroid growth kinetics compared to X-irradiation plus temozolomide or dimethyl fumarate as a combination therapy.

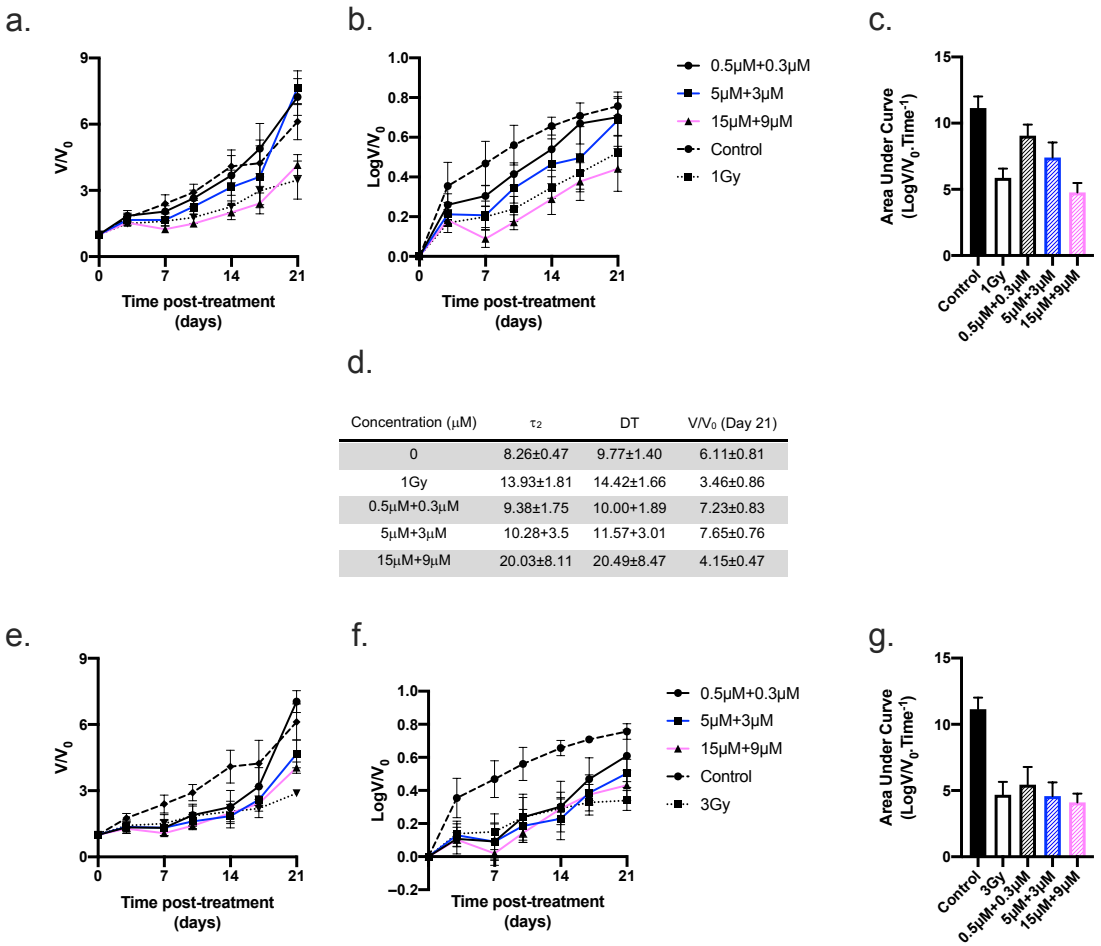

d.

Concentration (μM)	τ_2	DT	V/V_0 (Day 21)
0	8.26±0.47	9.77±1.40	6.11±0.81
1Gy	13.93±1.81	14.42±1.66	3.46±0.86
0.5μM+0.3μM	9.38±1.75	10.00+1.89	7.23±0.83
5μM+3μM	10.28+3.5	11.57+3.01	7.65±0.76
15μM+9μM	20.03±8.11	20.49±8.47	4.15±0.47

h.

Concentration (μM)	τ_2	DT	V/V_0 (Day 21)
0	8.26±0.47	9.77±1.40	6.11±0.81
3Gy	19.13±2.65	19.74±1.94	2.88±0.25
0.5μM+0.3μM	9.82±3.80	12.17±3.31	7.04±0.49
5μM+3μM	15.03±3.36	14.80±2.96	4.66±0.63
15μM+9μM	15.35±3.00	15.07±2.97	4.09±0.26

Figure 6.7: Growth curves of UVW human glioblastoma spheroids in response to increasing doses of the temozolomide-dimethyl fumarate combination, plus 1Gy (**a.**) or 3Gy (**e.**) of external beam X-irradiation. Log transformed data is shown for 1 and 3Gy treated UVW spheroids is shown in **b.** and **f.** respectively. Growth kinetics for each treatment are shown in **d.** and **h.** respectively. Area under the curve for each treatment was calculated and is shown in Figure 6.2 **c.**, and **g.** Data shown is the average of three independent experiments ± standard error of the mean (SEM). Kruskal-Wallis analysis with Dunn's post hoc testing for multiple comparisons was performed using Graphpad Prism 8 software, with p-values of <0.05 = *, <0.01=** and 0.001 = *** reported as significant. **Continued.**

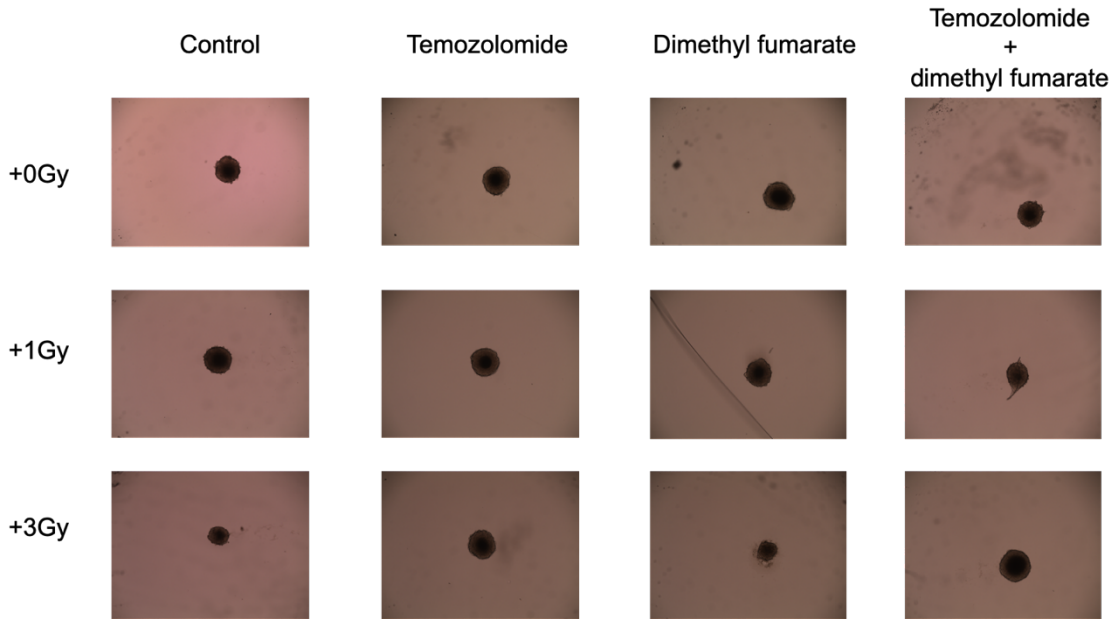

Figure 6.7 (Continued): Representative images of UVW human glioblastoma spheroids at Day 21 following treatment with 15μM temozolomide, 9μM dimethyl fumarate or 15μM+9μM of the temozolomide-dimethyl fumarate combination ± 1 or 3Gy of external beam X-irradiation.

When combined with external beam X-irradiation, the temozolomide-dimethyl fumarate combination delayed T98g spheroid growth in a dose dependent manner compared to untreated spheroids as measured by change in volume, τ_2, DT and area under the curve values, with a dose independent increase in both growth delay and doubling time compared to untreated controls (Figure 6.8d & h). Treatment with 400μM+25μM of the temozolomide-dimethyl fumarate combination significantly increased τ_2 to 16.55±2.28 when combined with 1Gy and to 13.54±1.93 when combined with 3Gy compared to a growth delay of 7.26±0.34 in untreated T98g spheroids.

When compared to external beam X-irradiation as a single agent, the X-irradiated temozolomide-dimethyl fumarate combination increased τ_2, DT and area under the curve values compared to X-irradiation as single agent. This was not statistically significant (p-value >0.05). This is indicative of the X-irradiated temozolomide-dimethyl fumarate combination not being more effective at altering T98g spheroid growth kinetics compared to X-irradiation as a single treatment.

The addition of X-irradiation to the temozolomide-dimethyl fumarate combination increased the growth delay and doubling time of T98g spheroids compared to spheroids treated with the temozolomide-dimethyl fumarate combination alone (Figure 6.3l), however this was not found to be statistically significant (p-value >0.05).

Compared to the combinations of temozolomide and external beam X-irradiation and dimethyl fumarate and external beam X-irradiation, the X-irradiated temozolomide-dimethyl fumarate combination increased the growth delay and doubling time of T98g spheroids, however there was no significant difference between these groups (p-value >0.05). This is indicative of the X-irradiated temozolomide-dimethyl fumarate combination not being more effective at altering T98g spheroid growth kinetics compared to X-irradiation plus temozolomide or dimethyl fumarate as a combination therapy.

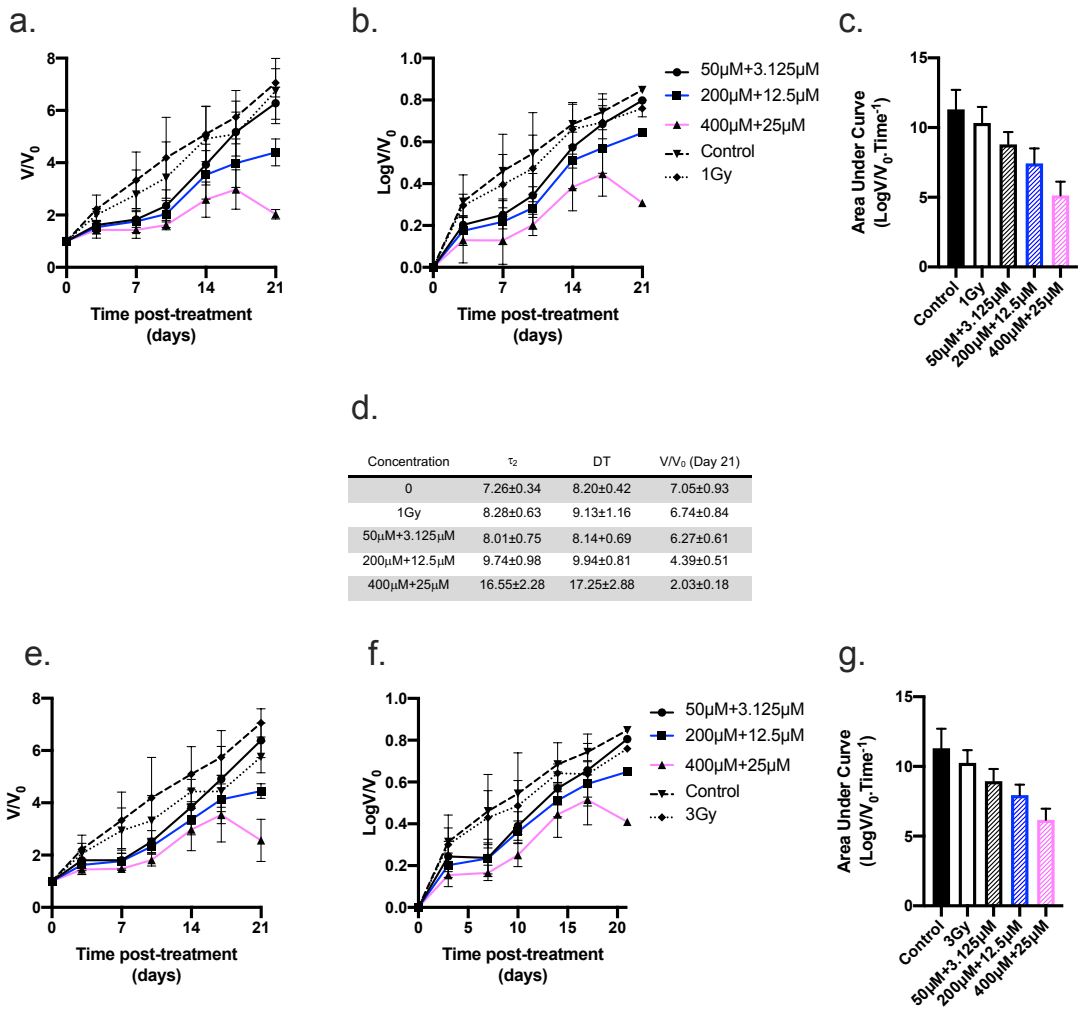

Concentration	τ_2	DT	V/V_0 (Day 21)
0	7.26±0.34	8.20±0.42	7.05±0.93
1Gy	8.28±0.63	9.13±1.16	6.74±0.84
50μM+3.125μM	8.01±0.75	8.14+0.69	6.27±0.61
200μM+12.5μM	9.74±0.98	9.94±0.81	4.39±0.51
400μM+25μM	16.55±2.28	17.25±2.88	2.03±0.18

Concentration	τ_2	DT	V/V_0 (Day 21)
0	7.26±0.34	8.20±0.42	7.05±0.93
3Gy	8.40±0.35	9.45±0.71	5.75±0.60
50μM+3.125μM	8.07±0.61	8.32±0.50	6.39±0.65
200μM+12.5μM	9.67±0.67	10.06±0.68	4.45±0.28
400μM+25μM	13.54±1.93	14.03±2.09	2.56±0.80

Figure 6.8: Growth curves of T98g human glioblastoma spheroids in response to increasing doses of the temozolomide-dimethyl fumarate combination, plus 1Gy (**a.**) or 3Gy (**e.**) of external beam X-irradiation. Log transformed data is shown for 1 and 3Gy treated UVW spheroids is shown in **b.** and **f.** respectively. Growth kinetics for each treatment are shown in **d.** and **h.** respectively. Area under the curve for each treatment was calculated and is shown in Figure 6.2 **c.,** and **g.** Data shown is the average of three independent experiments ± standard error of the mean (SEM). Kruskal-Wallis analysis with Dunn's post hoc testing for multiple comparisons was performed using Graphpad Prism 8 software, with p-values of <0.05 = *, <0.01=** and 0.001 = *** reported as significant. **(Continued).**

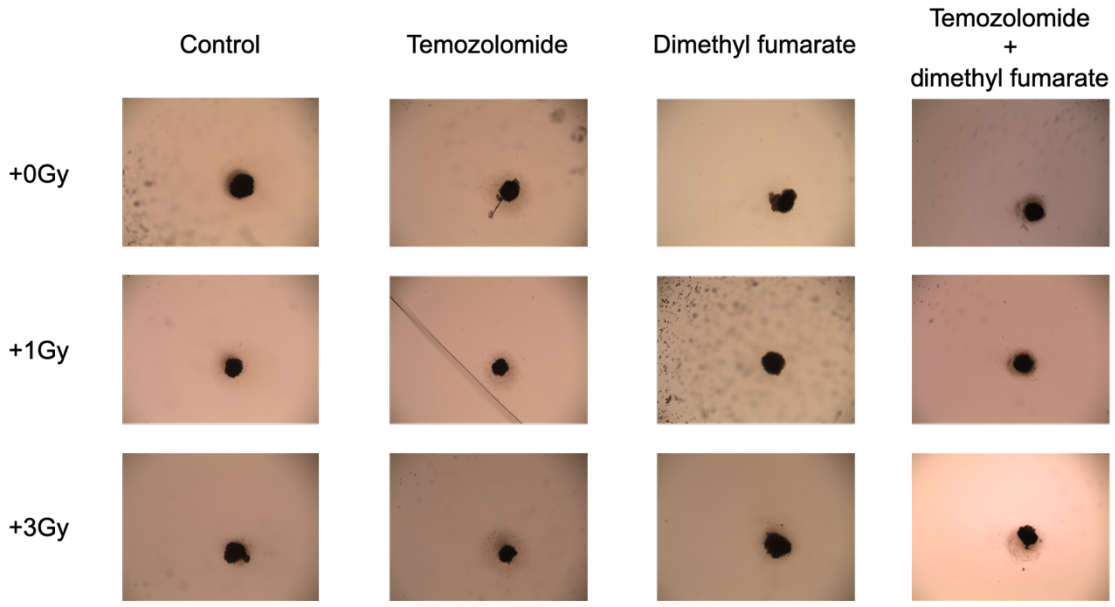

Figure 6.8 (Continued): Representative images of T98g human glioblastoma spheroids at Day 21 following treatment with 400μM temozolomide, 25μM dimethyl fumarate or 400μM+25μM of the temozolomide-dimethyl fumarate combination ± 1 or 3Gy of external beam X-irradiation.

6.5 Discussion

The post -omics age that we have entered has shown that there are limitations to the use of immortalised cell lines in the cancer drug development pipeline, and there appears to be a paradigm shift towards the use of patient samples as the gold standard in *in vitro* biology. That being said, immortalised cell lines still form the backbone of most *in vitro* research and the use of 3D *in vitro* models and xenografts still represents an important milestone in both discovery and translational biology. The use of cell lines also allows rapid screening and advancement of therapy development allowing much quicker and efficient integration of research into animal models, while the high throughput nature of cell lines allows us to keep to the 3R's – the reduction, refinement & replacement of animal models.

There are a number of reasons why multicellular tumour spheroids (MCTS; spheroids) can be viewed as a superior model to traditional monolayer culture. Spheroids model tumours to a better degree than monolayer culture, with increased hypoxia and necrosis, asynchronous cellular growth rates and variable waste, oxygen and nutrient gradients. This is coupled with a greater degree of genetic heterogeneity, meaning that there are different gene expression patterns throughout the spheroid mass, mirroring *in situ* tumours.

Spheroids, over monolayer culture, have an increased hypoxic compartment which is correlated with the increase treatment resistance of spheroids due to decreased levels of oxidative stress, and increased levels of resistance factors such as p-GP (Däster *et al*., 2016; Riffle *et al*., 2017; Wartenberg *et al*., 2003). As well as increased hypoxia, spheroids progress through the cell cycle at varied speeds. Cells cultured in monolayer cycle at the same rate, leading to weighted outcomes with treatment that rely on rapidly cycling cells to elicit their effects (Riffle *et al*., 2017). This makes spheroids more robust models for assessing cycle specific agents such as radiotherapy and temozolomide, as spheroids can model aspects of *in situ* tumours that monolayer culture cannot. Spheroid models form an important step in the discovery and translational cancer biology pipeline and can inform on aspects of cancer biology that traditional monolayer culture cannot before the establishment of *in vivo* models.

6.5.1 Response of UVW and T98g human glioblastoma spheroids to single agents and in combination with external beam X-irradiation

6.5.1.1 External beam X-irradiation

Radiotherapy is the standard of care for high-grade glioblastoma as suggested by the EORTC and ESMO (Stupp *et al*., 2009, 2010). 60Gy of hyperfractionated stereotactic radiotherapy (HFSRT) is given in 6 rounds of 10Gy in 2Gy fractions to every glioma patient when safe to do so as suggested by the EORTC. This is also given concomitantly with temozolomide (Fogh *et al*., 2010; Omuro *et al*., 2014; Stupp *et al*., 2005, 2007, 2009, 2010).

In order to determine the effects of external beam X-irradiation on spheroid growth, a dose of radiation above and below a patient clinical fraction was used as a single agent and in combination with temozolomide, dimethyl fumarate and the temozolomide-dimethyl fumarate combination.

2D cultures of both the UVW and T98g cell line displayed a similar level of cell kill when treated with 1 or 3Gy of external beam X-irradiation, suggesting that both cell lines have a similar degree of radiosensitivity. However, as discussed in Section 4.5.1, we hypothesise that the T98g cell line is radioresistant compared to UVW cells as determined by DNA damage repair response (Figure 4.8 & 4.9) and cytotoxicity at high dose (Figure 4.1).

Multicellular tumour spheroids show this hypothesised resistance to X-irradiation exquisitely. UVW spheroids responded to treatment with 1 or 3Gy as hypothesised, with a dose dependent increase in both growth delay and doubling time and a significantly reduced overall spheroid volume at the final time point assessed. T98g spheroids, however, had no significant response to the same X-irradiation parameters, displaying similar growth kinetics as non-irradiated spheroids. This is in keeping with our knowledge of the response of the T98g cell line to external beam X-irradiation, with X-irradiation having little effect on T98g survival and viability at comparable doses (Murad *et al*., 2018).

We believe that T98g cells have shown a greater ability to repair DNA double stranded breaks in two-dimensional culture, with a decrease in γH2a.X levels 24-hours post-irradiation (Figure 4.9), this has also been acknowledged in the literature (Short *et al*., 2007; de Sousa *et al*., 2017). In Chapter 4, the UVW cell line showed an increase in γH2a.X levels between 4 and 24-hours post X-irradiation (Figure 4.8), indicating sustained activation of the DNA damage repair response without resolution. Sustained levels of γH2a.X can be indicative of irreparable DNA damage (Short *et al*., 2007), correlating with an increase in apoptosis following X-irradiation (Figure 4.12) (Dikomey *et al*., 1998). This does not translate to two-dimensional cell kill, with both UVW and T98g cell lines being equally affected by 1 or 3Gy of external beam X-irradiation (Figure 4.1).

The resolution of γH2a.X in the T98g cell line may be due to increased levels of the double stranded break repair-associated proteins Rad-51 (Lambert and Lopez, 2000; Short *et al*., 2007), BRCA1 and NBS1 (Momota *et al*., 2003). However, Rad51 has also been shown to be increased in the UVW cell line following similar doses of external beam X-irradiation (Galloway, 2016). This suggest that there may be other factors that are influencing the radiosensitivity of the UVW cell line in three-dimensional culture.

One of the main radioresistance factors in glioblastoma is hypoxia (Kelley *et al*., 2016; Sheehan *et al*., 2010), one of the aspects of *in situ* tumours that spheroids are capable of replicating. Hypoxic tissue has increased radioresistance due to the lower level of ionisable oxygen (Cooke *et al*., 2003; Rey *et al*., 2017) found in hypoxic tissue. Ionisation of oxygen to reactive oxygen species is the main mechanism of radiation induced DNA double stranded breaks (Cooke *et al*., 2003; Niemantsverdriet *et al*., 2012), meaning that hypoxia confers radioresistance by limiting the generation of reactive oxygen species.

We believe that the differential response between spheroid models of the UVW and T98 cell lines to external beam X-irradiation is not due to hypoxia, as both UVW and T98g spheroids will have a hypoxic region due to structure of the spheroid and the limited permeability of oxygen towards the centre of the spheroid mass.

Hypoxia is known to supress the DNA damage repair response (Bristow and Hill, 2008; Olcina *et al*., 2010; Scanlon and Glazer, 2015), however suppression of this effect may be less pronounced in T98g cells as they appear from our studies to have higher basal level of DNA damage repair. We believe that hypoxia reduces the DNA damage

response of UVW spheroids to a point at which external beam X-irradiation can elicit cell kill and halt growth. As we suggest that the T98g cell line has a higher capacity for double stranded break repair, there will be less reduction in of the response in hypoxic tissue, and therefore less cell kill and growth arrest.

The response of each cell line to external beam X-irradiation suggests that spheroid models are a more valid representation of the response of glioblastoma cells to external beam X-irradiation than traditional monolayer culture. All hypotheses surrounding temozolomide and dimethyl fumarate in combination with external beam X-irradiation were based on the response of UVW and T98g cells to external beam x-irradiation in two-dimensional culture. The enhanced response of spheroids to external beam X-irradiation may mean that results from two-dimensional culture may not translate to spheroid models of glioblastoma.

6.5.1.2 Temozolomide

In two-dimensional cell culture, temozolomide induced a pronounced dose dependant reduction on UVW cell kill, both as a single agent and in conjunction with 1 or 3Gy of external beam X-irradiation. Conversely T98g cells were resistant to temozolomide. Cell kill was still achieved, albeit at concentrations that are not currently clinically achievable. Furthermore temozolomide did not sensitise T98g cells to external beam X-irradiation, unlike the UVW cell line. This is likely due to the activity of MGMT in the T98g, but not the UVW cell line (Figure 3.1c) (Chalmers *et al*., 2009), however, as discussed in Section 4.5.1.2, there is little consensus on MGMT status and temozolomide mediated radiosensitisation in glioblastoma.

It was hypothesised that the effects of temozolomide in two-dimensional UVW and T98g cell culture would be observed when used as a single agent and in combination with external beam X-irradiation to treat spheroid models of glioblastoma. We posited that MGMT status of each cell line would be predictive of spheroid response. Contrary to our hypothesis, temozolomide did not delay spheroid growth in the MGMT negative UVW cell line, with temozolomide treated spheroids following growth kinetics comparable to an untreated control and reaching a similar final volume to untreated spheroids. This result is contrary to literature reports of temozolomide treatment of spheroids.

It has previously been shown that temozolomide can delay growth and induce apoptosis in MGMT negative glioblastoma spheroids (Günther *et al*., 2003), an effect we have not been able to replicate. Growth delay occurred in the MGMT negative U87 cell line from concentrations as low as 5μM, a comparable concentration to the doses of temozolomide used throughout this study. A greater inhibitory effect was seen at concentrations of between 25 and 100μM, concentrations out with the range of the temozolomide-dimethyl fumarate combination. However, the Günther study did not replace treatment media, meaning spheroids were exposed to temozolomide for the duration of the imaging (Günther *et al*., 2003). We have found that continuous exposure to temozolomide significantly increases cytotoxicity to the point that there were no viable cells following 48-hours of continuous treatment (data not shown) despite the short half-life of temozolomide (Newlands *et al*., 1992). Continuous exposure is also unlikely to occur clinically, due to the pharmacokinetics of ADME criteria of both temozolomide and dimethyl fumarate (Bomprezzi, 2015; Brennan *et al*., 2015; Patel *et al*., 2003)

There are a number of possible reasons why temozolomide did not induce the expected growth delay in UVW spheroids. The most apparent may be that concentrations of temozolomide were simply too low. In order to maintain the continuity of the temozolomide-dimethyl fumarate combination used throughout these studies, the concentrations of temozolomide used in previous two-dimensional studies were utilised for all spheroid models. To induce the same effect in 3D culture as in 2D, it is often necessary to increase drug concentration (Galateanu *et al*., 2016; Kerr *et al*., 1988). Increased concentration allows for increased drug penetration into the spheroid mass (Kerr *et al*., 1988; Ong *et al*., 2010). However, in order to maintain continuity throughout these studies, the concentrations of temozolomide and dimethyl fumarate were kept constant. Increasing concentrations in the UVW cell line would have increased temozolomide concentrations out with an achievable clinical concentration (Patel *et al*., 2003). Future studies should use an increased concentration range in the UVW cell line and a reduced concentration range in the T98g cell line to find the lowest possible concentration for inhibiting spheroid growth.

At the temozolomide concentration range (0.5-15μM) used in this study, the drug may fail to penetrate beyond the outer proliferative layer of the spheroid (Kerr *et al*., 1988). Confirmation of drug of penetration should be performed using ToF-Sims mass spectrometry (Armitage *et al*., 2013; Denbigh and Lockyer, 2015; Grun *et al*., 2009;

Kotze, 2012; Kotze *et al*., 2013). Future work should be performed to correlate ToF-Sims mass spectrometry data with immunohistochemistry markers for temozolomide activity, such as mismatch repair proteins MLH1, MSH3 and MSH6 and the double strand break associated protein γH2a.X (Perazzoli *et al*., 2015; Sobol Jr *et al*., 2006). This would allow for confirmation of the presence and action of temozolomide throughout the spheroid mass.

However, as the drug penetrates towards the centre of the spheroid resistance increases due to hypoxia, reduced metabolic output and slower growth (Däster *et al*., 2016; Nunes *et al*., 2019; Riffle *et al*., 2017). This is particularly important for temozolomide, which has a greater effect on rapidly dividing cells (Beier *et al*., 2008).

Concentrations of temozolomide used throughout this study are known to be cytotoxic as a single agent and in combination with external beam X-irradiation (Figures 3.4a & 4.2a). In three dimensional models of glioblastoma single temozolomide treatment may only target the rapidly dividing cells of the proliferating outer region (Figure 6.1), allowing for selection of only slow growing, temozolomide resistant cells. Due to the short half-life of temozolomide, single treatment may not be potent enough to induce growth delay in the three dimensional spheroid models. Multiple dosing has been shown to reduce the IC50 of temozolomide in MGMT negative glioblastoma spheroids (Günther *et al*., 2003), and multiple dosing may induce a greater effect in UVW spheroids, in line with our hypothesis.

When combined with external beam X-irradiation, temozolomide treated UVW spheroids did not show the hypothesised increase in growth delay compared to external beam X-irradiation as a single agent. However, the spheroid doubling time and growth delay was increased compared to spheroids treated with temozolomide as a single agent, indicating that there is a synergistic interaction between temozolomide and external beam X-irradiation.

This change in growth kinetics appeared to be dependent on the dose of X-irradiation, with spheroids treated with 1Gy and temozolomide having significantly lower growth delay and spheroid doubling time compared to spheroids treated with 3Gy and temozolomide. This correlated to a dose dependent decrease in overall spheroid volume, suggesting that the combination of temozolomide and external beam X-

irradiation alters growth kinetics and decreases spheroid volume compared to temozolomide, but not external beam X-irradiation as a single agent. We have shown that, in two-dimensional culture, the interaction between temozolomide and external beam X-irradiation is synergistic in the MGMT negative UVW cell line, indicating that temozolomide acts as radiosensitiser (Figure 4.2a & b). This is in keeping with our knowledge of the combination of temozolomide and external beam X-irradiation from the literature (Carlson *et al*., 2009).

We believe that two-dimensional culture results may have weighted our hypotheses regarding the combination of temozolomide and external beam x-irradiation. As discussed, the response of UVW spheroids to external beam X-irradiation was more pronounced than expected and the response to temozolomide was less pronounced given the response of monolayer cultures of UVW cells to each agent (Figures 3.2 & 4.1 respectively). Again, this may be due to poor penetration of temozolomide throughout the spheroid mass as discussed above, preventing radiosensitisation. Based on the increased doubling time of spheroids treated with temozolomide and external beam X-irradiation compared to temozolomide alone, we still believe and interaction between the two agents is occurring. However, we suggest that this interaction results in the outcome being poorer than when external beam X-irradiation is used as a single agent. Temozolomide induces activation of break excision repair, mismatch repair and homologous recombination (Caporali *et al*., 2004; Liu *et al*., 2009; Sobol Jr *et al*., 2006; Trivedi *et al*., 2005), and the combination of temozolomide and X-irradiation is likely to induce a greater level of DNA damage repair than temozolomide or X-irradiation alone.

An increase in DNA damage repair proteins will correlate with increased DNA repair and therefore increased survival. This is seen with radiation, and a principle known as hyper-radiosensitivity and induced radioresistance (HRS/IRR), where low dose radiation increases cell kill over high dose radiation due to low dose radiation inducing a lower level of DNA damage repair response while still causing lethal damage (Schoenherr *et al*., 2013; Thomas *et al*., 2013).

T98g spheroids were not expected to respond to temozolomide treatment. Surprisingly, T98g spheroids responded to temozolomide treatment, despite minimal effect in 2D culture. Paradoxically, this response is potentially due to MGMT expression in this cell line. MGMT is a suicide enzyme, meaning that the action of removing methyl groups

from the base guanine irreversibly inhibits the enzyme (Christmann *et al*., 2011). Depletion of MGMT by excess temozolomide may therefore sensitise T98g spheroids to temozolomide (Günther *et al*., 2003).

However, this response may occur as the concentrations of temozolomide used in this study were high enough to penetrate the spheroid mass. Again, ToF-Sims mass spectrometry and immunohistochemistry for markers for temozolomide activity, such as mismatch repair proteins MLH1, MSH3 and MSH6 and γH2a.X (Perazzoli *et al*., 2015; Sobol Jr *et al*., 2006) could be used to allow for confirmation of the presence and action of temozolomide throughout the spheroid mass.

T98g spheroids did not appear to be radiosensitised by temozolomide. Temozolomide treated spheroids and spheroids treated with temozolomide and external beam X-irradiation displayed comparable growth kinetics. This is also seen in 2D culture, with little synergistic interaction occurring between temozolomide and external beam X-irradiation (Figure 4.3a & b). We believe that this is due to the increased DNA damage repair capacity of T98g cells discussed above.

6.5.1.3 Dimethyl fumarate

We believe that this is the first report of dimethyl fumarate being used to treat three-dimensional models of human cancer.

In monolayer models, dimethyl fumarate induced cytotoxicity as a single agent but showed no radiosensitisation of UVW or T98g human glioblastoma cell lines following treatment with 1 or 3Gy of external beam X-irradiation. Spheroid growth delay was expected to be observed due to the increased dependence of hypoxic glioma cells on glutathione (Bump *et al*., 1982) and the ability of dimethyl fumarate to deplete glutathione in both UVW and T98g cells (Figure 5.1a & c) (Brennan *et al*., 2015).

Although no radiosensitisation was seen in monolayer culture, it was expected that dimethyl fumarate would radiosensitise spheroids due to the increased hypoxic compartment (Riffle *et al*., 2017) and the ability of dimethyl fumarate to radiosensitise hypoxic cells (Held and Hopcia, 1993; Held *et al*., 1988, 1991).

Our hypothesis was not validated. In both cell lines dimethyl fumarate treated spheroids followed the same growth pattern and reached the same final volume as untreated spheroids. When combined with external beam X-irradiation, dimethyl fumarate did not significantly affect T98g spheroid volume compared to spheroids treated with external beam X-irradiation as single agent. This is likely due to poor drug penetration into the centre of spheroid (Kerr *et al*., 1988) and therefore no hypoxic radiosensitisation by dimethyl fumarate.

Again, we suggest ToF-Sims mass spectrometry to be undertaken that would allow for detection of dimethyl fumarate throughout the spheroid mass. This should be correlated with immunohistochemistry for markers of dimethyl fumarate activity such as NRF2 (Figure 5.8) (Brennan *et al*., 2015; Hammer *et al*., 2018).

6.5.2 Response of UVW and T98g human glioblastoma spheroids to the temozolomide-dimethyl fumarate combination

This is the first published report of the combination of temozolomide and dimethyl fumarate in three dimensional models of any cancer. In 2D culture, the temozolomide-dimethyl fumarate combination displayed synergy and increased cell kill compared to both temozolomide and dimethyl fumarate as single agents. The temozolomide-dimethyl fumarate combination also synergised with external beam X-irradiation to significantly increase cell kill.

In this study only the highest combination of the temozolomide-dimethyl fumarate combination increased growth delay and spheroid doubling time compared to temozolomide and dimethyl fumarate as single agents. In both cell lines, this was correlated with a decrease in spheroid volume compared to temozolomide and dimethyl fumarate as single agents. This is indicative of both cell kill and inhibition of cell growth. Given that the effects of the temozolomide-dimethyl fumarate combination are only seen at the highest dose used, this is indicative that the lower doses are not capable of interacting fully with the spheroid mass, again we hypothesise this occurred due to poor drug penetrations (Kerr *et al*., 1988).

For both cell lines we believe that the decrease in spheroid volume induced by the temozolomide-dimethyl fumarate combination is due to the mechanism discussed

extensively throughout Chapters 3, 4 and 5. Dimethyl fumarate will potentiate the effects of temozolomide, likely through inhibiting glutathione. This potentiation will occur through a bimodal mechanism; the inhibition will allow for higher intra-cellular concentrations of temozolomide, as well as allow for temozolomide to remain active within the cell for a sustained period of time. Decreased spheroid volume and increased growth delay was also seen when the temozolomide-dimethyl fumarate combination was used in combination with external beam X-irradiation. The response of the temozolomide-dimethyl fumarate combination with external beam X-irradiation did not occur in spheroids culture to the same extent as it occurred in two-dimensional culture. This likely due to the interpretation of 2D culture results, and the stronger than anticipated response of both cell lines to external beam X-irradiation discussed above. This highlights the importance of the utilisation of three-dimensional models in the drug development pipeline

We believe that we shown that the principle of glutathione depletion to chemosensitise glioblastoma cells translates to three-dimensional models of glioblastoma. Future work should be performed using mosaic spheroid models (Boyd *et al*., 2002). This would allow for drug penetration and modes of action in models that feature heterogeneous cell phenotypes and genotypes and asynchronous cellular growth.

We have shown that the combination of temozolomide, dimethyl fumarate and external beam X-irradiation is effective at delaying spheroid growth in both cell lines, but only at the highest concentrations used. This was contrary to our hypothesis and is likely due to the low concentrations of temozolomide and dimethyl fumarate used not penetrating the spheroid mass successfully.

Our hypotheses regarding temozolomide and dimethyl fumarate as single agents was not validated despite strong literature support and results from monolayer experiments. We believe that this highlights the need for screening novel treatments in more sophisticated models than traditional monolayer culture. We believe that failure to elicit the expected response occurred due to low drug concentrations not being able to penetrate the spheroid mass. This explains the discrepancy between two and three-dimensional culture results.

Unfortunately, we were not able to establish xenograft models of glioblastoma. This limits clinical advancement of the temozolomide-dimethyl fumarate combination as animal models are needed before the establishment of clinical trials. We believe that further work should focus on the establishment of animals of glioblastoma in which the temozolomide-dimethyl fumarate combination can be tested prior to clinical development.

Chapter 7

Discussion, conclusions and future work

Survival of patients diagnosed with glioblastoma multiforme is unacceptably low. Depending on molecular stratification from biopsy, 5-year survival can be as low as 1.9% in certain patient groups, and median 5-year survival is no higher than 4%.

We believe this is the first study to examine how the standard of care for high-grade glioblastoma could be improved using dimethyl fumarate as an adjuvant.

Vaccine immunologists use the term “dose sparing” to describe increased vaccine immunogenicity, while minimising the dose of vaccine needed to confer immunity. This concept can be applied to this project, where we aimed to increase anti-cancer activity of the current standard of care treatment for high-grade glioma while lowering doses of chemotherapy and X-irradiation. In this aim, the project was successful. This was most evident in the treatment resistant T98g cell line, where initially 400μM gave 50% cell. Using low dose dimethyl fumarate as an adjuvant to temozolomide and X-irradiation, cell kill was increased to 65% at just 50μM temozolomide and 1Gy of X-irradiation. Importantly, 50μM of temozolomide is an achievable clinical dose, and 1Gy is half of a current patient fraction.

It was hypothesised that dimethyl fumarate would potentiate the effects of temozolomide, likely through inhibition of glutathione. This potentiation was suggested to occur through a bimodal mechanism; the inhibition would allow for higher intra-cellular concentrations of temozolomide, as well as allow for temozolomide to remain active within the cell for a sustained period of time. When combined with external beam X-irradiation, we suggested that dimethyl fumarate inhibiting intracellular glutathione would result in higher intracellular temozolomide concentrations and higher reactive oxygen species levels, allowing for an increased level of DNA damage.

Our hypothesis that dimethyl fumarate would synergise with temozolomide was validated, showing a synergistic increase in cell kill in both MGMT positive and negative

cell lines. However, we were not able to suggest a mechanism of action for this increase in cell kill. We suggested that the increase in cell kill occurred due to dimethyl fumarate mediated depletion of glutathione. We have shown that the concentrations of dimethyl fumarate used in these studies are capable of significantly depleting intracellular glutathione levels, and increased glutathione levels increase chemoresistance towards temozolomide.

Depletion of glutathione was hypothesised to allow for higher intra-cellular concentrations of temozolomide, as well as allow for temozolomide to remain active within the cell for a sustained period of time. An increase in the efficacy of temozolomide was expected to be seen when cells were treated with the temozolomide-dimethyl fumarate combination compared to temozolomide alone. However, we were not able to show a significant increase in DNA damage as measured by γH2a.X formation, cell cycle arrest or induction of apoptosis with the combination of temozolomide and dimethyl fumarate compared to temozolomide alone.

We believe that depletion of glutathione by dimethyl fumarate is capable of activating the antioxidant transcription factor NRF2. We have shown that dimethyl fumarate is capable of activating NRF2 at the concentration used, however we have not been able to link glutathione depletion to activation of NRF2 directly. We have shown that activation and inhibition of NRF2 decrease and increase temozolomide sensitivity respectively. Activation of NRF2 by dimethyl fumarate may therefore limit the clinical deployment of dimethyl fumarate as an anti-cancer agent, or at least, activation of NRF2 should be a considered a potential adverse event. Future work should revolve around the development and application of the temozolomide-dimethyl fumarate to *in vivo* models of high-grade glioma. This would be one of the final steps before the potential implementation of small-scale safety and feasibility human studies.

Beyond the continuation of the temozolomide-dimethyl fumarate combination in high-grade glioma, there is the potential for the principle of glutathione depletion to be applied to other cancers that are treated with alkylating agents, spindle poisons and platinum-based alkylating-like agents.

There is still also still a huge amount to learn from the use of dimethyl fumarate as a single agent. The immunomodulatory effects of dimethyl fumarate are likely to have

significant effects on the tumour micro-environment, an area that is becoming increasingly studied and realised as site of therapeutic intervention. Dimethyl fumarate mediated modulation of signalling pathways such as the IL-6/STAT-3 pathway has the potential to be studied further. The emergent role of the tumour microenvironment and the interplay of the immune system with the tumour has opened up the possibility of dimethyl fumarate having a more diverse range of action in *in situ* tumours than in *in vitro* culture conditions. This should be fully examined to prevent events that would be not possible to detect in two-dimensional culture.

Any addition to the standard of care for glioblastoma that can improve treatment efficacy should be welcomed due to the continuously low survival rates seen in all patient groups. We believe that the potentiation of the standard of care for glioblastoma that we have demonstrated by the addition of sub-clinically achievable doses of dimethyl fumarate is significant. Dimethyl fumarate is safe, well tolerated, and importantly, is capable of crossing the blood brain barrier. We believe that dimethyl fumarate is an appropriate agent worthy of further investigation.

We strongly believe that dimethyl fumarate mediated depletion of glutathione is a treatment modality that should be investigated further in glioblastoma.

Chapter 8:

Outputs

Papers:

Potentiation of gold-standard treatment for glioblastoma multiforme using the immunomodulatory agent dimethyl fumarate [in preparation]

Posters:

Improving efficacy of gold standard chemotherapy for high-grade glioma using repurposed drugs – CRUK brain tumour conference, London, 02/04/18

Developing Novel Combinations for Brain Cancers – Medical Research Scotland event, Perth, 19/04/16

Curing Cancer with Purple Dots – Meet the Researcher (public engagement event) Glasgow and Dundee Science centres 27+28/02/19

Talks:

Things I wish I knew before I started my PhD – Medical Research Scotland event, Perth, 11/04/19

Developing Novel Combinations for Brain Cancers – SIPBS research day, Glasgow 11/11/16

Developing Novel Combinations for Brain Cancers – The “PATH” to Personalised Cancer Medicine, Glasgow, 16/08/18

Chapter 9:

References

Aasland, D., Götzinger, L., Hauck, L., Berte, N., Meyer, J., Effenberger, M., Schneider, S., Reuber, E.E., Roos, W.P., Tomicic, M.T., *et al*. (2019). Temozolomide Induces Senescence and Repression of DNA Repair Pathways in Glioblastoma Cells via Activation of ATR–CHK1, p21, and NF-κB. Cancer Res. *79*, 99–113.

Adamson, C., Kanu, O.O., Mehta, A.I., Di, C., Lin, N., Mattox, A.K., and Bigner, D.D. (2009). Glioblastoma multiforme: a review of where we have been and where we are going. Expert Opin. Investig. Drugs *18*, 1061–1083.

Agarwal, M.L., Agarwal, A., Taylor, W.R., and Stark, G.R. (1995). p53 controls both the G2/M and the G1 cell cycle checkpoints and mediates reversible growth arrest in human fibroblasts. Proc. Natl. Acad. Sci. *92*, 8493–8497.

Agnihotri, S., Burrell, K.E., Wolf, A., Jalali, S., Hawkins, C., Rutka, J.T., and Zadeh, G. (2013). Glioblastoma, a brief review of history, molecular genetics, animal models and novel therapeutic strategies. Arch. Immunol. Ther. Exp. (Warsz.) *61*, 25–41.

Agosti, R.M., Leuthold, M., Gullick, W.J., Yasargil, M.G., and Wiestler, O.D. (1992). Expression of the epidermal growth factor receptor in astrocytic tumours is specifically associated with glioblastoma multiforme. Virchows Arch. A *420*, 321–325.

Ahmed, L.A., Shehata, N.I., Abdelkader, N.F., and Khattab, M.M. (2014). Tempol, a Superoxide Dismutase Mimetic Agent, Ameliorates Cisplatin-Induced Nephrotoxicity through Alleviation of Mitochondrial Dysfunction in Mice. PLOS ONE *9*, e108889.

Alan Mitteer, R., Wang, Y., Shah, J., Gordon, S., Fager, M., Butter, P.-P., Jun Kim, H., Guardiola-Salmeron, C., Carabe-Fernandez, A., and Fan, Y. (2015). Proton beam radiation induces DNA damage and cell apoptosis in glioma stem cells through reactive oxygen species. Sci. Rep. *5*.

Albrecht, P., Bouchachia, I., Goebels, N., Henke, N., Hofstetter, H.H., Issberner, A., Kovacs, Z., Lewerenz, J., Lisak, D., Maher, P., *et al*. (2012). Effects of dimethyl fumarate on neuroprotection and immunomodulation. J. Neuroinflammation *9*, 163.

Aldape, K., Zadeh, G., Mansouri, S., Reifenberger, G., and von Deimling, A. (2015). Glioblastoma: pathology, molecular mechanisms and markers. Acta Neuropathol. (Berl.) *129*, 829–848.

Ali-Osman, F., Brunner, J.M., Kutluk, T.M., and Hess, K. (1997). Prognostic significance of glutathione S-transferase pi expression and subcellular localization in human gliomas. Clin. Cancer Res. *3*, 2253–2261.

Allalunis-Turner, M.J., Day, R.S., McKean, J.D., Petruk, K.C., Allen, P.B., Aronyk, K.E., Weir, B.K., Huyser-Wierenga, D., Fulton, D.S., and Urtasun, R.C. (1991). Glutathione

levels and chemosensitizing effects of buthionine sulfoximine in human malignant glioma cells. J. Neurooncol. *11*, 157–164.

An, Z., Aksoy, O., Zheng, T., Fan, Q.-W., and Weiss, W.A. (2018). Epidermal growth factor receptor and EGFRvIII in glioblastoma: signaling pathways and targeted therapies. Oncogene *37*, 1561–1575.

Antonelli, M.C., Guillemin, G.J., Raisman-Vozari, R., Del-Bel, E.A., Aschner, M., Collins, M.A., Tizabi, Y., Moratalla, R., and West, A.K. (2012). New Strategies in Neuroprotection and Neurorepair. Neurotox. Res. *21*, 49–56.

Apte, R.N., Dotan, S., Elkabets, M., White, M.R., Reich, E., Carmi, Y., Song, X., Dvozkin, T., Krelin, Y., and Voronov, E. (2006). The involvement of IL-1 in tumorigenesis, tumor invasiveness, metastasis and tumor-host interactions. Cancer Metastasis Rev. *25*, 387–408.

Armitage, E.G., Kotze, H.L., Fletcher, J.S., Henderson, A., Williams, K.J., Lockyer, N.P., and Vickerman, J.C. (2013). Time-of-flight SIMS as a novel approach to unlocking the hypoxic properties of cancer. Surf. Interface Anal. *45*, 282–285.

Armstrong, J.S., Steinauer, K.K., Hornung, B., Irish, J.M., Lecane, P., Birrell, G.W., Peehl, D.M., and Knox, S.J. (2002). Role of glutathione depletion and reactive oxygen species generation in apoptotic signaling in a human B lymphoma cell line. Cell Death Differ. Rome *9*, 252–263.

Arvelo, F., Sojo, F., and Cotte, C. (2016). Tumour progression and metastasis. Ecancermedicalscience *10*.

Ashburn, T.T., and Thor, K.B. (2004). Drug repositioning: identifying and developing new uses for existing drugs. Nat. Rev. Drug Discov. *3*, 673–683.

Baker, G.J., Yadav, V.N., Motsch, S., Koschmann, C., Calinescu, A.-A., Mineharu, Y., Camelo-Piragua, S.I., Orringer, D., Bannykh, S., Nichols, W.S., *et al*. (2014). Mechanisms of glioma formation: iterative perivascular glioma growth and invasion leads to tumor progression, VEGF-independent vascularization, and resistance to antiangiogenic therapy. Neoplasia N. Y. N *16*, 543–561.

Balendiran, G.K., Dabur, R., and Fraser, D. (2004). The role of glutathione in cancer. Cell Biochem. Funct. *22*, 343–352.

Banin, S. (1998). Enhanced Phosphorylation of p53 by ATM in Response to DNA Damage. Science *281*, 1674–1677.

Bao, S., Wu, Q., McLendon, R.E., Hao, Y., Shi, Q., Hjelmeland, A.B., Dewhirst, M.W., Bigner, D.D., and Rich, J.N. (2006). Glioma stem cells promote radioresistance by preferential activation of the DNA damage response. Nature *444*, 756–760.

Bar, E.E., Lin, A., Mahairaki, V., Matsui, W., and Eberhart, C.G. (2010). Hypoxia Increases the Expression of Stem-Cell Markers and Promotes Clonogenicity in Glioblastoma Neurospheres. Am. J. Pathol. *177*, 1491–1502.

Barciszewska, A.-M., Gurda, D., Głodowicz, P., Nowak, S., and Naskręt-Barciszewska, M.Z. (2015). A New Epigenetic Mechanism of Temozolomide Action in Glioma Cells. PLOS ONE *10*, e0136669.

Barker, F.G., Simmons, M.L., Chang, S.M., Prados, M.D., Larson, D.A., Sneed, P.K., Wara, W.M., Berger, M.S., Chen, P., Israel, M.A., *et al*. (2001). EGFR overexpression and radiation response in glioblastoma multiforme. Int. J. Radiat. Oncol. *51*, 410–418.

Barrié, M., Couprie, C., Dufour, H., Figarella-Branger, D., Muracciole, X., Hoang-Xuan, K., Braguer, D., Martin, P.M., Peragut, J.C., Grisoli, F., *et al*. (2005). Temozolomide in combination with BCNU before and after radiotherapy in patients with inoperable newly diagnosed glioblastoma multiforme. Ann. Oncol. *16*, 1177–1184.

Bartek, J., and Lukas, J. (2003). Chk1 and Chk2 kinases in checkpoint control and cancer. Cancer Cell *3*, 421–429.

Baskar, R., Lee, K.A., Yeo, R., and Yeoh, K.-W. (2012). Cancer and Radiation Therapy: Current Advances and Future Directions. Int. J. Med. Sci. *9*, 193–199.

Bassan, F., Peter, F., Houbre, B., Brennstuhl, M. j., Costantini, M., Speyer, E., and Tarquinio, C. (2014). Adherence to oral antineoplastic agents by cancer patients: definition and literature review. Eur. J. Cancer Care (Engl.) *23*, 22–35.

Bastien, J.I.L., McNeill, K.A., and Fine, H.A. (2015). Molecular characterizations of glioblastoma, targeted therapy, and clinical results to date. Cancer *121*, 502–516.

Batchelor, T.T., Sorensen, A.G., di Tomaso, E., Zhang, W.-T., Duda, D.G., Cohen, K.S., Kozak, K.R., Cahill, D.P., Chen, P.-J., Zhu, M., *et al*. (2007). AZD2171, a pan-VEGF receptor tyrosine kinase inhibitor, normalizes tumor vasculature and alleviates edema in glioblastoma patients. Cancer Cell *11*, 83–95.

Batista, L.F.Z., Roos, W.P., Christmann, M., Menck, C.F.M., and Kaina, B. (2007). Differential Sensitivity of Malignant Glioma Cells to Methylating and Chloroethylating Anticancer Drugs: p53 Determines the Switch by Regulating xpc, ddb2, and DNA Double-Strand Breaks. Cancer Res. *67*, 11886–11895.

Behnan, J., Finocchiaro, G., and Hanna, G. (2019). The landscape of the mesenchymal signature in brain tumours. Brain *142*, 847–866.

Beier, C.P., Kumar, P., Meyer, K., Leukel, P., Bruttel, V., Aschenbrenner, I., Riemenschneider, M.J., Fragoulis, A., Rümmele, P., Lamszus, K., *et al*. (2012). The Cancer Stem Cell Subtype Determines Immune Infiltration of Glioblastoma. Stem Cells Dev. *21*, 2753–2761.

Beier, D., Rohrl, S., Pillai, D.R., Schwarz, S., Kunz-Schughart, L.A., Leukel, P., Proescholdt, M., Brawanski, A., Bogdahn, U., Trampe-Kieslich, A., *et al*. (2008). Temozolomide Preferentially Depletes Cancer Stem Cells in Glioblastoma. Cancer Res. *68*, 5706–5715.

van den Bent, M.J., Brandes, A.A., Rampling, R., Kouwenhoven, M.C.M., Kros, J.M., Carpentier, A.F., Clement, P.M., Frenay, M., Campone, M., Baurain, J.-F., *et al*. (2009). Randomized Phase II Trial of Erlotinib Versus Temozolomide or Carmustine in Recurrent Glioblastoma: EORTC Brain Tumor Group Study 26034. J. Clin. Oncol. *27*, 1268–1274.

Bernardy, C.C.F., Zarpelon, A.C., Pinho-Ribeiro, F.A., Calixto-Campos, C., Carvalho, T.T., Fattori, V., Borghi, S.M., Casagrande, R., and Verri, W.A. (2017). Tempol, a Superoxide Dismutase Mimetic Agent, Inhibits Superoxide Anion-Induced Inflammatory Pain in Mice. BioMed Res. Int.

Bieńkowski, M., Piaskowski, S., Stoczyńska-Fidelus, E., Szybka, M., Banaszczyk, M., Witusik-Perkowska, M., Jesień-Lewandowicz, E., Jaskólski, D.J., Radomiak-Załuska, A., Jesionek-Kupnicka, D., *et al*. (2013). Screening for EGFR Amplifications with a Novel Method and Their Significance for the Outcome of Glioblastoma Patients. PLOS ONE *8*, e65444.

Bloom, D., Dhakshinamoorthy, S., and Jaiswal, A.K. (2002). Site-directed mutagenesis of cysteine to serine in the DNA binding regionof Nrf2 decreases its capacity to upregulate antioxidant responseelement-mediated expression and antioxidant induction of NAD(P)H:quinone oxidoreductase1 gene. Oncogene *21*, 2191–2200.

Bobola, M.S., Kolstoe, D.D., Blank, A., and Silber, J.R. (2010). Minimally Cytotoxic Doses of Temozolomide Produce Radiosensitization in Human Glioblastoma Cells Regardless of MGMT Expression. Mol. Cancer Ther. *9*, 1208–1218.

Bodell, W.J., Gaikwad, N.W., Miller, D., and Berger, M.S. (2003). Formation of DNA Adducts and Induction of lacI Mutations in Big Blue Rat-2 Cells Treated with Temozolomide: Implications for the Treatment of Low-Grade Adult and Pediatric Brain Tumors. Cancer Epidemiol. Prev. Biomark. *12*, 545–551.

Bomprezzi, R. (2015). Dimethyl fumarate in the treatment of relapsing–remitting multiple sclerosis: an overview. Ther. Adv. Neurol. Disord. *8*, 20–30.

Booth, L., Cruickshanks, N., Tavallai, S., Roberts, J.L., Peery, M., Poklepovic, A., and Dent, P. (2014). Regulation of dimethyl-fumarate toxicity by proteasome inhibitors. Cancer Biol. Ther. *15*, 1646–1657.

Bota, D.A., Desjardins, A., Quinn, J.A., Affronti, M.L., and Friedman, H.S. (2007). Interstitial chemotherapy with biodegradable BCNU (Gliadel®) wafers in the treatment of malignant gliomas. Ther. Clin. Risk Manag. *3*, 707–715.

Boveia, V., and Schutz-Geschwender, A. (2015). Quantitative Analysis of Signal Transduction with In-Cell Western Immunofluorescence Assays. Methods Mol. Biol. Clifton NJ *1314*, 115–130.

Boyd, M., Mairs, S.C., Stevenson, K., Livingstone, A., Clark, A.M., Ross, S.C., and Mairs, R.J. (2002). Transfectant mosaic spheroids: a new model for evaluation of tumour cell killing in targeted radiotherapy and experimental gene therapy. J. Gene Med. *4*, 567–576.

Brada, M., Pijls-Johannesma, M., and De Ruysscher, D. (2007). Proton Therapy in Clinical Practice: Current Clinical Evidence. J. Clin. Oncol. *25*, 965–970.

Brandes, A.A., Ermani, M., Basso, U., Amistà, P., Berti, F., Scienza, R., Rotilio, A., Pinna, G., Gardiman, M., and Monfardini, S. (2001). Temozolomide as a second-line systemic regimen in recurrent high-grade glioma: A phase II study. Ann. Oncol. *12*, 255–257.

Bray, F., Ferlay, J., Soerjomataram, I., Siegel, R.L., Torre, L.A., and Jemal, A. (2018). Global cancer statistics 2018: GLOBOCAN estimates of incidence and mortality worldwide for 36 cancers in 185 countries. CA. Cancer J. Clin. *68*, 394–424.

Bredel, M., Bredel, C., Juric, D., Duran, G.E., Yu, R.X., Harsh, G.R., Vogel, H., Recht, L.D., Scheck, A.C., and Sikic, B.I. (2006). Tumor necrosis factor-alpha-induced protein 3 as a putative regulator of nuclear factor-kappaB-mediated resistance to O6-alkylating agents in human glioblastomas. J. Clin. Oncol. Off. J. Am. Soc. Clin. Oncol. *24*, 274–287.

Bregy, A., Shah, A.H., Diaz, M.V., Pierce, H.E., Ames, P.L., Diaz, D., and Komotar, R.J. (2013). The role of Gliadel wafers in the treatment of high-grade gliomas. Expert Rev. Anticancer Ther. *13*, 1453–1461.

Brennan, C.W., Verhaak, R.G.W., McKenna, A., Campos, B., Noushmehr, H., Salama, S.R., Zheng, S., Chakravarty, D., Sanborn, J.Z., Berman, S.H., *et al*. (2013). The Somatic Genomic Landscape of Glioblastoma. Cell *155*, 462–477.

Brennan, M.S., Matos, M.F., Li, B., Hronowski, X., Gao, B., Juhasz, P., Rhodes, K.J., and Scannevin, R.H. (2015). Dimethyl Fumarate and Monoethyl Fumarate Exhibit Differential Effects on KEAP1, NRF2 Activation, and Glutathione Depletion In Vitro. PLOS ONE *10*, e0120254.

Bristow, R.G., and Hill, R.P. (2008). Hypoxia and metabolism: Hypoxia, DNA repair and genetic instability. Nat. Rev. Cancer *8*, 180–192.

Brown, J.M. (2000). Exploiting the hypoxic cancer cell: mechanisms and therapeutic strategies. Mol. Med. Today *6*, 157–162.

von Bueren, A.O., Bacolod, M.D., Hagel, C., Heinimann, K., Fedier, A., Kordes, U., Pietsch, T., Koster, J., Grotzer, M.A., Friedman, H.S., *et al*. (2012). Mismatch repair deficiency: a temozolomide resistance factor in medulloblastoma cell lines that is uncommon in primary medulloblastoma tumours. Br. J. Cancer *107*, 1399–1408.

Bump, E., Yu, N., and Brown, J. (1982). Radiosensitization of hypoxic tumor cells by depletion of intracellular glutathione. Science *217*, 544–545.

Burma, S., Chen, B.P., Murphy, M., Kurimasa, A., and Chen, D.J. (2001). ATM Phosphorylates Histone H2AX in Response to DNA Double-strand Breaks. J. Biol. Chem. *276*, 42462–42467.

Cabrini, G., Fabbri, E., Nigro, C.L., Dechecchi, M.C., and Gambari, R. (2015). Regulation of expression of O6-methylguanine-DNA methyltransferase and the treatment of glioblastoma (Review). Int. J. Oncol. *47*, 417–428.

Cahill, D.P., Levine, K.K., Betensky, R.A., Codd, P.J., Romany, C.A., Reavie, L.B., Batchelor, T.T., Futreal, P.A., Stratton, M.R., Curry, W.T., *et al*. (2007). Loss of the Mismatch Repair Protein MSH6 in Human Glioblastomas Is Associated with Tumor Progression during Temozolomide Treatment. Clin. Cancer Res. *13*, 2038–2045.

Candolfi, M., Curtin, J.F., Nichols, W.S., Muhammad, AKM.G., King, G.D., Pluhar, G.E., McNiel, E.A., Ohlfest, J.R., Freese, A.B., Moore, P.F., *et al*. (2007). Intracranial

glioblastoma models in preclinical neuro-oncology: neuropathological characterization and tumor progression. J. Neurooncol. *85*, 133–148.

Caporali, S., Falcinelli, S., Starace, G., Russo, M.T., Bonmassar, E., Jiricny, J., and D'Atri, S. (2004). DNA Damage Induced by Temozolomide Signals to both ATM and ATR: Role of the Mismatch Repair System. Mol. Pharmacol. *66*, 478–491.

Carlson, B.L., Grogan, P.T., Mladek, A.C., Schroeder, M.A., Kitange, G.J., Decker, P.A., Giannini, C., Wu, W., Ballman, K.A., James, C.D., *et al*. (2009). Radiosensitizing Effects of Temozolomide Observed in vivo only in a Subset of O6-Methylguanine-DNA Methyltransferase Methylated Glioblastoma Multiforme Xenografts. Int. J. Radiat. Oncol. *75*, 212–219.

Castedo, M., Perfettini, J.-L., Roumier, T., Andreau, K., Medema, R., and Kroemer, G. (2004). Cell death by mitotic catastrophe: a molecular definition. Oncogene *23*, 2825–2837.

Cekanova, M., and Rathore, K. (2014). Animal models and therapeutic molecular targets of cancer: utility and limitations. Drug Des. Devel. Ther. *8*, 1911–1922.

Chakravarti, A., Zhai, G., Suzuki, Y., Sarkesh, S., Black, P.M., Muzikansky, A., and Loeffler, J.S. (2004). The Prognostic Significance of Phosphatidylinositol 3-Kinase Pathway Activation in Human Gliomas. J. Clin. Oncol. *22*, 1926–1933.

Chakravarti, A., Erkkinen, M.G., Nestler, U., Stupp, R., Mehta, M., Aldape, K., Gilbert, M.R., Black, P.McL., and Loeffler, J.S. (2006). Temozolomide-Mediated Radiation Enhancement in Glioblastoma: A Report on Underlying Mechanisms. Clin. Cancer Res. *12*, 4738–4746.

Chakravarti, A., Wang, M., Robins, H.I., Lautenschlaeger, T., Curran, W.J., Brachman, D.G., Schultz, C.J., Choucair, A., Dolled-Filhart, M., Christiansen, J., *et al*. (2013). RTOG 0211: A Phase 1/2 Study of Radiation Therapy With Concurrent Gefitinib for Newly Diagnosed Glioblastoma Patients. Int. J. Radiat. Oncol. *85*, 1206–1211.

Chalmers, A.J., Ruff, E.M., Martindale, C., Lovegrove, N., and Short, S.C. (2009a). Cytotoxic Effects of Temozolomide and Radiation are Additive- and Schedule-Dependent. Int. J. Radiat. Oncol. *75*, 1511–1519.

Chang, K.-Y., Hsu, T.-I., Hsu, C.-C., Tsai, S.-Y., Liu, J.-J., Chou, S.-W., Liu, M.-S., Liou, J.-P., Ko, C.-Y., Chen, K.-Y., *et al*. (2017). Specificity protein 1-modulated superoxide dismutase 2 enhances temozolomide resistance in glioblastoma, which is independent of O6-methylguanine-DNA methyltransferase. Redox Biol. *13*, 655–664.

Chen, C.-H., Chang, Y.-J., Ku, M.S.B., Chung, K.-T., and Yang, J.-T. (2011). Enhancement of temozolomide-induced apoptosis by valproic acid in human glioma cell lines through redox regulation. J. Mol. Med. *89*, 303–315.

Chen, J., Yu, Y., Ji, T., Ma, R., Chen, M., Li, G., Li, F., Ding, Q., Kang, Q., Huang, D., *et al*. (2016). Clinical implication of Keap1 and phosphorylated Nrf2 expression in hepatocellular carcinoma. Cancer Med. *5*, 2678–2687.

Cheon, D.-J., and Orsulic, S. (2011). Mouse Models of Cancer. Annu. Rev. Pathol. Mech. Dis. *6*, 95–119.

Chia, A.J.L., Goldring, C.E., Kitteringham, N.R., Wong, S.Q., Morgan, P., and Park, B.K. (2010). Differential effect of covalent protein modification and glutathione depletion on the transcriptional response of Nrf2 and NF-κB. Biochem. Pharmacol. *80*, 410–421.

Chinot, O.L., Wick, W., Mason, W., Henriksson, R., Saran, F., Nishikawa, R., Carpentier, A.F., Hoang-Xuan, K., Kavan, P., Cernea, D., *et al*. (2014). Bevacizumab plus Radiotherapy–Temozolomide for Newly Diagnosed Glioblastoma. N. Engl. J. Med. *370*, 709–722.

Cho, S.-G., Lee, Y.H., Park, H.-S., Ryoo, K., Kang, K.W., Park, J., Eom, S.-J., Kim, M.J., Chang, T.-S., Choi, S.-Y., *et al*. (2001). Glutathione *S* -Transferase Mu Modulates the Stress-activated Signals by Suppressing Apoptosis Signal-regulating Kinase 1. J. Biol. Chem. *276*, 12749–12755.

Chou, T.-C. (2006). Theoretical Basis, Experimental Design, and Computerized Simulation of Synergism and Antagonism in Drug Combination Studies. Pharmacol. Rev. *58*, 621–681.

Chou, T.-C. (2010). Drug Combination Studies and Their Synergy Quantification Using the Chou-Talalay Method. Cancer Res. *70*, 440–446.

Chou, T.-C., and Talalay, P. (1984). Quantitative analysis of dose-effect relationships: the combined effects of multiple drugs or enzyme inhibitors. Adv. Enzyme Regul. *22*, 27–55.

Christensen, B., Smith, A., Zheng, S., Koestler, D., Houseman, E.A., Marsit, C.J., Wiemels, J.L., Nelson, H.H., Karagas, M.R., Wrensch, M.R., *et al*. (2010). Om-33. *idh* Mutation Defines Methylation Class And Survival In Human Glioma. Neuro-Oncol. *12*.

Christmann, M., Verbeek, B., Roos, W.P., and Kaina, B. (2011). O6-Methylguanine-DNA methyltransferase (MGMT) in normal tissues and tumors: Enzyme activity, promoter methylation and immunohistochemistry. Biochim. Biophys. Acta BBA - Rev. Cancer *1816*, 179–190.

Clarke, G., Johnston, S., Corrie, P., Kuhn, I., and Barclay, S. (2015). Withdrawal of anticancer therapy in advanced disease: a systematic literature review. BMC Cancer *15*, 892.

Cloughesy, T.F., Yoshimoto, K., Nghiemphu, P., Brown, K., Dang, J., Zhu, S., Hsueh, T., Chen, Y., Wang, W., Youngkin, D., *et al*. (2008). Antitumor Activity of Rapamycin in a Phase I Trial for Patients with Recurrent PTEN-Deficient Glioblastoma. PLOS Med. *5*, e8.

Cohen, M.H., Shen, Y.L., Keegan, P., and Pazdur, R. (2009). FDA Drug Approval Summary: Bevacizumab (Avastin®) as Treatment of Recurrent Glioblastoma Multiforme. The Oncologist *14*, 1131–1138.

Colditz, M.J., Leyen, K. van, and Jeffree, R.L. (2012). Aminolevulinic acid (ALA)–protoporphyrin IX fluorescence guided tumour resection. Part 2: Theoretical, biochemical and practical aspects. J. Clin. Neurosci. *19*, 1611–1616.

Collins, K., Jacks, T., and Pavletich, N.P. (1997). The cell cycle and cancer. Proc. Natl. Acad. Sci. *94*, 2776–2778.

Comerford, K.M., Wallace, T.J., Karhausen, J., Louis, N.A., Montalto, M.C., and Colgan, S.P. (2002). Hypoxia-inducible Factor-1-dependent Regulation of the Multidrug Resistance (MDR1) Gene. Cancer Res. *62*, 3387–3394.

Cong, Z.-X., wang, H.-D., Zhou, Y., Wang, J.-W., Pan, H., Zhang, D.-D., Zhang, L., and Zhu, L. (2014). Temozolomide and irradiation combined treatment-induced Nrf2 activation increases chemoradiation sensitivity in human glioblastoma cells. J. Neurooncol. *116*, 41–48.

Conklin, K.A. (2004). Chemotherapy-Associated Oxidative Stress: Impact on Chemotherapeutic Effectiveness. Integr. Cancer Ther. *3*, 294–300.

Cooke, J., and Losordo, D. (2002). Nitric Oxide and Angiogenesis. Circulation *105*, 2133–2135.

Cooke, M.S., Evans, M.D., Dizdaroglu, M., and Lunec, J. (2003). Oxidative DNA damage: mechanisms, mutation, and disease. FASEB J. *17*, 1195–1214.

Crellin, A. (2018). The Road Map for National Health Service Proton Beam Therapy. Clin. Oncol. *30*, 277–279.

Crespo, I., Vital, A.L., Nieto, A.B., Rebelo, O., Tão, H., Lopes, M.C., Oliveira, C.R., French, P.J., Orfao, A., and Tabernero, M.D. (2011). Detailed Characterization of Alterations of Chromosomes 7, 9, and 10 in Glioblastomas as Assessed by Single-Nucleotide Polymorphism Arrays. J. Mol. Diagn. JMD *13*, 634–647.

Croker, A.K., and Allan, A.L. (2012). Inhibition of aldehyde dehydrogenase (ALDH) activity reduces chemotherapy and radiation resistance of stem-like ALDHhiCD44^{+} human breast cancer cells. Breast Cancer Res. Treat. *133*, 75–87.

CRUK (2015). Brain, other CNS and intracranial tumours incidence statistics.

Cuadrado, A. (2015). Structural and functional characterization of Nrf2 degradation by glycogen synthase kinase 3/β-TrCP. Free Radic. Biol. Med. *88*, 147–157.

Cui, X., Hartanto, Y., and Zhang, H. (2017). Advances in multicellular spheroids formation. J. R. Soc. Interface *14*, 20160877.

Cunningham, D., Humblet, Y., Siena, S., Khayat, D., Bleiberg, H., Santoro, A., Bets, D., Mueser, M., Harstrick, A., Verslype, C., *et al*. (2004). Cetuximab Monotherapy and Cetuximab plus Irinotecan in Irinotecan-Refractory Metastatic Colorectal Cancer. N. Engl. J. Med. *351*, 337–345.

Dandy, W.E. (1928). REMOVAL OF RIGHT CEREBRAL HEMISPHERE FOR CERTAIN TUMORS WITH HEMIPLEGIA: PRELIMINARY REPORT. J. Am. Med. Assoc. *90*, 823–825.

Darzynkiewicz, Z., Huang, X., and Zhao, H. (2017). Analysis of Cellular DNA Content by Flow Cytometry. Curr. Protoc. Immunol. *119*, 5.7.1-5.7.20.

Däster, S., Amatruda, N., Calabrese, D., Ivanek, R., Turrini, E., Droeser, R.A., Zajac, P., Fimognari, C., Spagnoli, G.C., Iezzi, G., *et al*. (2016). Induction of hypoxia and necrosis

in multicellular tumor spheroids is associated with resistance to chemotherapy treatment. Oncotarget *8*, 1725–1736.

D'Atri, S., Tentori, L., Lacal, P.M., Graziani, G., Pagani, E., Benincasa, E., Zambruno, G., Bonmassar, E., and Jiricny, J. (1998). Involvement of the Mismatch Repair System in Temozolomide-Induced Apoptosis. Mol. Pharmacol. *54*, 334–341.

De Bonis, P., Anile, C., Pompucci, A., Fiorentino, A., Balducci, M., Chiesa, S., Lauriola, L., Maira, G., and Mangiola, A. (2013). The influence of surgery on recurrence pattern of glioblastoma. Clin. Neurol. Neurosurg. *115*, 37–43.

De Nicola, M., and Ghibelli, L. (2014). Glutathione depletion in survival and apoptotic pathways. Front. Pharmacol. *5*.

Deimling, A. von, Eibl, R.H., Ohgaki, H., Louis, D.N., Ammon, K. von, Petersen, I., Kleihues, P., Chung, R.Y., Wiestler, O.D., and Seizinger, B.R. (1992). p53 Mutations Are Associated with 17p Allelic Loss in Grade II and Grade III Astrocytoma. Cancer Res. *52*, 2987–2990.

Dell'Anno, A., Fabiano, M., Duineveld, G.C.A., Kok, A., and Danovaro, R. (1998). Nucleic Acid (DNA, RNA) Quantification and RNA/DNA Ratio Determination in Marine Sediments: Comparison of Spectrophotometric, Fluorometric, and HighPerformance Liquid Chromatography Methods and Estimation of Detrital DNA. Appl. Environ. Microbiol. *64*, 3238–3245.

Demuth, T., and Berens, M.E. (2004). Molecular mechanisms of glioma cell migration and invasion. J. Neurooncol. *70*, 217–228.

Denbigh, J.L., and Lockyer, N.P. (2015). ToF-SIMS as a tool for profiling lipids in cancer and other diseases. Mater. Sci. Technol. *31*, 137–147.

DeSantis, C.E., Lin, C.C., Mariotto, A.B., Siegel, R.L., Stein, K.D., Kramer, J.L., Alteri, R., Robbins, A.S., and Jemal, A. (2014). Cancer treatment and survivorship statistics, 2014. CA. Cancer J. Clin. *64*, 252–271.

Dikomey, E., Dahm-Daphi, J., Brammer, I., Martensen, R., and Kaina, B. (1998). Correlation between cellular radiosensitivity and non-repaired double-strand breaks studied in nine mammalian cell lines. Int. J. Radiat. Biol. *73*, 269–278.

Dolan, M.E., Mitchell, R.B., Mummert, C., Moschel, R.C., and Pegg, A.E. (1991). Effect of O6-benzylguanine analogues on sensitivity of human tumor cells to the cytotoxic effects of alkylating agents. Cancer Res. *51*, 3367–3372.

Dolcet, X., Llobet, D., Pallares, J., and Matias-Guiu, X. (2005). NF-kB in development and progression of human cancer. Virchows Arch. *446*, 475–482.

Dolecek, T.A., Propp, J.M., Stroup, N.E., and Kruchko, C. (2012). CBTRUS statistical report: primary brain and central nervous system tumors diagnosed in the United States in 2005-2009. Neuro-Oncol. *14 Suppl 5*, v1-49.

Don, A.S.A., and Zheng, X.F.S. (2011). Recent clinical trials of mTOR-targeted cancer therapies. Rev. Recent Clin. Trials *6*, 24–35.

Donato, V., Papaleo, A., Castrichino, A., Banelli, E., Giangaspero, F., Salvati, M., and Delfini, R. (2007). Prognostic Implication of Clinical and Pathologic Features in Patients with Glioblastoma Multiforme Treated with Concomitant Radiation plus Temozolomide. Tumori J. *93*, 248–256.

Doroshow, J.H., and Simon, R.M. (2017). On the Design of Combination Cancer Therapy. Cell *171*, 1476–1478.

Dorr, R.T., Liddil, J.D., and Soble, M.J. (1986). Cytotoxic effects of glutathione synthesis inhibition by L-buthionine-(SR)-sulfoximine on human and murine tumor cells. Invest. New Drugs *4*, 305–313.

Doucette, T., Rao, G., Rao, A., Shen, L., Aldape, K., Wei, J., Dziurzynski, K., Gilbert, M., and Heimberger, A.B. (2013). Immune Heterogeneity of Glioblastoma Subtypes: Extrapolation from the Cancer Genome Atlas. Cancer Immunol. Res. *1*, 112–122.

Dressler, E.V., Liu, M., Garcia, C.R., Dolecek, T.A., Pittman, T., Huang, B., and Villano, J.L. (2019). Patterns and disparities of care in glioblastoma. Neuro-Oncol. Pract. *6*, 37–46.

Dringen, R., Gutterer, J.M., and Hirrlinger, J. (2000). Glutathione metabolism in brain. Eur. J. Biochem. *267*, 4912–4916.

Dronkert, M.L.G., and Kanaar, R. (2001). Repair of DNA interstrand cross-links. Mutat. Res. Repair *486*, 217–247.

Dunn, J., Baborie, A., Alam, F., Joyce, K., Moxham, M., Sibson, R., Crooks, D., Husband, D., Shenoy, A., Brodbelt, A., *et al*. (2009). Extent of MGMT promoter methylation correlates with outcome in glioblastomas given temozolomide and radiotherapy. Br. J. Cancer *101*, 124–131.

Dunne-Daly, C.F. (1999). Principles of radiotherapy and radiobiology. Semin. Oncol. Nurs. *15*, 250–259.

Duronio, V. (2008). The life of a cell: apoptosis regulation by the PI3K/PKB pathway. Biochem. J. *415*, 333–344.

Eggler, A.L., Liu, G., Pezzuto, J.M., Breemen, R.B. van, and Mesecar, A.D. (2005). Modifying specific cysteines of the electrophile-sensing human Keap1 protein is insufficient to disrupt binding to the Nrf2 domain Neh2. Proc. Natl. Acad. Sci. *102*, 10070–10075.

Egorina, E.M., Sovershaev, M.A., and Østerud, B. (2006). In-Cell Western assay: a new approach to visualize tissue factor in human monocytes. J. Thromb. Haemost. *4*, 614–620.

Ekstrand, A.J., Sugawa, N., James, C.D., and Collins, V.P. (1992). Amplified and rearranged epidermal growth factor receptor genes in human glioblastomas reveal deletions of sequences encoding portions of the N- and/or C-terminal tails. Proc. Natl. Acad. Sci. U. S. A. *89*, 4309–4313.

Eljamel, S. (2015). 5-ALA Fluorescence Image Guided Resection of Glioblastoma Multiforme: A Meta-Analysis of the Literature. Int. J. Mol. Sci. *16*, 10443–10456.

Endersby, R., and Baker, S.J. (2008). PTEN signaling in brain: neuropathology and tumorigenesis. Oncogene *27*, 5416–5430.

Engelhard, H.H. (2000). The role of interstitial BCNU chemotherapy in the treatment of malignant glioma. Surg. Neurol. *53*, 458–464.

Eriksson, D., and Stigbrand, T. (2010). Radiation-induced cell death mechanisms. Tumor Biol. *31*, 363–372.

Eruslanov, E., and Kusmartsev, S. (2010). Identification of ROS using oxidized DCFDA and flow-cytometry. Methods Mol. Biol. Clifton NJ *594*, 57–72.

Esteller, M., Goodman, S.N., and Herman, J.G. (2000). Inactivation of the DNA-Repair Gene MGMT and the Clinical Response of Gliomas to Alkylating Agents. N. Engl. J. Med. 5.

Eyler, C.E., Wu, Q., Yan, K., MacSwords, J.M., Chandler-Militello, D., Misuraca, K.L., Lathia, J.D., Forrester, M.T., Lee, J., Stamler, J.S., *et al*. (2011). Glioma Stem Cell Proliferation and Tumor Growth Are Promoted by Nitric Oxide Synthase-2. Cell *146*, 53–66.

Fan, Q.-W., and Weiss, W.A. (2010). Targeting the RTK-PI3K-mTOR Axis in Malignant Glioma: Overcoming Resistance. In Phosphoinositide 3-Kinase in Health and Disease, C. Rommel, B. Vanhaesebroeck, and P.K. Vogt, eds. (Berlin, Heidelberg: Springer Berlin Heidelberg), pp. 279–296.

Fan, C.-H., Liu, W.-L., Cao, H., Wen, C., Chen, L., and Jiang, G. (2013). O 6 -methylguanine DNA methyltransferase as a promising target for the treatment of temozolomide-resistant gliomas. Cell Death Dis. *4*, e876–e876.

Felsberg, J., Thon, N., Eigenbrod, S., Hentschel, B., Sabel, M.C., Westphal, M., Schackert, G., Kreth, F.W., Pietsch, T., Löffler, M., *et al*. (2011). Promoter methylation and expression of MGMT and the DNA mismatch repair genes MLH1, MSH2, MSH6 and PMS2 in paired primary and recurrent glioblastomas. Int. J. Cancer *129*, 659–670.

Felsberg, J., Hentschel, B., Kaulich, K., Gramatzki, D., Zacher, A., Malzkorn, B., Kamp, M., Sabel, M., Simon, M., Westphal, M., *et al*. (2017). Epidermal Growth Factor Receptor Variant III (EGFRvIII) Positivity in EGFR-Amplified Glioblastomas: Prognostic Role and Comparison between Primary and Recurrent Tumors. Clin. Cancer Res. *23*, 6846–6855.

Fernandez-Medarde, A., and Santos, E. (2011). Ras in Cancer and Developmental Diseases. Genes Cancer *2*, 344–358.

Firat, E., Gaedicke, S., Tsurumi, C., Esser, N., Weyerbrock, A., and Niedermann, G. (2011). Delayed cell death associated with mitotic catastrophe in γ-irradiated stem-like glioma cells. Radiat. Oncol. *6*, 71.

Fogh, S.E., Andrews, D.W., Glass, J., Curran, W., Glass, C., Champ, C., Evans, J.J., Hyslop, T., Pequignot, E., Downes, B., *et al*. (2010). Hypofractionated Stereotactic Radiation Therapy: An Effective Therapy for Recurrent High-Grade Gliomas. J. Clin. Oncol. *28*, 3048–3053.

Foresti, R., Bains, S.K., Pitchumony, T.S., de Castro Brás, L.E., Drago, F., Dubois-Randé, J.-L., Bucolo, C., and Motterlini, R. (2013). Small molecule activators of the Nrf2-HO-1 antioxidant axis modulate heme metabolism and inflammation in BV2 microglia cells. Pharmacol. Res. *76*, 132–148.

Forman, H.J., Zhang, H., and Rinna, A. (2009). Glutathione: Overview of its protective roles, measurement, and biosynthesis. Mol. Aspects Med. *30*, 1–12.

Fragkos, M., Jurvansuu, J., and Beard, P. (2009). H2AX Is Required for Cell Cycle Arrest via the p53/p21 Pathway. Mol. Cell. Biol. *29*, 2828–2840.

Franke, T.F., Hornik, C.P., Segev, L., Shostak, G.A., and Sugimoto, C. (2003). PI3K/Akt and apoptosis: size matters. Oncogene *22*, 8983–8998.

Franken, N.A.P., Rodermond, H.M., Stap, J., Haveman, J., and van Bree, C. (2006). Clonogenic assay of cells in vitro. Nat. Protoc. *1*, 2315–2319.

Frezza, C., Tennant, D.A., and Gottlieb, E. (2010). IDH1 mutations in gliomas: when an enzyme loses its grip. Cancer Cell *17*, 7–9.

Friedman, H.S., McLendon, R.E., Kerby, T., Dugan, M., Bigner, S.H., Henry, A.J., Ashley, D.M., Krischer, J., Lovell, S., Rasheed, K., *et al*. (1998). DNA Mismatch Repair and 0 6 -Alkylguanine-DNA Alkyltransferase Analysis and Response to Temodal in Newly Diagnosed Malignant Glioma. 8.

Friedman, H.S., Kerby, T., and Calvert, H. Temozolomide and Treatment of Malignant Glioma. 13.

Fu, Y., Huang, R., Du, J., Yang, R., An, N., and Liang, A. (2010). Glioma-derived mutations in IDH: From mechanism to potential therapy. Biochem. Biophys. Res. Commun. *397*, 127–130.

Fujisawa, H., Reis, R.M., Nakamura, M., Colella, S., Yonekawa, Y., Kleihues, P., and Ohgaki, H. (2000). Loss of Heterozygosity on Chromosome 10 Is More Extensive in Primary (De Novo) Than in Secondary Glioblastomas. Lab. Invest. *80*, 65–72.

Fuller, C.D., Choi, M., Forthuber, B., Wang, S.J., Rajagiriyil, N., Salter, B.J., and Fuss, M. (2007). Standard fractionation intensity modulated radiation therapy (IMRT) of primary and recurrent glioblastoma multiforme. Radiat. Oncol. *2*, 26.

Fults, D., Brockmeyer, D., Tullous, M.W., Pedone, C.A., and Cawthon, R.M. (1992). p53 Mutation and Loss of Heterozygosity on Chromosomes 17 and 10 during Human Astrocytoma Progression. Cancer Res. *52*, 674–679.

Galateanu, B., Hudita, A., Negrei, C., Ion, R.-M., Costache, M., Stan, M., Nikitovic, D., Hayes, A.W., Spandidos, D.A., Tsatsakis, A.M., *et al*. (2016). Impact of multicellular tumor spheroids as an in vivo-like tumor model on anticancer drug response. Int. J. Oncol. *48*, 2295–2302.

Galloway, R.J. (2016). Combined chemo-radiotherapy utilising Olaparib and Mirin in combination with X-rays and targeted radionuclide therapy. Thesis PhD --University of Strathclyde.

Gariboldi, M.B., Ravizza, R., Petterino, C., Castagnaro, M., Finocchiaro, G., and Monti, E. (2003). Study of in vitro and in vivo effects of the piperidine nitroxide Tempol—a potential new therapeutic agent for gliomas. Eur. J. Cancer *39*, 829–837.

Garinis, G.A., Patrinos, G.P., Spanakis, N.E., and Menounos, P.G. (2002). DNA hypermethylation: when tumour suppressor genes go silent. Hum. Genet. *111*, 115–127.

Genderen, H. van, Kenis, H., Lux, P., Ungeth, L., Maassen, C., Deckers, N., Narula, J., Hofstra, L., and Reutelingsperger, C. (2006). In vitro measurement of cell death with the annexin A5 affinity assay. Nat. Protoc. *1*, 363–367.

Ghods, A., Glick, R., Braun, D., and Feinstein, D. (2013). Beneficial actions of the anti-inflammatory dimethyl fumarate in glioblastomas. Surg. Neurol. Int. *4*, 160.

Giese, A., Bjerkvig, R., Berens, M.E., and Westphal, M. (2003). Cost of Migration: Invasion of Malignant Gliomas and Implications for Treatment. J. Clin. Oncol. *21*, 1624–1636.

Gilbert, M.R., Dignam, J.J., Armstrong, T.S., Wefel, J.S., Blumenthal, D.T., Vogelbaum, M.A., Colman, H., Chakravarti, A., Pugh, S., Won, M., *et al*. (2014). A Randomized Trial of Bevacizumab for Newly Diagnosed Glioblastoma. N. Engl. J. Med. *370*, 699–708.

Ginestier, C., Hur, M.H., Charafe-Jauffret, E., Monville, F., Dutcher, J., Brown, M., Jacquemier, J., Viens, P., Kleer, C.G., Liu, S., *et al*. (2007). ALDH1 is a marker of normal and malignant human mammary stem cells and a predictor of poor clinical outcome. Cell Stem Cell *1*, 555–567.

Głębska, J., Skolimowski, J., Kudzin, Z., Gwoździński, K., Grzelak, A., and Bartosz, G. (2003). Pro-oxidative activity of nitroxides in their reactions with glutathione. Free Radic. Biol. Med. *35*, 310–316.

Goodenberger, M.L., and Jenkins, R.B. (2012). Genetics of adult glioma. Cancer Genet. *205*, 613–621.

Gray, G.K., McFarland, B.C., Nozell, S.E., and Benveniste, E.N. (2014). NF-κB and STAT3 in glioblastoma: therapeutic targets coming of age. Expert Rev. Neurother. *14*, 1293–1306.

Grossman, S.A., Ye, X., Piantadosi, S., Desideri, S., Nabors, L.B., Rosenfeld, M., Fisher, J., and for the NABTT CNS Consortium (2010). Survival of Patients with Newly Diagnosed Glioblastoma Treated with Radiation and Temozolomide in Research Studies in the United States. Clin. Cancer Res. *16*, 2443–2449.

Grossman, S.A., Ye, X., Lesser, G., Sloan, A., Carraway, H., Desideri, S., and Piantadosi, S. (2011). Immunosuppression in Patients with High-Grade Gliomas Treated with Radiation and Temozolomide. Clin. Cancer Res. *17*, 5473–5480.

Grun, B., Benjamin, E., Sinclair, J., Timms, J.F., Jacobs, I.J., Gayther, S.A., and Dafou, D. (2009). Three-dimensional in vitro cell biology models of ovarian and endometrial cancer. Cell Prolif. *42*, 219–228.

Günther, W., Pawlak, E., Damasceno, R., Arnold, H., and Terzis, A.J. (2003). Temozolomide induces apoptosis and senescence in glioma cells cultured as multicellular spheroids. Br. J. Cancer *88*, 463–469.

Halasi, M., Wang, M., Chavan, T.S., Gaponenko, V., Hay, N., and Gartel, A.L. (2013). ROS inhibitor *N* -acetyl-L-cysteine antagonizes the activity of proteasome inhibitors. Biochem. J. *454*, 201–208.

Hall, E.J. (2000). Radiobiology for the radiologist (Philadelphia: Lippincott Williams & Wilkins).

Hall, E.J., and Giaccia, A.J. (2012). Radiobiology for the radiologist (Philadelphia: Wolters Kluwer Health/Lippincott Williams & Wilkins).

Hammer, A., Waschbisch, A., Kuhbandner, K., Bayas, A., Lee, D.-H., Duscha, A., Haghikia, A., Gold, R., and Linker, R.A. (2018). The NRF2 pathway as potential biomarker for dimethyl fumarate treatment in multiple sclerosis. Ann. Clin. Transl. Neurol. *5*, 668–676.

Han, F., Hu, R., Yang, H., Liu, J., Sui, J., Xiang, X., Wang, F., Chu, L., and Song, S. (2016). PTEN gene mutations correlate to poor prognosis in glioma patients: a meta-analysis. OncoTargets Ther. *9*, 3485–3492.

Hanahan, D., and Weinberg, R.A. (2000). The Hallmarks of Cancer. Cell *100*, 57–70.

Hanahan, D., and Weinberg, R.A. (2011). Hallmarks of Cancer: The Next Generation. Cell *144*, 646–674.

Harrison, L.B. (2002). Impact of Tumor Hypoxia and Anemia on Radiation Therapy Outcomes. The Oncologist *7*, 492–508.

Hartmann, C., Hentschel, B., Wick, W., Capper, D., Felsberg, J., Simon, M., Westphal, M., Schackert, G., Meyermann, R., Pietsch, T., *et al*. (2010). Patients with IDH1 wild type anaplastic astrocytomas exhibit worse prognosis than IDH1-mutated glioblastomas, and IDH1 mutation status accounts for the unfavorable prognostic effect of higher age: implications for classification of gliomas. Acta Neuropathol. (Berl.) *120*, 707–718.

Harvey, C.J., Thimmulappa, R.K., Singh, A., Blake, D.J., Ling, G., Wakabayashi, N., Fujii, J., Myers, A., and Biswal, S. (2009). Nrf2-regulated glutathione recycling independent of biosynthesis is critical for cell survival during oxidative stress. Free Radic. Biol. Med. *46*, 443–453.

Hay, N., and Sonenberg, N. (2004). Upstream and downstream of mTOR. Genes Dev. *18*, 1926–1945.

Hayat, M.A. (2014). Tumors of the Central Nervous System, Volume 12 (Dordrecht: Springer Netherlands).

Hayes, J.D., and McMahon, M. (2009). NRF2 and KEAP1 mutations: permanent activation of an adaptive response in cancer. Trends Biochem. Sci. *34*, 176–188.

He, X., and Ma, Q. (2009). NRF2 Cysteine Residues Are Critical for Oxidant/Electrophile-Sensing, Kelch-Like ECH-Associated Protein-1-Dependent Ubiquitination-Proteasomal Degradation, and Transcription Activation. Mol. Pharmacol. *76*, 1265–1278.

He, J., Shan, Z., Li, L., Liu, F., Liu, Z., Song, M., and Zhu, H. (2011). Expression of glioma stem cell marker CD133 and O6-methylguanine-DNA methyltransferase is associated with resistance to radiotherapy in gliomas. Oncol. Rep. *26*, 1305–1313.

Heddleston, J.M., Li, Z., McLendon, R.E., Hjelmeland, A.B., and Rich, J.N. (2009). The hypoxic microenvironment maintains glioblastoma stem cells and promotes reprogramming towards a cancer stem cell phenotype. Cell Cycle *8*, 3274–3284.

Hegi, M.E., Diserens, A.-C., Godard, S., Dietrich, P.-Y., Regli, L., Ostermann, S., Otten, P., Van Melle, G., de Tribolet, N., and Stupp, R. (2004). Clinical Trial Substantiates the Predictive Value of ***O-6-Methylguanine-DNA Methyltransferase*** Promoter Methylation in Glioblastoma Patients Treated with Temozolomide. Clin. Cancer Res. *10*, 1871–1874.

Hegi, M.E., Diserens, A.-C., Gorlia, T., Hamou, M.-F., de Tribolet, N., Weller, M., Kros, J.M., Hainfellner, J.A., Mason, W., Mariani, L., *et al*. (2005). MGMT Gene Silencing and Benefit from Temozolomide in Glioblastoma. N. Engl. J. Med. *352*, 997–1003.

Heimberger, A.B., Hlatky, R., Suki, D., Yang, D., Weinberg, J., Gilbert, M., Sawaya, R., and Aldape, K. (2005). Prognostic Effect of Epidermal Growth Factor Receptor and EGFRvIII in Glioblastoma Multiforme Patients. Clin. Cancer Res. *11*, 1462–1466.

Held, K.D., and Hopcia, K.L. (1993). Role of protein thiols in intrinsic radiation protection of DNA and cells. Mutat. Res. Toxicol. *299*, 261–269.

Held, K.D., Epp, E.R., Clark, E.P., and Biaglow, J.E. (1988). Effect of Dimethyl Fumarate on the Radiation Sensitivity of Mammalian Cells in Vitro. Radiat. Res. *115*, 495–502.

Held, K.D., Epp, E.R., Awad, S., and Biaglow, J.E. (1991). Postirradiation Sensitization of Mammalian Cells by the Thiol-Depleting Agent Dimethyl Fumarate. Radiat. Res. *127*, 75–80.

Hensley, K., Mou, S., and Pye, Q.N. (2003). Nitrite Determination by Colorimetric and Fluorometric Griess Diazotization Assays. In Methods in Biological Oxidative Stress, K. Hensley, and R.A. Floyd, eds. (Totowa, NJ: Humana Press), pp. 185–193.

Hermanto, U., Frija, E.K., Lii, M.J., Chang, E.L., Mahajan, A., and Woo, S.Y. (2007). Intensity-modulated radiotherapy (IMRT) and conventional three-dimensional conformal radiotherapy for high-grade gliomas: does IMRT increase the integral dose to normal brain? Int. J. Radiat. Oncol. Biol. Phys. *67*, 1135–1144.

Hermisson, M., Klumpp, A., Wick, W., Wischhusen, J., Nagel, G., Roos, W., Kaina, B., and Weller, M. (2006). O6-methylguanine DNA methyltransferase and p53 status predict temozolomide sensitivity in human malignant glioma cells. J. Neurochem. *96*, 766–776.

Hirose, Y., Berger, M.S., and Pieper, R.O. (2001). p53 Effects Both the Duration of G2/M Arrest and the Fate of Temozolomide-treated Human Glioblastoma Cells. Cancer Res. *61*, 8.

Hirschhaeuser, F., Menne, H., Dittfeld, C., West, J., Mueller-Klieser, W., and Kunz-Schughart, L.A. (2010). Multicellular tumor spheroids: An underestimated tool is catching up again. J. Biotechnol. *148*, 3–15.

Hoffman, S., Propp, J.M., and McCarthy, B.J. (2006). Temporal trends in incidence of primary brain tumors in the United States, 1985–1999. Neuro-Oncol. *8*, 27–37.

Hong, X., Jiang, F., Kalkanis, S.N., Zhang, Z.G., Zhang, X.-P., deCarvalho, A.C., Katakowski, M., Bobbitt, K., Mikkelsen, T., and Chopp, M. (2006). SDF-1 and CXCR4 are up-regulated by VEGF and contribute to glioma cell invasion. Cancer Lett. *236*, 39–45.

van Horssen, J., Schreibelt, G., Bö, L., Montagne, L., Drukarch, B., van Muiswinkel, F.L., and de Vries, H.E. (2006). NAD(P)H:quinone oxidoreductase 1 expression in multiple sclerosis lesions. Free Radic. Biol. Med. *41*, 311–317.

Hothi, P., Martins, T.J., Chen, L., Deleyrolle, L., Yoon, J.-G., Reynolds, B., and Foltz, G. (2012). High-Throughput Chemical Screens Identify Disulfiram as an Inhibitor of Human Glioblastoma Stem Cells. Oncotarget *3*, 1124–1136.

Houillier, C., Wang, X., Kaloshi, G., Mokhtari, K., Guillevin, R., Laffaire, J., Paris, S., Boisselier, B., Idbaih, A., Laigle-Donadey, F., *et al*. (2010). IDH1 or IDH2 mutations predict longer survival and response to temozolomide in low-grade gliomas. Neurology *75*, 1560–1566.

Hu, X., Pandolfi, P.P., Li, Y., Koutcher, J.A., Rosenblum, M., and Holland, E.C. (2005). mTOR promotes survival and astrocytic characteristics induced by Pten/AKT signaling in glioblastoma. Neoplasia N. Y. N *7*, 356–368.

Huang, H.-C., Nguyen, T., and Pickett, C.B. (2002). Phosphorylation of Nrf2 at Ser-40 by Protein Kinase C Regulates Antioxidant Response Element-mediated Transcription. J. Biol. Chem. *277*, 42769–42774.

Huang, X.-J., Li, C.-T., Zhang, W.-P., Lu, Y.-B., Fang, S.-H., and Wei, E.-Q. (2008). Dihydroartemisinin Potentiates the Cytotoxic Effect of Temozolomide in Rat C6 Glioma Cells. Pharmacology *82*, 1–9.

Hung, K.S., Hong, C.Y., Lee, J., Lin, S.K., Huang, S.C., Wang, T.M., Tse, V., Sliverberg, G.D., Weng, S.C., and Hsiao, M. (2000). Expression of p16(INK4A) induces dominant suppression of glioblastoma growth in situ through necrosis and cell cycle arrest. Biochem. Biophys. Res. Commun. *269*, 718–725.

Hunter, C., Smith, R., Cahill, D.P., Stephens, P., Stevens, C., Teague, J., Greenman, C., Edkins, S., Bignell, G., Davies, H., *et al*. (2006). A Hypermutation Phenotype and Somatic MSH6 Mutations in Recurrent Human Malignant Gliomas after Alkylator Chemotherapy. Cancer Res. *66*, 3987–3991.

Ishizuka, M., Abe, F., Sano, Y., Takahashi, K., Inoue, K., Nakajima, M., Kohda, T., Komatsu, N., Ogura, S., and Tanaka, T. (2011). Novel development of 5-aminolevurinic acid (ALA) in cancer diagnoses and therapy. Int. Immunopharmacol. *11*, 358–365.

Ius, T., Isola, M., Budai, R., Pauletto, G., Tomasino, B., Fadiga, L., and Skrap, M. (2012). Low-grade glioma surgery in eloquent areas: volumetric analysis of extent of resection

and its impact on overall survival. A single-institution experience in 190 patients. J. Neurosurg. 1039–1052.

Iwamoto, F.M., Abrey, L.E., Beal, K., Gutin, P.H., Rosenblum, M.K., Reuter, V.E., DeAngelis, L.M., and Lassman, A.B. (2009). Patterns of relapse and prognosis after bevacizumab failure in recurrent glioblastoma. Neurology *73*, 1200–1206.

Jackson, S.P., and Bartek, J. (2009). The DNA-damage response in human biology and disease. Nature *461*, 1071–1078.

Jaiswal, A.K. (2004). Nrf2 signaling in coordinated activation of antioxidant gene expression. Free Radic. Biol. Med. *36*, 1199–1207.

Jamieson, E.L., Harrison, J.D., and Campbell, J.C. (2015). Chemical analysis of multicellular tumour spheroids. Analyst *140*, 3910–3920.

Jensen, M.M., Jørgensen, J.T., Binderup, T., and Kjær, A. (2008). Tumor volume in subcutaneous mouse xenografts measured by microCT is more accurate and reproducible than determined by 18F-FDG-microPET or external caliper. BMC Med. Imaging *8*, 16.

Jensen, R.L., Ragel, B.T., Whang, K., and Gillespie, D. (2006). Inhibition of hypoxia inducible factor-1α (HIF-1α) decreases vascular endothelial growth factor (VEGF) secretion and tumor growth in malignant gliomas. J. Neurooncol. *78*, 233–247.

Jing, X., Shi, H., Zhang, C., Ren, M., Han, M., Wei, X., Zhang, X., and Lou, H. (2015). Dimethyl fumarate attenuates 6-OHDA-induced neurotoxicity in SH-SY5Y cells and in animal model of Parkinson's disease by enhancing Nrf2 activity. Neuroscience *286*, 131–140.

Johannessen, T.-C.A., and Bjerkvig, R. (2012). Molecular mechanisms of temozolomide resistance in glioblastoma multiforme. Expert Rev. Anticancer Ther. *12*, 635–642.

Joo, M.S., Kim, W.D., Lee, K.Y., Kim, J.H., Koo, J.H., and Kim, S.G. (2016). AMPK Facilitates Nuclear Accumulation of Nrf2 by Phosphorylating at Serine 550. Mol. Cell. Biol. *36*, 1931–1942.

Jordan, C.T., Guzman, M.L., and Noble, M. (2006). Cancer stem cells. N. Engl. J. Med. *355*, 1253–1261.

Kaina, B. (2003). DNA damage-triggered apoptosis: critical role of DNA repair, double-strand breaks, cell proliferation and signaling. Biochem. Pharmacol. *66*, 1547–1554.

Kaina, B., Christmann, M., Naumann, S., and Roos, W.P. (2007). MGMT: Key node in the battle against genotoxicity, carcinogenicity and apoptosis induced by alkylating agents. DNA Repair *6*, 1079–1099.

Kansanen, E., Kuosmanen, S.M., Leinonen, H., and Levonen, A.-L. (2013). The Keap1-Nrf2 pathway: Mechanisms of activation and dysregulation in cancer. Redox Biol. *1*, 45–49.

Kanzawa, T., Germano, I.M., Komata, T., Ito, H., Kondo, Y., and Kondo, S. (2004). Role of autophagy in temozolomide-induced cytotoxicity for malignant glioma cells. Cell Death Differ. *11*, 448–457.

Kappelle, A.C., Postma, T.J., Taphoorn, M.J.B., Groeneveld, G.J., Bent, M.J. van den, Groeningen, C.J. van, Zonnenberg, B.A., Sneeuw, K.C.A., and Heimans, J.J. (2001). PCV chemotherapy for recurrent glioblastoma multiforme. Neurology *56*, 118–120.

Karimian, A., Ahmadi, Y., and Yousefi, B. (2016). Multiple functions of p21 in cell cycle, apoptosis and transcriptional regulation after DNA damage. DNA Repair *42*, 63–71.

Kastan, M.B., and Bartek, J. (2004). Cell-cycle checkpoints and cancer. Nature *432*, 316–323.

Kastrati, I., Siklos, M.I., Calderon-Gierszal, E.L., El-Shennawy, L., Georgieva, G., Thayer, E.N., Thatcher, G.R., and Frasor, J. (2016). Dimethyl fumarate inhibits the nuclear factor κB pathway in breast cancer cells by covalent modification of p65 protein. J. Biol. Chem. *291*, 3639–3647.

Kaur, B., Khwaja, F.W., Severson, E.A., Matheny, S.L., Brat, D.J., and Van Meir, E.G. (2005). Hypoxia and the hypoxia-inducible-factor pathway in glioma growth and angiogenesis. Neuro-Oncol. *7*, 134–153.

Keles, G.E., Chang, E.F., Lamborn, K.R., Tihan, T., Chang, C.-J., Chang, S.M., and Berger, M.S. (2006). Volumetric extent of resection and residual contrast enhancement on initial surgery as predictors of outcome in adult patients with hemispheric anaplastic astrocytoma. J. Neurosurg. 34–40.

Kelley, K., Knisely, J., Symons, M., and Ruggieri, R. (2016). Radioresistance of Brain Tumors. Cancers *8*, 42.

Kensler, T.W., Wakabayashi, N., and Biswal, S. (2007). Cell Survival Responses to Environmental Stresses Via the Keap1-Nrf2-ARE Pathway. Annu. Rev. Pharmacol. Toxicol. *47*, 89–116.

Kerr, D.J., Wheldon, T.E., Hydns, S., and Kaye, S.B. (1988). Cytotoxic drug penetration studies in multicellular tumour spheroids. Xenobiotica *18*, 641–648.

Keunen, O., Johansson, M., Oudin, A., Sanzey, M., Rahim, S.A.A., Fack, F., Thorsen, F., Taxt, T., Bartos, M., Jirik, R., *et al*. (2011). Anti-VEGF treatment reduces blood supply and increases tumor cell invasion in glioblastoma. Proc. Natl. Acad. Sci. *108*, 3749–3754.

Khani, P., Nasri, F., Chamani, F.K., Saeidi, F., Nahand, J.S., Tabibkhooei, A., and Mirzaei, H. (2019). Genetic and epigenetic contribution to astrocytic gliomas pathogenesis. J. Neurochem. *148*, 188–203.

Kil, W.J., Cerna, D., Burgan, W.E., Beam, K., Carter, D., Steeg, P.S., Tofilon, P.J., and Camphausen, K. (2008). In vitro and In vivo Radiosensitization Induced by the DNA Methylating Agent Temozolomide. Clin. Cancer Res. *14*, 931–938.

Kim, J., Lee, I.-H., Cho, H.J., Park, C.-K., Jung, Y.-S., Kim, Y., Nam, S.H., Kim, B.S., Johnson, M.D., Kong, D.-S., *et al*. (2015). Spatiotemporal Evolution of the Primary Glioblastoma Genome. Cancer Cell *28*, 318–328.

Kim, T.-H., Hur, E. -g., Kang, S.-J., Kim, J.-A., Thapa, D., Lee, Y.M., Ku, S.K., Jung, Y., and Kwak, M.-K. (2011). NRF2 Blockade Suppresses Colon Tumor Angiogenesis by Inhibiting Hypoxia-Induced Activation of HIF-1. Cancer Res. *71*, 2260–2275.

Kislin, K.L., McDonough, W.S., Eschbacher, J.M., Armstrong, B.A., and Berens, M.E. (2009). NHERF-1: Modulator of Glioblastoma Cell Migration and Invasion. Neoplasia *11*, 377-IN7.

Kobayashi, A., Kang, M.-I., Watai, Y., Tong, K.I., Shibata, T., Uchida, K., and Yamamoto, M. (2006). Oxidative and electrophilic stresses activate Nrf2 through inhibition of ubiquitination activity of Keap1. Mol. Cell. Biol. *26*, 221–229.

Koch, D., Hundsberger, T., Boor, S., and Kaina, B. (2007). Local intracerebral administration of O6-benzylguanine combined with systemic chemotherapy with temozolomide of a patient suffering from a recurrent glioblastoma. J. Neurooncol. *82*, 85–89.

Kogias, E., Osterberg, N., Baumer, B., Psarras, N., Koentges, C., Papazoglou, A., Saavedra, J.E., Keefer, L.K., and Weyerbrock, A. (2012). Growth-inhibitory and chemosensitizing effects of the glutathione-S-transferase-π-activated nitric oxide donor PABA/NO in malignant gliomas. Int. J. Cancer *130*, 1184–1194.

Koivunen, P., Hirsilä, M., Remes, A.M., Hassinen, I.E., Kivirikko, K.I., and Myllyharju, J. (2007). Inhibition of Hypoxia-inducible Factor (HIF) Hydroxylases by Citric Acid Cycle Intermediates: POSSIBLE LINKS BETWEEN CELL METABOLISM AND STABILIZATION OF HIF. J. Biol. Chem. *282*, 4524–4532.

Kostourou, V., Cartwright, J.E., Johnstone, A.P., Boult, J.K.R., Cullis, E.R., Whitley, Gs., and Robinson, S.P. (2011). The role of tumour-derived iNOS in tumour progression and angiogenesis. Br. J. Cancer *104*, 83–90.

Kotze, H.L. (2012). Systems biology of chemotherapy in hypoxia environements. University of Manchester.

Kotze, H.L., Armitage, E.G., Fletcher, J.S., Henderson, A., Williams, K.J., Lockyer, N.P., and Vickerman, J.C. (2013). ToF-SIMS as a tool for metabolic profiling small biomolecules in cancer systems. Surf. Interface Anal. *45*, 277–281.

Krueger, D.A., Care, M.M., Holland, K., Agricola, K., Tudor, C., Mangeshkar, P., Wilson, K.A., Byars, A., Sahmoud, T., and Franz, D.N. (2010). Everolimus for Subependymal Giant-Cell Astrocytomas in Tuberous Sclerosis. N. Engl. J. Med. *363*, 1801–1811.

Kumari, N., Dwarakanath, B.S., Das, A., and Bhatt, A.N. (2016). Role of interleukin-6 in cancer progression and therapeutic resistance. Tumour Biol. J. Int. Soc. Oncodevelopmental Biol. Med. *37*, 11553–11572.

Kunz-Schughart, L.A. (1999). Multicellular tumor spheroids: intermediates between monolayer culture and in vivo tumor. Cell Biol. Int. *23*, 157–161.

Labussière, M., Rahimian, A., Giry, M., Boisselier, B., Schmitt, Y., Polivka, M., Mokhtari, K., Delattre, J.-Y., Idbaih, A., Labreche, K., *et al*. (2016). Chromosome 17p Homodisomy Is Associated With Better Outcome in 1p19q Non-Codeleted and IDH-Mutated Gliomas. The Oncologist *21*, 1131–1135.

Lai, D., Visser-Grieve, S., and Yang, X. (2012). Tumour suppressor genes in chemotherapeutic drug response. Biosci. Rep. *32*, 361–374.

Lambert, S., and Lopez, B.S. (2000). Characterization of mammalian RAD51 double strand break repair using non-lethal dominant-negative forms. EMBO J. *19*, 3090–3099.

Lampreht Tratar, U., Horvat, S., and Cemazar, M. (2018). Transgenic Mouse Models in Cancer Research. Front. Oncol. *8*.

Lan, F., Lan, F., Yang, Y., Yang, Y., Han, J., Han, J., Wu, Q., Wu, Q., Yu, H., Yu, H., *et al*. (2016). Sulforaphane reverses chemo-resistance to temozolomide in glioblastoma cells by NF-κB-dependent pathway downregulating MGMT expression. Int. J. Oncol. *48*, 559–568.

Larjavaara, S., Mäntylä, R., Salminen, T., Haapasalo, H., Raitanen, J., Jääskeläinen, J., and Auvinen, A. (2007). Incidence of gliomas by anatomic location. Neuro-Oncol. *9*, 319–325.

Lathia, J.D., Mack, S.C., Mulkearns-Hubert, E.E., Valentim, C.L.L., and Rich, J.N. (2015). Cancer stem cells in glioblastoma. Genes Dev. *29*, 1203–1217.

Lee, S.Y. (2016). Temozolomide resistance in glioblastoma multiforme. Genes Dis. *3*, 198–210.

Lee, E.Y.H.P., and Muller, W.J. (2010). Oncogenes and Tumor Suppressor Genes. Cold Spring Harb. Perspect. Biol. *2*, a003236–a003236.

Lee, J.H., Lee, J.E., Kahng, J.Y., Kim, S.H., Park, J.S., Yoon, S.J., Um, J.-Y., Kim, W.K., Lee, J.-K., Park, J., *et al*. (2018). Human glioblastoma arises from subventricular zone cells with low-level driver mutations. Nature *560*, 243.

Legler, J.M., Ries, L.A.G., Smith, M.A., Warren, J.L., Heineman, E.F., Kaplan, R.S., and Linet, M.S. (1999). Brain and Other Central Nervous System Cancers: Recent Trends in Incidence and Mortality. JNCI J. Natl. Cancer Inst. *91*, 1382–1390.

Li, G.-M. (2008). Mechanisms and functions of DNA mismatch repair. Cell Res. *18*, 85–98.

Li, M., Xiao, A., Floyd, D., Olmez, I., Lee, J., Godlewski, J., Bronisz, A., Bhat, K.P.L., Sulman, E.P., Nakano, I., *et al*. (2017). CDK4/6 inhibition is more active against the glioblastoma proneural subtype. Oncotarget *8*, 55319–55331.

Li, W., Yu, S.-W., and Kong, A.-N.T. (2006). Nrf2 Possesses a Redox-sensitive Nuclear Exporting Signal in the Neh5 Transactivation Domain. J. Biol. Chem. *281*, 27251–27263.

Li, X., Wu, C., Chen, N., Gu, H., Yen, A., Cao, L., Wang, E., and Wang, L. (2016). PI3K/Akt/mTOR signaling pathway and targeted therapy for glioblastoma. Oncotarget *7*, 33440–33450.

Li, Y., Paonessa, J.D., and Zhang, Y. (2012a). Mechanism of Chemical Activation of Nrf2. PLOS ONE *7*, e35122.

Li, Y., Wang, L., Pappan, L., Galliher-Beckley, A., and Shi, J. (2012b). IL-1β promotes stemness and invasiveness of colon cancer cells through Zeb1 activation. Mol. Cancer *11*, 87.

Li, Z., Bao, S., Wu, Q., Wang, H., Eyler, C., Sathornsumetee, S., Shi, Q., Cao, Y., Lathia, J., McLendon, R.E., *et al*. (2009). Hypoxia-Inducible Factors Regulate Tumorigenic Capacity of Glioma Stem Cells. Cancer Cell *15*, 501–513.

Limón-Pacheco, J.H., Hernández, N.A., Fanjul-Moles, M.L., and Gonsebatt, M.E. (2007). Glutathione depletion activates mitogen-activated protein kinase (MAPK) pathways that display organ-specific responses and brain protection in mice. Free Radic. Biol. Med. *43*, 1335–1347.

Lin, S.X., Lisi, L., Russo, C.D., Polak, P.E., Sharp, A., Weinberg, G., Kalinin, S., and Feinstein, D.L. (2011). The Anti-Inflammatory Effects of Dimethyl Fumarate in Astrocytes Involve Glutathione and Haem Oxygenase-1. ASN Neuro *3*, AN20100033.

Liotta, L.A., and Kohn, E.C. (2001). The microenvironment of the tumour–host interface. Nature *411*, 375.

Liu, L. (2006). Targeted Modulation of MGMT: Clinical Implications. Clin. Cancer Res. *12*, 328–331.

Liu, C., Sage, J.C., Miller, M.R., Verhaak, R.G.W., Hippenmeyer, S., Vogel, H., Foreman, O., Bronson, R.T., Nishiyama, A., Luo, L., *et al*. (2011). Mosaic Analysis with Double Markers Reveals Tumor Cell of Origin in Glioma. Cell *146*, 209–221.

Liu, X., Han, E.K., Anderson, M., Shi, Y., Semizarov, D., Wang, G., McGonigal, T., Roberts, L., Lasko, L., Palma, J., *et al*. (2009). Acquired Resistance to Combination Treatment with Temozolomide and ABT-888 Is Mediated by Both Base Excision Repair and Homologous Recombination DNA Repair Pathways. Mol. Cancer Res. *7*, 1686–1692.

Liu, X., Ide, J.L., Norton, I., Marchionni, M.A., Ebling, M.C., Wang, L.Y., Davis, E., Sauvageot, C.M., Kesari, S., Kellersberger, K.A., *et al*. (2013). Molecular imaging of drug transit through the blood-brain barrier with MALDI mass spectrometry imaging. Sci. Rep. *3*, 2859.

Livak, K.J., and Schmittgen, T.D. (2001). Analysis of relative gene expression data using real-time quantitative PCR and the 2(-Delta Delta C(T)) Method. Methods San Diego Calif *25*, 402–408.

Loboda, A., Damulewicz, M., Pyza, E., Jozkowicz, A., and Dulak, J. (2016). Role of Nrf2/HO-1 system in development, oxidative stress response and diseases: an evolutionarily conserved mechanism. Cell. Mol. Life Sci. *73*, 3221–3247.

Loeffler, J.S., and Durante, M. (2013). Charged particle therapy—optimization, challenges and future directions. Nat. Rev. Clin. Oncol. *10*, 411–424.

Longbrake, E.E., Cantoni, C., Chahin, S., Cignarella, F., Cross, A.H., and Piccio, L. (2018). Dimethyl fumarate induces changes in B- and T-lymphocyte function independent of the effects on absolute lymphocyte count. Mult. Scler. J. *24*, 728–738.

Lopez-Gines, C., Cerda-Nicolas, M., Gil-Benso, R., Pellin, A., Lopez-Guerrero, J.A., Callaghan, R., Benito, R., Roldan, P., Piquer, J., Llacer, J., *et al*. (2005). Association of chromosome 7, chromosome 10 and EGFR gene amplification in glioblastoma multiforme. Clin. Neuropathol. *24*, 209–218.

Lottaz, C., Beier, D., Meyer, K., Kumar, P., Hermann, A., Schwarz, J., Junker, M., Oefner, P.J., Bogdahn, U., Wischhusen, J., *et al*. (2010). Transcriptional Profiles of CD133+ and CD133− Glioblastoma-Derived Cancer Stem Cell Lines Suggest Different Cells of Origin. Cancer Res. *70*, 2030–2040.

Louis, D.N., Perry, A., Reifenberger, G., von Deimling, A., Figarella-Branger, D., Cavenee, W.K., Ohgaki, H., Wiestler, O.D., Kleihues, P., and Ellison, D.W. (2016a). The 2016 World Health Organization Classification of Tumors of the Central Nervous System: a summary. Acta Neuropathol. (Berl.) *131*, 803–820.

Lowenstein, C.J., and Padalko, E. (2004). iNOS (NOS2) at a glance. J. Cell Sci. *117*, 2865–2867.

Lu, S.C. (2013). GLUTATHIONE SYNTHESIS. Biochim. Biophys. Acta *1830*, 3143–3153.

Luchman, H.A., Stechishin, O.D.M., Nguyen, S.A., Lun, X.Q., Cairncross, J.G., and Weiss, S. (2014). Dual mTORC1/2 Blockade Inhibits Glioblastoma Brain Tumor Initiating Cells In Vitro and In Vivo and Synergizes with Temozolomide to Increase Orthotopic Xenograft Survival. Clin. Cancer Res. *20*, 5756–5767.

Ludwig, K., and Kornblum, H.I. (2017). Molecular markers in glioma. J. Neurooncol. *134*, 505–512.

Ma, D.J., Galanis, E., Anderson, S.K., Schiff, D., Kaufmann, T.J., Peller, P.J., Giannini, C., Brown, P.D., Uhm, J.H., McGraw, S., *et al*. (2015a). A phase II trial of everolimus, temozolomide, and radiotherapy in patients with newly diagnosed glioblastoma: NCCTG N057K. Neuro-Oncol. *17*, 1261–1269.

Ma, L., Liu, J., Zhang, X., Qi, J., Yu, W., and Gu, Y. (2015b). p38 MAPK-dependent Nrf2 induction enhances the resistance of glioma cells against TMZ. Med. Oncol. *32*, 69.

Macphail, S.E., Gibney, C.A., Brooks, B.M., Booth, C.G., Flanagan, B.F., and Coleman, J.W. (2003). Nitric oxide regulation of human peripheral blood mononuclear cells: critical time dependence and selectivity for cytokine versus chemokine expression. J. Immunol. Baltim. Md 1950 *171*, 4809–4815.

Maemondo, M., Inoue, A., Kobayashi, K., Sugawara, S., Oizumi, S., Isobe, H., Gemma, A., Harada, M., Yoshizawa, H., Kinoshita, I., *et al*. (2010). Gefitinib or Chemotherapy for Non–Small-Cell Lung Cancer with Mutated EGFR. N. Engl. J. Med. *362*, 2380–2388.

Mairs, R.J., Hughes, K., Fitzsimmons, S., Prise, K.M., Livingstone, A., Wilson, L., Baig, N., Clark, A.M., Timpson, A., Patel, G., *et al*. (2007). Microsatellite analysis for

determination of the mutagenicity of extremely low-frequency electromagnetic fields and ionising radiation in vitro. Mutat. Res. Toxicol. Environ. Mutagen. *626*, 34–41.

Mak, I.W., Evaniew, N., and Ghert, M. (2014). Lost in translation: animal models and clinical trials in cancer treatment. Am. J. Transl. Res. *6*, 114–118.

Makin, G. (2018). Principles of chemotherapy. Paediatr. Child Health *28*, 183–188.

Malla, R., Gopinath, S., Alapati, K., Gondi, C.S., Gujrati, M., Dinh, D.H., Mohanam, S., and Rao, J.S. (2010). Downregulation of uPAR and Cathepsin B Induces Apoptosis via Regulation of Bcl-2 and Bax and Inhibition of the PI3K/Akt Pathway in Gliomas. PLOS ONE *5*, e13731.

Mansilla, S., Priebe, W., and Portugal, J. (2006). Mitotic Catastrophe Results in Cell Death by Caspase-Dependent and Caspase-Independent Mechanisms. Cell Cycle *5*, 53–60.

Marcotte, D., Zeng, W., Hus, J.-C., McKenzie, A., Hession, C., Jin, P., Bergeron, C., Lugovskoy, A., Enyedy, I., Cuervo, H., *et al*. (2013). Small molecules inhibit the interaction of Nrf2 and the Keap1 Kelch domain through a non-covalent mechanism. Bioorg. Med. Chem. *21*, 4011–4019.

Matheson, C.J., Backos, D.S., and Reigan, P. (2016). Targeting WEE1 Kinase in Cancer. Trends Pharmacol. Sci. *37*, 872–881.

McDonald, J.T., Kim, K., Norris, A.J., Vlashi, E., Phillips, T.M., Lagadec, C., Donna, L.D., Ratikan, J., Szelag, H., Hlatky, L., *et al*. (2010). Ionizing Radiation Activates the Nrf2 Antioxidant Response. Cancer Res. *70*, 8886–8895.

McGinely, N.L. (2015). Solid and hollow gold nanoparticles as radiosensitisers in combination with x-ray radiation and targeted radiopharmaceuticals (Thesis PhD -- University of Strathclyde).

McGirt, M.J., and Brem, H. (2010). Carmustine Wafers (Gliadel) Plus Concomitant Temozolomide Therapy After Resection of Malignant Astrocytoma: Growing Evidence for Safety and Efficacy. Ann. Surg. Oncol. *17*, 1729–1731.

McKinney, P.A. (2004). Brain tumours: incidence, survival, and aetiology. J. Neurol. Neurosurg. Psychiatry *75*, ii12–ii17.

McKnight, J.A. (2003). Principles of chemotherapy. Clin. Tech. Small Anim. Pract. *18*, 67–72.

McMahon, M., Thomas, N., Itoh, K., Yamamoto, M., and Hayes, J.D. (2004). Redox-regulated turnover of Nrf2 is determined by at least two separate protein domains, the redox-sensitive Neh2 degron and the redox-insensitive Neh6 degron. J. Biol. Chem. *279*, 31556–31567.

McMillan, T.J., Tobi, S., Mateos, S., and Lemon, C. (2001). The use of DNA double-strand break quantification in radiotherapy. Int. J. Radiat. Oncol. *49*, 373–377.

Meissner, M., Valesky, E.M., Kippenberger, S., and Kaufmann, R. (2012). Dimethyl fumarate - only an anti-psoriatic medication? JDDG J. Dtsch. Dermatol. Ges. *10*, 793–801.

Mikuni, N., and Miyamoto, S. (2010). Surgical Treatment for Glioma: Extent of Resection Applying Functional Neurosurgery. Neurol. Med. Chir. (Tokyo) *50*, 720–726.

Mimura, J., Kosaka, K., Maruyama, A., Satoh, T., Harada, N., Yoshida, H., Satoh, K., Yamamoto, M., and Itoh, K. (2011). Nrf2 regulates NGF mRNA induction by carnosic acid in T98G glioblastoma cells and normal human astrocytes. J. Biochem. (Tokyo) *150*, 209–217.

Mitchell, P., Ellison, D.W., and Mendelow, A.D. (2005). Surgery for malignant gliomas: mechanistic reasoning and slippery statistics. Lancet Neurol. *4*, 413–422.

Mizumoto, M., Yamamoto, T., Takano, S., Ishikawa, E., Matsumura, A., Ishikawa, H., Okumura, T., Sakurai, H., Miyatake, S.-I., and Tsuboi, K. (2015). Long-term survival after treatment of glioblastoma multiforme with hyperfractionated concomitant boost proton beam therapy. Pract. Radiat. Oncol. *5*, e9–e16.

Mohyeldin, A., Garzón-Muvdi, T., and Quiñones-Hinojosa, A. (2010). Oxygen in stem cell biology: a critical component of the stem cell niche. Cell Stem Cell *7*, 150–161.

Mok, T.S., Wu, Y.-L., Thongprasert, S., Yang, C.-H., Chu, D.-T., Saijo, N., Sunpaweravong, P., Han, B., Margono, B., Ichinose, Y., *et al*. (2009). Gefitinib or Carboplatin–Paclitaxel in Pulmonary Adenocarcinoma. N. Engl. J. Med. *361*, 947–957.

Molenaar, R.J., Verbaan, D., Lamba, S., Zanon, C., Jeuken, J.W.M., Boots-Sprenger, S.H.E., Wesseling, P., Hulsebos, T.J.M., Troost, D., van Tilborg, A.A., *et al*. (2014). The combination of IDH1 mutations and MGMT methylation status predicts survival in glioblastoma better than either IDH1 or MGMT alone. Neuro-Oncol. *16*, 1263–1273.

Momota, H., Ichimiya, S., Kondo, N., Kikuchi, T., Torigoe, T., Yamaki, T., Houkin, K., and Sato, N. (2003). Histone H2AX sensitizes glioma cells to genotoxic stimuli by recruiting DNA double-strand break repair proteins. Int. J. Oncol. *23*, 311–315.

Montaldi, A.P., and Sakamoto-Hojo, E.T. (2013). Methoxyamine sensitizes the resistant glioblastoma T98G cell line to the alkylating agent temozolomide. Clin. Exp. Med. *13*, 279–288.

Montano, N., Cenci, T., Martini, M., D'Alessandris, Q.G., Pelacchi, F., Ricci-Vitiani, L., Maira, G., De Maria, R., Larocca, L.M., and Pallini, R. (2011). Expression of EGFRvIII in Glioblastoma: Prognostic Significance Revisited. Neoplasia N. Y. N *13*, 1113–1121.

Morbidelli, L., Donnini, S., and Ziche, M. (2003). Role of nitric oxide in the modulation of angiogenesis. Curr. Pharm. Des. *9*, 521–530.

Morbidelli, L., Donnini, S., and Ziche, M. (2004). Role of nitric oxide in tumor angiogenesis. Cancer Treat. Res. *117*, 155–167.

Moreno, L., and Pearson, A.D. (2013). How can attrition rates be reduced in cancer drug discovery? Expert Opin. Drug Discov. *8*, 363–368.

Murad, H., Alghamian, Y., Aljapawe, A., and Madania, A. (2018). Effects of ionizing radiation on the viability and proliferative behavior of the human glioblastoma T98G cell line. BMC Res. Notes *11*, 330.

Mytilineou, C., Kramer, B.C., and Yabut, J.A. (2002). Glutathione depletion and oxidative stress. Parkinsonism Relat. Disord. *8*, 385–387.

Nakamura, M., Watanabe, T., Yonekawa, Y., Kleihues, P., and Ohgaki, H. (2001). Promoter methylation of the DNA repair gene MGMT in astrocytomas is frequently associated with G:C → A:T mutations of the TP53 tumor suppressor gene. Carcinogenesis *22*, 1715–1719.

Nan, Y., Guo, L., Song, Y., Wang, L., Yu, K., Huang, Q., and Zhong, Y. (2017). Combinatorial therapy with adenoviral-mediated PTEN and a PI3K inhibitor suppresses malignant glioma cell growth in vitro and in vivo by regulating the PI3K/AKT signaling pathway. J. Cancer Res. Clin. Oncol. *143*, 1477–1487.

Nath, S., and Devi, G.R. (2016). Three-dimensional culture systems in cancer research: Focus on tumor spheroid model. Pharmacol. Ther. *163*, 94–108.

Neidle, S. (2011). Cancer Drug Design and Discovery (Elsevier).

Nelson, W.G., and Kastan, M.B. (1994). DNA strand breaks: the DNA template alterations that trigger p53-dependent DNA damage response pathways. Mol. Cell. Biol. *14*, 1815–1823.

Newlands, E.S., Blackledge, G.R.P., Slack, J.A., Rustin, G.J., Smith, D.B., Stuart, N.S., Quarterman, C.P., Hoffman, R., Stevens, M.F.G., Brampton, M.H., *et al*. (1992). Phase I trial of temozolomide (CCRG 81045: M&B 39831: NSC 362856). Br. J. Cancer *65*, 287–291.

Newton, H.B., Bromberg, J., Junck, L., Page, M.A., and Greenberg, H.S. (1993). Comparison between BCNU and procarbazine chemotherapy for treatment of gliomas. J. Neurooncol. *15*, 257–263.

Ng, W.H., Wan, G.Q., and Too, H.P. (2007). Higher glioblastoma tumour burden reduces efficacy of chemotherapeutic agents: in vitro evidence. J. Clin. Neurosci. *14*, 261–266.

Niemantsverdriet, M., van Goethem, M.-J., Bron, R., Hogewerf, W., Brandenburg, S., Langendijk, J.A., van Luijk, P., and Coppes, R.P. (2012). High and Low LET Radiation Differentially Induce Normal Tissue Damage Signals. Int. J. Radiat. Oncol. *83*, 1291–1297.

van Nifterik, K.A., van den Berg, J., Stalpers, L.J.A., Lafleur, M.V.M., Leenstra, S., Slotman, B.J., Hulsebos, T.J.M., and Sminia, P. (2007). Differential Radiosensitizing Potential of Temozolomide in MGMT Promoter Methylated Glioblastoma Multiforme Cell Lines. Int. J. Radiat. Oncol. *69*, 1246–1253.

Nioi, P., Nguyen, T., Sherratt, P.J., and Pickett, C.B. (2005). The Carboxy-Terminal Neh3 Domain of Nrf2 Is Required for Transcriptional Activation. Mol. Cell. Biol. *25*, 10895–10906.

Nishikawa, R., Ji, X.D., Harmon, R.C., Lazar, C.S., Gill, G.N., Cavenee, W.K., and Huang, H.J. (1994). A mutant epidermal growth factor receptor common in human glioma confers enhanced tumorigenicity. Proc. Natl. Acad. Sci. U. S. A. *91*, 7727–7731.

Norden, A.D., Young, G.S., Setayesh, K., Muzikansky, A., Klufas, R., Ross, G.L., Ciampa, A.S., Ebbeling, L.G., Levy, B., Drappatz, J., *et al*. (2008). Bevacizumab for recurrent malignant gliomas: efficacy, toxicity, and patterns of recurrence. Neurology *70*, 779–787.

Normanno, N., De Luca, A., Bianco, C., Strizzi, L., Mancino, M., Maiello, M.R., Carotenuto, A., De Feo, G., Caponigro, F., and Salomon, D.S. (2006). Epidermal growth factor receptor (EGFR) signaling in cancer. Gene *366*, 2–16.

Noushmehr, H., Weisenberger, D.J., Diefes, K., Phillips, H.S., Pujara, K., Berman, B.P., Pan, F., Pelloski, C.E., Sulman, E.P., Bhat, K.P., *et al*. (2010). Identification of a CpG island methylator phenotype that defines a distinct subgroup of glioma. Cancer Cell *17*, 510–522.

Nunes, A.S., Barros, A.S., Costa, E.C., Moreira, A.F., and Correia, I.J. (2019). 3D tumor spheroids as in vitro models to mimic in vivo human solid tumors resistance to therapeutic drugs. Biotechnol. Bioeng. *116*, 206–226.

Ochs, K., and Kaina, B. (2000). Apoptosis Induced by DNA Damage O -Methylguanine Is Bcl-2 and Caspase-9/3 Regulated and Fas/Caspase-8 Independent. Cancer Res. *60*, 5815–5824.

Ohgaki, H., and Kleihues, P. (2013). The Definition of Primary and Secondary Glioblastoma. Clin. Cancer Res. *19*, 764–772.

Ohgaki, H., Dessen, P., Jourde, B., Horstmann, S., Nishikawa, T., Di Patre, P.-L., Burkhard, C., Schüler, D., Probst-Hensch, N.M., Maiorka, P.C., *et al*. (2004). Genetic pathways to glioblastoma: a population-based study. Cancer Res. *64*, 6892–6899.

Okcu, M.F., Selvan, M., Wang, L.-E., Stout, L., Erana, R., Airewele, G., Adatto, P., Hess, K., Ali-Osman, F., Groves, M., *et al*. (2004). Glutathione S-Transferase Polymorphisms and Survival in Primary Malignant Glioma. Clin. Cancer Res. *10*, 2618–2625.

Olcina, M., Lecane, P.S., and Hammond, E.M. (2010). Targeting Hypoxic Cells through the DNA Damage Response. Clin. Cancer Res. *16*, 5624–5629.

Omuro, A., and DeAngelis, L.M. (2013). Glioblastoma and other malignant gliomas: a clinical review. JAMA *310*, 1842–1850.

Omuro, A., Beal, K., Gutin, P., Karimi, S., Correa, D.D., Kaley, T.J., DeAngelis, L.M., Chan, T.A., Gavrilovic, I.T., Nolan, C., *et al*. (2014). Phase II Study of Bevacizumab, Temozolomide, and Hypofractionated Stereotactic Radiotherapy for Newly Diagnosed Glioblastoma. Clin. Cancer Res. *20*, 5023–5031.

Ong, S.-M., Zhao, Z., Arooz, T., Zhao, D., Zhang, S., Du, T., Wasser, M., van Noort, D., and Yu, H. (2010). Engineering a scaffold-free 3D tumor model for in vitro drug penetration studies. Biomaterials *31*, 1180–1190.

Ostrom, Q.T., Bauchet, L., Davis, F.G., Deltour, I., Fisher, J.L., Langer, C.E., Pekmezci, M., Schwartzbaum, J.A., Turner, M.C., Walsh, K.M., *et al*. (2014). The epidemiology of glioma in adults: a “state of the science” review. Neuro-Oncol. *16*, 896–913.

Pang, B.-C., Wan, W.-H., Lee, C.-K., Khu, K.J., and Ng, W.-H. (2007). The Role of Surgery in High-grade Glioma – Is Surgical Resection Justified? A Review of the Current Knowledge. *36*, 6.

Park, C.-M., Park, M.-J., Kwak, H.-J., Lee, H.-C., Kim, M.-S., Lee, S.-H., Park, I.-C., Rhee, C.H., and Hong, S.-I. (2006). Ionizing Radiation Enhances Matrix Metalloproteinase-2 Secretion and Invasion of Glioma Cells through Src/Epidermal Growth Factor Receptor–Mediated p38/Akt and Phosphatidylinositol 3-Kinase/Akt Signaling Pathways. Cancer Res. *66*, 8511–8519.

Parker, N.R., Khong, P., Parkinson, J.F., Howell, V.M., and Wheeler, H.R. (2015). Molecular Heterogeneity in Glioblastoma: Potential Clinical Implications. Front. Oncol. *5*.

Parsons, D.W., Jones, S., Zhang, X., Lin, J.C.-H., Leary, R.J., Angenendt, P., Mankoo, P., Carter, H., Siu, I.-M., Gallia, G.L., *et al*. (2008). An Integrated Genomic Analysis of Human Glioblastoma Multiforme. Science *321*, 1807–1812.

Patel, M., McCully, C., Godwin, K., and Balis, F.M. (2003). Plasma and Cerebrospinal Fluid Pharmacokinetics of Intravenous Temozolomide in Non-human Primates. J. Neurooncol. *61*, 203–207.

Paz, M.F., and Yaya-Tur, R. (2004). CpG Island Hypermethylation of the DNA Repair Enzyme Methyltransferase Predicts Response to Temozolomide in Primary Gliomas. Cancer Res. *7*.

Peereboom, D.M., Shepard, D.R., Ahluwalia, M.S., Brewer, C.J., Agarwal, N., Stevens, G.H.J., Suh, J.H., Toms, S.A., Vogelbaum, M.A., Weil, R.J., *et al*. (2010). Phase II trial of erlotinib with temozolomide and radiation in patients with newly diagnosed glioblastoma multiforme. J. Neurooncol. *98*, 93–99.

Peirson, S.N., and Butler, J.N. (2007). RNA Extraction From Mammalian Tissues. In Circadian Rhythms: Methods and Protocols, E. Rosato, ed. (Totowa, NJ: Humana Press), pp. 315–327.

Peitzsch, C., Tyutyunnykova, A., Pantel, K., and Dubrovska, A. (2017). Cancer stem cells: The root of tumor recurrence and metastases. Semin. Cancer Biol. *44*, 10–24.

Pelicano, H., Carney, D., and Huang, P. (2004). ROS stress in cancer cells and therapeutic implications. Drug Resist. Updat. *7*, 97–110.

Perazzoli, G., Prados, J., Ortiz, R., Caba, O., Cabeza, L., Berdasco, M., Gónzalez, B., and Melguizo, C. (2015). Temozolomide Resistance in Glioblastoma Cell Lines: Implication of MGMT, MMR, P-Glycoprotein and CD133 Expression. PLOS ONE *10*, e0140131.

Perry, J., Chambers, A., Spithoff, K., and Laperriere, N. (2007). Gliadel wafers in the treatment of malignant glioma: a systematic review. Curr. Oncol. Tor. Ont *14*, 189–194.

Perry, J., Okamoto, M., Guiou, M., Shirai, K., Errett, A., and Chakravarti, A. (2012). Novel Therapies in Glioblastoma.

Persano, L., Pistollato, F., Rampazzo, E., Della Puppa, A., Abbadi, S., Frasson, C., Volpin, F., Indraccolo, S., Scienza, R., and Basso, G. (2012). BMP2 sensitizes glioblastoma stem-like cells to Temozolomide by affecting HIF-1α stability and MGMT expression. Cell Death Dis. *3*, e412–e412.

Phillips, J., and Fox, R. (2013). BG-12 in Multiple Sclerosis. Semin. Neurol. *33*, 056–065.

Phillips, H.S., Kharbanda, S., Chen, R., Forrest, W.F., Soriano, R.H., Wu, T.D., Misra, A., Nigro, J.M., Colman, H., Soroceanu, L., *et al*. (2006). Molecular subclasses of high-grade glioma predict prognosis, delineate a pattern of disease progression, and resemble stages in neurogenesis. Cancer Cell *9*, 157–173.

Pietenpol, J.A., and Stewart, Z.A. (2002). Cell cycle checkpoint signaling:: Cell cycle arrest versus apoptosis. Toxicology *181*, 475–481.

Pistollato, F., Abbadi, S., Rampazzo, E., Persano, L., Della Puppa, A., Frasson, C., Sarto, E., Scienza, R., D'avella, D., and Basso, G. (2010). Intratumoral hypoxic gradient drives stem cells distribution and MGMT expression in glioblastoma. Stem Cells Dayt. Ohio *28*, 851–862.

Popescu, A.M., Purcaru, S.O., Alexandru, O., and Dricu, A. (2016). New perspectives in glioblastoma antiangiogenic therapy. Contemp. Oncol. *20*, 109–118.

Portugal, J., Mansilla, S., and Bataller, M. (2010). Mechanisms of Drug-Induced Mitotic Catastrophe in Cancer Cells. Curr. Pharm. Des. *16*, 69–78.

Pradère, J.-P., Hernandez, C., Koppe, C., Friedman, R.A., Luedde, T., and Schwabe, R.F. (2016). Negative regulation of NF-κB p65 activity by serine 536 phosphorylation. Sci. Signal. *9*, ra85–ra85.

Prados, M.D., Chang, S.M., Butowski, N., DeBoer, R., Parvataneni, R., Carliner, H., Kabuubi, P., Ayers-Ringler, J., Rabbitt, J., Page, M., *et al*. (2009). Phase II Study of Erlotinib Plus Temozolomide During and After Radiation Therapy in Patients With Newly Diagnosed Glioblastoma Multiforme or Gliosarcoma. J. Clin. Oncol. *27*, 579–584.

Preusser, M., de Ribaupierre, S., Wöhrer, A., Erridge, S.C., Hegi, M., Weller, M., and Stupp, R. (2011). Current concepts and management of glioblastoma. Ann. Neurol. *70*, 9–21.

Pritchard, J.R., Bruno, P.M., Gilbert, L.A., Capron, K.L., Lauffenburger, D.A., and Hemann, M.T. (2013). Defining principles of combination drug mechanisms of action. Proc. Natl. Acad. Sci. *110*, E170–E179.

Quinn, J.A., Jiang, S.X., Reardon, D.A., Desjardins, A., Vredenburgh, J.J., Rich, J.N., Gururangan, S., Friedman, A.H., Bigner, D.D., Sampson, J.H., *et al*. (2009). Phase II Trial of Temozolomide Plus O^6-Benzylguanine in Adults With Recurrent, Temozolomide-Resistant Malignant Glioma. J. Clin. Oncol. *27*, 1262–1267.

Raizer, J.J., Abrey, L.E., Lassman, A.B., Chang, S.M., Lamborn, K.R., Kuhn, J.G., Yung, W.K.A., Gilbert, M.R., Aldape, K.A., Wen, P.Y., *et al*. (2010). A phase II trial of erlotinib in patients with recurrent malignant gliomas and nonprogressive glioblastoma multiforme postradiation therapy. Neuro-Oncol. *12*, 95–103.

Ravizza, R., Cereda, E., Monti, E., and Gariboldi, M. (2004). The piperidine nitroxide Tempol potentiates the cytotoxic effects of temozolomide in human glioblastoma cells. Int. J. Oncol.

Raymond, E., Faivre, S., and Armand, J.P. (2000). Epidermal Growth Factor Receptor Tyrosine Kinase as a Target for Anticancer Therapy. Drugs *60*, 15–23.

Reed, M. (2009). Principles of cancer treatment by surgery. Surg. Oxf. *27*, 178–181.

Reitman, Z.J., Jin, G., Karoly, E.D., Spasojevic, I., Yang, J., Kinzler, K.W., He, Y., Bigner, D.D., Vogelstein, B., and Yan, H. (2011). Profiling the effects of isocitrate dehydrogenase 1 and 2 mutations on the cellular metabolome. Proc. Natl. Acad. Sci. *108*, 3270–3275.

Reliene, R., and Schiestl, R.H. (2006). Glutathione depletion by buthionine sulfoximine induces DNA deletions in mice. Carcinogenesis *27*, 240–244.

Rey, S., Schito, L., Koritzinsky, M., and Wouters, B.G. (2017). Molecular targeting of hypoxia in radiotherapy. Adv. Drug Deliv. Rev. *109*, 45–62.

Ricci-Vitiani, L., Pallini, R., Biffoni, M., Todaro, M., Invernici, G., Cenci, T., Maira, G., Parati, E.A., Stassi, G., Larocca, L.M., *et al*. (2010). Tumour vascularization via endothelial differentiation of glioblastoma stem-like cells. Nature *468*, 824–828.

Rich, J.N. (2007). Cancer Stem Cells in Radiation Resistance. Cancer Res. *67*, 8980–8984.

Riffle, S., Pandey, R.N., Albert, M., and Hegde, R.S. (2017). Linking hypoxia, DNA damage and proliferation in multicellular tumor spheroids. BMC Cancer *17*, 338.

Rishton, G.M. (2005). Failure and Success in Modern Drug Discovery: Guiding Principles in the Establishment of High Probability of Success Drug Discovery Organizations.

Rivera, A.L., Pelloski, C.E., Gilbert, M.R., Colman, H., De La Cruz, C., Sulman, E.P., Bekele, B.N., and Aldape, K.D. (2010). MGMT promoter methylation is predictive of response to radiotherapy and prognostic in the absence of adjuvant alkylating chemotherapy for glioblastoma. Neuro-Oncol. *12*, 116–121.

Rocha, C.R.R., Garcia, C.C.M., Vieira, D.B., Quinet, A., de Andrade-Lima, L.C., Munford, V., Belizário, J.E., and Menck, C.F.M. (2014). Glutathione depletion sensitizes cisplatin- and temozolomide-resistant glioma cells in vitro and in vivo. Cell Death Dis. *5*, e1505.

Rocha, C.R.R., Kajitani, G.S., Quinet, A., Fortunato, R.S., and Menck, C.F.M. (2016). NRF2 and glutathione are key resistance mediators to temozolomide in glioma and melanoma cells. Oncotarget *7*, 48081–48092.

Roos, W.P., and Kaina, B. (2006). DNA damage-induced cell death by apoptosis. Trends Mol. Med. *12*, 440–450.

Roos, W., Baumgartner, M., and Kaina, B. (2004). Apoptosis triggered by DNA damage O 6 -methylguanine in human lymphocytes requires DNA replication and is mediated by p53 and Fas/CD95/Apo-1. Oncogene *23*, 359–367.

Roos, W.P., Batista, L.F.Z., Naumann, S.C., Wick, W., Weller, M., Menck, C.F.M., and Kaina, B. (2007). Apoptosis in malignant glioma cells triggered by the temozolomide-induced DNA lesion O6-methylguanine. Oncogene *26*, 186–197.

Rutledge, W.C., Kong, J., Gao, J., Gutman, D.A., Cooper, L.A.D., Appin, C., Park, Y., Scarpace, L., Mikkelsen, T., Cohen, M.L., *et al*. (2013). Tumor-Infiltrating Lymphocytes in Glioblastoma Are Associated with Specific Genomic Alterations and Related to Transcriptional Class. Clin. Cancer Res. *19*, 4951–4960.

Saidu, N.E.B., Noé, G., Cerles, O., Cabel, L., Kavian-Tessler, N., Chouzenoux, S., Bahuaud, M., Chéreau, C., Nicco, C., Leroy, K., *et al*. (2017). Dimethyl Fumarate Controls the NRF2/DJ-1 Axis in Cancer Cells: Therapeutic Applications. Mol. Cancer Ther. *16*, 529–539.

Saile, B., Matthes, N., El Armouche, H., Neubauer, K., and Ramadori, G. (2001). The bcl, NFκB and p53/p21WAF1 systems are involved in spontaneous apoptosis and in the anti-apoptotic effect of TGF-β or TNF-α on activated hepatic stellate cells. Eur. J. Cell Biol. *80*, 554–561.

Saito, S., Goodarzi, A.A., Higashimoto, Y., Noda, Y., Lees-Miller, S.P., Appella, E., and Anderson, C.W. (2002). ATM Mediates Phosphorylation at Multiple p53 Sites, Including Ser ^{46} , in Response to Ionizing Radiation. J. Biol. Chem. *277*, 12491–12494.

Sakariassen, P.Ø., Immervoll, H., and Chekenya, M. (2007). Cancer Stem Cells as Mediators of Treatment Resistance in Brain Tumors: Status and Controversies. Neoplasia *9*, 882–892.

Sanson, M., Marie, Y., Paris, S., Idbaih, A., Laffaire, J., Ducray, F., El Hallani, S., Boisselier, B., Mokhtari, K., Hoang-Xuan, K., *et al*. (2009). Isocitrate Dehydrogenase 1 Codon 132 Mutation Is an Important Prognostic Biomarker in Gliomas. J. Clin. Oncol. *27*, 4150–4154.

Sant, S., and Johnston, P.A. (2017). The production of 3D tumor spheroids for cancer drug discovery. Drug Discov. Today Technol. *23*, 27–36.

Sarkaria, J.N., Carlson, B.L., Decker, P.A., Schroeder, M.J., Kitange, G.J., Ballman, K.V., and James, C. (2006). MGMT methylation status correlates with temozolomide-mediated radiosensitization in a panel of GBM orthotopic xenografts. J. Clin. Oncol. *24*, 1509–1509.

Sarkaria, J.N., Kitange, G.J., James, C.D., Plummer, R., Calvert, H., Weller, M., and Wick, W. (2008). Mechanisms of Chemoresistance in Malignant Glioma. Clin. Cancer Res. Off. J. Am. Assoc. Cancer Res. *14*, 2900–2908.

Scanlon, S.E., and Glazer, P.M. (2015). Multifaceted control of DNA repair pathways by the hypoxic tumor microenvironment. DNA Repair *32*, 180–189.

Schäfer, A., Teufel, J., Ringel, F., Bettstetter, M., Hoepner, I., Rasper, M., Gempt, J., Koeritzer, J., Schmidt-Graf, F., Meyer, B., *et al*. (2012). Aldehyde dehydrogenase 1A1--a new mediator of resistance to temozolomide in glioblastoma. Neuro-Oncol. *14*, 1452–1464.

Schindelin, J., Arganda-Carreras, I., Frise, E., Kaynig, V., Longair, M., Pietzsch, T., Preibisch, S., Rueden, C., Saalfeld, S., Schmid, B., *et al*. (2012). Fiji: an open-source platform for biological-image analysis. Nat. Methods *9*, 676–682.

Schmidt, M.M., and Dringen, R. (2010). Fumaric acid diesters deprive cultured primary astrocytes rapidly of glutathione. Neurochem. Int. *57*, 460–467.

Schmidt, T.J., Ak, M., and Mrowietz, U. (2007). Reactivity of dimethyl fumarate and methylhydrogen fumarate towards glutathione and N-acetyl-l-cysteine—Preparation of S-substituted thiosuccinic acid esters. Bioorg. Med. Chem. *15*, 333–342.

Schmittgen, T.D., and Livak, K.J. (2008). Analyzing real-time PCR data by the comparative C_T method. Nat. Protoc. *3*, 1101–1108.

Schnelldorfer, T., Gansauge, S., Gansauge, F., Schlosser, S., Beger, H.G., and Nussler, A.K. (2000). Glutathione depletion causes cell growth inhibition and enhanced apoptosis in pancreatic cancer cells. Cancer *89*, 1440–1447.

Schoenherr, D., Krueger, S.A., Martin, L., Marignol, L., Wilson, G.D., and Marples, B. (2013). Determining if low dose hyper-radiosensitivity (HRS) can be exploited to provide a therapeutic advantage: A cell line study in four glioblastoma multiforme (GBM) cell lines. Int. J. Radiat. Biol. *89*, 1009–1016.

Schumacker, P.T. (2015). Reactive Oxygen Species in Cancer: A Dance with the Devil. Cancer Cell *27*, 156–157.

Semenza, G.L. (2012). Hypoxia-Inducible Factors in Physiology and Medicine. Cell *148*, 399–408.

Shafer, D.A., Chen, Z., Harris, T., Tombes, M.B., Shrader, E., Strickler, K., Ryan, A.A., Dent, P., and Malkin, M.G. (2017). Phase I trial of dimethyl fumarate, temozolomide, and radiation therapy in glioblastoma multiforme. J. Clin. Oncol. *35*, 2060–2060.

Shannon, A.M., Bouchier-Hayes, D.J., Condron, C.M., and Toomey, D. (2003). Tumour hypoxia, chemotherapeutic resistance and hypoxia-related therapies. Cancer Treat. Rev. *29*, 297–307.

Sheehan, J.P., Shaffrey, M.E., Gupta, B., Larner, J., Rich, J.N., and Park, D.M. (2010). Improving the radiosensitivity of radioresistant and hypoxic glioblastoma. Future Oncol. *6*, 1591–1601.

Shepherd, F.A., Rodrigues Pereira, J., Ciuleanu, T., Tan, E.H., Hirsh, V., Thongprasert, S., Campos, D., Maoleekoonpiroj, S., Smylie, M., Martins, R., *et al*. (2005). Erlotinib in Previously Treated Non–Small-Cell Lung Cancer. N. Engl. J. Med. *353*, 123–132.

Sherr, C.J. (2004). Principles of tumor suppression. Cell *116*, 235–246.

Sherr, C.J., and McCormick, F. (2002). The RB and p53 pathways in cancer. Cancer Cell *2*, 103–112.

Short, S.C., Martindale, C., Bourne, S., Brand, G., Woodcock, M., and Johnston, P. (2007). DNA repair after irradiation in glioma cells and normal human astrocytes. Neuro-Oncol. *9*, 404–411.

Sidaway, P. (2017). CNS cancer: Glioblastoma subtypes revisited. Nat. Rev. Clin. Oncol. *14*, 587.

Sies, H. (1999). Glutathione and its role in cellular functions. Free Radic. Biol. Med. *27*, 916–921.

Sigismund, S., Avanzato, D., and Lanzetti, L. (2019). Emerging functions of the EGFR in cancer. Mol. Oncol. 3–20.

Simons, B.W., and Brayton, C. (2017). Chapter 3 - Challenges and Limitations of Mouse Xenograft Models of Cancer. In Patient Derived Tumor Xenograft Models, R. Uthamanthil, and P. Tinkey, eds. (Academic Press), pp. 25–36.

Singh, A., Venkannagari, S., Oh, K.H., Zhang, Y.-Q., Rohde, J.M., Liu, L., Nimmagadda, S., Sudini, K., Brimacombe, K.R., Gajghate, S., *et al*. (2016). Small molecule inhibitor of NRF2 selectively intervenes therapeutic resistance in KEAP1-deficient NSCLC tumors. ACS Chem. Biol. *11*, 3214–3225.

Singh, S.K., Hawkins, C., Clarke, I.D., Squire, J.A., Bayani, J., Hide, T., Henkelman, R.M., Cusimano, M.D., and Dirks, P.B. (2004). Identification of human brain tumour initiating cells. Nature *432*, 396–401.

Singh, S.P., Wishnok, J.S., Keshive, M., Deen, W.M., and Tannenbaum, S.R. (1996). The chemistry of the S-nitrosoglutathione/glutathione system. Proc. Natl. Acad. Sci. *93*, 14428–14433.

Slater, K. (2001). Cytotoxicity tests for high-throughput drug discovery. Curr. Opin. Biotechnol. *12*, 70–74.

Smith, J.S., Tachibana, I., Passe, S.M., Huntley, B.K., Borell, T.J., Iturria, N., O'Fallon, J.R., Schaefer, P.L., Scheithauer, B.W., James, C.D., *et al*. (2001). PTEN Mutation, EGFR Amplification, and Outcome in Patients With Anaplastic Astrocytoma and Glioblastoma Multiforme. JNCI J. Natl. Cancer Inst. *93*, 1246–1256.

Smoll, N.R., and Hamilton, B. (2014). Incidence and relative survival of anaplastic astrocytomas. Neuro-Oncol. *16*, 1400–1407.

Sneed, P.K., Gutin, P.H., Larson, D.A., Malec, M.K., Phillips, T.L., Prados, M.D., Scharfen, C.O., Weaver, K.A., and Wara, W.M. (1994). Patterns of recurrence of glioblastoma multiforme after external irradiation followed by implant boost. Int. J. Radiat. Oncol. Biol. Phys. *29*, 719–727.

Sobol Jr, R.W., Tawbi, H., Jukic, D.M., Mule, K., Mascari, R., and Kirkwood, J.M. (2006). Mismatch repair (MMR) and base excision repair (BER) protein expression correlates with clinical response to dacarbazine (DTIC)/temozolomide (TMZ) therapy of patients with metastatic melanoma. J. Clin. Oncol. *24*, 8015–8015.

SongTao, Q., Lei, Y., Si, G., YanQing, D., HuiXia, H., XueLin, Z., LanXiao, W., and Fei, Y. (2012). IDH mutations predict longer survival and response to temozolomide in secondary glioblastoma. Cancer Sci. *103*, 269–273.

Sottoriva, A., Spiteri, I., Piccirillo, S.G.M., Touloumis, A., Collins, V.P., Marioni, J.C., Curtis, C., Watts, C., and Tavare, S. (2013). Intratumor heterogeneity in human glioblastoma reflects cancer evolutionary dynamics. Proc. Natl. Acad. Sci. *110*, 4009–4014.

de Sousa, J.F., Torrieri, R., Serafim, R.B., Di Cristofaro, L.F.M., Escanfella, F.D., Ribeiro, R., Zanette, D.L., Paçó-Larson, M.L., da Silva, W.A., Tirapelli, D.P. da C., *et al*. (2017). Expression signatures of DNA repair genes correlate with survival prognosis of astrocytoma patients. Tumor Biol. *39*, 101042831769455.

Squatrito, M., Brennan, C.W., Helmy, K., Huse, J.T., Petrini, J.H., and Holland, E.C. (2010). Loss of ATM/Chk2/p53 Pathway Components Accelerates Tumor Development and Contributes to Radiation Resistance in Gliomas. Cancer Cell *18*, 619–629.

Stichel, D., Ebrahimi, A., Reuss, D., Schrimpf, D., Ono, T., Shirahata, M., Reifenberger, G., Weller, M., Hänggi, D., Wick, W., *et al*. (2018). Distribution of EGFR amplification, combined chromosome 7 gain and chromosome 10 loss, and TERT promoter mutation in brain tumors and their potential for the reclassification of IDHwt astrocytoma to glioblastoma. Acta Neuropathol. (Berl.) *136*, 793–803.

Straetemans, R., O'Brien, T., Wouters, L., Van Dun, J., Janicot, M., Bijnens, L., Burzykowski, T., and Aerts, M. (2005). Design and Analysis of Drug Combination Experiments. Biom. J. *47*, 299–308.

Stratton, M.R., Campbell, P.J., and Futreal, P.A. (2009). The cancer genome. Nature *458*, 719–724.

Stupp, R., Weller, M., Belanger, K., Bogdahn, U., Ludwin, S.K., Lacombe, D., and Mirimanoff, R.O. (2005). Radiotherapy plus Concomitant and Adjuvant Temozolomide for Glioblastoma. N. Engl. J. Med. 10.

Stupp, R., Hegi, M.E., Gilbert, M.R., and Chakravarti, A. (2007). Chemoradiotherapy in Malignant Glioma: Standard of Care and Future Directions. J. Clin. Oncol. *25*, 4127–4136.

Stupp, R., Hegi, M.E., and Mason, W.P. (2009). Effects of radiotherapy with concomitant and adjuvant temozolomide versus radiotherapy alone on survival in glioblastoma in a randomised phase III study: 5-year analysis of the EORTC-NCIC trial. *10*, 8.

Stupp, R., Tonn, J.-C., Brada, M., Pentheroudakis, G., and On behalf of the ESMO Guidelines Working Group (2010). High-grade malignant glioma: ESMO Clinical Practice Guidelines for diagnosis, treatment and follow-up. Ann. Oncol. *21*, v190–v193.

Sukumari-Ramesh, S., Prasad, N., Alleyne, C.H., Vender, J.R., and Dhandapani, K.M. (2015). Overexpression of Nrf2 attenuates Carmustine-induced cytotoxicity in U87MG human glioma cells. BMC Cancer *15*.

Sullivan, L.B., Martinez-Garcia, E., Nguyen, H., Mullen, A.R., Dufour, E., Sudarshan, S., Licht, J.D., Deberardinis, R.J., and Chandel, N.S. (2013). The Proto-oncometabolite

Fumarate Binds Glutathione to Amplify ROS-Dependent Signaling. Mol. Cell *51*, 236–248.

Sun, J., Chen, Y., Li, M., and Ge, Z. (1998). Role of Antioxidant Enzymes on Ionizing Radiation Resistance. Free Radic. Biol. Med. *24*, 586–593.

Szerlip, N.J., Pedraza, A., Chakravarty, D., Azim, M., McGuire, J., Fang, Y., Ozawa, T., Holland, E.C., Huse, J.T., Jhanwar, S., *et al*. (2012). Intratumoral heterogeneity of receptor tyrosine kinases EGFR and PDGFRA amplification in glioblastoma defines subpopulations with distinct growth factor response. Proc. Natl. Acad. Sci. U. S. A. *109*, 3041–3046.

Taguchi, K., Motohashi, H., and Yamamoto, M. (2011). Molecular mechanisms of the Keap1–Nrf2 pathway in stress response and cancer evolution. Genes Cells Devoted Mol. Cell. Mech. *16*, 123–140.

Tajima, M., Kurashima, Y., Sugiyama, K., Ogura, T., and Sakagami, H. (2009). The redox state of glutathione regulates the hypoxic induction of HIF-1. Eur. J. Pharmacol. *606*, 45–49.

Tate, M.C., and Aghi, M.K. (2009). Biology of angiogenesis and invasion in glioma. Neurotherapeutics *6*, 447–457.

The Cancer Genome Atlas Research Network (2008). Comprehensive genomic characterization defines human glioblastoma genes and core pathways. Nature *455*, 1061–1068.

Thomas, C., Martin, J., Devic, C., Bräuer-Krisch, E., Diserbo, M., Thariat, J., and Foray, N. (2013). Impact of dose-rate on the low-dose hyper-radiosensitivity and induced radioresistance (HRS/IRR) response. Int. J. Radiat. Biol. *89*, 813–822.

To, C., Ringelberg, C.S., Royce, D.B., Williams, C.R., Risingsong, R., Sporn, M.B., and Liby, K.T. (2015). Dimethyl fumarate and the oleanane triterpenoids, CDDO-imidazolide and CDDO-methyl ester, both activate the Nrf2 pathway but have opposite effects in the A/J model of lung carcinogenesis. Carcinogenesis *36*, 769–781.

Torre, L.A., Bray, F., Siegel, R.L., Ferlay, J., Lortet-Tieulent, J., and Jemal, A. (2015). Global cancer statistics, 2012. CA. Cancer J. Clin. *65*, 87–108.

Townsend, D.M., and Tew, K.D. (2003). The role of glutathione-S-transferase in anti-cancer drug resistance. Oncogene *22*, 7369–7375.

Traverso, N., Ricciarelli, R., Nitti, M., Marengo, B., Furfaro, A.L., Pronzato, M.A., Marinari, U.M., and Domenicotti, C. (2013). Role of Glutathione in Cancer Progression and Chemoresistance. Oxid. Med. Cell. Longev. *2013*, 1–10.

Trivedi, R.N., Almeida, K.H., Fornsaglio, J.L., Schamus, S., and Sobol, R.W. (2005). The Role of Base Excision Repair in the Sensitivity and Resistance to Temozolomide-Mediated Cell Death. Cancer Res. *65*, 6394–6400.

Tsai, W.-C., Hueng, D.-Y., Lin, C.-R., Yang, T., and Gao, H.-W. (2016). Nrf2 Expressions Correlate with WHO Grades in Gliomas and Meningiomas. Int. J. Mol. Sci. *17*, 722.

Tsao, M.-S., Sakurada, A., Cutz, J.-C., Zhu, C.-Q., Kamel-Reid, S., Squire, J., Lorimer, I., Zhang, T., Liu, N., Daneshmand, M., *et al*. (2005). Erlotinib in Lung Cancer — Molecular and Clinical Predictors of Outcome. N. Engl. J. Med. *353*, 133–144.

Tso, C.-L., Freije, W.A., Day, A., Chen, Z., Merriman, B., Perlina, A., Lee, Y., Dia, E.Q., Yoshimoto, K., Mischel, P.S., *et al*. (2006). Distinct Transcription Profiles of Primary and Secondary Glioblastoma Subgroups. Cancer Res. *66*, 159–167.

Uhm, J.H., Ballman, K.V., Wu, W., Giannini, C., Krauss, J.C., Buckner, J.C., James, C.D., Scheithauer, B.W., Behrens, R.J., Flynn, P.J., *et al*. (2011). Phase II Evaluation of Gefitinib in Patients With Newly Diagnosed Grade 4 Astrocytoma: Mayo/North Central Cancer Treatment Group Study N0074. Int. J. Radiat. Oncol. *80*, 347–353.

Vakifahmetoglu, H., Olsson, M., and Zhivotovsky, B. (2008). Death through a tragedy: mitotic catastrophe. Cell Death Differ. Rome *15*, 1153–1162.

Valesky, E.M., Hrgovic, I., Doll, M., Wang, X.-F., Pinter, A., Kleemann, J., Kaufmann, R., Kippenberger, S., and Meissner, M. (2016). Dimethylfumarate effectively inhibits lymphangiogenesis via p21 induction and G1 cell cycle arrest. Exp. Dermatol. *25*, 200–205.

Van Cutsem, E., Köhne, C.-H., Hitre, E., Zaluski, J., Chang Chien, C.-R., Makhson, A., D'Haens, G., Pintér, T., Lim, R., Bodoky, G., *et al*. (2009). Cetuximab and Chemotherapy as Initial Treatment for Metastatic Colorectal Cancer. N. Engl. J. Med. *360*, 1408–1417.

Velichkova, M., and Hasson, T. (2005). Keap1 Regulates the Oxidation-Sensitive Shuttling of Nrf2 into and out of the Nucleus via a Crm1-Dependent Nuclear Export Mechanism. Mol. Cell. Biol. *25*, 4501–4513.

Verhaak, R.G.W., Hoadley, K.A., Purdom, E., Wang, V., Qi, Y., Wilkerson, M.D., Miller, C.R., Ding, L., Golub, T., Mesirov, J.P., *et al*. (2010). Integrated genomic analysis identifies clinically relevant subtypes of glioblastoma characterized by abnormalities in PDGFRA, IDH1, EGFR, and NF1. Cancer Cell *17*, 98–110.

Vescovi, A.L., Galli, R., and Reynolds, B.A. (2006). Brain tumour stem cells. Nat. Rev. Cancer *6*, 425–436.

Vignard, J., Mirey, G., and Salles, B. (2013). Ionizing-radiation induced DNA double-strand breaks: A direct and indirect lighting up. Radiother. Oncol. *108*, 362–369.

Vives, K.P., and Piepmeier, J.M. (1999). Complications and Expected Outcome of Glioma Surgery. J. Neurooncol. *42*, 289–302.

Vos, O., Schans, G.P. van der, and Roos-verheij, W.S.D. (1986). Reduction of Intracellular Glutathione Content and Radiosensitivity. Int. J. Radiat. Biol. Relat. Stud. Phys. Chem. Med. *50*, 155–165.

Wang, X., and Lin, Y. (2008). Tumor necrosis factor and cancer, buddies or foes? Acta Pharmacol. Sin. *29*, 1275–1288.

Wang, Q., Hu, B., Hu, X., Kim, H., Squatrito, M., Scarpace, L., deCarvalho, A.C., Lyu, S., Li, P., Li, Y., *et al*. (2017). Tumor Evolution of Glioma-Intrinsic Gene Expression

Subtypes Associates with Immunological Changes in the Microenvironment. Cancer Cell *32*, 42-56.e6.

Wang, T.-J., Huang, M.-S., Hong, C.-Y., Tse, V., Silverberg, G.D., and Hsiao, M. (2001). Comparisons of Tumor Suppressor p53, p21, and p16 Gene Therapy Effects on Glioblastoma Tumorigenicity in Situ. Biochem. Biophys. Res. Commun. *287*, 173–180.

Wang, X.-J., Sun, Z., Villeneuve, N.F., Zhang, S., Zhao, F., Li, Y., Chen, W., Yi, X., Zheng, W., Wondrak, G.T., *et al*. (2008). Nrf2 enhances resistance of cancer cells to chemotherapeutic drugs, the dark side of Nrf2. Carcinogenesis *29*, 1235–1243.

Waring, M.J., Arrowsmith, J., Leach, A.R., Leeson, P.D., Mandrell, S., Owen, R.M., Pairaudeau, G., Pennie, W.D., Pickett, S.D., Wang, J., *et al*. (2015). An analysis of the attrition of drug candidates from four major pharmaceutical companies. Nat. Rev. Drug Discov. *14*, 475–486.

Wartenberg, M., Ling, F.C., Müschen, M., Klein, F., Acker, H., Gassmann, M., Petrat, K., Pütz, V., Hescheler, J., and Sauer, H. (2003). Regulation of the multidrug resistance transporter P-glycoprotein in multicellular tumor spheroids by hypoxia-inducible factor (HIF-1) and reactive oxygen species. FASEB J. *17*, 503–505.

Watanabe, K., Sato, K., Biernat, W., Tachibana, O., Ammon, K. von, Ogata, N., Yonekawa, Y., Kleihues, P., and Ohgaki, H. (1997). Incidence and timing of p53 mutations during astrocytoma progression in patients with multiple biopsies. Clin. Cancer Res. *3*, 523–530.

Weathers, S.P., and De Groot, J. (2015). VEGF Manipulation in Glioblastoma. Oncol. Williston Park N *29*, 720–727.

Weaver, B.A.A., and Cleveland, D.W. (2005). Decoding the links between mitosis, cancer, and chemotherapy: The mitotic checkpoint, adaptation, and cell death. Cancer Cell *8*, 7–12.

Wedge, S.R., and Newlands, E.S. (1996). O6-benzylguanine enhances the sensitivity of a glioma xenograft with low O6-alkylguanine-DNA alkyltransferase activity to temozolomide and BCNU. Br. J. Cancer *73*, 1049–1052.

Wefel, J.S., and Schagen, S.B. (2012). Chemotherapy-Related Cognitive Dysfunction. Curr. Neurol. Neurosci. Rep. *12*, 267–275.

Weller, M. (2011). Novel diagnostic and therapeutic approaches to malignant glioma. Swiss Med. Wkly. *141*, w13210.

Westphal, M., Maire, C.L., and Lamszus, K. (2017). EGFR as a Target for Glioblastoma Treatment: An Unfulfilled Promise. CNS Drugs *31*, 723–735.

Whillier, S., Raftos, J.E., Chapman, B., and Kuchel, P.W. (2009). Role of N-acetylcysteine and cystine in glutathione synthesis in human erythrocytes. Redox Rep. *14*, 115–124.

White, J.B., Miller, G.M., Layton, K.F., and Krauss, W.E. (2007). Nonenhancing tumors of the spinal cord. J. Neurosurg. Spine *7*, 403–407.

Wilms, H., Sievers, J., Rickert, U., Rostami-Yazdi, M., Mrowietz, U., and Lucius, R. (2010). Research Dimethylfumarate inhibits microglial and astrocytic inflammation by suppressing the synthesis of nitric oxide, IL-1β, TNF-α and IL-6 in an in-vitro model of brain inflammation.

Wong, E.T., Gautam, S., Malchow, C., Lun, M., Pan, E., and Brem, S. (2011). Bevacizumab for Recurrent Glioblastoma Multiforme: A Meta-Analysis. J. Natl. Compr. Canc. Netw. *9*, 403–407.

Würth, R., Barbieri, F., and Florio, T. (2014). New Molecules and Old Drugs as Emerging Approaches to Selectively Target Human Glioblastoma Cancer Stem Cells. BioMed Res. Int. *2014*, 1–11.

Xie, C., Sheng, H., Zhang, N., Li, S., Wei, X., and Zheng, X. (2016). Association of MSH6 mutation with glioma susceptibility, drug resistance and progression (Review). Mol. Clin. Oncol. *5*, 236–240.

Xie, X., Zhao, Y., Ma, C.-Y., Xu, X.-M., Zhang, Y.-Q., Wang, C.-G., Jin, J., Shen, X., Gao, J.-L., Li, N., *et al*. (2015). Dimethyl fumarate induces necroptosis in colon cancer cells through GSH depletion/ROS increase/MAPKs activation pathway. Br. J. Pharmacol. *172*, 3929–3943.

Xu, Z., Zhang, F., Sun, F., Gu, K., Dong, S., and He, D. (2015). Dimethyl fumarate for multiple sclerosis. In Cochrane Database of Systematic Reviews, The Cochrane Collaboration, ed. (Chichester, UK: John Wiley & Sons, Ltd), p.

Yamada, J., Yoshimura, S., Yamakawa, H., Sawada, M., Nakagawa, M., Hara, S., Kaku, Y., Iwama, T., Naganawa, T., Banno, Y., *et al*. (2003). Cell permeable ROS scavengers, Tiron and Tempol, rescue PC12 cell death caused by pyrogallol or hypoxia/reoxygenation. Neurosci. Res. *45*, 1–8.

Yamamoto, T., Suzuki, T., Kobayashi, A., Wakabayashi, J., Maher, J., Motohashi, H., and Yamamoto, M. (2008). Physiological Significance of Reactive Cysteine Residues of Keap1 in Determining Nrf2 Activity. Mol. Cell. Biol. *28*, 2758–2770.

Yan, K., Yang, K., and Rich, J.N. (2013). The evolving landscape of glioblastoma stem cells. Curr. Opin. Neurol. *26*, 701–707.

Yang, D.-I., Yin, J.-H., Ju, T.-C., Chen, L.-S., and Hsu, C.Y. (2004). Nitric oxide and BCNU chemoresistance in C6 glioma cells: Role of S-nitrosoglutathione. Free Radic. Biol. Med. *36*, 1317–1328.

Yardley, D.A. (2013). Drug Resistance and the Role of Combination Chemotherapy in Improving Patient Outcomes.

Yokota, J. (2000). Tumor progression and metastasis. Carcinogenesis *21*, 497–503.

Yoshino, A., Ogino, A., Yachi, K., Ohta, T., Fukushima, T., Watanabe, T., Katayama, Y., Okamoto, Y., Naruse, N., Sano, E., *et al*. (2010). Gene expression profiling predicts response to temozolomide in malignant gliomas. Int. J. Oncol. *36*, 1367–1377.

Zaboronok, A., Isobe, T., Yamamoto, T., Sato, E., Takada, K., Sakae, T., Tsurushima, H., and Matsumura, A. (2014). Proton beam irradiation stimulates migration and invasion of human U87 malignant glioma cells. J. Radiat. Res. (Tokyo) *55*, 283–287.

Zagzag, D., Lukyanov, Y., Lan, L., Ali, M.A., Esencay, M., Mendez, O., Yee, H., Voura, E.B., and Newcomb, E.W. (2006). Hypoxia-inducible factor 1 and VEGF upregulate CXCR4 in glioblastoma: implications for angiogenesis and glioma cell invasion. Lab. Invest. *86*, 1221.

Zawlik, I., Kita, D., Vaccarella, S., Mittelbronn, M., Franceschi, S., and Ohgaki, H. (2009). Common Polymorphisms in the MDM2 and TP53 Genes and the Relationship between TP53 Mutations and Patient Outcomes in Glioblastomas. Brain Pathol. *19*, 188–194.

Zhang, D.D. (2006). Mechanistic studies of the Nrf2-Keap1 signaling pathway. Drug Metab. Rev. *38*, 769–789.

Zhang, L., and Wang, H. (2017). FTY720 inhibits the Nrf2/ARE pathway in human glioblastoma cell lines and sensitizes glioblastoma cells to temozolomide. Pharmacol. Rep. *69*, 1186–1193.

Zhang, J., Grek, C., Ye, Z.-W., Manevich, Y., Tew, K.D., and Townsend, D.M. (2014). Pleiotropic Functions of Glutathione S-Transferase P. Adv. Cancer Res. *122*, 143–175.

Zhang, W., Wang, Z., Shu, F., Jin, Y., Liu, H., Wang, Q., and Yang, Y. (2010). Activation of AMP-activated Protein Kinase by Temozolomide Contributes to Apoptosis in Glioblastoma Cells via p53 Activation and mTORC1 Inhibition. J. Biol. Chem. *285*, 40461–40471.

Zhang, X., Chen, T., Zhang, J., Mao, Q., Li, S., Xiong, W., Qiu, Y., Xie, Q., and Ge, J. (2012). Notch1 promotes glioma cell migration and invasion by stimulating β-catenin and NF-κB signaling via AKT activation. Cancer Sci. *103*, 181–190.

Zhang, Y., Dube, C., Gibert, M., Cruickshanks, N., Wang, B., Coughlan, M., Yang, Y., Setiady, I., Deveau, C., Saoud, K., *et al*. (2018). The p53 Pathway in Glioblastoma. Cancers *10*, 297.

Zhang, Z.-S., Wang, J., Shen, Y.-B., Guo, C.-C., Sai, K., Chen, F.-R., Mei, X., Han, F., and Chen, Z.-P. (2015). Dihydroartemisinin increases temozolomide efficacy in glioma cells by inducing autophagy. Oncol. Lett. *10*, 379–383.

Zhao, G., Liu, Y., Fang, J., Chen, Y., Li, H., and Gao, K. (2014). Dimethyl fumarate inhibits the expression and function of hypoxia-inducible factor-1α (HIF-1α). Biochem. Biophys. Res. Commun. *448*, 303–307.

Zhao, H., Huang, X., Halicka, H.D., and Darzynkiewicz, Z. (2019). Detection of Histone H2AX Phosphorylation on Ser-139 as an Indicator of DNA Damage.

Zhao, S., Lin, Y., Xu, W., Jiang, W., Zha, Z., Wang, P., Yu, W., Li, Z., Gong, L., Peng, Y., *et al*. (2009). Glioma-derived mutations in IDH1 dominantly inhibit IDH1 catalytic activity and induce HIF-1alpha. Science *324*, 261–265.

Zhitkovich, A. (2019). *N* -Acetylcysteine: Antioxidant, Aldehyde Scavenger, and More. Chem. Res. Toxicol. acs.chemrestox.9b00152.

Zhivotovsky, B., and Orrenius, S. (2010). Cell cycle and cell death in disease: past, present and future. J. Intern. Med. *268*, 395–409.

Zhu, J., Wang, H., Sun, Q., Ji, X., Zhu, L., Cong, Z., Zhou, Y., Liu, H., and Zhou, M. (2013). Nrf2 is required to maintain the self-renewal of glioma stem cells. BMC Cancer *13*.

Zhu, Z., Du, S., Du, Y., Ren, J., Ying, G., and Yan, Z. (2018). Glutathione reductase mediates drug resistance in glioblastoma cells by regulating redox homeostasis. J. Neurochem. *144*, 93–104.

Appendices

Appendix a

a.

	4hr				24hr			
	0	0.5μM	5μM	15μM	0	0.5μM	5μM	15μM
0	–	ns	ns	ns	–	G_2 **	G_2 **	G_2 **
0.5μM+0.3μM	ns	ns			ns	ns		
5μM+3μM	ns		ns		ns		ns	
15μM+9μM	ns			ns	G_2 **			ns

b.

	4hr				24hr			
	0	0.3μM	3μM	9μM	0	0.3μM	3μM	9μM
0	–	ns	ns	ns	–	ns	ns	ns
0.5μM+0.3μM	ns	ns			ns	ns		
5μM+3μM	ns		ns		ns		ns	
15μM+9μM	ns			ns	G_2 **			ns

c.

	4hr				24hr			
	0	50μM	200μM	400μM	0	50μM	200μM	400μM
0	–	ns	ns	ns	–	ns	ns	ns
50μM+3.125μM	ns	ns			ns	ns		
200μM+12.5μM	ns		ns		ns		ns	
400μM+25μM	G_2 *			ns	G_2 ***			ns

d.

	4hr				24hr			
	0	3.125μM	12.5μM	25μM	0	3.125μM	12.5μM	25μM
0	–	ns	ns	ns	–	ns	ns	ns
50μM+3.125μM	ns	ns			ns	ns		
200μM+12.5μM	ns		ns		ns		ns	
400μM+25μM	G_2 *			G_2 *	G_2 ***			G_2 **

Appendix A: Statistical analysis of data presented in Figure 3.9 and 10. a. comparison of cell cycle progression in temozolomide and temozolomide-dimethyl fumarate combination treated UVW cells. b. comparison of cell cycle progression in dimethyl fumarate and temozolomide-dimethyl fumarate combination treated UVW cells. c. comparison of cell cycle progression in temozolomide and temozolomide-dimethyl fumarate combination treated T98g cells. d. comparison of cell cycle progression in dimethyl fumarate and temozolomide-dimethyl fumarate combination treated T98g cells.

Appendix b

a.

	24hr				48hr				72hr			
	0	0.5μM	5μM	15μM	0	0.5μM	5μM	15μM	0	0.5μM	5μM	15μM
0	–	ns	ns	ns	–	ns	ns	ns	–	***	***	***
0.5μM+0.3μM	ns	ns			ns	ns			***	ns		
5μM+3μM	ns		ns		ns		ns		***		ns	
15μM+9μM	ns			ns	ns			ns	***			ns

b.

	24hr				48hr				72hr			
	0	0.3μM	3μM	9μM	0	0.3μM	3μM	9μM	0	0.3μM	3μM	9μM
0	–	ns	ns	ns	–	**	**	***	–	***	***	***
0.5μM+0.3μM	ns	ns			ns	**			***	ns		
5μM+3μM	ns		ns		ns		**		***		ns	
15μM+9μM	ns			ns	ns			**	***			ns

c.

	24hr			48hr			72hr		
	0.5μM	5μM	15μM	0.5μM	5μM	15μM	0.5μM	5μM	15μM
0.5μM+0.3μM	ns			ns			L** N**		
5μM+3μM		ns			ns			L** N**	
15μM+9μM			ns			ns			L* N**

d.

	24hr			48hr			72hr		
	0.3μM	3μM	9μM	0.3μM	3μM	9μM	0.3μM	3μM	9μM
0.5μM+0.3μM	ns			L**			L** N**		
5μM+3μM		ns			L**			L** N**	
15μM+9μM			ns			L**			L** N**

Appendix B1: Statistical analysis of data presented in Figure 3.10. a. comparison of apoptotic induction in temozolomide and temozolomide-dimethyl fumarate combination treated UVW cells. b. comparison of apoptotic induction in dimethyl fumarate and temozolomide-dimethyl fumarate combination treated UVW cells. c. comparison of apoptotic phase distribution in temozolomide and temozolomide-dimethyl fumarate combination treated UVW cells. d. comparison of apoptotic phase distribution in dimethyl fumarate and temozolomide-dimethyl fumarate combination treated UVW cells.

a.

	24hr				48hr				72hr			
	0	50μM	200μM	400μM	0	50μM	200μM	400μM	0	50μM	200μM	400μM
0	–	ns	ns	ns	–	ns	**	**	–	**	**	**
50μM+3.125μM	ns	ns			ns	ns			*	ns		
200μM+12μM	ns		ns		ns		ns		*		ns	
400μM+25μM	ns			ns	ns			ns	*			ns

b.

	24hr				48hr				72hr			
	0	3.125μM	12.5μM	25μM	0	3.125μM	12.5μM	25μM	0	3.125μM	12.5μM	25μM
0	–	ns	ns	ns	–	ns	ns	ns	–	**	**	**
50μM+3.125μM	ns	ns			ns	ns			*	*		
200μM+12μM	ns		ns		ns		ns		*		*	
400μM+25μM	ns			ns	ns			ns	*			*

c.

	24hr			48hr			72hr		
	50μM	200μM	400μM	50μM	200μM	400μM	50μM	200μM	400μM
50μM+3.125μM	ns			ns			ns		
200μM+12μM		ns			ns			ns	
400μM+25μM			ns			ns			ns

d.

	24hr			48hr			72hr		
	3.125μM	12.5μM	25μM	3.125μM	12.5μM	25μM	3.125μM	12.5μM	25μM
50μM+3.125μM	ns			ns			L*		
200μM+12μM		ns			ns			L*	
400μM+25μM			ns			ns			L*

Appendix B2: Statistical analysis of data presented in Figure 3.11. a. comparison of apoptotic induction in temozolomide and temozolomide-dimethyl fumarate combination treated T98g cells. b. comparison of apoptotic induction in dimethyl fumarate and temozolomide-dimethyl fumarate combination treated T98g cells. c. comparison of apoptotic phase distribution in temozolomide and temozolomide-dimethyl fumarate combination treated T98g cells. d. comparison of apoptotic phase distribution in dimethyl fumarate and temozolomide-dimethyl fumarate combination treated T98g cells.

Appendix c

a.

	0	1/3Gy	0.5μM	5μM	15μM
0	–	G_2**	G_2**	G_2**	G_2**
0.5μM+1Gy	ns	ns	ns		
0.5μM+3Gy	G_2*	ns	G_2*		
5μM+1Gy	ns	ns		ns	
5μM+3Gy	G_2*	ns		G_2**	
15μM+1Gy	ns	ns			ns
15μM+3Gy	G_2*	G_2*			G_2*

b.

	0	1/3Gy	0.3μM	3μM	9μM
0	–	G_2**	ns	ns	ns
0.3μM+1Gy	ns	ns	ns		
0.3μM+3Gy	ns	ns	ns		
3μM+1Gy	ns	ns		ns	
3μM+3Gy	ns	ns		ns	
9μM+1Gy	ns	ns			ns
9μM+3Gy	ns	ns			ns

c.

	0	1/3Gy	0.3μM+1/3Gy	3μM+1/3Gy	9μM+1/3Gy
0	–	G_2**	ns	ns	ns
0.5μM+0.3μM+1Gy	ns	ns	ns		
0.5μM+0.3μM+3Gy	G_2**	ns	G_2*		
5μM+3μM+1Gy	ns	ns		ns	
5μM+3μM+3Gy	G_2**	G_2*		G_2*	
15μM+9μM+1Gy	G_2*	ns			ns
15μM+9μM+3Gy	G_2**	G_2*			G_2*

d.

	0	1/3Gy	0.5μM+1/3Gy	5μM+1/3Gy	15μM+1/3Gy
0	–	G_2**	ns	ns	ns
0.5μM+0.3μM+1Gy	ns	ns	ns		
0.5μM+0.3μM+3Gy	G_2**	ns	ns		
5μM+3μM+1Gy	ns	ns		ns	
5μM+3μM+3Gy	G_2**	G_2*		ns	
15μM+9μM+1Gy	G_2*	ns			ns
15μM+9μM+3Gy	G_2**	G_2*			ns

e.

	0	1/3Gy	0.5μM+3μM	5μM+3μM	15μM+9μM
0	–	G_2**	ns	ns	ns
0.5μM+3μM+1Gy	ns	ns	ns		
0.5μM+3μM+3Gy	G_2**	ns	G_2**		
5μM+3μM+1Gy	ns	ns		ns	
5μM+3μM+3Gy	G_2**	G_2*		G_2**	
15μM+9μM+1Gy	G_2*	ns			ns
15μM+9μM+3Gy	G_2**	G_2*			G_2**

Appendix C1: Statistical analysis of data presented in Figure 4.10. a. comparison of cell cycle progression in temozolomide treated and temozolomide-X-irradiated exposed UVW cells. b. cell cycle progression in dimethyl fumarate treated and dimethyl fumarate-X-irradiated exposed UVW cells. c. cell cycle progression n in the temozolomide-dimethyl fumarate combination treated and the X-irradiated temozolomide-dimethyl fumarate combination treated UVW cells. d. cell cycle progression in X-irradiated and temozolomide treated and X-irradiated temozolomide-dimethyl fumarate combination treated UVW cells. e. cell cycle progression in X-irradiated and dimethyl fumarate treated and X-irradiated temozolomide-dimethyl fumarate combination treated UVW cells.

a.

	0	1/3Gy	50μM	200μM	400μM
0	–	3Gy G_2*	ns	ns	ns
50μM+1Gy	ns	ns	ns		
50μM+3Gy	ns	ns	G_2*		
200μM+1Gy	ns	ns		ns	
200μM+3Gy	G_2*	ns		ns	
400μM+1Gy	G_2*	ns			G_2*
400μM+3Gy	G_2**	ns			G_2*

b.

	0	1/3Gy	3.125μM	12.5μM	25μM
0	–	3Gy G_2*	ns	ns	ns
3.125μM+1Gy	ns	ns	ns		
3.125μM+3Gy	ns	ns	ns		
12.5μM+1Gy	ns	ns		ns	
12.5μM+3Gy	ns	ns		ns	
25μM+1Gy	ns	ns			ns
25μM+3Gy	ns	ns			ns

c.

	0	1/3Gy	50μM+3.125μM	200μM+12.5μM	400μM+25μM
0	–	G_2**	ns	ns	ns
50μM+3.125μM+1Gy	G_2**	G_2**	G_2**		
50μM+3.125μM+3Gy	G_2***	G_2*	G_2***		
200μM+12.5μM+1Gy	G_2**	G_2**		G_2**	
200μM+12.5μM+3Gy	G_2***	G_2*		G_2***	
400μM+25μM+1Gy	G_2**	G_2**			G_2**
400μM+25μM+3Gy	G_2***	G_2*			G_2***

d.

	0	1/3Gy	50μM+1/3Gy	200μM+1/3Gy	400μM+1/3Gy
0	–	G_2**	ns	ns	ns
50μM+3.125μM+1Gy	G_2**	G_2**	G_2**		
50μM+3.125μM+3Gy	G_2***	G_2*	G_2**		
200μM+12.5μM+1Gy	G_2**	G_2**		G_2**	
200μM+12.5μM+3Gy	G_2***	G_2*		G_2**	
400μM+25μM+1Gy	G_2**	G_2**			G_2**
400μM+25μM+3Gy	G_2***	G_2*			G_2**

e.

	0	1/3Gy	50μM+1/3Gy	200μM+1/3Gy	400μM+1/3Gy
0	–	G_2**	ns	3Gy G_2*	1Gy G_2* 3Gy G_2**
50μM+3.125μM+1Gy	G_2**	G_2**	G_2**		
50μM+3.125μM+3Gy	G_2***	G_2*	G_2**		
200μM+12.5μM+1Gy	G_2**	G_2**		G_2**	
200μM+12.5μM+3Gy	G_2***	G_2*		G_2**	
400μM+25μM+1Gy	G_2**	G_2**			G_2**
400μM+25μM+3Gy	G_2***	G_2*			G_2**

Appendix C2: Statistical analysis of data presented in Figure 4.11. a. comparison of cell cycle progression in temozolomide treated and temozolomide-X-irradiated exposed T98g cells. b. cell cycle progression in dimethyl fumarate treated and dimethyl fumarate-X-irradiated exposed T98g cells. c. cell cycle progression n in the temozolomide-dimethyl fumarate combination treated and the X-irradiated temozolomide-dimethyl fumarate combination treated T98g cells. d. cell cycle progression in X-irradiated and temozolomide treated and X-irradiated temozolomide-dimethyl fumarate combination treated T98g cells. e. cell cycle progression in X-irradiated and dimethyl fumarate treated and X-irradiated temozolomide-dimethyl fumarate combination treated T98g cells.

Appendix d

a.

	24hr					48hr					72hr				
	0	1/3Gy	0.5μM	5μM	15μM	0	1/3Gy	0.5μM	5μM	15μM	0	1/3Gy	0.5μM	5μM	15μM
0.5μM+1Gy	ns	ns	ns			*	ns	*			**	ns	ns		
0.5μM+3Gy	ns	ns	ns			*	ns	*			**	ns	ns		
5μM+1Gy	ns	ns		ns		*	ns		*		**	ns		ns	
5μM+3Gy	ns	ns		ns		*	ns		*		**	ns		ns	
15μM+1Gy	ns	ns			ns	*	ns			*	**	ns			ns
15μM+3Gy	ns	ns			ns	*	ns			*	**	ns			ns

b.

	24hr					48hr					72hr				
	0	1/3Gy	0.3μM	3μM	9μM	0	1/3Gy	0.3μM	3μM	9μM	0	1/3Gy	0.3μM	3μM	9μM
0.3μM+1Gy	ns	ns	ns			*	ns	ns			**	ns	ns		
0.3μM+3Gy	ns	ns	ns			*	ns	ns			**	ns	ns		
3μM+1Gy	ns	ns		ns		*	ns		ns		**	ns		ns	
3μM+3Gy	ns	ns		ns		*	ns		ns		**	ns		ns	
9μM+1Gy	ns	ns			ns	*	ns			ns	**	ns			ns

c.

	24hr					48hr					72hr				
	0	1/3Gy	0.5μM+0.3μM	5μM+3μM	15μM+9μM	0	1/3Gy	0.5μM+0.3μM	5μM+3μM	15μM+9μM	0	1/3Gy	0.5μM+0.3μM	5μM+3μM	15μM+9μM
0.5μM+0.3μM+1Gy	ns	ns	*			*	ns	**			**	ns	ns		
0.5μM+0.3μM+3Gy	ns	ns	**			*	ns	**			**	ns	ns		
5μM+3μM+1Gy	ns	ns		*		*	ns		**		**	ns		ns	
5μM+3μM+3Gy	ns	ns		**		*	ns		**		**	ns		ns	
15μM+9μM+1Gy	ns	ns			*	*	ns			**	**	ns			ns
15μM+9μM+3Gy	ns	ns			**	*	ns			**	**	ns			ns

d.

	24hr			48hr			72hr		
	0.5μM+1/3Gy	5μM+1/3Gy	15μM+1/3Gy	0.5μM+1/3Gy	5μM+1/3Gy	15μM+1/3Gy	0.5μM+1/3Gy	5μM+1/3Gy	15μM+1/3Gy
0.5μM+0.3μM+1Gy	ns			ns			ns		
0.5μM+0.3μM+3Gy	ns			ns			ns		
5μM+3μM+1Gy		ns			ns			ns	
5μM+3μM+3Gy		ns			ns			ns	
15μM+9μM+1Gy			ns			ns			ns
15μM+9μM+3Gy			ns			ns			ns

Appendix D1: Statistical analysis of data presented in Figure 4.13. a. comparison of apoptotic induction in temozolomide treated and temozolomide-X-irradiated exposed UVW cells. b. comparison of apoptotic induction in dimethyl fumarate treated and dimethyl fumarate-X-irradiated exposed UVW cells. c. comparison of apoptotic induction in the temozolomide-dimethyl fumarate combination treated and the X-irradiated temozolomide-dimethyl fumarate combination treated UVW cells. d. comparison of apoptotic induction in X-irradiated and temozolomide treated and X-irradiated temozolomide-dimethyl fumarate combination treated UVW cells. e. comparison of apoptotic induction in X-irradiated and dimethyl fumarate treated and X-irradiated temozolomide-dimethyl fumarate combination treated UVW cells.

a.

	24hr			48hr			72hr		
	0.5μM	5μM	15μM	0.5μM	5μM	15μM	0.5μM	5μM	15μM
0.5μM+1Gy	ns			L*			L** N***		
0.5μM+3Gy	ns			L*			L** N***		
5μM+1Gy		ns			L*			L** N***	
5μM+3Gy		ns			L*			L** N***	
15μM+1Gy			ns			L*			L** N***
15μM+3Gy			ns			L*			L** N***

b.

	24hr			48hr			72hr		
	0.3μM	3μM	9μM	0.3μM	3μM	9μM	0.3μM	3μM	9μM
0.3μM+1Gy	ns			L*			L** N***		
0.3μM+3Gy	ns			L*			L** N***		
3μM+1Gy		ns			L*			L** N***	
3μM+3Gy		ns			L*			L** N***	
9μM+1Gy			ns			L*			L** N***
9μM+3Gy			ns			L*			L** N***

c.

	24hr			48hr			72hr		
	0.5μM+0.3μM	5μM+3μM	15μM+9μM	0.5μM+0.3μM	5μM+3μM	15μM+9μM	0.5μM+0.3μM	5μM+3μM	15μM+9μM
0.5μM+0.3μM+1Gy	ns			L*			L* N***		
0.5μM+0.3μM+3Gy	ns			L*			L* N***		
5μM+3μM+1Gy		ns			L*			L* N***	
5μM+3μM+3Gy		ns			L*			L* N***	
15μM+9μM+1Gy			ns			L*			L* N***
15μM+9μM+3Gy			ns			L*			L* N***

d.

	24hr			48hr			72hr		
	0.5μM+1/3Gy	5μM+1/3Gy	15μM+1/3Gy	0.5μM+1/3Gy	5μM+1/3Gy	15μM+1/3Gy	0.5μM+1/3Gy	5μM+1/3Gy	15μM+1/3Gy
0.5μM+0.3μM+1Gy	ns			ns			ns		
0.5μM+0.3μM+3Gy	ns			ns			ns		
5μM+3μM+1Gy		ns			ns			ns	
5μM+3μM+3Gy		ns			ns			ns	
15μM+9μM+1Gy			ns			ns			ns
15μM+9μM+3Gy			ns			ns			ns

e.

	24hr			48hr			72hr		
	0.3μM+1/3Gy	3μM+1/3Gy	9μM+1/3Gy	0.3μM+1/3Gy	3μM+1/3Gy	9μM+1/3Gy	0.3μM+1/3Gy	3μM+1/3Gy	9μM+1/3Gy
0.5μM+0.3μM+1Gy	ns			ns			ns		
0.5μM+0.3μM+3Gy	ns			ns			ns		
5μM+3μM+1Gy		ns			ns			ns	
5μM+3μM+3Gy		ns			ns			ns	
15μM+9μM+1Gy			ns			ns			ns
15μM+9μM+3Gy			ns			ns			ns

Appendix D2: Statistical analysis of data presented in Figure 4.13. a. comparison of apoptotic phase distribution in temozolomide treated and temozolomide-X-irradiated exposed UVW cells. b. comparison of apoptotic phase distribution in dimethyl fumarate treated and dimethyl fumarate-X-irradiated exposed UVW cells. c. comparison of apoptotic phase distribution in the temozolomide-dimethyl fumarate combination treated and the X-irradiated temozolomide-dimethyl fumarate combination treated UVW cells. d. comparison of apoptotic phase distribution in X-irradiated and temozolomide treated and X-irradiated temozolomide-dimethyl fumarate combination treated UVW cells. e. comparison of apoptotic phase distribution in X-irradiated and dimethyl fumarate treated and X-irradiated temozolomide-dimethyl fumarate combination treated UVW cells.

a.

	24hr					48hr					72hr				
	0	1/3Gy	50μM	200μM	400μM	0	1/3Gy	50μM	200μM	400μM	0	1/3Gy	50μM	200μM	400μM
50μM+1Gy	ns	ns	ns			*	ns	ns			*	ns	ns		
50μM+3Gy	ns	ns	ns			*	ns	ns			*	ns	ns		
200μM+1Gy	ns	ns		ns		*	ns		ns		*	ns		ns	
200μM+3Gy	ns	ns		ns		*	ns		ns		*	ns		ns	
400μM+1Gy	ns	ns			ns	*	ns			ns	*	ns			ns
400μM+3Gy	ns	ns			ns	*	ns			ns	*	ns			ns

b.

	24hr					48hr					72hr				
	0	1/3Gy	3.125μM	12.5μM	25μM	0	1/3Gy	3.125μM	12.5μM	25μM	0	1/3Gy	3.125μM	12.5μM	25μM
3.125μM+1Gy	ns	ns	ns			ns	ns	ns			*	ns	**		
3.125μM+3Gy	ns	ns	ns			ns	ns	ns			*	ns	*		
12.5μM+1Gy	ns	ns		ns		*	ns		ns		*	ns		**	
12.5μM+3Gy	ns	ns		ns		*	ns		ns		*	ns		*	
25μM+1Gy	ns	ns			ns	*	ns			ns	*	ns			**
25μM+3Gy	ns	ns			ns	*	ns			ns	*	ns			*

c.

	24hr					48hr					72hr				
	0	1/3Gy	50μM+3.125μM	200μM+12.5μM	400μM+25μM	0	1/3Gy	50μM+3.125μM	200μM+12.5μM	400μM+25μM	0	1/3Gy	50μM+3.125μM	200μM+12.5μM	400μM+25μM
50μM+3.125μM+1Gy	ns	ns	ns			ns	ns	ns			*	ns	ns		
50μM+3.125μM+3Gy	ns	ns	ns			*	ns	ns			*	ns	ns		
200μM+12.5μM+1Gy	ns	ns		ns		*	ns		ns		*	ns		ns	
200μM+12.5μM+3Gy	ns	ns		ns		*	ns		ns		*	ns		ns	
400μM+25μM+1Gy	ns	ns			ns	*	ns			ns	*	ns			ns
400μM+25μM+3Gy	ns	ns			ns	*	ns			ns	*	ns			ns

d.

	24hr			48hr			72hr		
	50μM+1/3Gy	200μM+1/3Gy	400μM+1/3Gy	50μM+1/3Gy	200μM+1/3Gy	400μM+1/3Gy	50μM+1/3Gy	200μM+1/3Gy	400μM+1/3Gy
50μM+3.125μM+1Gy	ns			ns			ns		
50μM+3.125μM+3Gy	ns			ns			ns		
200μM+12.5μM+1Gy		ns			ns			ns	
200μM+12.5μM+2Gy		ns			ns			ns	
400μM+25μM+1Gy			ns			ns			ns
400μM+25μM+3Gy			ns			ns			ns

e.

	24hr			48hr			72hr		
	3.125+1/3Gy	12.5μM+1/3Gy	25μM+1/3Gy	3.125+1/3Gy	12.5μM+1/3Gy	25μM+1/3Gy	3.125+1/3Gy	12.5μM+1/3Gy	25μM+1/3Gy
50μM+3.125μM+1Gy	ns			ns			ns		
50μM+3.125μM+3Gy	ns			ns			ns		
200μM+12.5μM+1Gy		ns			ns			ns	
200μM+12.5μM+2Gy		ns			ns			ns	
400μM+25μM+1Gy			ns			ns			ns
400μM+25μM+3Gy			ns			ns			ns

Appendix D3: Statistical analysis of data presented in Figure 4.14. a. comparison of apoptotic induction in temozolomide treated and temozolomide-X-irradiated exposed T98g cells. b. comparison of apoptotic induction in dimethyl fumarate treated and dimethyl fumarate-X-irradiated exposed T98g cells. c. comparison of apoptotic induction in the temozolomide-dimethyl fumarate combination treated and the X-irradiated temozolomide-dimethyl fumarate combination treated T98g cells. d. comparison of apoptotic induction in X-irradiated and temozolomide treated and X-irradiated temozolomide-dimethyl fumarate combination treated T98g cells. e. comparison of apoptotic induction in X-irradiated and dimethyl fumarate treated and X-irradiated temozolomide-dimethyl fumarate combination treated T98g cells.

a.

	24hr			48hr			72hr		
	50μM	200μM	400μM	50μM	200μM	400μM	50μM	200μM	400μM
50μM+1Gy	ns			ns			ns		
50μM+3Gy	ns			ns			ns		
200μM+1Gy		ns			ns			ns	
200μM+3Gy		ns			ns			ns	
400μM+1Gy			ns			ns			ns
400μM+3Gy			ns			ns			ns

b.

	24hr			48hr			72hr		
	3.125μM	12.5μM	25μM	3.125μM	12.5μM	25μM	3.125μM	12.5μM	25μM
3.125μM+1Gy	ns			ns			L*		
3.125μM+3Gy	ns			ns			L*		
12.5μM+1Gy		ns			ns			L*	
12.5μM+3Gy		ns			ns			L*	
25μM+1Gy			ns			ns			L*
25μM+3Gy			ns			ns			L*

c.

	24hr			48hr			72hr		
	50μM+3.125μM	200μM+12.5μM	400μM+25μM	50μM+3.125μM	200μM+12.5μM	400μM+25μM	50μM+3.125μM	200μM+12.5μM	400μM+25μM
50μM+3.125μM+1Gy	ns			ns			ns		
50μM+3.125μM+3Gy	ns			ns			ns		
200μM+12.5μM+1Gy		ns			ns			ns	
200μM+12.5μM+2Gy		ns			ns			ns	
400μM+25μM+1Gy			ns			ns			ns
400μM+25μM+3Gy			ns			ns			ns

d.

	24hr			48hr			72hr		
	3.125+1/3Gy	12.5μM+1/3Gy	25μM+1/3Gy	3.125+1/3Gy	12.5μM+1/3Gy	25μM+1/3Gy	3.125+1/3Gy	12.5μM+1/3Gy	25μM+1/3Gy
50μM+3.125μM+1Gy	ns			ns			ns		
50μM+3.125μM+3Gy	ns			ns			ns		
200μM+12.5μM+1Gy		ns			ns			ns	
200μM+12.5μM+2Gy		ns			ns			ns	
400μM+25μM+1Gy			ns			ns			ns
400μM+25μM+3Gy			ns			ns			ns

e.

	24hr			48hr			72hr		
	50μM+1/3Gy	200μM+1/3Gy	400μM+1/3Gy	50μM+1/3Gy	200μM+1/3Gy	400μM+1/3Gy	50μM+1/3Gy	200μM+1/3Gy	400μM+1/3Gy
50μM+3.125μM+1Gy	ns			ns			ns		
50μM+3.125μM+3Gy	ns			ns			ns		
200μM+12.5μM+1Gy		ns			ns			ns	
200μM+12.5μM+2Gy		ns			ns			ns	
400μM+25μM+1Gy			ns			ns			ns
400μM+25μM+3Gy			ns			ns			ns

Appendix D4: Statistical analysis of data presented in Figure 4.14. a. comparison of apoptotic phase distribution in temozolomide treated and temozolomide-X-irradiated exposed T98 cells. b. comparison of apoptotic phase distribution in dimethyl fumarate treated and dimethyl fumarate-X-irradiated exposed T98g cells. c. comparison of apoptotic phase distribution in the temozolomide-dimethyl fumarate combination treated and the X-irradiated temozolomide-dimethyl fumarate combination treated T98g cells. d. comparison of apoptotic phase distribution in X-irradiated and temozolomide treated and X-irradiated temozolomide-dimethyl fumarate combination treated T98g cells. e. comparison of apoptotic phase distribution in X-irradiated and dimethyl fumarate treated and X-irradiated temozolomide-dimethyl fumarate combination treated T98g cells.